

---

# PLAXIS

---

PLAXIS 3D 2024.1

Material Models Manual 3D

---

**Bentley**<sup>®</sup>  
Advancing Infrastructure

Last Updated: December 29, 2023

# Table of Contents

<b>Chapter 1: Introduction .....</b>	<b>6</b>
1.1 Material Models and Licencing levels .....	6
1.2 On the use of different models .....	6
1.3 Limitations .....	10
<b>Chapter 2: Preliminaries on material modelling .....</b>	<b>14</b>
2.1 General definitions of stress .....	14
2.2 General definitions of strain .....	16
2.3 Elastic strains .....	17
2.4 Undrained effective stress analysis (effective stiffness parameters) .....	19
2.4.1 Skempton B-parameter .....	22
2.4.2 Biot pore pressure coefficient $\alpha_{\text{Biot}}$ [ULT] .....	23
2.5 Undrained effective stress analysis with effective strength parameters (Undrained A) .....	24
2.6 Undrained effective stress analysis with undrained strength parameters (Undrained B) .....	25
2.7 Undrained total stress analysis with undrained parameters (Undrained C) .....	26
2.8 The initial pre-consolidation stress in advanced models .....	27
2.9 On the initial stresses .....	29
<b>Chapter 3: Linear Elastic Perfectly Plastic Model (Mohr-Coulomb Model) .....</b>	<b>31</b>
3.1 Linear Elastic Perfectly - Plastic behaviour .....	31
3.2 Formulation of the Mohr-Coulomb model .....	32
3.3 Parameters of the Mohr-Coulomb model .....	34
3.4 Depth-dependency .....	40
3.5 On the use of the Mohr-Coulomb model in dynamics calculations [ULT] .....	41
<b>Chapter 4: The Hoek-Brown model (rock behaviour) .....</b>	<b>42</b>
4.1 Formulation of the Hoek-Brown model .....	42
4.2 Conversion of Hoek-Brown to Mohr-Coulomb .....	45
4.3 Parameters of the Hoek-Brown model .....	45
4.4 On the use of the Hoek-Brown model in dynamics calculations .....	54
<b>Chapter 5: The Jointed Rock model (anisotropy) .....</b>	<b>55</b>
5.1 Anisotropic elastic material stiffness matrix .....	56
5.2 Plastic behaviour in three directions .....	58
5.3 Parameters of the Jointed Rock model .....	60
5.4 On the use of the Jointed Rock model in dynamics calculations .....	66
<b>Chapter 6: The Hardening Soil model (Isotropic hardening) .....</b>	<b>67</b>
6.1 Hyperbolic relationship for standard drained triaxial test .....	68
6.2 Approximation of hyperbola by the Hardening Soil model .....	69
6.3 Plastic volumetric strain for triaxial states of stress .....	71
6.4 Parameters of the Hardening Soil Model .....	72
6.5 On the cap yield surface in the Hardening Soil model .....	78
6.6 State parameters in the Hardening Soil model .....	80

6.7	On the use of the Hardening Soil model in dynamics calculations .....	81
<b>Chapter 7: The Hardening Soil model with small-strain stiffness (HSsmall) .....</b>		<b>82</b>
7.1	Describing small-strain stiffness with a Simple Hyperbolic Law .....	83
7.2	Applying the Hardin-Drnevich relationship in the HS Model .....	84
7.3	Virgin (initial) loading vs unloading/reloading .....	86
7.4	Model Parameters .....	87
7.5	On the parameters $G_0$ and $\gamma_{0.7}$ .....	90
7.6	Model Initialization .....	91
7.7	State parameters in the Hardening Soil model with small-strain stiffness .....	92
7.8	On the use of the Hardening Soil model with small-strain stiffness in dynamics calculations .....	92
7.9	Other differences with the Hardening Soil model .....	93
<b>Chapter 8: Modified Cam-Clay model .....</b>		<b>95</b>
8.1	Formulation of the Modified Cam-Clay model .....	95
8.2	Parameters of the Modified Cam-Clay model .....	96
8.3	State parameters in the Modified Cam-Clay model .....	97
8.4	On the use of the Modified Cam-Clay model in dynamics calculations .....	98
8.5	Warning .....	98
<b>Chapter 9: The NGI-ADP model (anisotropic undrained shear strength) .....</b>		<b>99</b>
9.1	Formulation of the NGI-ADP model .....	99
9.1.1	1D model presentation .....	99
9.1.2	The NGI-ADP model in plane strain .....	100
9.1.3	The NGI-ADP model in 3D stress space .....	101
9.1.4	The NGI-ADP model traction criterion for interfaces in 2D .....	104
9.2	Parameters of the NGI-ADP model .....	104
9.3	State parameters in the NGI-ADP model .....	109
<b>Chapter 10: The Soft soil model [ADV] .....</b>		<b>110</b>
10.1	Isotropic states of stress and strain ( $\sigma'_1 = \sigma'_2 = \sigma'_3$ ) .....	111
10.2	Yield function .....	112
10.3	Parameters of the Soft Soil model .....	114
10.4	State parameters in the Soft Soil model .....	118
10.5	On the use of the Soft Soil model in dynamics calculations .....	118
<b>Chapter 11: Soft Soil Creep model (time dependent behaviour) [ADV] .....</b>		<b>120</b>
11.1	Introduction .....	120
11.2	Basics of one-dimensional creep .....	121
11.3	On the variables $\tau_c$ and $\epsilon_c$ .....	122
11.4	Differential law for 1D-creep .....	124
11.5	Three-dimensional-model .....	125
11.6	Formulation of elastic 3D-strains .....	128
11.7	Formulation of failure condition .....	129
11.8	Parameters of the Soft Soil Creep model .....	129
11.9	State parameters in the Soft Soil Creep model .....	133
11.10	On the use of the Soft Soil Creep model in dynamics calculations .....	133
11.11	On the use of the Soft Soil Creep model in practical applications .....	133
<b>Chapter 12: The Sekiguchi-Ohta model [ADV] .....</b>		<b>135</b>
12.1	Formulation of the Sekiguchi-Ohta model .....	135

12.1.1	Isotropic states of stress and strain ( $\sigma'_1 = \sigma'_2 = \sigma'_3$ ) .....	135
12.1.2	Inviscid (time-independent) formulation .....	136
12.1.3	Viscid (time-dependent) formulation .....	137
12.2	Parameters of the Sekiguchi-Ohta model .....	137
12.2.1	Model parameters of the inviscid model .....	138
12.2.2	Model parameters of the viscid model .....	140
12.3	State parameters in the Sekiguchi-Ohta model .....	142
<b>Chapter 13: The UDCAM-S model [ADV] .....</b>		<b>143</b>
13.1	Parameters of the UDCAM-S model .....	145
13.1.1	Ratio of the initial shear modulus to the degraded TXC shear strength ( $G_{max}/\tau_C$ ) ..	146
13.1.2	Shear strain at failure in triaxial compression ( $\gamma_f^C$ ) .....	146
13.1.3	Shear strain at failure in triaxial extension ( $\gamma_f^E$ ) .....	146
13.1.4	Shear strain at failure in direct simple shear ( $\gamma_f^{DSS}$ ) .....	146
13.1.5	Reference degraded TXC shear strength ( $\tau_{ref}^C$ ) .....	146
13.1.6	Reference depth ( $y_{ref}$ ) .....	147
13.1.7	Increase of degraded TXC shear strength with depth ( $\tau_{inc}^C$ ) .....	147
13.1.8	Ratio of the degraded TXE shear strength to the undrained TXC shear strength ( $\tau_E/\tau_C$ ) .....	147
13.1.9	Ratio of the degraded DSS shear strength to the undrained TXC shear strength ( $\tau_{DSS}/\tau_C$ ) .....	147
13.1.10	Initial mobilization ( $\tau_0/\tau_C$ ) .....	147
13.1.11	Poisson's ratio ( $\nu'$ ) .....	148
13.2	State parameters in the UDCAM-S model .....	148
13.3	On the use of the UDCAM-S model in dynamics calculations .....	149
<b>Chapter 14: The Concrete model [ADV] .....</b>		<b>150</b>
14.1	Formulation of the Concrete model .....	151
14.2	Strain hardening and softening .....	152
14.2.1	Compression .....	152
14.2.2	Tension .....	154
14.3	Time-dependency of the Concrete model .....	154
14.3.1	Strength and Stiffness .....	154
14.3.2	Plastic Deformability .....	156
14.3.3	Fracture energy .....	156
14.3.4	Viscoelastic Creep .....	157
14.3.5	Shrinkage .....	158
14.4	Parameters of the Concrete model .....	158
14.4.1	Recommended values for the parameters of the Concrete model .....	160
14.4.2	Summary of recommended parameters for Concrete model .....	162
14.5	State parameters in the Concrete model .....	164
14.6	On the use of the Concrete model in dynamics calculations .....	165
14.7	Warning .....	166
<b>Chapter 15: The UBC3D-PLM model [ULT] .....</b>		<b>167</b>
15.1	Elasto-plastic behaviour and hardening rule .....	168
15.2	Flow rule .....	170
15.3	Load state during liquefaction .....	171
15.4	Post-liquefaction rule and cyclic mobility .....	173
15.5	Parameters of the UBC3D-PLM model .....	174
15.6	State parameters in the UBC3D-PLM model .....	178

15.7	On the use of the UBC3D-PLM model in dynamics calculations .....	180
<b>Chapter 16: User-defined soil models [ADV]/[ULT] + [GSE] .....</b>		<b>181</b>
16.1	Introduction .....	181
16.2	Implementation of User Defined (UD) soil Models in calculations program .....	181
16.2.1	Main Functionalities UD Models .....	182
16.2.2	Using predefined subroutines from the source code .....	187
16.2.3	Definition of user-interface functions .....	187
16.2.4	UDSM additional information .....	190
16.2.5	Compiling the user subroutine .....	190
16.2.6	Debugging possibilities .....	191
16.3	Input of UD model parameters via user-interface .....	191
<b>Chapter 17: Application of advanced soil models .....</b>		<b>195</b>
17.1	Hardening Soil model: Response in drained and undrained triaxial tests .....	195
17.2	Application of the Hardening Soil model on real soil tests .....	199
17.2.1	Triaxial Test .....	200
17.2.2	Oedometer test .....	202
17.2.3	Pressiometer test .....	204
17.2.4	Conclusions of the Application of the Hardening Soil model on real soil tests .....	207
17.3	Application of the Hardening Soil model with small-strain stiffness on real soil tests .....	208
17.4	Soft Soil Creep model : Undrained triaxial tests at different loading rates .....	211
17.5	Soft Soil Creep model: Response in one-dimensional compression test .....	215
17.6	Soft Soil model: Response in isotropic compression test .....	221
17.7	Hardening Soil model and Hardening Soil model with small-strain stiffness: Excavation in Berlin sand .....	223
<b>Chapter 18: Structural Behaviour .....</b>		<b>227</b>
18.1	Anchors .....	227
18.2	3D Beams .....	227
18.3	3D Geogrids .....	229
18.4	3D Plates .....	230
18.5	3D Embedded beams .....	236
<b>Chapter 19: Hydraulic Models .....</b>		<b>239</b>
19.1	Van Genuchten model .....	239
19.2	Approximate Van Genuchten model .....	242
<b>Chapter 20: References .....</b>		<b>245</b>
<b>Appendices .....</b>		<b>250</b>
<b>Appendix A: Symbols .....</b>		<b>251</b>
<b>Appendix B: Applicability of the material model .....</b>		<b>256</b>
<b>Appendix C: Modelling of embedded structures .....</b>		<b>261</b>
<b>Appendix D: Fortran subroutines for User-defined soil models .....</b>		<b>263</b>
<b>Appendix E: Overview of Soil Models and Licence levels .....</b>		<b>266</b>

The mechanical behaviour of soils and rocks may be modelled at various degrees of accuracy. Hooke's law of linear, isotropic elasticity, for example, may be thought of as the simplest available stress-strain relationship. As it involves only two input parameters, i.e. Young's modulus,  $E$ , and Poisson's ratio,  $\nu$ , it is generally too crude to capture essential features of soil and rock behaviour. The linear elastic perfectly plastic model (Mohr-Coulomb) may be considered as a first order approximation of soil or rock behaviour. However, PLAXIS includes more advanced material models involving specific features such as stress-dependency of stiffness, strain-hardening / softening, memory of pre-consolidation, critical state, anisotropy, creep, swelling and shrinkage. Users are encouraged to employ the advanced models in an attempt to simulate the behaviour of soils and rocks more realistically, thereby obtaining more accurate results from their PLAXIS calculations. The use of the *SoilTest* facility may help in calibrating the corresponding model parameters. An overview of the applicability of the material models is given in [Applicability of the material model](#) (on page 256).

## 1.1 Material Models and Licencing levels

Soil/material models in PLAXIS 3D are offered for different licence levels (See [General Information Manual](#)). In this manual, soil models available for each licence level can be identified as follows:

- Material models with no identification - generally available for PLAXIS 3D licence.
- [ADV] - Material models available only for users with PLAXIS 2D/PLAXIS 3D Advanced licence.
- [ULT] - Material models available only for users with PLAXIS 2D/PLAXIS 3D Ultimate licence.
- [GSE] - Material models available only for users with Geotechnical SELECT subscription.

A compilation of the different soil models offered by PLAXIS 3D with their associated licence can be check in [Overview of Soil Models and Licence levels](#) (on page 266).

## 1.2 On the use of different models

### 1.2.1 *Linear Elastic model (LE)*

The Linear Elastic model is based on Hooke's law of isotropic elasticity. It involves two basic elastic parameters, i.e. Young's modulus  $E$  and Poisson's ratio  $\nu$ . Although the Linear Elastic model is not suitable to model soil, it may be used to model stiff volumes in the soil, like concrete walls, or intact rock formations.

### 1.2.2 *Mohr-Coulomb model (MC)*

The linear elastic perfectly-plastic Mohr-Coulomb model involves five input parameters, i.e.  $E$  and  $\nu$  for soil elasticity;  $\phi$  and  $c$  for soil plasticity and  $\psi$  as an angle of dilatancy. This Mohr-Coulomb model represents a 'first-order' approximation of soil or rock behaviour. It is recommended to use this model for a first analysis of the problem considered. For each layer one estimates a constant average stiffness or a stiffness that increases linearly with depth. Due to this constant stiffness, computations tend to be relatively fast and one obtains a first estimate of deformations.

### 1.2.3 *Hoek-Brown model (HB)*

The Hoek-Brown model is an isotropic elastic perfectly-plastic model for weathered rock based on the 2002 edition of the Hoek-Brown failure criterion. This non-linear stress-dependent criterion describes shear failure and tensile failure by a continuous function, and is familiar to most geologists and rock engineers. Besides the elastic parameters ( $E$  and  $\nu$ ), the model involves practical rock parameters such as the uni-axial compressive strength of the intact rock ( $\sigma_{ci}$ ), the Geological Strength Index ( $GSI$ ), and the disturbance factor ( $D$ ).

### 1.2.4 *Jointed Rock model (JR)*

The Jointed Rock model is an anisotropic elastic-plastic model, especially meant to simulate the behaviour of rock layers involving stratification and particular fault directions. Plasticity can only occur in a maximum of three shear directions (shear planes). Each plane has its own strength parameters  $\phi$  and  $c$ . The intact rock is considered to behave fully elastic with constant stiffness properties  $E$  and  $\nu$ . Reduced elastic properties may be defined for the stratification direction.

### 1.2.5 *Hardening Soil model (HS)*

The Hardening Soil model is an advanced model for the simulation of soil behaviour. As for the Mohr-Coulomb model, limiting states of stress are described by means of the friction angle,  $\phi$ , the cohesion,  $c$ , and the dilatancy angle,  $\psi$ . However, soil stiffness is described much more accurately by using three different input stiffnesses: the triaxial loading stiffness,  $E_{50}$ , the triaxial unloading stiffness,  $E_{ur}$ , and the oedometer loading stiffness,  $E_{oed}$ . As average values for various soil types,  $E_{ur} \approx 3E_{50}$  and  $E_{oed} \approx E_{50}$  are suggested as default settings, but both very soft and very stiff soils tend to give other ratios of  $E_{oed} / E_{50}$ , which can be entered by the user.

## Introduction

### On the use of different models

---

In contrast to the Mohr-Coulomb model, the Hardening Soil model also accounts for stress-dependency of stiffness moduli. This means that all stiffnesses increase with pressure. Hence, all three input stiffnesses relate to a reference stress, usually taken as 100 kPa (1 bar).

Besides the model parameters mentioned above, initial soil conditions, such as pre-consolidation, play an essential role in most soil deformation problems. This can be taken into account in the initial stress generation.

### 1.2.6 *Hardening Soil model with small-strain stiffness (HSsmall)*

The Hardening Soil model with small-strain stiffness (HSsmall) is a modification of the above Hardening Soil model that accounts for the increased stiffness of soils at small strains. At low strain levels most soils exhibit a higher stiffness than at engineering strain levels, and this stiffness varies non-linearly with strain. This behaviour is described in the HSsmall model using an additional strain-history parameter and two additional material parameters, i.e.  $G_0^{ref}$  and  $\gamma_{0.7}$ .  $G_0^{ref}$  is the small-strain shear modulus and  $\gamma_{0.7}$  is the strain level at which the shear modulus has reduced to about 70% of the small-strain shear modulus. The advanced features of the HSsmall model are most apparent in working load conditions. Here, the model gives more reliable displacements than the HS model. When used in dynamic applications, the Hardening Soil model with small-strain stiffness also introduces hysteretic material damping.

### 1.2.7 *Modified Cam-Clay model (MCC)*

The Modified Cam-Clay model is a well known model from international soil modelling literature; see for example [Muir Wood \(1990\)](#) (on page 248). It is meant primarily for the modelling of near normally-consolidated clay-type soils. This model has been added to PLAXIS to allow for a comparison with other codes.

### 1.2.8 *NGI-ADP model*

The NGI-ADP model is an anisotropic undrained shear strength model. The soil shear strength is defined by means of  $S_u$  values for active, passive and direct simple shear stress states. The model may be used for onshore and offshore applications in undrained clays and silts.

### 1.2.9 *Soft Soil model (SS) - [ADV]*

The Soft Soil model is a Cam-Clay type model especially meant for primary compression of near normally-consolidated clay-type soils. Although the modelling capabilities of this model are generally superseded by the Hardening Soil model, the Soft Soil model is better capable to model the compression behaviour of very soft soils.

### 1.2.10 *Soft Soil Creep model (SSC) - [ADV]*

The Hardening Soil model is generally suitable for all soils, but it does not account for viscous effects, i.e. creep and stress relaxation. In fact, all soils exhibit some creep and primary compression is thus followed by a certain amount of secondary compression.

## Introduction

### On the use of different models

---

The latter is most dominant in soft soils, i.e. normally consolidated clays, silts and peat, and PLAXIS thus implemented a model under the name Soft Soil Creep model. The Soft Soil Creep model has been developed primarily for application to settlement problems of foundations, embankments, etc. For unloading problems, as normally encountered in tunnelling and other excavation problems, the Soft Soil Creep model hardly supersedes the simple Mohr-Coulomb model. As for the Hardening Soil model, proper initial soil conditions are also essential when using the Soft Soil Creep model. This also includes data on the pre-consolidation stress, as the model accounts for the effect of overconsolidation. Note that the initial overconsolidation ratio also determines the initial creep rate.

#### 1.2.11 *Sekiguchi-Ohta model* - [ADV]

The Sekiguchi-Ohta model is a Cam-Clay type of model with anisotropic yield contour defined by  $K_{nc}^0$ . Two versions of the model exist: The inviscid model is a time independent model which has similarities with the Soft Soil model. The viscid model is time-dependent and has similarities with the Soft Soil Creep model. Both models have been developed in Japan. These models were previously available as user-defined models, but have become standard models in PLAXIS nowadays.

#### 1.2.12 *UDCAM-S model* - [ADV]

The Simplified UnDrained Cyclic Accumulation Model (UDCAM-S) is an advanced model to deal with undrained soil behaviour and degradation of the strength and stiffness in cyclic loading of clay or very low permeable silty soils. The UDCAM-S model is derived from the complex UDCAM model by NGI ([Andersen & Jostad, 2009](#) (on page 245)) with simplifications in order to be more suitable for engineering practice. The material model is based on the NGI-ADP model for the undrained behaviour of clays, implementing a pre-processing procedure called cyclic accumulation tool (See the Reference Manual - *Chapter 6 - Cyclic accumulation and optimisation tool*) to obtain the degraded parameter set based on the type of analysis the user has to perform.

#### 1.2.13 *Concrete model* - [ADV]

The Concrete model is an advanced elastoplastic model for concrete and shotcrete structures. It simulates the time-dependent strength and stiffness of concrete, strain hardening-softening in compression and tension as well as creep and shrinkage. The failure criterion involves a Mohr-Coulomb yield surface for deviatoric loading, which is combined with a Rankine yield surface in the tensile regime. The Concrete model employs 25 input parameters, but most of them can be derived from standard uniaxial tensile and compression tests and are generally familiar to structural engineers.

#### 1.2.14 *UBC3D-PLM model* - [ULT]

The UBC3D-PLM model is an advanced model for the simulation of liquefaction behaviour in dynamic applications. The UBC3D-PLM model employs two yield surfaces to guarantee a smooth transition near the mobilised friction angle. The UBC3D-PLM model uses the Mohr-Coulomb yield condition with an hardening law similar to the Hardening Soil model. For the secondary state, the UBC3D-PLM model incorporates a densification law through a second yield surface with a kinematic hardening rule based on the number of loading cycles. This correlation improves the precision of the evolution of the excess pore pressure.

The dynamic applications require a deep and extended investigation of the soil deposit. However, the UBC3D-PLM model implements a specific formulation with input parameters based on the most common tests: drained triaxial tests (CD TxC) or standard penetration tests (SPT).

#### 1.2.15 *Calibration of model parameters using the SoilTest facility - [GSE]*

The *SoilTest* facility may be used to check the performance of material models and the chosen model parameters in well defined soil lab test conditions as well as in arbitrary stress-strain conditions. In this way, users can compare the model response with real lab test data and get a feel for the accuracy at which real soil behaviour is approximated by the model. Even if a perfect match is obtained, it is good to realise that using calibrated material models in practical applications (where conditions are different than in the lab) may still lead to differences between the finite element model and reality. Nevertheless, the use of the *SoilTest* facility can help in understanding the capabilities and limitations of the material model and the influence of the model parameters.

### 1.3 Limitations

The PLAXIS code and its soil models have been developed to perform calculations of realistic geotechnical problems. In this respect PLAXIS can be considered as a geotechnical simulation tool. The soil models can be regarded as a qualitative representation of soil behaviour whereas the model parameters are used to quantify the soil characteristics. Although much care has been taken for the development of the PLAXIS code and its soil models, the simulation of reality remains an approximation, which implicitly involves some inevitable numerical and modelling errors. Moreover, the accuracy at which reality is approximated depends highly on the expertise of the user regarding the modelling of the problem, the understanding of the soil models and their limitations, the selection of model parameters, and the ability to judge the reliability of the computational results.

Some of the limitations in the currently available models are listed below:

#### 1.3.1 *Linear Elastic model*

Linear Elastic model Soil behaviour is highly non-linear and irreversible. The linear elastic model is insufficient to capture the essential features of soil. The use of the linear elastic model may, however, be considered to model strong massive structures in the soil or bedrock layers. Stress states in the linear elastic model are not limited in any way, which means that the model shows infinite strength. Be careful using this model for materials that are loaded up to their material strength.

#### 1.3.2 *Mohr-Coulomb model*

The linear elastic perfectly-plastic Mohr-Coulomb model is a first order model that includes only a limited number of features that soil behaviour shows in reality. Although the increase of stiffness with depth can be taken into account, the Mohr-Coulomb model does neither include stress-dependency nor stress-path dependency nor strain dependency of stiffness or anisotropic stiffness. In general, effective stress states at failure are quite well described using the Mohr-Coulomb failure criterion with effective strength parameters  $\varphi'$  and  $c'$ . For undrained materials, the Mohr-Coulomb model may be used with the friction angle  $\varphi$  set to  $0^\circ$  and the cohesion  $c$  set to  $c_u(S_u)$ , to enable a direct control of undrained shear strength. In that case note that the model does not automatically include the increase of shear strength with consolidation.

### 1.3.3 *Hoek-Brown model*

The Hoek-Brown model is an isotropic continuum model particularly meant to model weathered rock. Hence, the model is not suitable for stratified or jointed rock sections with a significant anisotropic stiffness or with one or more dominant sliding directions. For such behaviour, the Jointed Rock model is available.

### 1.3.4 *Hardening Soil model*

Although the Hardening Soil model can be regarded as an advanced soil model, there are a number of features of real soil behaviour the model does not include. It is a hardening model that does not account for softening due to soil dilatancy and de-bonding effects. In fact, it is an isotropic hardening model so that it models neither hysteretic and cyclic loading nor cyclic mobility. Moreover, the model does not distinguish between large stiffness at small strains and reduced stiffness at engineering strain levels. The user has to select the stiffness parameters in accordance with the dominant strain levels in the application. Last but not least, the use of the Hardening Soil model generally results in longer calculation times, since the material stiffness matrix is formed and decomposed in each calculation step.

### 1.3.5 *Hardening Soil model with small-strain stiffness*

As the Hardening Soil model with small-strain stiffness (HSsmall) incorporates the loading history of the soil and a strain-dependent stiffness, it can, to some extent, be used to model cyclic loading. However, it does not incorporate a gradual softening during cyclic loading, so is not suitable for cyclic loading problems in which softening plays a role. In fact, just as in the Hardening Soil model, softening due to soil dilatancy and debonding effects are not taken into account. Moreover, the HSsmall does not incorporate the accumulation of irreversible volumetric straining nor liquefaction behaviour with cyclic loading. The use of the HSsmall will generally result in calculation times that are even longer than those of the Hardening Soil model.

### 1.3.6 *Jointed Rock model*

The Jointed Rock model is a first order anisotropic model that includes a limited number of features that rock behaviour shows in reality. Plasticity can only occur in a maximum of three shear directions (shear planes). Each plane has its own shear strength parameters  $\varphi_i$  and  $c_i$  and tensile strength  $t_i$ . Hence, the maximum shear stress is linearly dependent on the normal stress, and not curved as in reality. The intact rock is considered to behave fully elastic with constant stiffness properties  $E$  and  $\nu$ . Reduced elastic properties may be defined for the stratification direction. Note that failure is limited to the predefined shear plane directions. It is possible that realistic potential failure mechanisms are not captured by the model because of the elastic behaviour in any other direction than the three shear planes.

### 1.3.7 *Modified Cam-Clay model*

The same limitations (including those in the Soft Soil Creep model) hold in the Modified Cam-Clay model. Moreover, the Modified Cam-Clay model may allow for unrealistically high shear stresses. This is particularly the case for overconsolidated stress states where the stress path crosses the critical state line. Furthermore, the Modified Cam-Clay model may give softening behaviour for such stress paths. Without special regularization

techniques, softening behaviour may lead to mesh dependency and convergence problems of iterative procedures. Moreover, the Modified Cam-Clay model cannot be used in combination with *Safety* analysis by means of  $\phi$ -c reduction.

#### 1.3.8 NGI-ADP model

The NGI-ADP model is an undrained shear strength model particularly meant to model undrained clays and silts. It can be used in a drained or effective stress analysis, but note that the shear strength is not automatically updated with changes of effective stress. Also note that the NGI-ADP model does not include a tension cut-off.

#### 1.3.9 Soft Soil model-[ADV]

The same limitations (including the ones for the Soft Soil Creep model) hold in the Soft Soil model. The utilization of the Soft Soil model should be limited to the situations that are dominated by compression. It is not recommended for use in excavation problems, since the model hardly supercedes the Mohr-Coulomb model in unloading problems.

#### 1.3.10 Soft Soil Creep model-[ADV]

All above limitations also hold true for the Soft Soil Creep model. In addition this model tends to over-predict the range of elastic soil behaviour. This is especially the case for excavation problems, including tunnelling. Care must also be taken with the generation of initial stresses for normally consolidated soils. Although it would seem logical to use  $OCR = 1.0$  for normally consolidated soils, such use would generally lead to an over-prediction of deformations in problems where the stress level is dominated by the initial self-weight stresses. Therefore, for such problems it is recommended to use a slightly increased OCR-value to generate the initial stress state. In fact, in reality most soils tend to show a slightly increased pre-consolidation stress in comparison with the initial effective stress. Before starting an analysis with external loading it is suggested to perform a single calculation phase with a short time interval and without loading to verify the surface settlement rate based on common practice.

#### 1.3.11 UDCAM-S model-[ADV]

The UDCAM-S model is an undrained shear strength model particularly meant to model undrained clays and silts under design storms. It can be used in a drained or effective stress analysis, but note that the shear strength is not automatically updated with changes of effective stress. Also note that the NGI-ADP model does not include a tension cut-off.

#### 1.3.12 Concrete model-[ADV]

The Concrete model is an elastoplastic time-dependent model particularly meant to model shotcrete or concrete structures. The design approach is separately implemented in the model through two safety factor parameters in order to avoid inconsistency between the different aspects computed by the Concrete model. The user should be careful in dynamics analysis because of the time interval difference between dynamic input and shotcrete hardening. The model is not suitable for failure involving low fracture energy.

### 1.3.13 Interfaces

Interface elements are generally modelled by means of the bi-linear Mohr-Coulomb model. When a more advanced model is used for the corresponding cluster material data set, the interface element will only pick up the relevant data ( $c$ ,  $\varphi$ ,  $\psi$ ,  $E$ ,  $\nu$ ) for the Mohr-Coulomb model, as described in the Reference Manual. In such cases the interface stiffness is set equal to the elastic soil stiffness. Hence,  $E = E_{ur}$  where  $E_{ur}$  is stress level dependent, following a power law with  $E_{ur}$  proportional to  $\sigma_m$ . For the Soft Soil model, Soft Soil Creep model and Modified Cam-Clay model the power  $m$  is equal to 1 and  $E_{ur}$  is largely determined by the swelling constant  $\kappa^*$ .

### 1.3.14 Undrained behaviour

In general, care must be taken in undrained conditions, since the effective stress path that is followed in any of the models may deviate significantly from reality. Although PLAXIS has options to deal with undrained behaviour in an effective stress analysis, the use of undrained shear strength ( $c_u$  or  $S_u$ ) may be preferred over the use of effective strength properties ( $\varphi'$  and  $c'$ ) in such cases. Please note that direct input on undrained shear strength does not automatically include the increase of shear strength with consolidation. If, for any reason, the user decides to use effective strength properties in undrained conditions, it is strongly recommended to check the resulting *mobilised shear strength* using the corresponding option in the PLAXIS Output program.

## Preliminaries on material modelling

A material model is described by a set of mathematical equations that give a relationship between stress and strain. Material models are often expressed in a form in which infinitesimal increments of stress (or 'stress rates') are related to infinitesimal increments of strain (or 'strain rates'). All material models implemented in PLAXIS are based on a relationship between the effective stress rates,  $\dot{\sigma}'$ , and the strain rates,  $\dot{\epsilon}'$ . In the following section it is described how stresses and strains are defined in PLAXIS. In subsequent sections the basic stress-strain relationship is formulated and the influence of pore pressures in undrained materials is described. Later sections focus on initial conditions for advanced material models.

This Material Models Manual is a general manual for all PLAXIS programs and uses the coordinate system as used in most programs ([Figure 1](#) (on page 14)). Please note that the PLAXIS 3D uses a different coordinate system where  $z$  is the vertical axis. Users should realize this when reading this manual.

### 2.1 General definitions of stress

Stress is a tensor which can be represented by a matrix in Cartesian coordinates:

$$\boldsymbol{\sigma} = \begin{bmatrix} \sigma_{xx} & \sigma_{xy} & \sigma_{xz} \\ \sigma_{yx} & \sigma_{yy} & \sigma_{yz} \\ \sigma_{zx} & \sigma_{zy} & \sigma_{zz} \end{bmatrix} \quad \text{Eq. [1]}$$

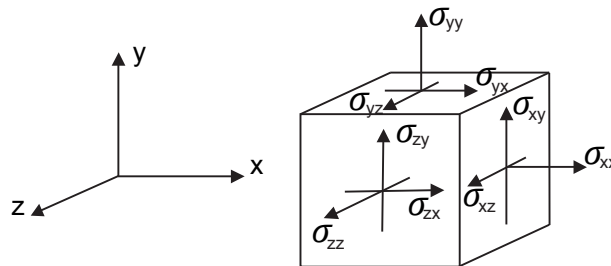


Figure 1: General three-dimensional coordinate system and sign convention for stresses

In the standard deformation theory, the stress tensor is symmetric such that  $\sigma_{xy} = \sigma_{yx}$ ,  $\sigma_{yz} = \sigma_{zy}$  and  $\sigma_{zx} = \sigma_{xz}$ . In this situation, stresses are often written in vector notation, which involve only six different components:

$$\underline{\sigma} = (\sigma_{xx} \ \sigma_{yy} \ \sigma_{zz} \ \sigma_{xy} \ \sigma_{yz} \ \sigma_{zx})^T \quad \text{Eq. [2]}$$

According to Terzaghi's principle, stresses in the soil are divided into effective stresses,  $\underline{\sigma}'$ , and pore pressures,  $q_w$ :

## Preliminaries on material modelling

### General definitions of stress

$$\underline{\sigma} = \underline{\sigma}' + \underline{\sigma}_w \quad \text{Eq. [3]}$$

Pore pressures are generally provided by water in the pores. Water is considered not to sustain any shear stresses. As a result, effective shear stresses are equal to total shear stresses. Positive normal stress components are considered to represent tension, whereas negative normal stress components indicate pressure (or compression). Moreover, water is considered to be fully isotropic, so all pore pressure components are equal. Hence, pore pressure can be represented by a single value,  $p_w$ :

$$\underline{\sigma}_w = (p_w \ p_w \ p_w \ 0 \ 0 \ 0)^T \quad \text{Eq. [4]}$$

Material models for soil and rock are generally expressed as a relationship between infinitesimal increments of effective stress and infinitesimal increments of strain. In such a relationship, infinitesimal increments of effective stress are represented by stress rates (with a dot above the stress symbol):

$$\dot{\underline{\sigma}}' = (\dot{\sigma}'_{xx} \ \dot{\sigma}'_{yy} \ \dot{\sigma}'_{zz} \ \dot{\sigma}'_{xy} \ \dot{\sigma}'_{yz} \ \dot{\sigma}'_{zx})^T \quad \text{Eq. [5]}$$

It is often useful to apply principal stresses rather than Cartesian stress components when formulating material models. Principal stresses are the stresses in such a coordinate system direction that all shear stress components are zero. Principal stresses are, in fact, the eigenvalues of the stress tensor. Principal effective stresses can be determined in the following way:

$$\det(\underline{\sigma} - \sigma' \underline{\mathbf{I}}) = 0 \quad \text{Eq. [6]}$$

where  $\underline{\mathbf{I}}$  is the identity matrix. This equation gives three solutions for  $\sigma'$ , i.e. the principal effective stresses ( $\sigma'_1$ ,  $\sigma'_2$ ,  $\sigma'_3$ ). In PLAXIS the principal effective stresses are arranged in algebraic order:

$$\sigma'_1 \leq \sigma'_2 \leq \sigma'_3 \quad \text{Eq. [7]}$$

Hence,  $\sigma'_1$  is the largest compressive principal stress and  $\sigma'_3$  is the smallest compressive principal stress. In this manual, models are often presented with reference to the principal stress space, as indicated in [Figure 2](#) (on page 15).

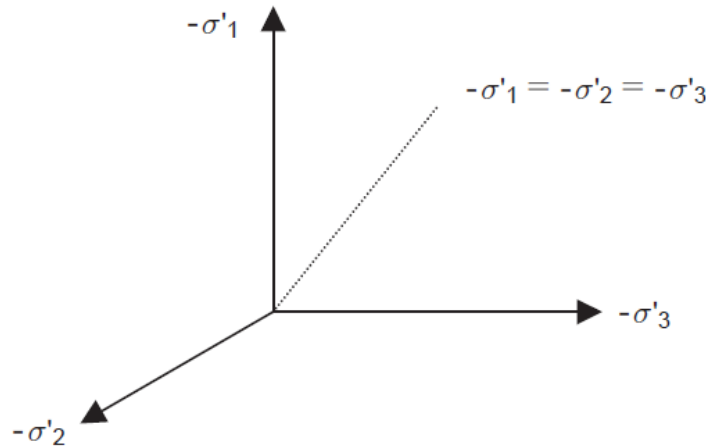


Figure 2: Principal stress space

In addition to principal stresses it is also useful to define invariants of stress, which are stress measures that are independent of the orientation of the coordinate system. Two useful stress invariants are:

$$p' = \frac{1}{3}(\sigma'_{xx} + \sigma'_{yy} + \sigma'_{zz}) \quad \text{Eq. [8]}$$

## Preliminaries on material modelling

### General definitions of strain

$$q = \sqrt{\frac{1}{2}((\sigma'_{xx} - \sigma'_{yy})^2 + (\sigma'_{yy} - \sigma'_{zz})^2 + (\sigma'_{zz} - \sigma'_{xx})^2 + 6(\sigma_{xy}^2 + \sigma_{yz}^2 + \sigma_{zx}^2))} \quad \text{Eq. [9]}$$

where

$$\begin{aligned} p' &= \text{Isotropic effective stress, or mean effective stress.} \\ q &= \text{Equivalent shear stress. It has the important property that it reduces to} \\ &\quad q = |\sigma'_1 - \sigma'_3| \text{ for triaxial stress states with } \sigma'_2 = \sigma'_3. \end{aligned}$$

Principal effective stresses can be written in terms of the invariants:

$$\sigma'_1 = p' + \frac{2}{3}q \sin(\theta - \frac{2}{3}\pi) \quad \text{Eq. [10]}$$

$$\sigma'_2 = p' + \frac{2}{3}q \sin(\theta) \quad \text{Eq. [11]}$$

$$\sigma'_3 = p' + \frac{2}{3}q \sin(\theta + \frac{2}{3}\pi) \quad \text{Eq. [12]}$$

in which  $\theta$  is referred to as Lode's angle (a third invariant), which is defined as:

$$\theta = \frac{1}{3} \arcsin\left(\frac{27}{2} \frac{J_3}{q^3}\right) \quad \text{Eq. [13]}$$

with

$$\begin{aligned} J_3 &= (\sigma'_{xx} - p')(\sigma'_{yy} - p')(\sigma'_{zz} - p') - (\sigma'_{yy} - p')\sigma_{zx}^2 \\ &\quad - (\sigma'_{xx} - p')\sigma_{yz}^2 - (\sigma'_{zz} - p')\sigma_{xy}^2 + 2\sigma_{xy}\sigma_{yz}\sigma_{zx} \end{aligned} \quad \text{Eq. [14]}$$

## 2.2 General definitions of strain

Strain is a tensor which can be represented by a matrix with Cartesian coordinates as:

$$\boldsymbol{\varepsilon} = \begin{bmatrix} \varepsilon_{xx} & \varepsilon_{xy} & \varepsilon_{xz} \\ \varepsilon_{yx} & \varepsilon_{yy} & \varepsilon_{yz} \\ \varepsilon_{zx} & \varepsilon_{zy} & \varepsilon_{zz} \end{bmatrix} \quad \text{Eq. [15]}$$

Strains are the derivatives of the displacement components, i.e.  $\varepsilon_{ij} = \frac{1}{2} \left( \frac{\partial u_i}{\partial j} + \frac{\partial u_j}{\partial i} \right)$

where  $i$  and  $j$  are either  $x, y$  or  $z$ .

According to the small deformation theory, only the sum of complementing Cartesian shear strain components  $\varepsilon_{ij}$  and  $\varepsilon_{ji}$  result in shear stress. This sum is denoted as the shear strain  $\gamma$ . Hence, instead of  $\varepsilon_{xy}, \varepsilon_{yx}, \varepsilon_{yz}, \varepsilon_{zy}, \varepsilon_{zx}$  and  $\varepsilon_{xz}$  the shear strain components  $\gamma_{xy}, \gamma_{yz}$  and  $\gamma_{zx}$  are used respectively. Under the above conditions, strains are often written in vector notation, which involve only six different components:

$$\boldsymbol{\varepsilon} = (\varepsilon_{xx} \ \varepsilon_{yy} \ \varepsilon_{zz} \ \gamma_{xy} \ \gamma_{yz} \ \gamma_{zx})^T \quad \text{Eq. [16]}$$

$$\varepsilon_{xx} = \frac{\partial}{\partial x} u_x \quad \text{Eq. [17]}$$

$$\varepsilon_{yy} = \frac{\partial}{\partial y} u_y \quad \text{Eq. [18]}$$

## Preliminaries on material modelling

### Elastic strains

---

$$\varepsilon_{zz} = \frac{\partial}{\partial z} u_z \quad \text{Eq. [19]}$$

$$\gamma_{xy} = \varepsilon_{xy} + \varepsilon_{yx} = \frac{\partial}{\partial y} u_x + \frac{\partial}{\partial x} u_y \quad \text{Eq. [20]}$$

$$\gamma_{yz} = \varepsilon_{yz} + \varepsilon_{zy} = \frac{\partial}{\partial z} u_y + \frac{\partial}{\partial y} u_z \quad \text{Eq. [21]}$$

$$\gamma_{zx} = \varepsilon_{zx} + \varepsilon_{xz} = \frac{\partial}{\partial x} u_z + \frac{\partial}{\partial z} u_x \quad \text{Eq. [22]}$$

Similarly as for stresses, positive normal strain components refer to extension, whereas negative normal strain components indicate compression.

In the formulation of material models, where infinitesimal increments of strain are considered, these increments are represented by strain rates (with a dot above the strain symbol). notation

$$\dot{\varepsilon} = (\dot{\varepsilon}_{xx} \dot{\varepsilon}_{yy} \dot{\varepsilon}_{zz} \dot{\gamma}_{xy} \dot{\gamma}_{yz} \dot{\gamma}_{zx})^T \quad \text{Eq. [23]}$$

In analogy to the invariants of stress, it is also useful to define invariants of strain. A strain invariant that is often used is the volumetric strain,  $\varepsilon_v$ , which is defined as the sum of all normal strain components in a standard calculation according to small deformation theory:

$$\varepsilon_v = \varepsilon_{xx} + \varepsilon_{yy} + \varepsilon_{zz} = \varepsilon_1 + \varepsilon_2 + \varepsilon_3 \quad \text{Eq. [24]}$$

In *Updated mesh* calculations the volumetric strain is calculated as:

$$\varepsilon_v = \varepsilon_{xx} + \varepsilon_{yy} + \varepsilon_{zz} + \varepsilon_{xx}\varepsilon_{yy} + \varepsilon_{xx}\varepsilon_{zz} + \varepsilon_{yy}\varepsilon_{zz} + \varepsilon_{xx}\varepsilon_{yy}\varepsilon_{zz} \quad \text{Eq. [25]}$$

The volumetric strain is defined as negative for compaction and as positive for dilatancy.

Another invariant is the deviatoric strain ( $\varepsilon_q$ ), which is calculated as:

$$\varepsilon_q = \sqrt{\frac{2}{9}[(\varepsilon_{xx} - \varepsilon_{yy})^2 + (\varepsilon_{yy} - \varepsilon_{zz})^2 + (\varepsilon_{zz} - \varepsilon_{xx})^2] + \frac{1}{3}(\gamma_{xy}^2 + \gamma_{yz}^2 + \gamma_{zx}^2)} \quad \text{Eq. [26]}$$

For triaxial conditions i.e.  $\varepsilon_2 = \varepsilon_3$  the deviatoric strain, reduces to:

$$\varepsilon_q = \frac{2}{3} | \varepsilon_1 - \varepsilon_3 | \quad \text{Eq. [27]}$$

where  $\varepsilon_1$  and  $\varepsilon_3$  are the major and minor principal strains components respectively. Furthermore, when volumetric strains are negligible ( $\varepsilon_v = 0$ ), then  $\varepsilon_3 = -1/2\varepsilon_1$ , so  $\varepsilon_q = | \varepsilon_1 |$

For elastoplastic models, as used in PLAXIS, strains are decomposed into elastic and plastic components:

$$\varepsilon = \varepsilon^e + \varepsilon^p \quad \text{Eq. [28]}$$

Throughout this manual, the superscript *e* will be used to denote elastic strains and the superscript *p* will be used to denote plastic strains.

## 2.3 Elastic strains

Material models for soil and rock are generally expressed as a relationship between infinitesimal increments of effective stress ('effective stress rates') and infinitesimal increments of strain ('strain rates'). This relationship may be expressed in the form:

## Preliminaries on material modelling

### Elastic strains

$$\dot{\boldsymbol{\sigma}}' = \mathbf{M} \dot{\boldsymbol{\varepsilon}} \quad \text{Eq. [29]}$$

where  $\mathbf{M}$  is a material stiffness matrix. Note that in this type of approach, pore-pressures are explicitly excluded from the stress-strain relationship.

The simplest material model in PLAXIS is based on Hooke's law for isotropic linear elastic behaviour. This model is available under the name Linear Elastic model, but it is also the basis of other models. Hooke's law can be given by the equation:

$$\begin{bmatrix} \dot{\sigma}_{xx}' \\ \dot{\sigma}_{yy}' \\ \dot{\sigma}_{zz}' \\ \dot{\sigma}_{xy}' \\ \dot{\sigma}_{yz}' \\ \dot{\sigma}_{zx}' \end{bmatrix} = \frac{E'}{(1-2\nu')(1+\nu')} \begin{bmatrix} 1-\nu' & \nu' & \nu' & 0 & 0 & 0 \\ \nu' & 1-\nu' & \nu' & 0 & 0 & 0 \\ \nu' & \nu' & 1-\nu' & 0 & 0 & 0 \\ 0 & 0 & 0 & \frac{1}{2}-\nu' & 0 & 0 \\ 0 & 0 & 0 & 0 & \frac{1}{2}-\nu' & 0 \\ 0 & 0 & 0 & 0 & 0 & \frac{1}{2}-\nu' \end{bmatrix} \begin{bmatrix} \dot{\varepsilon}_{xx}' \\ \dot{\varepsilon}_{yy}' \\ \dot{\varepsilon}_{zz}' \\ \dot{\varepsilon}_{xy}' \\ \dot{\varepsilon}_{yz}' \\ \dot{\varepsilon}_{zx}' \end{bmatrix} \quad \text{Eq. [30]}$$

The elastic material stiffness matrix is often denoted as  $\mathbf{D}^e$ . Two parameters are used in this model, the effective Young's modulus,  $E'$ , and the effective Poisson's ratio,  $\nu'$ . In the remaining part of this manual effective parameters are denoted without dash ('), unless a different meaning is explicitly stated. The symbols  $E$  and  $\nu$  are sometimes used in this manual in combination with the subscript *ur* to emphasize that the parameter is explicitly meant for unloading and reloading. A stiffness modulus may also be indicated with the subscript *ref* to emphasize that it refers to a particular reference level ( $y_{ref}$ )

According to Hooke's law, the relationship between Young's modulus  $E$  and other stiffness moduli, such as the shear modulus  $G$ , the bulk modulus  $K$ , and the oedometer modulus  $E_{oed}$ , is given by:

$$\begin{aligned} G &= \frac{E}{2(1+\nu)} & a) \\ K &= \frac{E}{3(1-2\nu)} & b) \\ E_{oed} &= \frac{(1-\nu)E}{(1-2\nu)(1+\nu)} & c) \end{aligned} \quad \text{Eq. [31]}$$

Using these auxiliary stiffness parameters, Hooke's law can be presented in an alternative form as:

$$\begin{bmatrix} \dot{p} \\ \dot{q} \end{bmatrix} = \begin{bmatrix} K & 0 \\ 0 & 3G \end{bmatrix} \begin{bmatrix} \dot{\varepsilon}_v \\ \dot{\varepsilon}_q \end{bmatrix} \quad \text{Eq. [32]}$$

During the input of material parameters for the Linear Elastic model or the Mohr-Coulomb model the values of  $G$  and  $E_{oed}$  are presented as auxiliary parameters (alternatives), calculated from Eq. [31]. Note that the alternatives are influenced by the input values of  $E$  and  $\nu$ . Entering a particular value for one of the alternatives  $G$  or  $E_{oed}$  results in a change of the  $E$  modulus, while  $\nu$  remains the same.

It is possible for the Linear Elastic model and the Mohr-Coulomb model to specify a stiffness that varies linearly with depth. This can be done by entering a value for  $E_{inc}$  which is the increment of stiffness per unit of depth, as indicated in Eq. [33]

Together with the input of  $E_{inc}$  the input of  $y_{ref}$  becomes relevant. Above  $y_{ref}$  the stiffness is equal to  $E_{ref}$ . Below the stiffness is given by:

$$E(y) = E_{ref} + (y_{ref} - y)E_{inc} \quad y < y_{ref} \quad \text{Eq. [33]}$$

## Preliminaries on material modelling

### Undrained effective stress analysis (effective stiffness parameters)

#### Note:

The Linear Elastic model is usually inappropriate to model the highly non-linear behaviour of soil, but it is of interest to simulate structural behaviour, such as thick concrete walls or plates, for which strength properties are usually very high compared with those of soil. For these applications, the Linear Elastic model will often be selected together with *Non-porous* drainage type in order to exclude pore pressures from these structural elements.

## 2.4 Undrained effective stress analysis (effective stiffness parameters)

In PLAXIS it is possible to specify undrained behaviour in an effective stress analysis using effective model parameters. This is achieved by identifying the type of material behaviour (*Drainage type*) of a soil layer as *Undrained A* or *Undrained B* ([Undrained effective stress analysis with effective strength parameters \(Undrained A\)](#) (on page 24) and [Undrained effective stress analysis with undrained strength parameters \(Undrained B\)](#) (on page 25)). In this section, it is explained how PLAXIS deals with this special option.

The presence of pore pressures in a soil body, usually caused by water, contributes to the total stress level. According to Terzaghi's principle, total stresses vector notation  $\sigma$  can be divided into effective stresses  $\sigma'$ , active pore pressure  $p_{active}$  and pore water pressures  $p_w$  (see also Eq. [3]). However, water is supposed not to sustain any shear stress, and therefore the effective shear stresses are equal to the total shear stresses:

$$\sigma = \sigma' + m p_{active} \quad \text{Eq. [34]}$$

where,

$$m = \begin{bmatrix} 1 \\ 1 \\ 1 \\ 0 \\ 0 \\ 0 \end{bmatrix} \text{ and } p_{active} = \alpha_{Biot} S_{eff} p_w \quad \text{Eq. [35]}$$

$$\sigma_{xx} = \sigma'_{xx} + \alpha_{Biot} S_{eff} p_w \quad \text{Eq. [36]}$$

$$\sigma_{yy} = \sigma'_{yy} + \alpha_{Biot} S_{eff} p_w \quad \text{Eq. [37]}$$

$$\sigma_{zz} = \sigma'_{zz} + \alpha_{Biot} S_{eff} p_w \quad \text{Eq. [38]}$$

$$\sigma_{xy} = \sigma'_{xy}$$

$$\sigma_{yz} = \sigma'_{yz} \quad \text{Eq. [39]}$$

$$\sigma_{zx} = \sigma'_{zx}$$

where

$$\begin{array}{ll} \alpha_{Biot} & = \text{Biot's pore pressure coefficient.} \\ S_{eff} & = \text{Effective degree of saturation.} \end{array}$$

## Preliminaries on material modelling

### Undrained effective stress analysis (effective stiffness parameters)

Considering incompressible grains, Biot's coefficient  $\alpha_{Biot}$  is equal to unity ( $\alpha_{Biot} = 1$ ). The situation of compressible grains or compressible solid material ( $\alpha_{Biot} < 1$ ) is explained in more detail at the end of this section.

Note that, similar to the total and the effective stress components,  $p_w$  is considered negative for pressure.

The product  $\alpha_{Biot} S_{eff} p_w$  is termed 'Active pore pressure',  $p_{active}$  in PLAXIS. A further distinction is made between steady state pore stress,  $p_{steady}$ , and excess pore stress,  $p_{excess}$ :

$$p_w = p_{steady} + p_{excess} \quad Eq. [40]$$

Steady state pore pressures are considered to be input data, i.e. generated on the basis of phreatic levels or by means of a groundwater flow calculation. Excess pore pressures are generated during plastic calculations for the case of undrained A or B material behaviour or during a consolidation analysis. Undrained material behaviour and the corresponding calculation of excess pore pressures are described below.

Since the time derivative of the steady state component equals zero, it follows:

$$\dot{p}_w = \dot{p}_{excess} \quad Eq. [41]$$

Hooke's law can be inverted to obtain:

$$\begin{bmatrix} \dot{\epsilon}_{xx}^e \\ \dot{\epsilon}_{yy}^e \\ \dot{\epsilon}_{zz}^e \\ \dot{\gamma}_{xy}^e \\ \dot{\gamma}_{yz}^e \\ \dot{\gamma}_{zx}^e \end{bmatrix} = \frac{1}{E'} \begin{bmatrix} 1 & -\nu' & -\nu' & 0 & 0 & 0 \\ -\nu' & 1 & -\nu' & 0 & 0 & 0 \\ -\nu' & -\nu' & 1 & 0 & 0 & 0 \\ 0 & 0 & 0 & 2+2\nu' & 0 & 0 \\ 0 & 0 & 0 & 0 & 2+2\nu' & 0 \\ 0 & 0 & 0 & 0 & 0 & 2+2\nu' \end{bmatrix} \begin{bmatrix} \dot{\sigma}_{xx}' \\ \dot{\sigma}_{yy}' \\ \dot{\sigma}_{zz}' \\ \dot{\sigma}_{xy}' \\ \dot{\sigma}_{yz}' \\ \dot{\sigma}_{zx}' \end{bmatrix} \quad Eq. [42]$$

Substituting Eq. [39] gives:

$$\begin{bmatrix} \dot{\epsilon}_{xx}^e \\ \dot{\epsilon}_{yy}^e \\ \dot{\epsilon}_{zz}^e \\ \dot{\gamma}_{xy}^e \\ \dot{\gamma}_{yz}^e \\ \dot{\gamma}_{zx}^e \end{bmatrix} = \frac{1}{E'} \begin{bmatrix} 1 & -\nu' & -\nu' & 0 & 0 & 0 \\ -\nu' & 1 & -\nu' & 0 & 0 & 0 \\ -\nu' & -\nu' & 1 & 0 & 0 & 0 \\ 0 & 0 & 0 & 2+2\nu' & 0 & 0 \\ 0 & 0 & 0 & 0 & 2+2\nu' & 0 \\ 0 & 0 & 0 & 0 & 0 & 2+2\nu' \end{bmatrix} \begin{bmatrix} \dot{\sigma}_{xx}' - \alpha_{Biot} \dot{p}_w \\ \dot{\sigma}_{yy}' - \alpha_{Biot} \dot{p}_w \\ \dot{\sigma}_{zz}' - \alpha_{Biot} \dot{p}_w \\ \dot{\sigma}_{xy}' \\ \dot{\sigma}_{yz}' \\ \dot{\sigma}_{zx}' \end{bmatrix} \quad Eq. [43]$$

Considering slightly compressible water, the rate of excess pore pressure is written as:

$$\dot{p}_{excess} = \frac{a_{biot} \dot{\epsilon}_v}{nC_w + (a_{biot} - n)C_s} \quad Eq. [44]$$

$$C_w = \frac{1}{k_w} \quad Eq. [45]$$

$$C_s = \frac{1}{k_s} \quad Eq. [46]$$

## Preliminaries on material modelling

### Undrained effective stress analysis (effective stiffness parameters)

in which  $K_w$  is the bulk modulus of the water,  $K_s$  is the bulk modulus of the solid material,  $C_w$  is the compressibility of the water,  $C_s$  is the compressibility of the solid material and  $n$  is the soil porosity.

$$n = \frac{e_0}{1 + e_0} \quad \text{Eq. [47]}$$

where  $e_0$  is the initial void ratio as specified in the general soil properties.

The inverted form of Hooke's law may be written in terms of the total stress rates and the undrained parameters  $E_u$  and  $v_u$ :

$$\begin{bmatrix} \dot{\varepsilon}_{xx}^e \\ \dot{\varepsilon}_{yy}^e \\ \dot{\varepsilon}_{zz}^e \\ \dot{\gamma}_{xy}^e \\ \dot{\gamma}_{yz}^e \\ \dot{\gamma}_{zx}^e \end{bmatrix} = \frac{1}{E_u} \begin{bmatrix} 1 & -v_u & -v_u & 0 & 0 & 0 \\ -v_u & 1 & -v_u & 0 & 0 & 0 \\ -v_u & -v_u & 1 & 0 & 0 & 0 \\ 0 & 0 & 0 & 2+2v_u & 0 & 0 \\ 0 & 0 & 0 & 0 & 2+2v_u & 0 \\ 0 & 0 & 0 & 0 & 0 & 2+2v_u \end{bmatrix} \begin{bmatrix} \dot{\sigma}_{xx}' \\ \dot{\sigma}_{yy}' \\ \dot{\sigma}_{zz}' \\ \dot{\sigma}_{xy}' \\ \dot{\sigma}_{yz}' \\ \dot{\sigma}_{zx}' \end{bmatrix} \quad \text{Eq. [48]}$$

where:

$$\begin{aligned} E_u &= 2G(1 + v_u); \\ v_u &= \frac{3v' + \alpha_{Biot} B(1 - 2v')}{3 - \alpha_{Biot} B(1 - 2v')} \\ B &= \frac{\alpha_{Biot}}{\alpha_{Biot} + n \left( \frac{K'}{K_w} + \alpha_{Biot} - 1 \right)} \end{aligned} \quad \text{Eq. [49]}$$

where  $B$  is Skempton's B-parameter.

Hence, the special option for undrained behaviour in PLAXIS (*Undrained A* or *Undrained B*) is such that the effective parameters  $G$  and  $v'$  are transformed into undrained parameters  $E_u$  and  $v_u$  according to Eq. [49]. Note that the index  $u$  is used to indicate auxiliary parameters for undrained soil. Hence,  $E_u$  and  $v_u$  should not be confused with  $E_{ur}$  and  $v_{ur}$  as used to denote unloading / reloading.

Fully incompressible behaviour is obtained for  $v_u = 0.5$ . However, taking  $v_u = 0.5$  leads to singularity of the stiffness matrix. In fact, water is not fully incompressible, but a realistic bulk modulus for water is very large. In order to avoid numerical problems caused by an extremely low compressibility,  $v_u$  is, by default, taken as 0.495, which makes the undrained soil body slightly compressible. In order to ensure realistic computational results, the bulk modulus of the water must be high compared with the bulk modulus of the soil skeleton, i.e.  $K_w \gg n K'$ . This condition is sufficiently ensured by requiring  $v' \leq 0.35$ .

Consequently, for material behaviour *Undrained A* or *Undrained B*, a bulk modulus for water is automatically added to the stiffness matrix. The bulk modulus of water is obtained in three ways: automatically from Eq. [50] (*v-undrained definition - Direct*), automatically but by specifying the Skempton's B-parameter (*v-undrained definition - Skempton B based*) and manually by directly specifying  $K_w$  and  $\alpha_{Biot}$  (*Biot effective stress concept*).

$$\frac{K_w}{n} = \frac{3(v_u - v')}{(1 - 2v_u)(1 + v')} \quad K' = \frac{0.495 - v'}{1 + v'} 300K' \geq 30K' \quad (\text{For } \alpha_{Biot} = 1) \quad \text{Eq. [50]}$$

## Preliminaries on material modelling

### Undrained effective stress analysis (effective stiffness parameters)

**Note:** In the UBC3D-PLM model, the implicit Poisson's ratio ( $\nu'$ ) is defined based on the elastic bulk modulus  $K$  and the elastic shear modulus  $G$  at the current stress state,  $\nu' = (3K - 2G)/(6K + 2G)$ . For this reason, the value follows the evolution of the stiffnesses and it is not constant.

Hence,  $K_w/n$  is larger than  $30K'$ , at least for  $\nu' \leq 0.35$  and  $\alpha_{Biot} = 1$ . The bulk stiffness of water  $K_w$ , calculated in this way, is a numerical value related to the soil stiffness. It is lower than or equal to the real bulk stiffness of pure water,  $K_w^0$  ( $2 \cdot 10^6$  kN/m<sup>2</sup>). In retrospect it is worth mentioning here a review about the Skempton B-parameter.

#### 2.4.1 Skempton B-parameter

When the *Drainage type* is set to *Undrained A* or *Undrained B*, PLAXIS automatically assumes an implicit undrained bulk modulus,  $K_u$ , for the soil as a whole (soil skeleton + water) and distinguishes between total stress rates, effective stress rates and rates of excess pore pressure:

$$\text{Total stress :} \quad \dot{p} = K_u \dot{\varepsilon}_v \quad \text{Eq. [51]}$$

$$\text{Excess pore pressure :} \quad \dot{p}_{excess} = B \dot{p} = \frac{\alpha_{biot} \dot{\varepsilon}_v}{nC_w + (\alpha_{biot} - n)C_s} \quad \text{Eq. [52]}$$

$$\text{Effective stress :} \quad \dot{p}' = (1 - \alpha_{Biot} B) \dot{p} = K' \dot{\varepsilon}_v \quad \text{Eq. [53]}$$

Note that for *Undrained A* or *Undrained B* effective stiffness parameters should be entered in the material data set, i.e.  $E'$  and  $\nu'$  and not  $E_u$  and  $\nu_u$ , or the respective stiffness parameters in advanced models; the latter should be done for *Undrained C* behaviour in a total stress analysis ([Undrained total stress analysis with undrained parameters \(Undrained C\)](#) (on page 26)). The undrained bulk modulus is automatically calculated by PLAXIS using Hooke's law of elasticity:

$$K_u = \frac{2G(1 + \nu_u)}{3(1 - 2\nu_u)} \quad \text{where} \quad G = \frac{E'}{2(1 + \nu')} \quad \text{Eq. [54]}$$

When using the  *$\nu$ -undrained* option with suboption *Direct*, by default  $\nu_u = 0.495$  (but can be changed) and  $\alpha_{Biot} = 1$ , whereas when using the  *$\nu$ -undrained* option with suboption *Skempton B based* with input of Skempton's B-parameter or the option *Biot effective stress concept*,  $\nu_u$  is calculated as:

$$\nu_u = \frac{3\nu' + \alpha_{Biot} B(1 - 2\nu')}{3 - \alpha_{Biot} B(1 - 2\nu')} \quad \text{Eq. [55]}$$

If the soil is only partially saturated, the pores contain both air and water and the equivalent bulk modulus of the pore fluid  $K_w^{unsat}$  is expected to be much smaller compared to that of pure water, in the case of fully saturated soil  $K_w$ . PLAXIS assumes a constant gas pressure i.e. air is always drained, the drainage type of soil only relates to the drainage type of liquid water. Excess pore pressure change will therefore depend on the bulk modulus of liquid water and the surface tension (capillary effect). This assumption allows to establish the following rigorous relationship for the unsaturated bulk modulus of the pore fluid:

$$K_w^{unsat} = \frac{K_w}{1 + \frac{K_w}{S_w} \left( -\frac{\partial S_w}{\partial p_w} \right)} \quad \text{Eq. [56]}$$

where is the derivative of saturation w.r.t. pore water pressure (suction), i.e. the slope of water retention curve

## Preliminaries on material modelling

### Undrained effective stress analysis (effective stiffness parameters)

The value of Skempton's B-parameter is calculated from the ratio of the bulk stiffnesses of the soil skeleton and the pore fluid, as already defined in Eq. [50]:

$$B = \frac{\alpha_{Biot}}{\alpha_{Biot} + n \left( \frac{K'}{K_w} + \alpha_{Biot} - 1 \right)} \quad Eq. [57]$$

The rate of excess pore pressure is calculated from the (small) volumetric strain rate, according to:

$$\dot{p}_{excess} = \frac{\alpha_{Biot} \dot{\epsilon}_v}{n C_w + (\alpha_{Biot} - n) C_s} \quad Eq. [58]$$

The types of elements used in PLAXIS are sufficiently adequate to avoid mesh locking effects for nearly incompressible materials.

This special option to model undrained material behaviour on the basis of effective model parameters is available for most material models in PLAXIS. This enables undrained calculations to be executed with effective stiffness parameters, with explicit distinction between effective stresses and (excess) pore pressures. However, shear induced (excess) pore pressure may not be sufficiently included.

Such an analysis requires effective soil parameters and is therefore highly convenient when such parameters are available. For soft soil projects, accurate data on effective parameters may not always be available. Instead, in situ tests and laboratory tests may have been performed to obtain undrained soil parameters. In such situations measured undrained Young's moduli can be easily converted into effective Young's moduli based on Hooke's law:

$$E' = \frac{2(1 + \nu')}{3} E_u \quad Eq. [59]$$

For advanced models there is no such direct conversion possible. In that case it is recommended to estimate the required effective stiffness parameter from the measured undrained stiffness parameter, then perform a simple undrained test to check the resulting undrained stiffness and adapt the effective stiffness if needed. The *Soil test* facility (Reference Manual) may be used as a convenient tool to perform such test.

### 2.4.2 Biot pore pressure coefficient $\alpha_{Biot}$ [ULT]

In general, for geotechnical applications, the compressibility of the soil skeleton is much higher than the compressibility of the individual grains, so deformations of the grains themselves can be ignored. However, in the case of very deep soil layers at very high pressures, the stiffness of the soil or rock matrix comes close to the stiffness of the solid material of which the soil grains or the rock is composed of, and, therefore, the compressibility of the solid material cannot be ignored. This has consequences for the division of total stress into effective stress and pore pressure. Considering compressible solid material, Terzaghi's effective stress definition changes into:

$$\sigma' = \sigma - \alpha_{biot} S_{eff} \underline{m} p_w \quad Eq. [60]$$

Where  $\alpha_{Biot}$  is Biot's pore pressure coefficient,  $S_{eff}$  is the effective degree of saturation,  $\underline{m}$  is a vector with unity values (1) for the normal components and 0-values for the shear components, and  $p_w$  is the pore water pressure. The alpha coefficient is defined as:

$$\alpha_{biot} = 1 - \frac{K'}{K_s} \quad Eq. [61]$$

## Preliminaries on material modelling

### Undrained effective stress analysis with effective strength parameters (*Undrained A*)

---

Where  $K'$  is the effective bulk modulus of the soil matrix and  $K_s$  is the bulk modulus of the solid material. Indeed, for incompressible solid material ( $K_s = \infty$ ) Terzaghi's original stress definition is retained. A lower value of  $\alpha_{Biot}$  implies that for a given value of total stress and pore water pressure, the resulting effective stress is higher than when considering incompressible solid material ( $\alpha_{Biot} = 1$ ).

In the case of undrained soil behaviour (*Undrained A* or *B* in PLAXIS 3D), Biot's pore pressure coefficient also affects the undrained Poisson's ratio  $\nu_u$  that is automatically calculated by PLAXIS 3D based on a manual input of  $K_w$  parameter (see Eq. Eq. [49]).

The default value of Biot's pore pressure coefficient is 1.0 (*v-undrained definition* option), but users may change this value in the range of [0.001, 1.0] for the *Biot effective stress concept* option.

## 2.5 Undrained effective stress analysis with effective strength parameters (*Undrained A*)

In principle, undrained effective stress analysis as described in [Undrained effective stress analysis \(effective stiffness parameters\)](#) (on page 19) can be used in combination with effective strength parameters  $\phi'$  and  $c'$  to model the material's undrained shear strength (*Undrained A*). In this case, the development of the pore pressure plays a crucial role in providing the right effective stress path that leads to failure at a realistic value of undrained shear strength ( $c_u$  or  $s_u$ ). However, note that most soil models are not capable of providing the right effective stress path in undrained loading. As a result, they will produce the wrong undrained shear strength if the material strength has been specified on the basis of effective strength parameters. Another problem is that for undrained materials effective strength parameters are usually not available from soil investigation data. In order to overcome these problems, some models allow for a direct input of undrained shear strength. This approach is described in [Undrained effective stress analysis with undrained strength parameters \(Undrained B\)](#) (on page 25).

If the user wants to model the material strength of undrained materials using the effective strength parameters  $\phi'$  and  $c'$ , this can be done in PLAXIS in the same way as for drained materials. However, in this case the *Drainage type* must be set to *Undrained A*. As a result, PLAXIS will automatically add the stiffness of water to the stiffness matrix (see [Undrained effective stress analysis \(effective stiffness parameters\)](#) (on page 19)) in order to distinguish between effective stresses and (excess) pore pressures (= effective stress analysis). The advantage of using effective strength parameters in undrained loading conditions is that after consolidation a qualitatively increased shear strength is obtained, although this increased shear strength could also be quantitatively wrong, for the same reason as explained before.

## Preliminaries on material modelling

Undrained effective stress analysis with undrained strength parameters (*Undrained B*)

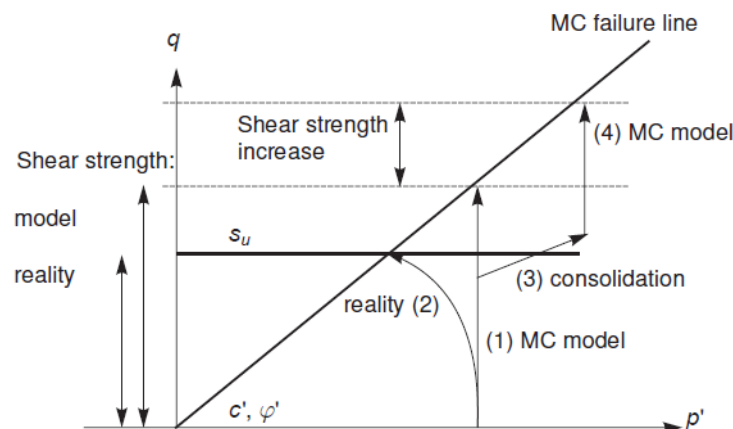


Figure 3: Illustration of stress paths; reality vs Mohr-Coulomb model

[Undrained effective stress analysis \(effective stiffness parameters\)](#) (on page 19) illustrates an example using the Mohr-Coulomb model. When the *Drainage type* is set to *Undrained A*, the model will follow an effective stress path where the mean effective stress,  $p'$ , remains constant all the way up to failure (1). It is known that especially soft soils, like normally consolidated clays and peat, will follow an effective stress path in undrained loading where  $p'$  reduces significantly as a result of shear induced pore pressure (2). As a result, the maximum deviatoric stress that can be reached in the model is over-estimated in the Mohr-Coulomb model. In other words, the mobilised shear strength in the model supersedes the available undrained shear strength.

If, at some stress state, the soil is consolidated, the mean effective stress will increase (3). Upon further undrained loading with the Mohr-Coulomb model, the observed shear strength will be increased (4) compared to the previous shear strength, but this increased shear strength may again be unrealistic, especially for soft soils.

On the other hand, advanced models do include, to some extent, the reduction of mean effective stress in undrained loading, but even when using advanced models it is generally advised to check the mobilised shear strength in the Output program against the available (undrained) shear strength when this approach is followed.

Note that whenever the *Drainage type* parameter is set to *Undrained A*, effective values must be entered for the stiffness parameters (Young's modulus  $E'$  and Poisson ratio  $\nu'$  in case of the Mohr-Coulomb model or the respective stiffness parameters in the advanced models).

Care must be taken when using *Undrained A* together with a non-zero dilatancy angle  $\psi$ . The use of a positive dilatancy angle may lead to unrealistically large tensile pore stresses and, as a result, an unrealistically large shear strength. The use of a negative dilatancy angle may lead to unrealistically high pore pressure and unrealistic liquefaction type of behaviour. Hence, for *Undrained A* it is recommended to use  $\psi = 0$ .

## 2.6 Undrained effective stress analysis with undrained strength parameters (*Undrained B*)

For undrained soil layers with a known undrained shear strength profile, PLAXIS offers for some models the possibility of an undrained effective stress analysis, as described in [Undrained effective stress analysis \(effective stiffness parameters\)](#) (on page 19), with direct input of the undrained shear strength, i.e. setting the friction

## Preliminaries on material modelling

### Undrained total stress analysis with undrained parameters (*Undrained C*)

angle to zero and the cohesion equal to the undrained shear strength ( $\varphi = \varphi_u = 0^\circ$ ;  $c = s_u$ ) (*Drainage type = Undrained B*). Also in this case, distinction is made between pore pressures and effective stresses. Although the pore pressures and effective stress path may not be fully correct, the resulting undrained shear strength is not affected, since it is directly specified as an input parameter.

The option to perform an undrained effective stress analysis with undrained strength properties is only available for the Mohr-Coulomb model, the Hardening Soil model, the Hardening Soil model with small-strain stiffness and the NGI-ADP model. Since most soils show an increasing shear strength with depth, it is possible to specify the increase per unit of depth in PLAXIS in the **Stress dependency** blocks on the **Mechanical** tabsheet of the **Soil** window.

Note that if the Hardening Soil model or the Hardening Soil model with small-strain stiffness is used with  $\varphi = 0^\circ$ , the stiffness moduli in the model are no longer stress-dependent and the model exhibits no compression hardening, although the model retains its separate unloading-reloading modulus and shear hardening. Also note that a direct input of undrained shear strength does not automatically give the increase of shear strength with consolidation.

Further note that whenever the *Drainage type* parameter is set to *Undrained B*, effective values must be entered for the stiffness parameters (Young's modulus  $E'$  and Poisson ratio  $\nu'$  in case of the Mohr-Coulomb model or the respective stiffness parameters in the advanced models).

## 2.7 Undrained total stress analysis with undrained parameters (*Undrained C*)

If, for any reason, it is desired not to use the *Undrained A* or *Undrained B* options in PLAXIS to perform an undrained effective stress analysis, one may simulate undrained behaviour using a conventional total stress analysis with all parameters specified as undrained. In that case, stiffness is modelled using an undrained Young's modulus  $E_u$  and an undrained Poisson ratio  $\nu_u$ , and strength is modelled using an undrained shear strength  $s_u$  and  $\varphi = \varphi_u = 0^\circ$ . Typically, for the undrained Poisson ratio a value close to 0.5 is selected (between 0.495 and 0.499). A value of 0.5 exactly is not possible, since this would lead to singularity of the stiffness matrix.

In PLAXIS it is possible to perform a total stress analysis with undrained parameters if the Mohr-Coulomb model or the NGI-ADP model is used. In this case, one should select *Undrained C* as the *Drainage type*. The disadvantage of the undrained total stress analysis is that no distinction is made between effective stresses and pore pressures. Hence, all output referring to effective stresses should now be interpreted as total stresses and all pore pressures are equal to zero.

Note that a direct input of undrained shear strength does not automatically give the increase of shear strength with consolidation. In fact, it does not make sense to perform a consolidation analysis since there are no pore pressures to consolidate. Also note that the  $K_0$ -value to generate initial stresses refers to total stresses rather than effective stresses in this case. This type of approach is not possible for most advanced models.

### 2.7.1 Overview of models and allowable drainage types

Material model	Drainage type
Linear Elastic model	Drained, Undrained A, Undrained C, Non-porous

## Preliminaries on material modelling

The initial pre-consolidation stress in advanced models

Material model	Drainage type
Mohr-Coulomb model	Drained, Undrained A, Undrained B, Undrained C, Non-porous
Hardening Soil model	Drained, Undrained A, Undrained B
Hardening Soil model with small-strain stiffness	Drained, Undrained A, Undrained B
UBC3D-PLM model	Drained, Undrained A
Soft Soil model	Drained, Undrained A
Soft Soil Creep model	Drained, Undrained A
Jointed Rock model	Drained, Non-porous
Modified Cam-Clay model	Drained, Undrained A
NGI-ADP model	Drained, Undrained C
UDCAM-S model	Undrained C
Hoek-Brown model	Drained, Non-porous
Sekiguchi-Ohta model	Drained, Undrained A
Concrete model	Drained, Non-porous
User-defined soil models	Drained, Undrained A, Non-porous

## 2.8 The initial pre-consolidation stress in advanced models

When using advanced models in PLAXIS an initial pre-consolidation stress has to be determined. In the engineering practice it is common to use a vertical pre-consolidation stress,  $\sigma_p$ , but PLAXIS needs an equivalent isotropic pre-consolidation stress,  $p_p^{eq}$  to determine the initial position of a cap-type yield surface. If a material is overconsolidated, information is required about the overconsolidation Ratio (OCR), i.e. the ratio of the greatest effective vertical stress previously reached,  $\sigma_p$  (see [Figure 4](#) (on page 28)), and the in-situ effective vertical stress,  $\sigma'_{yy}{}^0$  (note that in PLAXIS 3D the vertical (effective) stress is  $\sigma'_{zz}{}^0$ ).

$$OCR = \frac{\sigma_p}{\sigma'_{yy}{}^0} \quad Eq. [62]$$

The two ways of specifying the vertical pre-consolidation stress are illustrated in [Figure 4](#) (on page 28).

## Preliminaries on material modelling

The initial pre-consolidation stress in advanced models

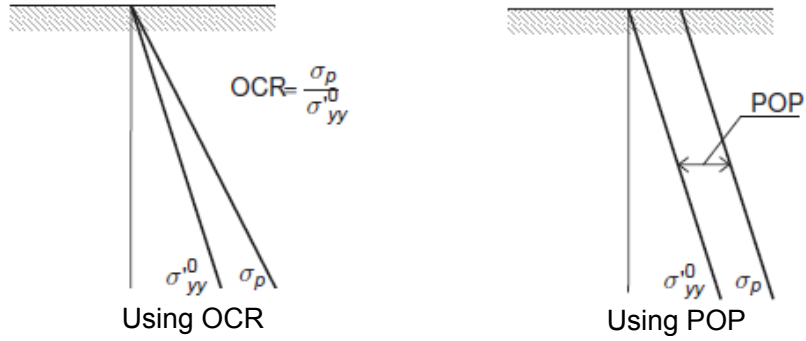


Figure 4: Illustration of vertical pre-consolidation stress in relation to the in-situ vertical stress

It is also possible to specify the initial stress state using the Pre-Overburden Pressure (POP) as an alternative to prescribing the overconsolidation ratio. The Pre-Overburden Pressure is defined by:

$$POP = \left| \sigma_p - \sigma_{yy}^0 \right| \quad \text{Eq. [63]}$$

The pre-consolidation stress  $\sigma_p$  is used to compute the equivalent pre-consolidation pressure  $p_p^{eq}$  which determines the initial position of a cap-type yield surface in the advanced soil models. The calculation of  $p_p^{eq}$  is based on the principal stress history  $(\sigma'_{1,max}, \sigma'_2, \sigma'_3)$ . The actual determination of  $p_p^{eq}$  depends on the constitutive model being used. The principal stress history is initialised in the *Initial phase (K0-procedure or Gravity loading)* based on the *Cartesian effective stress* components and the *pre-overburden pressure (POP)* or *overconsolidation ratio (OCR)* defined in the boreholes or data set. From this, Cartesian pre-consolidation stress levels are calculated based on the following equations:

$$\begin{aligned} \sigma'_{xx,c} &= K_0^{nc} OCR \sigma'_{yy} \\ \sigma'_{xx,c} &= OCR \sigma'_{yy} \\ \sigma'_{zz,c} &= K_0^{nc} OCR \sigma'_{yy} \\ \sigma_{xy,c} &= \sigma_{xy} \end{aligned} \quad \text{Eq. [64]}$$

where

$$K_0^{nc} = K_0\text{-value associated with normally consolidated states of stress.}$$

### Note:

- $K_0^{nc}$  is a model parameter in advanced constitutive models and estimated in simple models ( $K_0^{nc} = 1 - \sin \varphi$ ).
- Models that do not have  $\varphi$  as input parameter use  $K_0^{nc} = 0.5$  ( $\varphi = 30^\circ$ ).

For the Modified Cam-Clay model,  $K_0^{nc}$  is automatically determined based on the parameter  $M$  as entered by the user. The exact relationship between  $M$  and  $K_0^{nc}$  can be formulated as (Bringreave, 1994) (on page 246):

$$M = 3 \sqrt{\frac{(1 - K_0^{nc})^2}{(1 + 2K_0^{nc})^2} + \frac{(1 - K_0^{nc})(1 - 2v_{ur})(\lambda^*/k^* - 1)}{(1 + 2K_0^{nc})(1 - 2v_{ur})\lambda^*/k^* - (1 - K_0^{nc})(1 + v_{ur})}} \quad \text{Eq. [65]}$$

For more details see [Modified Cam-Clay model](#) (on page 95).

The Cartesian stress components  $(\sigma'_{xx,c}, \sigma'_{yy,c}, \sigma'_{zz,c}, \sigma'_{xy,c})$  are transformed to principal stress components  $(\sigma'_{1,max}, \sigma'_2, \sigma'_3)$  and the maximum major principal stress,  $\sigma'_{1,max}$  is kept as a general state parameter which is

## Preliminaries on material modelling

### On the initial stresses

available for succeeding phases. In subsequent phases,  $\sigma'_{1,max}$  is updated if the major principal stress is larger than the current one.

If, in later calculation phases, the soil behaviour is changed to an(other) advanced material model, the equivalent pre-consolidation pressure  $p_p^{eq}$  is initialised according to the current (updated) principal stress history ( $\sigma'_{1,max}$ ,  $\sigma'_2$ ,  $\sigma'_3$ ).

The stress state at pre-consolidation stress level is expressed in (p, q):

$$p' = -\frac{1}{3}(1 + 2K_0^{nc})\sigma_p \quad \text{and} \quad q = (1 - K_0^{nc})\sigma_p \quad Eq. [66]$$

The equivalent isotropic pre-consolidation stress is calculated depending on the model used.

Note that *OCR* and *POP* are only taken into account in the  $K_0$ -procedure (initial calculation phase). Gravity loading does not consider *OCR* or *POP*, and always gives a normally-consolidated stress state. If an advanced soil model (involving pre-consolidation stress) is activated in a later calculation phase, i.e.

- The corresponding soil cluster is activated for the first time, or
- The material data of a soil is changed from a 'simple' soil model without pre-consolidation stress to an 'advanced' soil model with the pre-consolidation stress as a state parameter

then the stress state at the beginning of that phase is assumed to be normally-consolidated, i.e. the pre-consolidation stress is initiated in accordance with the current stress state. If, in such a case, an overconsolidated stress state is to be modelled, the overconsolidation has to be simulated by applying and removing an overburden load.

## 2.9 On the initial stresses

In overconsolidated soils the coefficient of lateral earth pressure for the initial stress state is larger than for normally consolidated soils. This effect is automatically taken into account for advanced soil models when generating the initial stresses using the  $K_0$ -procedure. The procedure that is followed here is described below. The procedure is described for the lateral stress in x-direction ( $\sigma'_{xx}$  based on  $K_{0,x}$ ), but a similar procedure is followed for the lateral stress in z-direction ( $\sigma'_{zz}$  based on  $K_{0,z}$ ).

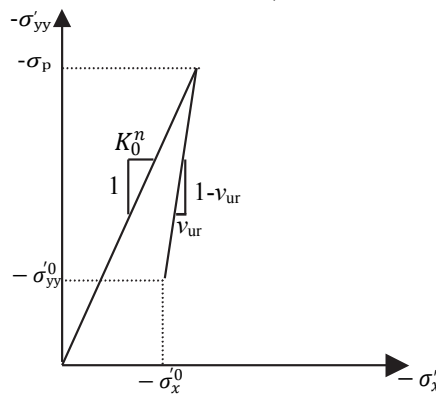


Figure 5: Overconsolidated stress state obtained from primary loading and subsequent unloading

Consider a one-dimensional compression test, preloaded to  $\sigma'_{yy} = \sigma_p$  and subsequently unloaded to  $\sigma'_{yy} = \sigma'_{yy}^0$ . During unloading the sample behaves elastically and the incremental stress ratio is, according to Hooke's law, given by (see [Figure 5](#) (on page 29)):

## Preliminaries on material modelling

### On the initial stresses

---

$$\frac{\Delta \sigma'_{xx}}{\Delta \sigma'_{yy}} = \frac{K_0^{nc} \sigma_p - \sigma'_{xx}}{\sigma_p - \sigma'_{yy}} = \frac{K_0^{nc} OCR \sigma'_{yy} - \sigma'_{xx}}{(OCR - 1) \sigma'_{yy}} = \frac{v_{ur}}{1 - v_{ur}} \quad Eq. [67]$$

where  $K_0^{nc}$  is the stress ratio in the normally consolidated state. Hence, the default stress ratio of the overconsolidated soil sample is given by:

$$K_{0,x} = \frac{\sigma'_{xx}}{\sigma'_{yy}} = K_0^{nc} OCR - \frac{v_{ur}}{1 - v_{ur}} (OCR - 1) \quad Eq. [68]$$

When using POP as an alternative way to define overconsolidation, the default initial horizontal stress is defined by:

$$\sigma'_{xx} = K_0^{nc} \sigma_p - \frac{v_{ur}}{1 - v_{ur}} POP \quad Eq. [69]$$

The use of a small Poisson's ratio will lead to a relatively large ratio of lateral stress and vertical stress, as generally observed in overconsolidated soils. Note that Eq. [68] and Eq. [69] are only valid in the elastic domain, because the formulas are derived from Hooke's law of elasticity. If a soil sample is unloaded by a large amount, resulting in a high degree of overconsolidation, the stress ratio will be limited by the Mohr-Coulomb failure condition.

Note that the above initial stress ratio's are only suggested (default) values, and may be overruled by the user if more precise data are available or if other values seem more appropriate.

## Linear Elastic Perfectly Plastic Model (Mohr-Coulomb Model)

Soils behave rather non-linear when subjected to changes of stress or strain. In reality, the stiffness of soil depends at least on the stress level, the stress path and the strain level. Some such features are included in the advanced soil models in PLAXIS. The Mohr-Coulomb model, however, is a simple and well-known linear elastic perfectly plastic model, which can be used as a first approximation of soil behaviour. The linear elastic part of the Mohr-Coulomb model is based on Hooke's law of isotropic elasticity ([Linear Elastic Perfectly - Plastic behaviour](#) (on page 31)). The perfectly plastic part is based on the Mohr-Coulomb failure criterion, formulated in a non-associated plasticity framework.

Plasticity involves the development of irreversible strains. In order to evaluate whether or not plasticity occurs in a calculation, a yield function,  $f$ , is introduced as a function of stress and strain. Plastic yielding is related with the condition  $f = 0$ . This condition can often be presented as a surface in principal stress space. A perfectly-plastic model is a constitutive model with a fixed yield surface, i.e. a yield surface that is fully defined by model parameters and not affected by (plastic) straining. For stress states represented by points within the yield surface, the behaviour is purely elastic and all strains are reversible.

### 3.1 Linear Elastic Perfectly - Plastic behaviour

The basic principle of elastoplasticity is that strains and strain rates are decomposed into an elastic part and a plastic part:

$$\boldsymbol{\varepsilon} = \boldsymbol{\varepsilon}^e + \boldsymbol{\varepsilon}^p \quad \dot{\boldsymbol{\varepsilon}} = \dot{\boldsymbol{\varepsilon}}^e + \dot{\boldsymbol{\varepsilon}}^p \quad \text{Eq. [70]}$$

Hooke's law is used to relate the stress rates to the elastic strain rates. Substitution of Eq. [70] into Hooke's law Eq. [30] leads to:

$$\dot{\boldsymbol{\sigma}} = \mathbf{D}^e \dot{\boldsymbol{\varepsilon}}^e = \mathbf{D}^e (\dot{\boldsymbol{\varepsilon}} - \dot{\boldsymbol{\varepsilon}}^p) \quad \text{Eq. [71]}$$

According to the classical theory of plasticity, plastic strain rates are proportional to the derivative of the yield function with respect to the stresses. This means that the plastic strain rates can be represented as vectors perpendicular to the yield surface. This classical form of the theory is referred to as associated plasticity. However, for Mohr-Coulomb type yield functions, the theory of associated plasticity overestimates dilatancy. Therefore, in addition to the yield function, a plastic potential function  $g$  is introduced. The case  $g \neq f$  is denoted as non-associated plasticity. In general, the plastic strain rates are written as:

$$\dot{\boldsymbol{\varepsilon}}^p = \lambda \frac{\partial g}{\partial \boldsymbol{\sigma}} \quad \text{Eq. [72]}$$

## Linear Elastic Perfectly Plastic Model (Mohr-Coulomb Model)

### Formulation of the Mohr-Coulomb model

in which  $\lambda$  is the plastic multiplier. For purely elastic behaviour  $\lambda$  is zero, whereas in the case of plastic behaviour  $\lambda$  is positive:

$$\lambda = 0 \text{ for : } f < 0 \text{ or : } \frac{\partial f}{\partial \mathbf{a}'} \mathbf{D}^e \dot{\boldsymbol{\varepsilon}} \leq 0 \quad (\text{Elasticity}) \quad \text{Eq. [73]}$$

$$\lambda > 0 \text{ for : } f = 0 \text{ and : } \frac{\partial f}{\partial \mathbf{a}'} \mathbf{D}^e \dot{\boldsymbol{\varepsilon}} > 0 \quad (\text{Plasticity}) \quad \text{Eq. [74]}$$

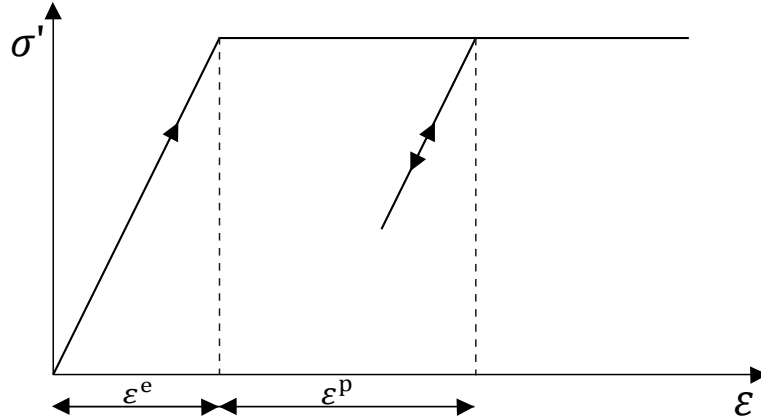


Figure 6: Basic idea of an elastic perfectly plastic model

These equations may be used to obtain the following relationship between the effective stress rates and strain rates for elastic perfectly-plastic behaviour ([Smith & Griffiths \[1982\]](#) (on page 249); [Vermeer & Borst \[1984\]](#) (on page 249)):

$$\dot{\mathbf{a}}' = \left( \mathbf{D}^e - \frac{\alpha}{d} \mathbf{D}^e \frac{\partial \mathbf{g}}{\partial \mathbf{a}'} \frac{\partial f}{\partial \mathbf{a}'} \mathbf{D}^e \right) \dot{\boldsymbol{\varepsilon}} \quad \text{Eq. [75]}$$

where:

$$d = \left( \frac{\partial f}{\partial \mathbf{a}'} \mathbf{D}^e \frac{\partial \mathbf{g}}{\partial \mathbf{a}'} \right) \quad \text{Eq. [76]}$$

The parameter  $\alpha$  is used as a switch. If the material behaviour is elastic, as defined by Eq. [73], the value of  $\alpha$  is equal to zero, whilst for plasticity, as defined by Eq. [74], the value of  $\alpha$  is equal to unity.

The above theory of plasticity is restricted to smooth yield surfaces and does not cover a multi surface yield contour as present in the full Mohr-Coulomb model. For such a yield surface the theory of plasticity has been extended by [Koiter \(1960\)](#) (on page 247) and others to account for flow vertices involving two or more plastic potential functions:

$$\dot{\boldsymbol{\varepsilon}}^p = \lambda_1 \frac{\partial \mathbf{g}_1}{\partial \mathbf{a}'} + \lambda_2 \frac{\partial \mathbf{g}_2}{\partial \mathbf{a}'} + \dots \quad \text{Eq. [77]}$$

Similarly, several quasi independent yield functions ( $f_1, f_2, \dots$ ) are used to determine the magnitude of the multipliers ( $\lambda_1, \lambda_2, \dots$ ).

## 3.2 Formulation of the Mohr-Coulomb model

The Mohr-Coulomb yield condition is an extension of Coulomb's friction law to general states of stress. In fact, this condition ensures that Coulomb's friction law is obeyed in any plane within a material element.

The full Mohr-Coulomb yield condition consists of six yield functions when formulated in terms of principal stresses (see for instance [Smith & Griffiths, 1982](#) (on page 249)):

$$\begin{aligned}
 f_{1a} &= \frac{1}{2}(\sigma'_2 - \sigma'_3) + \frac{1}{2}(\sigma'_2 + \sigma'_3)\sin(\phi) - c\cos(\phi) \leq 0 & a) \\
 f_{2a} &= \frac{1}{2}(\sigma'_3 - \sigma'_2) + \frac{1}{2}(\sigma'_3 + \sigma'_2)\sin(\phi) - c\cos(\phi) \leq 0 & b) \\
 f_{2a} &= \frac{1}{2}(\sigma'_3 - \sigma'_1) + \frac{1}{2}(\sigma'_3 + \sigma'_1)\sin(\phi) - c\cos(\phi) \leq 0 & c) \\
 f_{2b} &= \frac{1}{2}(\sigma'_1 - \sigma'_3) + \frac{1}{2}(\sigma'_1 + \sigma'_3)\sin(\phi) - c\cos(\phi) \leq 0 & d) \\
 f_{3a} &= \frac{1}{2}(\sigma'_1 - \sigma'_2) + \frac{1}{2}(\sigma'_1 + \sigma'_2)\sin(\phi) - c\cos(\phi) \leq 0 & e) \\
 f_{3b} &= \frac{1}{2}(\sigma'_2 - \sigma'_1) + \frac{1}{2}(\sigma'_2 + \sigma'_1)\sin(\phi) - c\cos(\phi) \leq 0 & f)
 \end{aligned}$$

*Eq. [78]*

The two plastic model parameters appearing in the yield functions are the well-known friction angle  $\phi$  and the cohesion  $c$ . The condition  $f_i = 0$  for all yield functions together (where  $f_i$  is used to denote each individual yield function) represents a fixed hexagonal cone in principal stress space as shown in [Figure 7](#) (on page 33).

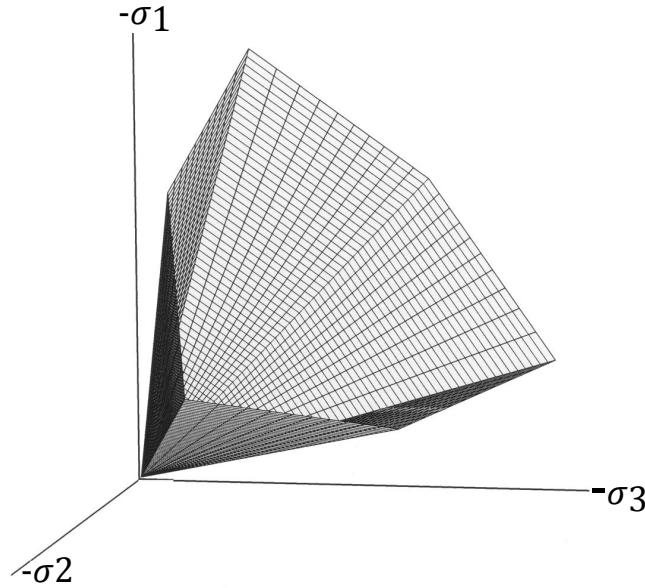


Figure 7: The Mohr-Coulomb yield surface in principal stress space ( $c = 0$ )

In addition to the yield functions, six plastic potential functions are defined for the Mohr-Coulomb model:

## Linear Elastic Perfectly Plastic Model (Mohr-Coulomb Model)

Parameters of the Mohr-Coulomb model

$$\begin{aligned}
 g_{1a} &= \frac{1}{2}(\sigma'_2 - \sigma'_3) + \frac{1}{2}(\sigma'_2 + \sigma'_3)\sin(\psi) \leq 0 & a) \\
 g_{1b} &= \frac{1}{2}(\sigma'_3 - \sigma'_2) + \frac{1}{2}(\sigma'_3 + \sigma'_2)\sin(\psi) \leq 0 & b) \\
 g_{2a} &= \frac{1}{2}(\sigma'_3 - \sigma'_1) + \frac{1}{2}(\sigma'_3 + \sigma'_1)\sin(\psi) \leq 0 & c) \\
 g_{2b} &= \frac{1}{2}(\sigma'_1 - \sigma'_3) + \frac{1}{2}(\sigma'_1 + \sigma'_3)\sin(\psi) \leq 0 & d) \\
 g_{3a} &= \frac{1}{2}(\sigma'_1 - \sigma'_2) + \frac{1}{2}(\sigma'_1 + \sigma'_2)\sin(\psi) \leq 0 & e) \\
 g_{3b} &= \frac{1}{2}(\sigma'_2 - \sigma'_1) + \frac{1}{2}(\sigma'_2 + \sigma'_1)\sin(\psi) \leq 0 & f)
 \end{aligned}$$

*Eq. [79]*

The plastic potential functions contain a third plasticity parameter, the dilatancy angle  $\psi$ . This parameter is required to model positive plastic volumetric strain increments (dilatancy) as actually observed for dense soils. A discussion of all of the model parameters used in the Mohr-Coulomb model is given in the next section.

When implementing the Mohr-Coulomb model for general stress states, special treatment is required for the intersection of two yield surfaces. Some programs use a smooth transition from one yield surface to another, i.e. the rounding-off of the corners (see for example [Smith & Griffiths, 1982](#) (on page 249)). In PLAXIS, however, the exact form of the full Mohr-Coulomb model is implemented, using a sharp transition from one yield surface to another. For a detailed description of the corner treatment the reader is referred to the literature ([Koiter, 1960](#) (on page 247); [van Langen & Vermeer, 1990](#) (on page 249)).

For  $c > 0$ , the standard Mohr-Coulomb criterion allows for tension. In fact, allowable tensile stresses increase with cohesion. In reality, soil can sustain none or only very small tensile stresses. This behaviour can be included in a PLAXIS analysis by specifying a tension cut-off. In this case, Mohr circles with positive principal stresses are not allowed. The tension cut-off introduces three additional yield functions, defined as:

$$\begin{aligned}
 f_4 &= \sigma'_1 - \sigma_t \leq 0 & a) \\
 f_5 &= \sigma'_2 - \sigma_t \leq 0 & b) \\
 f_6 &= \sigma'_3 - \sigma_t \leq 0 & c)
 \end{aligned}$$

*Eq. [80]*

When this tension cut-off procedure is used, the allowable tensile stress,  $\sigma_t$ , is, by default, taken equal to zero, but this value can be changed by the user. For these three yield functions an associated flow rule is adopted.

For stress states within the yield surface, the behaviour is elastic and obeys Hooke's law for isotropic linear elasticity, as discussed in . Hence, besides the plasticity parameters  $c$ ,  $\varphi$ , and  $\psi$ , input is required on the elastic Young's modulus  $E$  and Poisson's ratio  $\nu$ . The model described here is officially called the linear elastic perfectly plastic model with Mohr-Coulomb failure criterion. For simplicity, this model is called the Mohr-Coulomb model in PLAXIS.

## Linear Elastic Perfectly Plastic Model (Mohr-Coulomb Model)

Parameters of the Mohr-Coulomb model

### 3.3 Parameters of the Mohr-Coulomb model

The linear elastic perfectly-plastic Mohr-Coulomb model requires a total of five parameters, 2 stiffness parameters and 3 strength parameters, which are generally familiar to most geotechnical engineers and which can be obtained from basic tests on soil samples. The stiffness parameters with their standard units are:

$E_{ref}$	Young's modulus	[kN/m <sup>2</sup> ]
$\nu$	Poisson's ratio	[-]

Instead of using the Young's modulus as a stiffness parameter, alternative stiffness parameters can be entered. These parameters with their standard units are listed below:

$G$	Shear modulus	[kN/m <sup>2</sup> ]
$E_{oed}$	Oedometer modulus	[kN/m <sup>2</sup> ]

The strength parameters of the Mohr-Coulomb model are:

$c$	Cohesion	[kN/m <sup>2</sup> ]
$\varphi$	Friction angle	[°]
$\psi$	Dilatancy angle	[°]
$\sigma_t$	Tension cut-off and tensile strength	[kN/m <sup>2</sup> ]

Parameters can either be effective parameters (indicated by a prime sign (')) or undrained parameters (indicated by a subscript u), depending on the selected drainage type.

[ULT] In the case of dynamic applications, alternative and/or additional parameters may be used to define stiffness based on wave velocities. These parameters are listed below:

$V_p$	Compression wave velocity	[m/s]
$V_s$	Shear wave velocity	[m/s]

#### 3.3.1 Young's modulus (E)

PLAXIS uses the Young's modulus as the basic stiffness modulus in the elastic model and the Mohr-Coulomb model, but some alternative stiffness moduli are displayed as well. A stiffness modulus has the dimension of stress. The values of the stiffness parameter adopted in a calculation require special attention as many geomaterials show a non-linear behaviour from the very beginning of loading. In triaxial testing of soil samples the initial slope of the stress-strain curve (tangent modulus) is usually indicated as  $E_0$  and the secant modulus at 50% strength is denoted as  $E_{50}$  (see [Figure 8](#) (on page 36)). For materials with a large linear elastic range it is realistic to use  $E_0$ , but for loading of soils one generally uses  $E_{50}$ . Considering unloading problems, as in the case of tunnelling and excavations, one needs an unload-reload modulus ( $E_{ur}$ ) instead of  $E_{50}$ .

## Linear Elastic Perfectly Plastic Model (Mohr-Coulomb Model)

### Parameters of the Mohr-Coulomb model

For soils, both the unloading modulus,  $E_{ur}$ , and the first loading modulus,  $E_{50}$ , tend to increase with the confining pressure. Hence, deep soil layers tend to have greater stiffness than shallow layers. Moreover, the observed stiffness depends on the stress path that is followed. The stiffness is much higher for unloading and reloading than for primary loading. Also, the observed soil stiffness in terms of a Young's modulus may be lower for (drained) compression than for shearing. Hence, when using a constant stiffness modulus to represent soil behaviour one should choose a value that is consistent with the stress level and the stress path development. Note that some stress-dependency of soil behaviour is taken into account in the advanced models in PLAXIS which are described in subsequent chapters. For the Mohr-Coulomb model, PLAXIS offers a special option for the input of a stiffness increasing with depth (see [Depth-dependency](#) (on page 40)). Note that for material data sets where the drainage type is set to *Undrained (A)* or *Undrained (B)*, Young's modulus has the meaning of an effective Young's modulus, whilst PLAXIS automatically takes care of the incompressibility ([Undrained effective stress analysis \(effective stiffness parameters\)](#) (on page 19)).

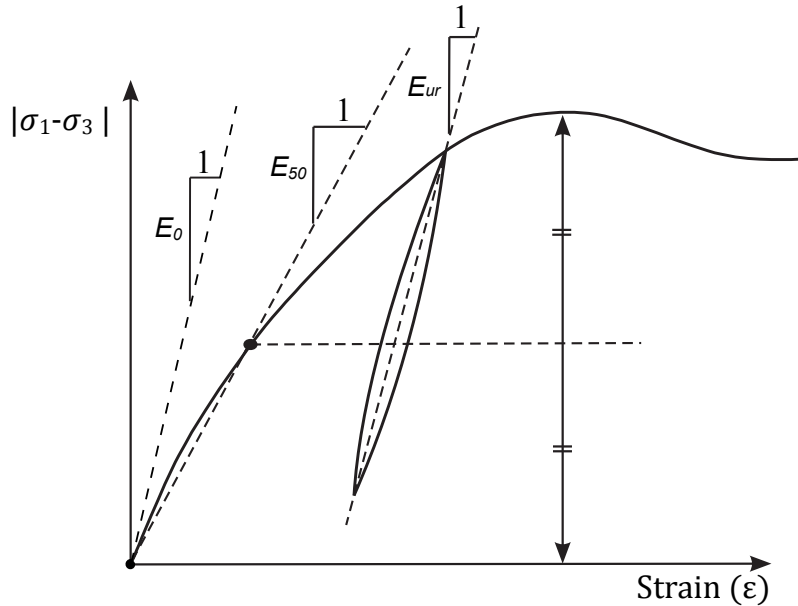


Figure 8: Definition of  $E_0$ ,  $E_{50}$  and  $E_{ur}$  for drained triaxial test results

### 3.3.2 Poisson's ratio ( $\nu$ )

Standard drained triaxial tests may yield a significant rate of volume decrease at the very beginning of axial loading and, consequently, a low initial value of Poisson's ratio ( $\nu_0$ ). For some cases, such as particular unloading problems, it may be realistic to use such a low initial value, but in general when using the Mohr-Coulomb model the use of a higher value is recommended.

The selection of a Poisson's ratio is particularly simple when the elastic model or Mohr-Coulomb model is used for gravity loading under conditions of one-dimensional compression. For this type of loading PLAXIS should give realistic ratios of  $K_0 = \sigma'_h / \sigma'_v$ .

As both models will give the well-known ratio of  $\sigma'_h / \sigma'_v = \nu / (1 - \nu)$  for one-dimensional compression it is easy to select a Poisson's ratio that gives a realistic value of  $K_0$ . Hence,  $\nu$  is evaluated by matching  $K_0$ . In many cases one will obtain  $\nu$  values in the range between 0.3 and 0.4. In general, such values can also be used for loading conditions other than one-dimensional compression. Please note that in this way it is not possible to create  $K_0$  values larger than 1, as may be observed in highly overconsolidated stress states. For unloading conditions, however, it is more appropriate to use values in the range between 0.15 and 0.25.

## Linear Elastic Perfectly Plastic Model (Mohr-Coulomb Model)

### Parameters of the Mohr-Coulomb model

---

Further note that for material data sets where the drainage type is set to *Undrained (A)* or *Undrained (B)*, Poisson's ratio has the meaning of an effective Poisson's ratio, whilst PLAXIS automatically takes care of the incompressibility ( [Undrained effective stress analysis \(effective stiffness parameters\)](#) (on page 19)). To ensure that the soil skeleton is much more compressible than the pore water, the effective Poisson's ratio should be smaller than 0.35 for *Undrained (A)* or *Undrained (B)* materials.

### 3.3.3 Shear modulus ( $G$ )

The shear modulus,  $G$ , has the dimension of stress. According to Hooke's law, the relationship between Young's modulus  $E$  and the shear modulus is given by (see Eq. [31] a):

$$G = \frac{E}{2(1 + \nu)} \quad \text{Eq. [81]}$$

Entering a particular value for one of the alternatives  $G$  or  $E_{oed}$  results in a change of the  $E$  modulus whilst  $\nu$  remains the same.

### 3.3.4 Oedometer modulus ( $E_{oed}$ )

The oedometer modulus,  $E_{oed}$ , or constrained modulus, has the dimension of stress. According to Hooke's law, the relationship between Young's modulus  $E$  and the oedometer modulus is given by (see Eq. [31] c)).

$$E_{oed} = \frac{(1 - \nu)E}{(1 - 2\nu)(1 + \nu)} \quad \text{Eq. [82]}$$

Entering a particular value for one of the alternatives  $G$  or  $E_{oed}$  results in a change of the  $E$  modulus whilst  $\nu$  remains the same.

### 3.3.5 Compression wave velocity $V_p$ [ULT]

The compression wave velocity,  $V_p$ , in a confined one-dimensional soil is a function of stiffness,  $E_{oed}$ , and the mass density,  $\rho$ , as:

$$V_p = \sqrt{\frac{E_{oed}}{\rho}} \quad \text{where } E_{oed} = \frac{(1 - \nu)E}{(1 + \nu)(1 - 2\nu)} \quad \text{and} \quad \rho = \frac{\gamma_{unsat}}{g} \quad \text{Eq. [83]}$$

in which  $\gamma_{unsat}$  is the total unsaturated unit weight and  $g$  is the gravity acceleration (9.8 m/s<sup>2</sup>).

### 3.3.6 Shear wave velocity $V_s$ [ULT]

The shear wave velocity,  $V_s$ , in a confined one-dimensional soil is a function of shear stiffness,  $G$ , and the mass density,  $\rho$ , as:

$$V_s = \sqrt{\frac{G}{\rho}} \quad \text{where } G = \frac{E}{2(1 + \nu)} \quad \text{and} \quad \rho = \frac{\gamma_{unsat}}{g} \quad \text{Eq. [84]}$$

in which  $\gamma_{unsat}$  is the total unsaturated unit weight and  $g$  is the gravity acceleration (9.8 m/s<sup>2</sup>).

## Linear Elastic Perfectly Plastic Model (Mohr-Coulomb Model)

### Parameters of the Mohr-Coulomb model

---

#### 3.3.7 Cohesion ( $c$ ) or undrained shear strength ( $s_u$ )

The cohesive strength has the dimension of stress. In the Mohr-Coulomb model, the cohesion parameter may be used to model the effective cohesion  $c'$  of the soil (cohesion intercept), in combination with a realistic effective friction angle  $\varphi'$  (see [Figure 9](#) (on page 39) (a)). This may not only be done for drained soil behaviour, but also if the type of material behaviour is set to *Undrained (A)*, as in both cases PLAXIS will perform an effective stress analysis. Alternatively, the cohesion parameter may be used to model the undrained shear strength  $s_u$  of the soil, in combination with  $\varphi = \varphi_u = 0$  when the *Drainage type* is set to *Undrained (B)* or *Undrained (C)*. In that case the Mohr-Coulomb failure criterion reduces to the well-known Tresca criterion. PLAXIS allows for an increase of shear strength with depth using the  $s_{u,inc}$  parameter ([Depth-dependency](#) (on page 40)).

The disadvantage of using effective strength parameters  $c'$  and  $\varphi'$  in combination with the drainage type being set to *Undrained (A)* is that the undrained shear strength as obtained from the model may deviate from the undrained shear strength in reality because of differences in the actual stress path being followed. In this respect, advanced soil models generally perform better than the Mohr-Coulomb model, but in all cases it is recommended to compare the resulting stress state in all calculation phases with the present shear strength in reality ( $|\sigma_1 - \sigma_3| \leq 2 s_u$ ).

On the other hand, the advantage of using effective strength parameters is that the change in shear strength with consolidation is obtained automatically, although it is still recommended to check the resulting stress state after consolidation.

The advantage of using the cohesion parameter to model undrained shear strength in combination with  $\varphi = 0$  (*Undrained (B)* or *Undrained (C)*) is that the user has direct control over the shear strength, independent of the actual stress state and stress path followed. Please note that this option may not be appropriate when using advanced soil models.

PLAXIS can handle cohesionless sands ( $c = 0$ ), but some options may not perform well. To avoid complications, non-experienced users are advised to enter at least a small value in soil layers near the ground surface (use  $c > 0.2$  kPa). Please note that a positive value for the cohesion may lead to a tensile strength, which may be unrealistic for soils. By default, the *Tension cut-off* option is used to reduce the tensile strength.

PLAXIS offers a special option for the input of layers in which the cohesion increases with depth (see [Depth-dependency](#) (on page 40)).

#### 3.3.8 Friction angle ( $\varphi$ )

The friction angle  $\varphi$  (phi) is entered in degrees. In general the friction angle is used to model the effective friction of the soil, in combination with an effective cohesion  $c'$  ([Figure 9](#) (on page 39) (a)). This may not only be done for drained soil behaviour, but also if the type of material behaviour is set to *Undrained (A)*, since in both cases PLAXIS will perform an effective stress analysis. Alternatively, the soil strength is modelled by setting the cohesion parameter equal to the undrained shear strength of the soil, in combination with  $\varphi = 0$  (*Undrained (B)* or *Undrained (C)*) ([Figure 9](#) (on page 39) (b)). In that case the Mohr-Coulomb failure criterion reduces to the well-known Tresca criterion.

## Linear Elastic Perfectly Plastic Model (Mohr-Coulomb Model)

Parameters of the Mohr-Coulomb model

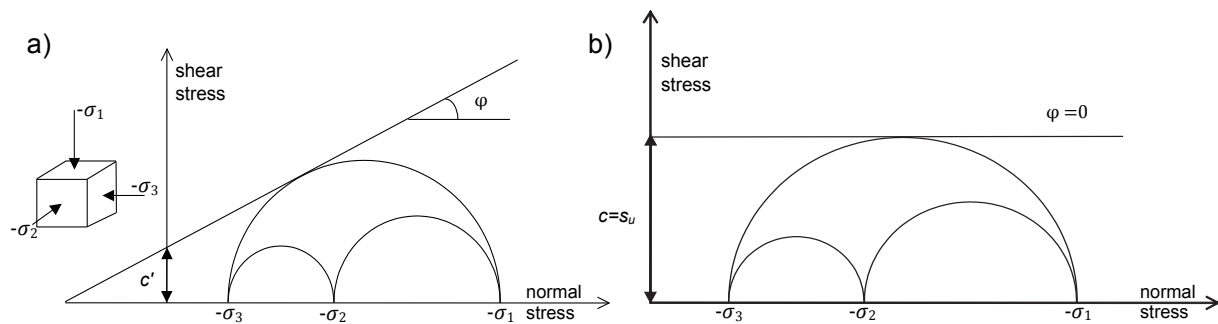


Figure 9: Stress circles at yield; one touches Coulomb's envelope. a) Using effective strength parameters (Mohr-Coulomb) - b) Using undrained strength parameters (Tresca).

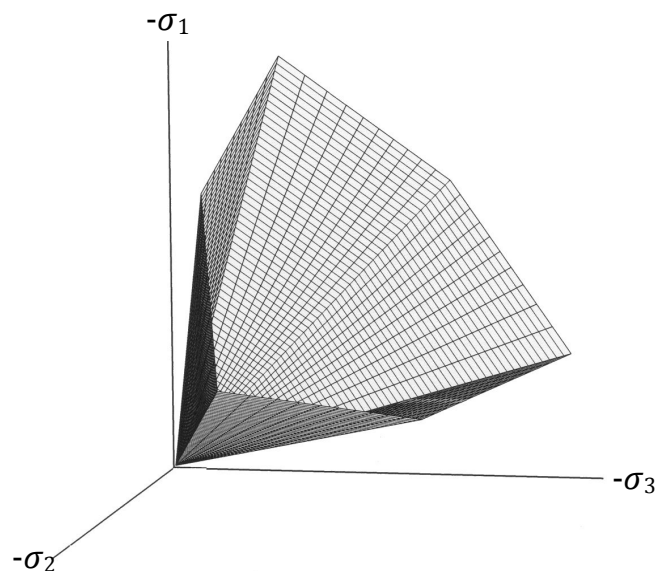


Figure 10: Failure surface in principal stress space for cohesionless soil

High friction angles, as sometimes obtained for dense sands, will substantially increase plastic computational effort. Moreover, high friction may be subjected to strain-softening behaviour, which means that such high friction angles are not sustainable under (large) deformation. Hence, high friction angles should be avoided when performing preliminary computations for a particular project\*. The friction angle largely determines the shear strength as shown in [Figure 9](#) (on page 39) by means of Mohr's stress circles. A more general representation of the yield criterion is shown in [Figure 10](#) (on page 39). The Mohr-Coulomb failure criterion proves to be better for describing soil strength for general stress states than the Drucker-Prager approximation.

**Note:** \*The friction angles are in the order of 20 - 30 degrees for clay and silt (the more plastic the clay, the lower the friction), and 30 - 40 degrees for sand and gravel (the denser the sand, the higher the friction).

### 3.3.9 Dilatancy angle ( $\psi$ )

The dilatancy angle,  $\psi$  (psi), is specified in degrees. Apart from heavily overconsolidated layers, clay soils tend to show little dilatancy ( $\psi \approx 0$ ). The dilatancy of sand depends on both the density and the friction angle. In general

## Linear Elastic Perfectly Plastic Model (Mohr-Coulomb Model)

### Depth-dependency

---

the dilatancy angle of soils is much smaller than the friction angle. For quartz sands the order of magnitude is  $\psi \approx \varphi - 30^\circ$ . For  $\varphi$ -values of less than  $30^\circ$ , however, the angle of dilatancy is mostly zero. A small negative value for  $\psi$  is only realistic for extremely loose sands. In the Hardening Soil model or Hardening Soil model with small-strain stiffness the end of dilatancy, as generally observed when the soil reaches the critical state, can be modelled using the *Dilatancy cut-off*. However, this option is not available for the Mohr-Coulomb model. For further information about the link between the friction angle and dilatancy, see [Bolton \(1986\)](#). (on page 246).

A positive dilatancy angle implies that in drained conditions the soil will continue to dilate as long as shear deformation occurs. This is clearly unrealistic, as most soils will reach a critical state at some point and further shear deformation will occur without volume changes. In undrained conditions a positive dilatancy angle, combined with the restriction on volume changes, leads to a generation of tensile pore stresses. In an undrained effective stress analysis therefore the strength of the soil may be overestimated.

When the soil strength is modelled as undrained shear strength,  $s_u$ , and  $\varphi = 0$ , (*Undrained (B)* or *Undrained (C)*) the dilatancy angle is automatically set to zero. Great care must be taken when using a positive value of dilatancy in combination with drainage type set to *Undrained (A)*. In that case the model will show unlimited soil strength due to tensile pore stresses. These tensile pore stresses can be limited by setting the cavitation cut-off.

### 3.3.10 Tension cut-off

In some practical problems an area with tensile stresses may develop. According to the Coulomb envelope shown in [Figure 9](#) (on page 39) this is allowed when the shear stress (radius of Mohr circle) is sufficiently small. However, the soil surface near a trench in clay sometimes shows tensile cracks. This indicates that soil may also fail in tension instead of in shear. Such behaviour can be included in a PLAXIS analysis by selecting the tension cut-off. In this case Mohr circles with positive principal stresses are not allowed. When selecting the tension cut-off the allowable tensile strength may be entered. For the Mohr-Coulomb model the tension cut-off is, by default, selected with a tensile strength of zero.

## 3.4 Depth-dependency

The advanced features comprise the increase of stiffness and cohesive strength with depth and the use of a tension cut-off. In fact, the latter option is used by default, but it may be deactivated here, if desired. These parameters are defined in the *Depth-dependency* blocks on the **Mechanical** tabsheet of the **Soil** window.

### 3.4.1 Increase of stiffness ( $E_{inc}$ )

In real soils, the stiffness depends significantly on the stress level, which means that the stiffness generally increases with depth. When using the Mohr-Coulomb model, the stiffness is a constant value. In order to account for the increase of the stiffness with depth the  $E_{inc}$ -value may be used, which is the increase of the Young's modulus per unit of depth (expressed in the unit of stress per unit depth). At the level given by the  $y_{ref}$  parameter, and above, the stiffness is equal to the reference Young's modulus,  $E_{ref}$ , as entered on the **Mechanical** tabsheet. Below, the stiffness is given by:

$$E(y) = E_{ref} + (y_{ref} - y)E_{inc} \quad (y < y_{ref}) \quad Eq. [85]$$

## Linear Elastic Perfectly Plastic Model (Mohr-Coulomb Model)

On the use of the Mohr-Coulomb model in dynamics calculations [ULT]

where  $y$  represents the vertical direction. The actual value of Young's modulus in the stress points is obtained from the reference value and  $E_{inc}$ . Note that during calculations a stiffness increasing with depth does not change as a function of the stress state.

**Note:** Note that in PLAXIS 3D the vertical coordinate is  $z$  instead of  $y$ .

### 3.4.2 Increase of cohesion or shear strength with depth ( $c_{inc}$ or $s_{u,inc}$ )

PLAXIS offers an advanced option for the input of clay layers in which the cohesion,  $c$ , (or undrained shear strength,  $s_u$ ) increases with depth. In order to account for the increase of the cohesion with depth the  $c_{inc}$ -value may be used, which is the increase of cohesion per unit of depth (expressed in the unit of stress per unit depth). At the level given by the  $y_{ref}$  parameter, and above, the cohesion is equal to the (reference) cohesion,  $c_{ref}$ , as entered on the **Mechanical** tabsheet. Below, the cohesive strength is given by:

$$\begin{aligned} c(y) &= c_{ref} + (y_{ref} - y)c_{inc} & (y < y_{ref}) & \quad a) \\ s_u(y) &= s_{u,ref} + (y_{ref} - y)s_{u,inc} & (y < y_{ref}) & \quad b) \end{aligned} \quad Eq. [86]$$

where  $y$  represents the vertical direction. Note that when using effective strength properties ( $\varphi' > 0$ ) it is generally not necessary to use an increase of cohesion with depth, since the friction together with the initial effective stress will result in an increasing shear strength with depth.

## 3.5 On the use of the Mohr-Coulomb model in dynamics calculations [ULT]

When using the Mohr-Coulomb model in dynamics calculations, the stiffness parameters need to be selected such that the model correctly predicts wave velocities in the soil (Eq. [83] and Eq. [84]). This generally requires a much larger small strain stiffness rather than a stiffness at engineering strain levels. When subjected to dynamic or cyclic loading, the Mohr-Coulomb model may generate plastic strains if stress points reach the Mohr-Coulomb failure criterion, which will lead to damping in dynamics calculations. However, it should be noted that the stress cycles within the Mohr-Coulomb failure contour will only generate elastic strains and no (hysteretic) damping, nor accumulation of strains or pore pressure or liquefaction. In order to simulate the soil's damping characteristics in cyclic loading, Rayleigh damping may be defined.

## The Hoek-Brown model (rock behaviour)

The material behaviour of rock differs from the behaviour of soils in the sense that it is generally stiffer and stronger. The dependency of the stiffness on the stress level is almost negligible, so stiffness of rocks can be considered constant. On the other hand, the dependency of the (shear) strength on the stress level is significant. In this respect, heavily jointed or weathered rock can be regarded a frictional material. A first approach is to model the shear strength of rock by means of the Mohr-Coulomb failure criterion. However, considering the large range of stress levels where rock may be subjected to, a linear stress-dependency, as obtained from the Mohr-Coulomb model, is generally not sufficient. Furthermore, rock may also show a significant tensile strength. The Hoek-Brown failure criterion is a better non-linear approximation of the strength of rocks. It involves shear strength as well as tensile strength in a continuous formulation. Together with Hooke's law of isotropic linear elastic behaviour it forms the Hoek-Brown model for rock behaviour. The 2002 edition of this model ([Hoek, Carranza-Torres & Corkum, 2002](#)) (on page 247) has been implemented in PLAXIS 3D to simulate the isotropic behaviour of rock-type materials. The implementation of the model, including the material strength factorization, is based on [Bentz, Schwab, Vermeer & Kauther, \(2007\)](#) (on page 246). More background information on the Hoek-Brown model and the selection of model parameters can be found in [Hoek, 2006](#) (on page 247). For anisotropic behaviour of stratified rock reference is made to [The Jointed Rock model \(anisotropy\)](#) (on page 55).

### 4.1 Formulation of the Hoek-Brown model

The generalised Hoek-Brown failure criterion can be formulated as a non-linear relationship between the major and minor effective principal stresses (considering tension positive and compression negative):

$$\sigma_1' = \sigma_3' - |\sigma_{ci}| \left( m_b \frac{\sigma_3'}{\sigma_{ci}} + s \right)^a \quad \text{Eq. [87]}$$

where  $m_b$  is a reduced value of the intact rock parameter  $m_i$ , which also depends on the Geological Strength Index (GSI) and the Disturbance Factor (D):

$$m_b = m_i \exp\left(\frac{GSI - 100}{28 - 14D}\right) \quad \text{Eq. [88]}$$

$s$  and  $a$  are auxiliary material constants for the rock mass, that can be expressed as:

$$s = \exp\left(\frac{GSI - 100}{9 - 3D}\right) \quad \text{Eq. [89]}$$

$$a = \frac{1}{2} + \frac{1}{6} \left[ \exp\left(\frac{-GSI}{15}\right) - \exp\left(\frac{-20}{3}\right) \right] \quad \text{Eq. [90]}$$

$\sigma_{ci}$  is the uni-axial compressive strength of the intact rock material (defined as a positive value). From this value, the uni-axial compressive strength of the specific rock under consideration,  $\sigma_c$ , can be obtained by:

## The Hoek-Brown model (rock behaviour)

Formulation of the Hoek-Brown model

$$\sigma_c = - |\sigma_{ci}| s^a \quad \text{Eq. [91]}$$

The tensile strength of the specific rock under consideration,  $\sigma_t$ , can be obtained by:

$$\sigma_t = \frac{s |\sigma_{ci}|}{m_b} \quad \text{Eq. [92]}$$

The Hoek-Brown failure criterion is illustrated in [Figure 11](#) (on page 43).

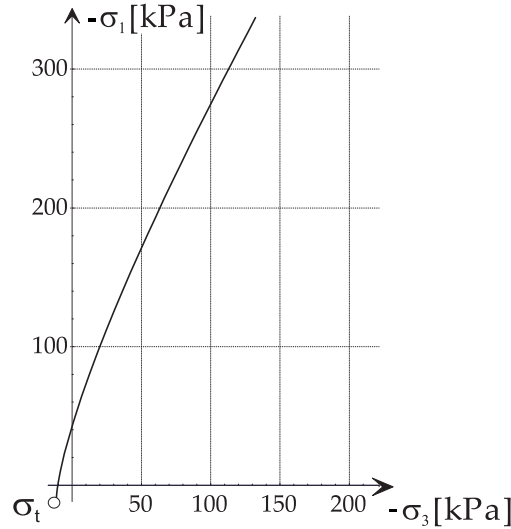


Figure 11: Hoek-Brown failure criterion in principal stresses

In the framework of plasticity theory, the Hoek-Brown failure criterion is reformulated into the following yield function:

$$f_{HB} = \sigma'_1 - \sigma'_3 + \bar{f}(\sigma'_3) \quad \text{where} \quad \bar{f}(\sigma'_3) = |\sigma_{ci}| \left( m_b \frac{-\sigma'_3}{|\sigma_{ci}|} + s \right)^a \quad \text{Eq. [93]}$$

For general three-dimensional stress states, more than one yield function is required to deal with the corners of the yield contour, similar to the full Mohr-Coulomb criterion. Defining compression as negative and considering ordering of principal stresses such that  $\sigma'_1 \leq \sigma'_2 \leq \sigma'_3$ , the full criterion can be captured by two yield functions:

$$f_{HB,13} = \sigma'_1 - \sigma'_3 + \bar{f}(\sigma'_3) \quad \text{where} \quad \bar{f}(\sigma'_3) = |\sigma_{ci}| \left( m_b \frac{-\sigma'_3}{|\sigma_{ci}|} + s \right)^a \quad \text{Eq. [94]}$$

$$f_{HB,12} = \sigma'_1 - \sigma'_2 + \bar{f}(\sigma'_2) \quad \text{where} \quad \bar{f}(\sigma'_2) = |\sigma_{ci}| \left( m_b \frac{-\sigma'_2}{|\sigma_{ci}|} + s \right)^a \quad \text{Eq. [95]}$$

The full Hoek-Brown failure contour ( $f_i = 0$ ) in principal stress space is illustrated in [Figure 12](#) (on page 44)

## The Hoek-Brown model (rock behaviour)

### Formulation of the Hoek-Brown model

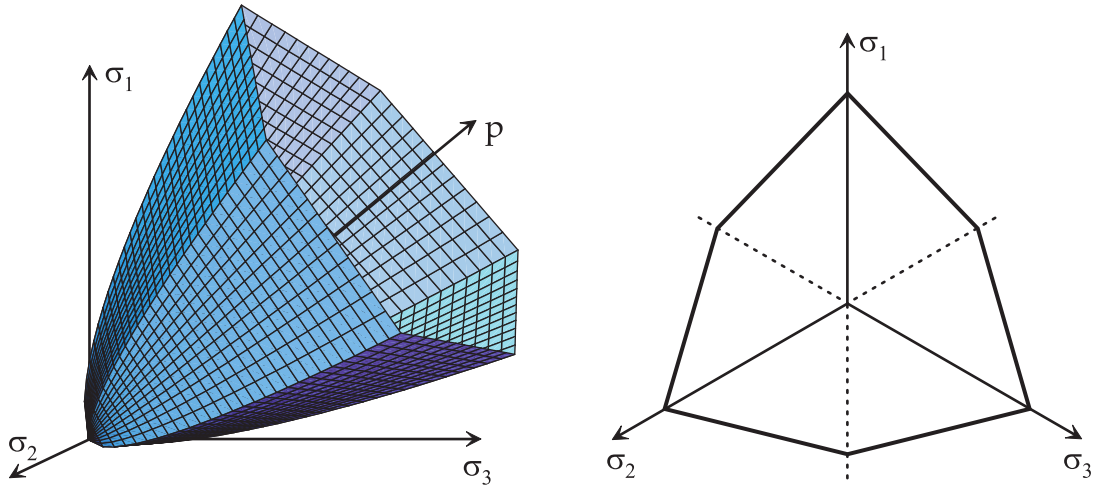


Figure 12: The Hoek-Brown failure contour in principal stress space

In addition to the two yield functions, two corresponding plastic potential functions are defined for the Hoek-Brown model:

$$g_{HB,13} = S_1 - \left( \frac{1 + \sin(\psi_{mob})}{1 - \sin(\psi_{mob})} \right) S_3 \quad Eq. [96]$$

$$g_{HB,12} = S_1 - \left( \frac{1 + \sin(\psi_{mob})}{1 - \sin(\psi_{mob})} \right) S_2 \quad Eq. [97]$$

where  $S_i$  are the transformed stresses, defined as:

$$S_i = \left( \frac{-\sigma_i}{m_b |\sigma_{ci}|} + \frac{s}{m_b^2} \right) \quad for \quad i = 1, 2, 3 \quad Eq. [98]$$

$\psi_{mob}$  is the mobilised dilatancy angle, varying with  $\sigma'_3$  from its input value at ( $\sigma'_3 = 0$ ) down to zero at  $-\sigma'_3 = \sigma_\psi$  and beyond:

$$\psi_{mob} = \frac{\sigma_\psi + \sigma'_3}{\sigma_\psi} \psi \geq 0 \quad (0 \geq -\sigma'_3 \geq \sigma_\psi) \quad Eq. [99]$$

Moreover, in order to allow for plastic expansion in the tensile zone, an increased artificial value of the mobilised dilatancy is used:

$$\psi_{mob} = \psi + \frac{\sigma'_3}{\sigma_t} (90^\circ - \psi) \quad (\sigma'_t \geq \sigma'_3 \geq 0) \quad Eq. [100]$$

The evolution of the mobilised dilatancy angle as a function of  $\sigma'_3$  is visualized in [Figure 13](#) (on page 45).

## The Hoek-Brown model (rock behaviour)

Conversion of Hoek-Brown to Mohr-Coulomb

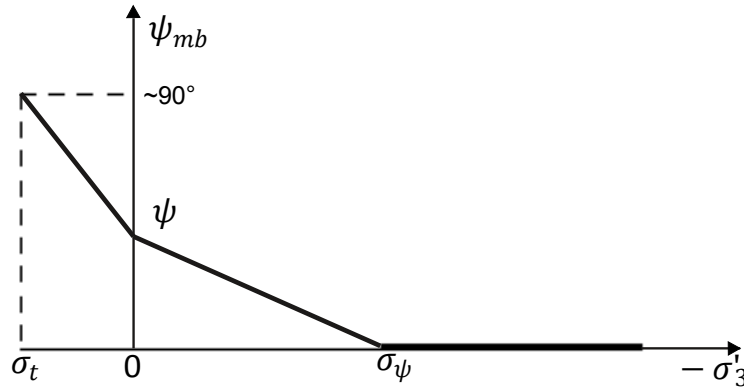


Figure 13: Evolution of mobilised dilatancy angle

Regarding the elastic behaviour of the Hoek-Brown model, Hooke's law of isotropic linear elastic behaviour, as described in [Elastic strains](#) (on page 17), is adopted. This part of the model involves Young's modulus,  $E$ , representing the in-situ stiffness of the jointed rock mass before failure, and Poisson's ratio,  $\nu$ , describing transverse straining.

## 4.2 Conversion of Hoek-Brown to Mohr-Coulomb

In order to compare the Hoek-Brown failure criterion with the well-known Mohr-Coulomb failure criterion for practical applications involving a particular stress range, a balanced fit can be made for confining stresses in the range (considering tension positive and compression negative):

$$-\sigma_t < \sigma'_3 < -\sigma'_{3,\max}$$

This gives the following expressions for the Mohr-Coulomb effective strength parameters  $\phi'$  and  $c'$  ([Carranza-Torres, 2004](#) (on page 246)):

$$\sin(\phi') = \frac{6am_b(s + m_b\sigma'_{3n})^{a-1}}{2(1+a)(2+a) + 6am_b(s + m_b\sigma'_{3n})^{a-1}} \quad \text{Eq. [101]}$$

$$c' = \frac{|\sigma_{ci}| \left[ (1+2a)s + (1-a)m_b\sigma'_{3n}(s + m_b\sigma'_{3n})^{a-1} \right]}{(1+a)(2+a) \sqrt{1 + \frac{6am_b(s + m_b\sigma'_{3n})^{a-1}}{(1+a)(2+a)}}} \quad \text{Eq. [102]}$$

where  $\sigma'_{3n} = -\sigma'_{3\max}/|\sigma_{ci}|$ . The upper limit of the confining stress,  $\sigma'_{3\max}$ , depends on the application.

## 4.3 Parameters of the Hoek-Brown model

The Hoek-Brown model involves a total of 8 parameters, which are generally familiar to geologists and mining engineers. These parameters with their standard units are listed below:

## The Hoek-Brown model (rock behaviour)

### Parameters of the Hoek-Brown model

$E_{rm}$	The rock mass Young's modulus	[kN/m <sup>2</sup> ]
$\nu$	Poisson's ratio	[-]
$ \sigma_{ci} $	Uni-axial compressive strength of the intact rock (>0)	[kN/m <sup>2</sup> ]
$m_i$	Intact rock parameter	[-]
$GSI$	Geological Strength Index	[-]
$D$	Disturbance factor	[-]
$\psi_{max}$	Dilatancy angle (at $\sigma'_3 = 0$ )	[°]
$\sigma_\psi$	Absolute value of confining pressure $\sigma'_3$ at which $\psi = 0^\circ$	[kN/m <sup>2</sup> ]

On the *Mechanical* tabsheet the rock mass intrinsic parameters are also displayed:

$m_b$	Rock mass parameter	[-]
$s$	Rock mass parameter	[-]
$a$	Rock mass parameter	[-]
$\sigma_t$	Rock mass tensile strength	[kN/m <sup>2</sup> ]
$\sigma_c$	Rock mass uni-axial compressive strength	[kN/m <sup>2</sup> ]

**Note:** Note that it is common in rock mechanics to express  $E$ ,  $\sigma_{ci}$  and  $\sigma_\psi$  in the unit MPa (megaPascal = MN/m<sup>2</sup>), whereas the input values in PLAXIS are given in standard units as defined in the project properties.

The Hoek-Brown model is the most used failure criterion for rock masses, nevertheless there are some uncertainties regarding the input parameters that require a consolidated experience. For this reason, PLAXIS implements in the side panel of the *Mechanical* tabsheet of the Hoek-Brown model a pre-processing tool to guide the user in the determination of the rock mass strength and stiffness parameters.

- *Analysis*: shows the Hoek-Brown failure envelope in the plane of principal effective stresses  $\sigma'_3 - \sigma'_1$ , in order to visualise the effects of changing of rock mass parameters on the failure envelope.
- The second tabsheet is specific to determine the parameter  $|\sigma_{ci}|$ ,  $m_i$ ,  $GSI$  and  $D$ . More details are given below.

### 4.3.1 The rock mass Young's modulus $E_{rm}$

In principle, Young's modulus can be measured from axial compression tests or direct shear tests on rock samples. However, this modulus is more applicable to the intact rock material, and should be reduced to obtain a representative stiffness of the in-situ rock mass. The rock mass Young's modulus  $E_{rm}$  is assumed to be a constant value for the considered rock layer. The rock mass stiffness  $E_{rm}$  can be estimated through one of the suggested empirical correlations.

- Generalised [Hoek & Diederichs \(2006\)](#) (on page 247):

## The Hoek-Brown model (rock behaviour)

Parameters of the Hoek-Brown model

$$E_{rm} = E_i \left( 0.02 + \frac{1 - D/2}{1 + e^{(60+15D-GSI)/11}} \right) \quad Eq. [103]$$

where

$$\begin{aligned} E_i &= \text{The intact rock modulus.} \\ GSI &= \text{Geological strength Index.} \\ D &= \text{Disturbance factor.} \end{aligned}$$

When no direct values of the intact rock modulus  $E_i$  are available or where undisturbed sampling for measurement of  $E_i$  is difficult, it is possible to estimate the intact rock modulus from the following relationship:

$$E_i = MR \sigma_{ci} \quad Eq. [104]$$

where

$$MR = \text{The Modulus Ratio originally proposed by [Deere, 1968](#) (on page 246) and reported in [Table 1](#) (on page 47) and } \sigma_{ci} \text{ is the uni-axial compressive strength.}$$

**Table 1: Guidelines for the selection of modulus ratio (MR) values (Hoek & Diederichs (2006))**

Name	Rock type	Texture	MR	MR±
Agglomerate	Igneous	Coarse	500	100
Amphibolites	Metamorphic	Medium	450	50
Andesite	Igneous	Medium	400	100
Anhydrite	Sedimentary	Fine	350	0
Basalt	Igneous	Fine	350	100
Breccia	Igneous	Medium	500	0
Breccia	Sedimentary	Coarse	290	60
Chalk	Sedimentary	Very fine	1000	0
Claystones	Sedimentary	Very fine	250	50
Conglomerates	Sedimentary	Coarse	350	50
Crystalline limestone	Sedimentary	Coarse	500	100
Dacite	Igneous	Fine	400	50
Diabase	Igneous	Fine	325	25
Diorite	Igneous	Medium	325	25
Dolerite	Igneous	Medium	350	50

## The Hoek-Brown model (rock behaviour)

Parameters of the Hoek-Brown model

Name	Rock type	Texture	MR	MR±
Dolomites	Sedimentary	Very fine	425	75
Gabbro	Igneous	Coarse	450	50
Gneiss	Metamorphic	Fine	525	225
Granite	Igneous	Coarse	425	125
Granodiorite	Igneous	Coarse, Medium	425	25
Greywackes	Sedimentary	Fine	350	0
Gypsum	Sedimentary	Medium	350	0
Hornfels	Metamorphic	Medium	550	150
Marble	Metamorphic	Coarse	850	150
Marls	Sedimentary	Very fine	175	25
Metasandstone	Metamorphic	Medium	250	50
Micritic limestones	Sedimentary	Fine	900	100
Migmatite	Metamorphic	Coarse	375	25
Norite	Igneous	Coarse, Medium	375	25
Peridotite	Igneous	Very fine	275	25
Phyllites	Metamorphic	Fine	550	250
Porphyries	Igneous	Coarse, Medium	400	0
Quartzites	Metamorphic	Fine	375	75
Rhyolite	Igneous	Medium	400	100
Sandstones	Sedimentary	Medium	275	75
Schists	Metamorphic	Medium	675	425
Shales	Sedimentary	Very fine	200	50
Siltstones	Sedimentary	Fine	375	25
Slates	Metamorphic	Very fine	500	100
Sparitic limestones	Sedimentary	Medium	700	100
Tuff	Igneous	Fine	300	100

## The Hoek-Brown model (rock behaviour)

### Parameters of the Hoek-Brown model

- Simplified [Hoek & Diederichs \(2006\)](#) (on page 247) that depends only in  $GSI$  and  $D$ :

$$E_{rm}(MPa) = 100000 \left( \frac{1 - D/2}{1 + e^{((75+25D-GSI)/11)}} \right) \quad Eq. [105]$$

Note that the input of Young's modulus in PLAXIS is generally in  $kN/m^2$  ( $= kPa = 10^{-3} MPa$ ), which means that the value obtained from the above formula must be multiplied by  $10^3$ .

### 4.3.2 Poisson's ratio $\nu$

Poisson's ratio,  $\nu$ , is generally in the range of 0.1 - 0.4. Typical values for particular rock types are listed in [Figure 14](#) (on page 49).

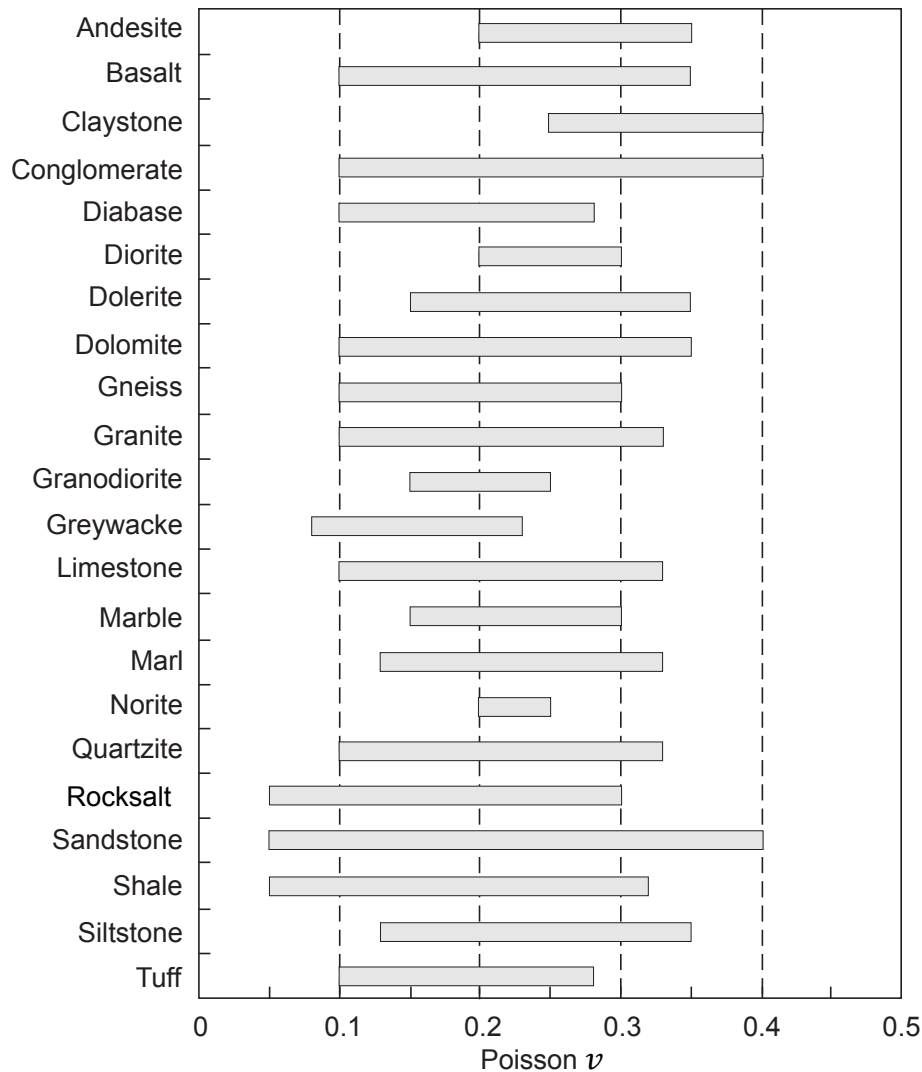


Figure 14: Typical Poisson's ratio values

## The Hoek-Brown model (rock behaviour)

### Parameters of the Hoek-Brown model

---

#### 4.3.3 Uni-axial compressive strength of intact rock $|\sigma_{ci}|$

The uni-axial strength of intact rock  $|\sigma_{ci}|$  can be determined in laboratory testing, e.g. axial compression. Laboratory testing is often conducted on intact rock so that  $GSI = 100$  and  $D = 0$ . In accordance with estimation methods generally executed in the field (i.e. geological hammer, pocket knife), typical values are reported in the side panel of the pre-processing tool.

#### 4.3.4 Intact rock parameter $m_i$

The intact rock parameter  $m_i$  is an empirical model parameter. Typical values are given in the side panel of the pre-processing tool which are based on the rock type as reported by [Marinos & Hoek \(2001\)](#) (on page 247) and [Wyllie & Mah \(2004\)](#) (on page 249) (see also Reference Manual - *Chapter 6 - Hoek-Brown pre-processing tool - Table: Values of the constant  $m_i$  for intact rock.*)

# The Hoek-Brown model (rock behaviour)

## Parameters of the Hoek-Brown model

The screenshot shows the 'Soil - Hoek-Brown - <NoName>' window in PLAXIS. The left panel contains several tabs: General, Mechanical, Groundwater, Interfaces, and Initial. The 'Mechanical' tab is active, showing a table of properties and values. The right panel, titled 'Analysis', shows a list of materials with their corresponding  $m_i$  values.

Property	Unit	Value
<b>Stiffness</b>		
$E_{rm}$	kN/m <sup>2</sup>	0.000
$\nu$ (nu)		0.000
<b>Alternatives</b>		
$G_{ref}$	kN/m <sup>2</sup>	0.000
<b>Strength</b>		
<b>Uniaxial compressive strength of intact rock</b>		
$ \sigma_{ci} $	kN/m <sup>2</sup>	0.000
<b>Hoek-Brown parameters</b>		
Determination	Derived	
$m_b$		0.000
$s$		0.02605E-3
$a$		0.6192
$m_i$		0.000
GSI		5.000
D		0.000
<b>Rock mass parameters</b>		
$\sigma_t$	kN/m <sup>2</sup>	0.000
$\sigma_c$	kN/m <sup>2</sup>	0.000
<b>Tension</b>		
Tension cut-off		<input type="checkbox"/>
<b>Dilatancy</b>		
$\psi_{max}$	°	0.000
$\sigma_\psi$	kN/m <sup>2</sup>	0.000
<b>Excess pore pressure calculation</b>		
Determination	v-undrained definition	
$v_u$ definition method	Direct	
$v_{u, equivalent}$ (nu)		0.4950
Skempton B		0.9933
$K_{w, ref}/n$	kN/m <sup>2</sup>	0.000

Name	$m_i$
Agglomerate igneous, coarse	19 ± 3
Amphibolites metamorphic, medium	26 ± 6
Andesite igneous, medium	25 ± 5
Anhydrite sedimentary, fine	12 ± 2
Basalt igneous, fine	25 ± 5
Breccia (igneous) igneous, medium	19 ± 5
Breccia (sedimentary) sedimentary, coarse	19 ± 5
Chalk sedimentary, very fine	7 ± 2
Claystones sedimentary, very fine	4 ± 2
Conglomerates sedimentary, coarse	21 ± 3
Crystalline limestone sedimentary, coarse	12 ± 3
Dacite igneous, fine	25 ± 3
Diabase igneous, fine	15 ± 5
Diorite igneous, medium	25 ± 5
Dolerite igneous, medium	16 ± 5

Figure 15: Intact rock parameter  $m_i$  for Hoek-Brown model

## 4.3.5 Geological Strength Index $GSI$

The GSI parameter can be computed thanks to the side panel of the pre-processing tool. The *GSI* tabsheet allows to choose between two rock types: *General* and *Flysch*. An intact rock is equivalent to  $GSI = 100$ , whereas a soil structure is in proximity to  $GSI = 0$ . Based on the selected rock type, the  $GSI$  can be chosen taking the structure and the surface conditions of the rock mass into account.

# The Hoek-Brown model (rock behaviour)

## Parameters of the Hoek-Brown model

**Soil - Hoek-Brown - <NoName>**

General \* Mechanical Groundwater Interfaces Initial

Property Unit Value

**Stiffness**

$E_m$  kN/m<sup>2</sup> 0.000

$\nu$  (nu) 0.000

**Alternatives**

$G_{ref}$  kN/m<sup>2</sup> 0.000

**Strength**

**Uniaxial compressive strength of intact rock**

$| \sigma_{ci} |$  kN/m<sup>2</sup> 0.000

**Hoek-Brown parameters**

Determination Derived

$m_b$  0.000

$s$  0.02609E-3

$a$  0.6192

$m_i$  0.000

GSI 5.000

$D$  0.000

**Rock mass parameters**

$\sigma_c$  kN/m<sup>2</sup> 0.000

$\sigma_c$  kN/m<sup>2</sup> 0.000

**Tension**

Tension cut-off ☒

Tensile strength kN/m<sup>2</sup> 0.000

**Dilatancy**

$\psi_{max}$  ° 0.000

$\sigma_\psi$  kN/m<sup>2</sup> 0.000

**Excess pore pressure calculation**

Determination v-undrained definition

$v_u$  definition method Direct

$v_{u, equivalent}$  (nu) 0.4950

Skempton B 0.9933

Analysis GSI

Rock type: General

STRUCTURE	VERY GOOD Very rough, fresh unweathered surfaces.	GOOD Slightly weathered, iron stained surfaces.	FAIR Moderately weathered surfaces.	POOR Highly weathered surfaces with complete fillings with angular fragments.	VERY POOR Disintegrated, highly weathered
<b>INTACT OR MASSIVE</b> Intact rock specimens or massive in situ rock with few widely spaced discontinuities.	90			N/A	N/A
<b>BLOCKY</b> Well interlocked undisturbed rock mass consisting of cubical blocks formed by three intersecting discontinuity sets.	80	70			
<b>VERY BLOCKY</b> Interlocked, partially disturbed mass with multi-faceted angular blocks formed by 4 or more joint sets.		60	50		
<b>BLOCKY DISTURBED/SEAMY</b> Folded with angular blocks formed by many intersecting discontinuity sets. Persistence of bedding planes or schistosity.			40	30	
<b>DISINTEGRATED</b> Poorly interlocked, heavily broken rock mass with mixture of angular and rounded rock pieces.				20	
<b>LAMINATED/SHEARED</b> Lack of blockiness due to close spacing of weak schistosity or shear planes.	N/A	N/A			10

Next OK Cancel

Figure 16: Geological Strength Index GSI for Hoek-Brown model

### 4.3.6 Disturbance factor $D$

The *Disturbance factor*,  $D$ , is a parameter that depends on the amount of disturbance of the rock as a result of mechanical processes in open excavations, tunnels or mines, such as blasting, tunnel boring, machine driven or manual excavation. No disturbance is equivalent to  $D = 0$ , whereas severe disturbance is equivalent to  $D = 1$ . For more information see [Hoek \(2006\)](#) (on page 247). Typical values are given in the side panel of the pre-processing tool.

# The Hoek-Brown model (rock behaviour)

## Parameters of the Hoek-Brown model

The screenshot shows the PLAXIS 3D software interface for the Hoek-Brown model. The left pane displays a tree view of parameters, and the right pane shows a list of disturbance factor  $D$  values for different excavation scenarios.

Property	Unit	Value
<b>Stiffness</b>		
$E_{rm}$	kN/m <sup>2</sup>	0.000
$\nu$ ( $\nu_u$ )		0.000
<b>Alternatives</b>		
$G_{ref}$	kN/m <sup>2</sup>	0.000
<b>Strength</b>		
<b>Uniaxial compressive strength of intact</b>		
$ \sigma_{ci} $	kN/m <sup>2</sup>	0.000
<b>Hoek-Brown parameters</b>		
Determination	Derived	
$m_b$		0.000
$s$		0.02605E-3
$a$		0.6192
$m_i$		0.000
GSI		5.000
$D$		0.000
<b>Rock mass parameters</b>		
$\sigma_c$	kN/m <sup>2</sup>	0.000
$\sigma_t$	kN/m <sup>2</sup>	0.000
<b>Tension</b>		
Tension cut-off		<input checked="" type="checkbox"/>
Tensile strength	kN/m <sup>2</sup>	0.000
<b>Dilatancy</b>		
$\psi_{max}$	°	0.000
$\sigma_\psi$	kN/m <sup>2</sup>	0.000
<b>Excess pore pressure calculation</b>		
Determination	v-undrained definition	
$v_u$ definition method	Direct	
$v_{u, equivalent}$ ( $\nu_u$ )		0.4950
Skempton B		0.9933

**Disturbance factor  $D$  for Hoek-Brown model**

- Tunnel excavation by TBM or blasting of excellent quality.  $D = 0.000$
- Tunnel excavation by hand or using a mechanical process rather than blasting, in poor quality rock. There are no squeezing problems leading to floor heave, or these are mitigated using a temporary invert.  $D = 0.000$
- Tunnel excavation by hand or using a mechanical process rather than blasting, in poor quality rock. There are unmitigated squeezing problems leading to floor heave.  $D = 0.5000$
- Tunnel excavation using blasting of very poor quality, leading to severe local damage.  $D = 0.8000$
- Slope created using controlled, small scale blasting of good quality.  $D = 0.7000$
- Slope created using small scale blasting of poor quality.  $D = 1.000$
- Slope in very large open pit mine, created using heavy production blasting.  $D = 1.000$
- Slope in very large open pit mine, created using mechanical excavation in softer rocks.  $D = 0.7000$

Figure 17: Disturbance factor  $D$  for Hoek-Brown model

**Note:** The disturbance factor  $D$  should only be applied to the actual zone of damaged rock in order to avoid greatly underestimation of the strength and overall stability. The thickness  $T$  of the blast damaged zone depends upon the design of the blast (Reference Manual- Chapter 6- Hoek-Brown preprocessing tool).

### 4.3.7 Tension cut-off

The Hoek-Brown model simulates the *Tensile strength* of the rock mass via the  $|\sigma_{ci}|$  parameter, calculated from rock properties  $\sigma_c$ ,  $s$  and  $m_b$ . To enhance modelling capabilities and flexibility, PLAXIS 3D allows to calibrate separately the rock tensile strength using tension cut-off facility. By default the tension cut-off option is disabled. When enabled, users can put a tensile strength value, and if that value is lower than  $\sigma_b$ , the tensile capacity will be cut-off at that value. This feature can be helpful in some situations, for instance in Safety analysis where this tension cut-off value (but not the  $\sigma_t$  parameter) is reduced with the safety factor.

### 4.3.8 Dilatancy $\psi$ and $\sigma_\psi$

Rocks may show dilatant material behaviour when subjected to shear under relatively low confining stress. At larger confining stress, dilatancy is suppressed. This behaviour is modelled by means of a specified value of  $\psi$  for

## The Hoek-Brown model (rock behaviour)

On the use of the Hoek-Brown model in dynamics calculations

---

$\sigma_3 = 0$ , with a linear decrease down to zero for  $\sigma'_3 = \sigma_\psi$ , where  $\sigma_\psi$  is an additional input parameter ([Figure 13](#) (on page 45)).

### 4.4 On the use of the Hoek-Brown model in dynamics calculations

When using the Hoek-Brown model in dynamics calculations, the stiffness need to be selected such that the model correctly predicts wave velocities in the soil (Eq. [84]). When subjected to dynamic or cyclic loading, the Hoek-Brown model may generate plastic strains if stress points reach the Hoek-Brown failure criterion, which will lead to damping in dynamics calculations. However, the stress cycles within the Hoek-Brown failure contour will only generate elastic strains and no (hysteretic) damping, nor accumulation of strains or pore pressure or liquefaction. In order to simulate the rock's damping characteristics in cyclic loading, Rayleigh damping may be defined.

## The Jointed Rock model (anisotropy)

Materials may have different properties in different directions. As a result, they may respond differently when subjected to particular conditions in one direction or another. This aspect of material behaviour is called anisotropy. When modelling anisotropy, distinction can be made between elastic anisotropy and plastic anisotropy. Elastic anisotropy refers to the use of different elastic stiffness properties in different directions. Plastic anisotropy may involve the use of different strength properties in different directions, as considered in the Jointed Rock model. Another form of plastic anisotropy is kinematic hardening. The latter is not considered in PLAXIS.

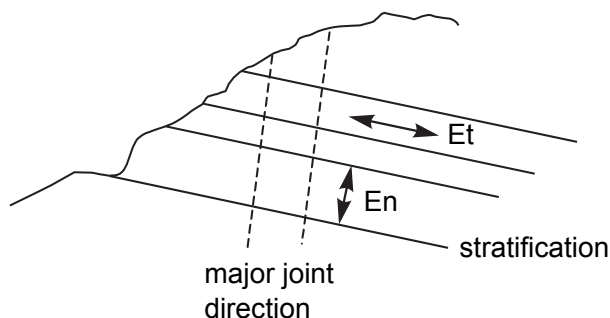


Figure 18: Visualization of concept behind the Jointed Rock model

The Jointed Rock model is an anisotropic elastic perfectly-plastic model, especially meant to simulate the behaviour of stratified and jointed rock layers. In this model it is assumed that there is intact rock with an optional stratification direction and major joint directions. The intact rock is considered to behave as a transversely anisotropic elastic material, quantified by five parameters and a direction. The anisotropy may result from stratification or from other phenomena. In the major joint directions it is assumed that shear stresses are limited according to Coulomb's criterion. Upon reaching the maximum shear stress in such a direction, plastic sliding will occur. A maximum of three sliding directions ('planes') can be defined, of which the first plane is assumed to coincide with the direction of elastic anisotropy. Each plane may have different shear strength properties. In addition to plastic shearing, the tensile stresses perpendicular to the three planes are limited according to a predefined tensile strength (tension cut-off).

The application of the Jointed Rock model is justified when families of joints or joint sets are present. These joint sets have to be parallel, not filled with fault gouge, and their spacing has to be small compared to the characteristic dimension of the structure.

Some basic characteristics of the Jointed Rock model are:

- Anisotropic elastic behaviour for intact rock: Parameters  $E_b$ ,  $E_m$ ,  $\nu_{nb}$ ,  $\nu_{ts}$ ,  $G_{nt}$
- Shear failure according to Coulomb in 3 directions: Parameters  $c_i$ ,  $\varphi_i$  and  $\psi_i$
- Limited tensile strength in three directions: Parameters  $\sigma_{t,i}$

## The Jointed Rock model (anisotropy)

### Anisotropic elastic material stiffness matrix

## 5.1 Anisotropic elastic material stiffness matrix

The elastic material behaviour in the Jointed Rock model is described by an elastic material stiffness matrix,  $\mathbf{D}^*$ . In contrast to Hooke's law, the  $\mathbf{D}^*$ -matrix as used in the Jointed Rock model is transversely anisotropic. Different stiffnesses can be used normal to and in a predefined direction ('plane 1'). This direction may correspond to the stratification direction or to any other direction with significantly different elastic stiffness properties.

Consider, for example, a horizontal stratification, where the stiffness in z- direction,  $E_n$ , is different from the stiffness in the rock as a continuum,  $E_t$ . In this case the 'plane 1' direction is parallel to the xy-plane and the following constitutive relations exist (See: Zienkiewicz & Taylor: The Finite Element Method, 4th Ed.):

$$\begin{aligned}
 \dot{\varepsilon}_{xx} &= \frac{\dot{\sigma}_{xx}}{E_t} - \frac{v_{nt}\dot{\sigma}_{yy}}{E_t} - \frac{v_{ts}\dot{\sigma}_{zz}}{E_n} & a) \\
 \dot{\varepsilon}_{yy} &= \frac{v_{nt}\dot{\sigma}_{xx}}{E_t} + \frac{\dot{\sigma}_{yy}}{E_t} - \frac{v_{ts}\dot{\sigma}_{zz}}{E_n} & b) \\
 \dot{\varepsilon}_{zz} &= \frac{v_{ts}\dot{\sigma}_{xx}}{E_n} - \frac{v_{ts}\dot{\sigma}_{yy}}{E_n} + \frac{\dot{\sigma}_{zz}}{E_n} & c) \\
 \dot{\gamma}_{xy} &= \frac{2(1+v_{nt})}{E_t}\dot{\sigma}_{xy} & d) \\
 \dot{\gamma}_{yz} &= \frac{\dot{\sigma}_{yz}}{G_{nt}} & e) \\
 \dot{\gamma}_{zx} &= \frac{\dot{\sigma}_{zx}}{G_{nt}} & f)
 \end{aligned}$$

Eq. [106]

The inverse of the anisotropic elastic material stiffness matrix,  $(\mathbf{D}^*)^{-1}$ , follows from the above relations. This matrix is symmetric. The regular material stiffness matrix  $\mathbf{D}^*$  can only be obtained by numerical inversion.

In order for the  $\mathbf{D}^*$  to remain positive definite, the following requirement has to be obeyed:

$$v_{ts} < \sqrt{\frac{E_n}{E_t} \left( \frac{1 - v_{nt}}{2} \right)} \quad \text{Eq. [107]}$$

In general, the stratification plane will not be parallel to the global xy-plane, but the above relations will generally hold for a local  $(n,s,t)$  coordinate system where the stratification plane is parallel to the st-plane. The orientation of this plane is defined by the *dip angle* (or shortly *dip*) and *strike* (see [Parameters of the Jointed Rock model](#) (on page 60)). As a consequence, the local material stiffness matrix has to be transformed from the local to the global coordinate system. Therefore we consider first a transformation of stresses and strains:

$$\sigma_{nst} = \mathbf{R}_\sigma \sigma_{xyz} \quad \sigma_{xyz} = \mathbf{R}_\sigma^{-1} \sigma_{nst} \quad \text{Eq. [108]}$$

$$\varepsilon_{nst} = \mathbf{R}_\varepsilon \varepsilon_{xyz} \quad \varepsilon_{xyz} = \mathbf{R}_\varepsilon^{-1} \varepsilon_{nst} \quad \text{Eq. [109]}$$

where

## The Jointed Rock model (anisotropy)

Anisotropic elastic material stiffness matrix

$$\mathbf{R}_o = \begin{bmatrix} n_x^2 & n_y^2 & n_z^2 & 2n_x n_y & 2n_y n_z & 2n_x n_z \\ s_x^2 & s_y^2 & s_z^2 & 2s_x s_y & 2s_y s_z & 2s_x s_z \\ t_x^2 & t_y^2 & t_z^2 & 2t_x t_y & 2t_y t_z & 2t_x t_z \\ n_x s_x & n_y s_y & n_z s_z & n_x s_y + n_y s_x & n_y s_z + n_z s_y & n_z s_x + n_x s_z \\ s_x t_x & s_y t_y & s_z t_z & s_x t_y + s_y t_x & s_y t_z + s_z t_y & s_x t_z + s_z t_x \\ n_x t_x & n_y t_y & n_z t_z & n_x t_y + n_y t_x & n_y t_z + n_z t_y & n_z t_x + n_x s_z \end{bmatrix} \quad Eq. [110]$$

and

$$\mathbf{R}_\varepsilon = \begin{bmatrix} n_x^2 & n_y^2 & n_z^2 & n_x n_y & n_y n_z & n_x n_z \\ s_x^2 & s_y^2 & s_z^2 & s_x s_y & s_y s_z & s_x s_z \\ t_x^2 & t_y^2 & t_z^2 & t_x t_y & t_y t_z & t_x t_z \\ 2n_x s_x & 2n_y s_y & 2n_z s_z & n_x s_y + n_y s_x & n_y s_z + n_z s_y & n_z s_x + n_x s_z \\ 2s_x t_x & 2s_y t_y & 2s_z t_z & s_x t_y + s_y t_x & s_y t_z + s_z t_y & s_x t_z + s_z t_x \\ 2n_x t_x & 2n_y t_y & 2n_z t_z & n_x t_y + n_y t_x & n_y t_z + n_z t_y & n_z t_x + n_x s_z \end{bmatrix} \quad Eq. [111]$$

$n_x, n_y, n_z, s_x, s_y, s_z, t_x, t_y$  and  $t_z$  are the components of the normalised  $n, s$  and  $t$ -vectors in global  $(x,y,z)$ -coordinates (i.e. 'sines' and 'cosines'; see [Parameters of the Jointed Rock model](#) (on page 60)). For plane strain condition  $n_z = s_z = t_x = t_y = 0$  and  $t_z = 1$ .

It further holds that:

$$\mathbf{R}_\varepsilon^T = \mathbf{R}_o^{-1} \quad \mathbf{R}_o^T = \mathbf{R}_\varepsilon^{-1} \quad Eq. [112]$$

A local stress-strain relationship in  $(n,s,t)$ -coordinates can be transformed to a global relationship in  $(x,y,z)$ -coordinates in the following way:

$$\left. \begin{aligned} \sigma_{nst} &= \mathbf{D}_{nst}^* \varepsilon_{nst} \\ \sigma_{nst} &= \mathbf{R}_{nst}^* \sigma_{xyz} \\ \varepsilon_{nst} &= \mathbf{R}_{nst}^* \varepsilon_{xyz} \end{aligned} \right\} \Rightarrow \mathbf{R}_o \sigma_{xyz} = \mathbf{D}_{nst}^* \mathbf{R}_\varepsilon \varepsilon_{xyz} \quad Eq. [113]$$

Hence,

$$\sigma_{xyz} = \mathbf{R}_o^{-1} \mathbf{D}_{nst}^* \mathbf{R}_\varepsilon \varepsilon_{xyz} \quad Eq. [114]$$

Using to above condition (Eq. [112])

$$\sigma_{xyz} = \mathbf{R}_\varepsilon^T \mathbf{D}_{nst}^* \mathbf{R}_\varepsilon \varepsilon_{xyz} = \mathbf{D}_{xyz}^* \varepsilon_{xyz} \quad \text{or} \quad \mathbf{D}_{xyz}^* = \mathbf{R}_\varepsilon^T \mathbf{D}_{nst}^* \mathbf{R}_\varepsilon \quad Eq. [115]$$

Actually, not the  $\mathbf{D}^*$ -matrix is given in local coordinates but the inverse matrix  $(\mathbf{D}^*)^{-1}$ .

$$\left. \begin{aligned} \varepsilon_{nst} &= \mathbf{D}_{nst}^* \sigma_{nst} \\ \sigma_{nst} &= \mathbf{R}_o^* \sigma_{xyz} \\ \varepsilon_{nst} &= \mathbf{R}_\varepsilon^* \varepsilon_{xyz} \end{aligned} \right\} \Rightarrow \varepsilon_{xyz} = \mathbf{R}_\varepsilon^{-1} \mathbf{D}_{nst}^{*-1} \mathbf{R}_o \sigma_{xyz} = \mathbf{R}_\varepsilon^T \mathbf{D}_{nst}^{*-1} \mathbf{R}_o \sigma_{xyz} \quad Eq. [116]$$

## The Jointed Rock model (anisotropy)

Plastic behaviour in three directions

Hence,

$$\mathbf{D}_{xyz}^{*-1} = \mathbf{R}_o^T \mathbf{D}_{nst}^{*-1} \mathbf{R}_o \quad \text{or} \quad \mathbf{D}_{xyz}^* = [\mathbf{R}_o^T \mathbf{D}_{nst}^{*-1} \mathbf{R}_o]^{-1} \quad \text{Eq. [117]}$$

Instead of inverting the  $(\mathbf{D}_{nst}^{*-1})$ -matrix in the first place, the transformation is considered first, after which the total is numerically inverted to obtain the global material stiffness matrix  $\mathbf{D}_{xyz}^*$ .

## 5.2 Plastic behaviour in three directions

A maximum of 3 sliding directions (sliding planes) can be defined in the Jointed Rock model. The first sliding plane corresponds to the direction of elastic anisotropy. In addition, a maximum of two other sliding directions may be defined. However, the formulation of plasticity on all planes is similar. On each plane a local Coulomb condition applies to limit the shear stress,  $|\tau|$ . Moreover, a tension cut-off criterion is used to limit the tensile stress on a plane. Each plane,  $i$ , has its own strength parameters  $c_i$ ,  $\varphi_i$ ,  $\psi_i$  and  $\sigma_{t,i}$ .

In order to check the plasticity conditions for a plane with local  $(n, s, t)$ -coordinates it is necessary to calculate the local stresses from the Cartesian stresses. The local stresses involve three components, i.e. a normal stress component,  $\sigma_n$ , and two independent shear stress components,  $\tau_s$  and  $\tau_t$ .

$$\underline{\sigma}_i = \mathbf{T}_i^T \underline{\sigma} \quad \text{Eq. [118]}$$

where

$$\begin{aligned} \underline{\sigma} &= (\sigma_n \ \tau_s \ \tau_t)^T & a) \\ \underline{\sigma} &= (\sigma_{xx} \ \sigma_{yy} \ \sigma_{zz} \ \sigma_{xy} \ \sigma_{yz} \ \sigma_{zx})^T & b) \end{aligned} \quad \text{Eq. [119]}$$

$\mathbf{T}_i^T = \text{transformation matrix } (3 \times 6), \text{ for plane } i$

As usual in PLAXIS, tensile (normal) stresses are defined as positive whereas compression is defined as negative.

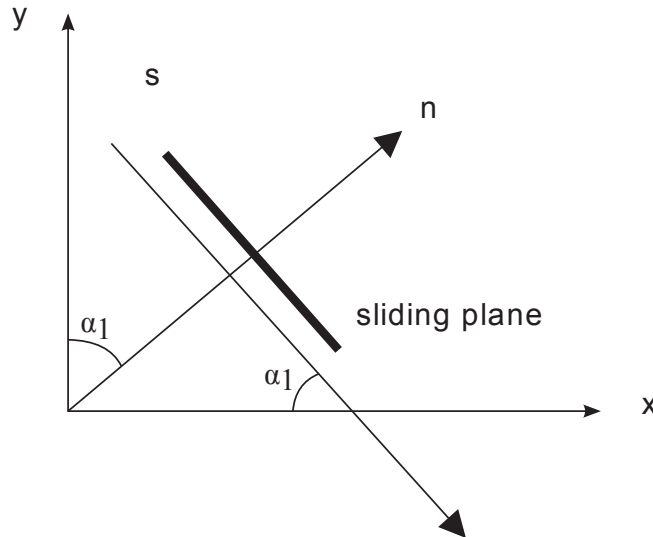


Figure 19: Plane strain situation with a single sliding plane and vectors  $n, s$

## The Jointed Rock model (anisotropy)

Plastic behaviour in three directions

Consider a plane strain situation as visualised in [Figure 19](#) (on page 58). Here a sliding plane is considered under an angle  $\alpha_1$  (= *dip*) with respect to the x-axis. In this case the transformation matrix  $\mathbf{T}^T$  becomes:

$$\mathbf{T}^T = \begin{bmatrix} s^2 & c^2 & 0 & -2sc & 0 & 0 \\ sc & -sc & 0 & -s^2 + c^2 & 0 & 0 \\ 0 & 0 & 0 & 0 & -c & -c \end{bmatrix} \quad \text{Eq. [120]}$$

where:

$$s = \sin(\alpha_1)$$

$$c = \cos(\alpha_1)$$

In the general three-dimensional case the transformation matrix is more complex, since it involves both *dip* and *strike* (see [Parameters of the Jointed Rock model](#) (on page 60)):

$$\mathbf{T}^T = \begin{bmatrix} n_x^2 & n_y^2 & n_z^2 & 2n_xn_y & 2n_y n_z & 2n_z n_x \\ n_x s_x & n_y s_y & n_z s_z & n_x s_y + n_y s_x & n_z s_y + n_y s_z & n_z s_x + n_x s_z \\ n_x t_x & n_y t_y & n_z t_z & n_y t_x + n_x t_y & n_y t_z + n_z t_y & n_z t_x + n_x t_z \end{bmatrix} \quad \text{Eq. [121]}$$

Note that the general transformation matrix,  $\mathbf{T}$ , for the calculation of local stresses corresponds to rows 1, 4 and 6 of  $\mathbf{R}_\sigma$  (see Eq. [110]).

After having determined the local stress components, the plasticity conditions can be checked on the basis of yield functions. The yield functions for plane *i* are defined as:

$$\begin{aligned} f_i^c &= |\tau_s| + \sigma_n \tan(\alpha_i) - c_i & (\text{Coulomb}) \\ f_i^c &= \sigma_n - \sigma_{t,i} (\sigma_{t,i} \leq c_i \cot(\phi_i)) & (\text{Tension cut-off}) \end{aligned} \quad \text{Eq. [122]}$$

[Figure 20](#) (on page 59) visualizes the full yield criterion on a single plane.

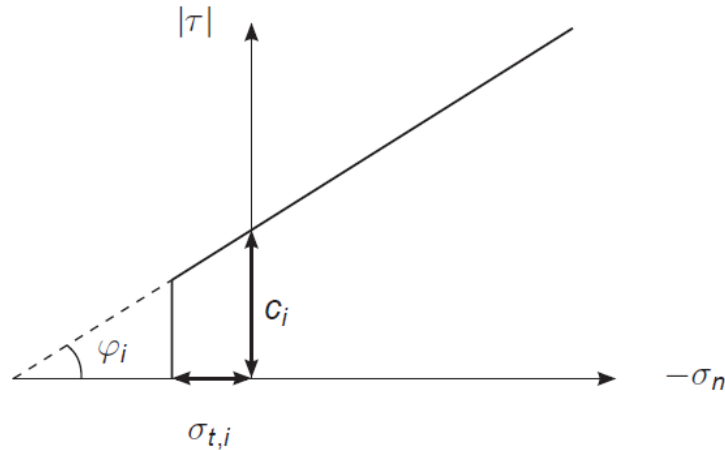


Figure 20: Yield criterion for individual plane

The local plastic strains are defined by:

## The Jointed Rock model (anisotropy)

Parameters of the Jointed Rock model

$$\Delta \varepsilon_j^p = \lambda_j \frac{\partial g_j^c}{\partial a_j} \quad \text{Eq. [123]}$$

where  $g_j$  is the local plastic potential function for plane  $j$ :

$$\begin{aligned} g_i^c &= |\tau_j| + \sigma_n \tan(\psi_i) - c_i & (\text{Coulomb}) \\ g_i^c &= \sigma_n - \sigma_{t,i} & (\text{Tension cut-off}) \end{aligned} \quad \text{Eq. [124]}$$

The transformation matrix,  $\mathbf{T}$ , is also used to transform the local plastic strain increments of plane  $j$ ,  $\Delta \varepsilon_j^p$ , into global plastic strain increments,  $\Delta \varepsilon^p$ :

$$\Delta \varepsilon^p = \mathbf{T}_j \Delta \varepsilon_j^p \quad \text{Eq. [125]}$$

The consistency condition requires that at yielding the value of the yield function must remain zero for all active yield functions. For all planes together, a maximum of 6 yield functions exist, so up to 6 plastic multipliers must be found such that all yield functions are at most zero and the plastic multipliers are non-negative.

$$\begin{aligned} f_i^c &= f_i^{c(e)} - \sum_{j=1}^{np} \langle \lambda_j^c \rangle \frac{\partial f_i^c}{\partial \sigma} T_i^T D T_j \frac{\partial g_j^c}{\partial \sigma} - \sum_{j=1}^{np} \langle \lambda_j^t \rangle \frac{\partial f_i^c}{\partial \sigma} T_i^T D T_j \frac{\partial g_j^t}{\partial \sigma} \\ f_i^t &= f_i^{t(e)} - \sum_{j=1}^{np} \langle \lambda_j^c \rangle \frac{\partial f_i^t}{\partial \sigma} T_i^T D T_j \frac{\partial g_j^c}{\partial \sigma} - \sum_{j=1}^{np} \langle \lambda_j^t \rangle \frac{\partial f_i^t}{\partial \sigma} T_i^T D T_j \frac{\partial g_j^t}{\partial \sigma} \end{aligned} \quad \text{Eq. [126]}$$

This means finding up to 6 values of  $\lambda_i \geq 0$  such that all  $f_i \leq 0$  and  $\lambda_i f_i = 0$ .

When the maximum of 3 planes are used, there are  $2^6 = 64$  possibilities of (combined) yielding. In the calculation process, all these possibilities are taken into account in order to provide an exact calculation of stresses.

### 5.3 Parameters of the Jointed Rock model

Most parameters of the Jointed Rock model coincide with those of the isotropic Mohr-Coulomb model. These are the basic elastic parameters and the basic strength parameters.

Elastic parameters as in Mohr-Coulomb model (see <a href="#">Parameters of the Mohr-Coulomb model</a> (on page 34))		
$E_t$	Young's modulus for rock as a continuum	[kN/m <sup>2</sup> ]
$\nu_{nt}$	Poisson's ratio for rock as a continuum	[-]
Anisotropic elastic parameters 'Plane 1' direction (e.g. stratification direction)		
$E_n$	Young's modulus perpendicular to 'Plane 1' direction	[kN/m <sup>2</sup> ]
$G_{nt}$	Shear modulus perpendicular to 'Plane 1' direction	[kN/m <sup>2</sup> ]

## The Jointed Rock model (anisotropy)

Parameters of the Jointed Rock model

Anisotropic elastic parameters 'Plane 1' direction (e.g. stratification direction)		
$\nu_{ts}$	Poisson's ratio perpendicular to 'Plane 1' direction $\nu_{ts} < \sqrt{\frac{E_n}{E_t} \left( \frac{1 - \nu_{nt}}{2} \right)}$	[-]
Strength parameters in joint directions (Plane i=1, 2, 3):		
$c_i$	Cohesion	[kN/m <sup>2</sup> ]
$\varphi_i$	Friction angle	[°]
$\psi_i$	Dilatancy angle	[°]
$\sigma_{t,i}$	Tensile strength	[kN/m <sup>2</sup> ]
Definition of joint directions (Plane i=1, 2, 3):		
Number of planes	Number of joint directions ( $1 \leq n \leq 3$ )	[-]
$\alpha_{1,i}$	Dip ( $-180 \leq \alpha_{1,i} \leq 180$ )	[°]
$\alpha_{2,i}$	Strike ( $-180 \leq \alpha_{2,i} \leq 180$ ) ( $\alpha_{2,i} = 90$ in PLAXIS 2D)	[°]

# The Jointed Rock model (anisotropy)

## Parameters of the Jointed Rock model

Figure 21: Parameters for the Jointed Rock model

### 5.3.1 Elastic parameters

The elastic parameters  $E_t$  and  $v_{nt}$  are the (constant) stiffness (Young's modulus) and Poisson's ratio of the rock as a continuum according to Hooke's law, i.e. as if it would not be anisotropic.

Elastic anisotropy in a rock formation may be introduced by stratification. The stiffness perpendicular to the stratification direction is usually reduced compared with the general stiffness. This reduced stiffness can be represented by the parameter  $E_n$ , together with a second Poisson's ratio,  $v_{ts}$ . In general, the elastic stiffness normal to the direction of elastic anisotropy is defined by the parameters  $E_n$  and  $v_{ts}$ . In order to avoid singularity of the material stiffness matrix, the input of  $v_{ts}$  is limited by:

$$v_{ts} < \sqrt{\frac{E_n}{E_t} \left( \frac{1 - v_{nt}}{2} \right)} \quad \text{Eq. [127]}$$

Elastic shearing in the stratification direction is also considered to be 'weaker' than elastic shearing in other directions. In general, the shear stiffness in the anisotropic direction can explicitly be defined by means of the elastic shear modulus  $G_{nt}$ . In contrast to Hooke's law of isotropic elasticity,  $G_{nt}$  is a separate parameter and is not simply related to Young's modulus by means of Poisson's ratio (see [Eq.106](#) (on page 56) (d) & (e)).

If the elastic behaviour of the rock is fully isotropic, then the parameters  $E_n$  and  $v_{ts}$  can be simply set equal to  $E_t$  and  $v_{nt}$  respectively, whereas  $G_{nt}$  should be set to  $1/2E_t/(1+v_{nt})$ .

## The Jointed Rock model (anisotropy)

### Parameters of the Jointed Rock model

---

#### 5.3.2 Strength parameters

Each sliding direction (plane) has its own strength properties  $c_i$ ,  $\varphi_i$  and  $\sigma_{t,i}$  and dilatancy angle  $\psi_i$ . The strength properties  $c_i$  and  $\varphi_i$  determine the allowable shear strength according to Coulomb's criterion and  $\sigma_t$  determines the tensile strength according to the tension cut-off criterion. The latter is displayed after pressing *Advanced* button. By default, the tension cut-off is active and the tensile strength is set to zero. The dilatancy angle,  $\psi_i$ , is used in the plastic potential function  $g$ , and determines the plastic volume expansion due to shearing.

#### 5.3.3 Definition of joint directions

It is assumed that the direction of elastic anisotropy corresponds with the first direction where plastic shearing may occur ('plane 1'). This direction must always be specified. In the case the rock formation is stratified without major joints, the *number of sliding planes* (= sliding directions) is still 1, and strength parameters must be specified for this direction anyway. A maximum of three sliding directions can be defined. These directions may correspond to the most critical directions of joints in the rock formation.

The sliding directions are defined by means of two parameters: The *Dip angle* ( $\alpha_1$ ) (or shortly *Dip*) and the *Strike* ( $\alpha_2$ ). The definition of both parameters is visualised in [Figure 22](#) (on page 64).

Consider a sliding plane, as indicated in [Figure 22](#) (on page 64). The sliding plane can be defined by the vectors  $(s, t)$ , which are both normal to the vector  $n$ . The vector  $n$  is the 'normal' to the sliding plane, whereas the vector  $s$  is the 'fall line' of the sliding plane (*dip*) and the vector  $t$  is the 'horizontal line' of the sliding plane (*strike*). The sliding plane makes an angle  $\alpha_1$  with respect to the horizontal plane, where the horizontal plane can be defined by the vectors  $(s^*, t)$ , which are both normal to the vertical axis. The angle  $\alpha_1$  is the *dip*, which is defined as the positive 'downward' inclination angle between the horizontal plane and the sliding plane. Hence,  $\alpha_1$  is the angle between the vectors  $s^*$  and  $s$ , measured clockwise from  $s^*$  to  $s$  when looking in the positive  $t$ -direction. The dip ought to be entered in the range  $[0^\circ, 90^\circ]$ , but negative values as well as values larger than  $90^\circ$  can also be entered.

## The Jointed Rock model (anisotropy)

Parameters of the Jointed Rock model

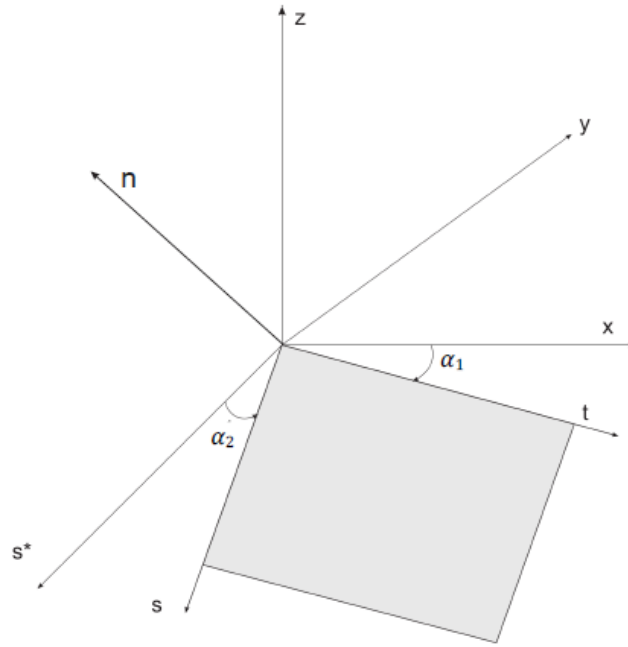


Figure 22: Definition of dip angle and strike

The orientation of the sliding plane is further defined by the *strike*,  $\alpha_2$ , which is defined in PLAXIS as the orientation of the vector  $t$  with respect to the  $x$ -direction. The strike is defined as the positive angle from the  $x$ -direction, measured clockwise to the  $t$ -axis. The dip direction is entered in the range  $[-180^\circ, 180^\circ]$ .

From the definitions as given above, it follows for PLAXIS 3D that:

$$\underline{n} = \begin{bmatrix} n_x \\ n_y \\ n_z \end{bmatrix} = \begin{bmatrix} -\sin(\alpha_1)\sin(\alpha_2) \\ -\sin(\alpha_1)\cos(\alpha_2) \\ \cos(\alpha_1) \end{bmatrix} \quad \text{Eq. [128]}$$

$$\underline{s} = \begin{bmatrix} s_x \\ s_y \\ s_z \end{bmatrix} = \begin{bmatrix} -\cos(\alpha_1)\sin(\alpha_2) \\ -\cos(\alpha_1)\cos(\alpha_2) \\ -\sin(\alpha_1) \end{bmatrix} \quad \text{Eq. [129]}$$

$$\underline{t} = \begin{bmatrix} t_x \\ t_y \\ t_z \end{bmatrix} = \begin{bmatrix} \cos(\alpha_2) \\ -\sin(\alpha_2) \\ -\sin(\alpha_1) \end{bmatrix} \quad \text{Eq. [130]}$$

whereas for PLAXIS 2D  $\alpha_2$  is taken by definition as  $\alpha_2 = 90^\circ$ , such that:

$$\underline{n} = \begin{bmatrix} n_x \\ n_y \\ n_z \end{bmatrix} = \begin{bmatrix} -\sin(\alpha_1) \\ \cos(\alpha_1) \\ 0 \end{bmatrix} \quad \text{Eq. [131]}$$

## The Jointed Rock model (anisotropy)

Parameters of the Jointed Rock model

$$s = \begin{bmatrix} s_x \\ s_y \\ s_z \end{bmatrix} = \begin{bmatrix} -\cos(\alpha_1) \\ -\sin(\alpha_2) \\ 0 \end{bmatrix} \quad Eq. [132]$$

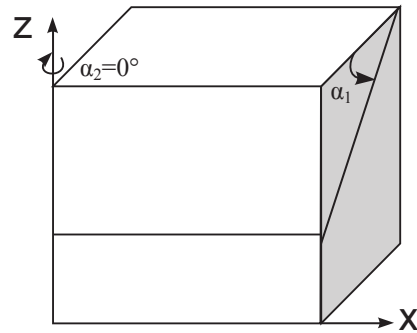
$$t = \begin{bmatrix} t_x \\ t_y \\ t_z \end{bmatrix} = \begin{bmatrix} 0 \\ 0 \\ 1 \end{bmatrix} \quad Eq. [133]$$

Figure 23 (on page 65) shows some examples of how sliding planes occur in a 3D models for different values of  $\alpha_1$  and  $\alpha_2$ . As it can be seen, for plane strain conditions (the cases considered in PLAXIS 2D) only  $\alpha_1$  is required. By default,  $\alpha_2$  is fixed at  $90^\circ$ .

Plaxis 3D

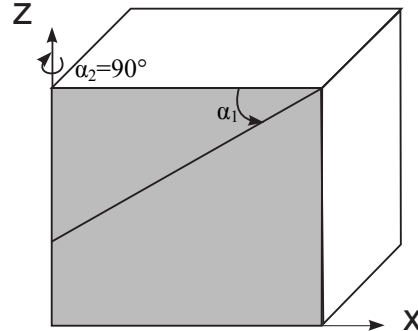
$$\alpha_1 = 30^\circ$$

$$\alpha_2 = 0^\circ$$



$$\alpha_1 = 30^\circ$$

$$\alpha_2 = 90^\circ$$



Plaxis 2D

$$\alpha_1 = 30^\circ$$

$$\alpha_2 = 90^\circ$$

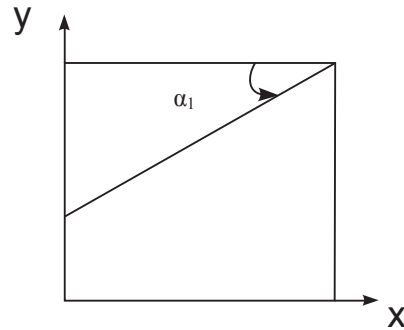


Figure 23: Examples of failure directions defined by  $\alpha_1$  and  $\alpha_2$

## The Jointed Rock model (anisotropy)

On the use of the Jointed Rock model in dynamics calculations

---

### 5.4 On the use of the Jointed Rock model in dynamics calculations

When using the Jointed Rock model in dynamics calculations, the stiffness need to be selected such that the model correctly predicts wave velocities in the soil (Equation Eq. [84]). When subjected to dynamic or cyclic loading, the Jointed Rock model may generate plastic strains if stress points reach the Coulomb failure criterion, which will lead to damping in dynamics calculations. However, it should be noted that stress cycles within the Coulomb failure contour will only generate elastic strains and no (hysteretic) damping, nor accumulation of strains or pore pressure or liquefaction. In order to simulate the rock's damping characteristics in cyclic loading, Rayleigh damping may be defined.

**Note:** A slightly modified version of the Jointed Rock model with generalised Mohr-Coulomb failure criterion in addition to the individual failure directions is available as user-defined soil model. Contact Plaxis for more information.

**Note:**

- In a geological context, *strike* is defined as the angle from the North to the *strike* of the *dipping plane* (positive towards East direction), whereas in PLAXIS definition *strike* is defined from the global *x-direction* to the strike of the dipping plane (with the same positive rotation direction). If we define the angle from the North direction to the *x-direction* of the PLAXIS model as declination, then strike in PLAXIS is the geological strike minus declination.
- Moreover, there might be confusion between true *strike* and its opposite direction ( $180^\circ$  direction). Hence, care must be taken when translating *strike* from geological data into PLAXIS input.

## The Hardening Soil model (Isotropic hardening)

In contrast to an elastic perfectly-plastic model, the yield surface of a hardening plasticity model is not fixed in principal stress space, but it can expand due to plastic straining. Distinction can be made between two main types of hardening, namely shear hardening and compression hardening. Shear hardening is used to model irreversible strains due to primary deviatoric loading. Compression hardening is used to model irreversible plastic strains due to primary compression in oedometer loading and isotropic loading. Both types of hardening are contained in the present model.

The Hardening Soil model is an advanced model for simulating the behaviour of different types of soil, both soft soils and stiff soils, [Shanz \(1998\)](#) (on page 248). When subjected to primary deviatoric loading, soil shows a decreasing stiffness and simultaneously irreversible plastic strains develop. In the special case of a drained triaxial test, the observed relationship between the axial strain and the deviatoric stress can be well approximated by a hyperbola. Such a relationship was first formulated by [Kondner \(1963\)](#) (on page 247) and later used in the well-known hyperbolic model ([Duncan & Chang, 1970](#)) (on page 246). The Hardening Soil model, however, supersedes the hyperbolic model by far: Firstly by using the theory of plasticity rather than the theory of elasticity, secondly by including soil dilatancy and thirdly by introducing a yield cap. Some basic characteristics of the model are:

- Stress dependent stiffness according to a power law: Input parameter  $m$
- Plastic straining due to primary deviatoric loading: Input parameter  $E_{50}^{ref}$
- Plastic straining due to primary compression: Input parameter  $E_{oed}^{ref}$
- Elastic unloading / reloading: Input parameters  $E_{ur}^{ref}$ ,  $v_{ur}$
- Failure according to the Mohr-Coulomb failure criterion: Parameters  $c$ ,  $\varphi$  and  $\psi$

A basic feature of the present Hardening Soil model is the stress dependency of soil stiffness. For oedometer conditions of stress and strain, the model implies for example the relationship  $E_{oed} = E_{oed}^{ref} (\sigma / p^{ref})^m$ . In the special case of soft soils it is realistic to use  $m = 1$ . In such situations there is also a simple relationship between the modified compression index  $\lambda^*$ , as used in models for soft soil and the oedometer loading modulus (see also [Parameters of the Soft Soil Creep model](#) (on page 129) ).

$$E_{oed}^{ref} = \frac{p^{ref}}{\lambda^*} \quad \lambda^* = \frac{\lambda}{(1 + e_0)} \quad Eq. [134]$$

where  $p^{ref}$  is a reference pressure. Here we consider a tangent oedometer modulus at a particular reference pressure  $p^{ref}$ . Hence, the primary loading stiffness relates to the modified compression index  $\lambda^*$  or to the standard Cam-Clay compression index  $\lambda$ .

Similarly, the unloading-reloading modulus relates to the modified swelling index  $\kappa^*$  or to the standard Cam-Clay swelling index  $\kappa$ . There is the approximate relationship:

## The Hardening Soil model (Isotropic hardening)

Hyperbolic relationship for standard drained triaxial test

$$E_{ur}^{ref} \approx \frac{2p^{ref}}{\kappa^*} \quad k^* = \frac{k}{(1+e_0)} \quad Eq. [135]$$

This relationship applies in combination with the input value  $m = 1$ .

### 6.1 Hyperbolic relationship for standard drained triaxial test

A basic idea for the formulation of the Hardening Soil model is the hyperbolic relationship between the vertical strain,  $\varepsilon_1$ , and the deviatoric stress,  $q$ , in primary triaxial loading. Here standard drained triaxial tests tend to yield curves that can be described by:

$$-\varepsilon_1 = \frac{1}{E_i} \frac{q}{1 - q/q_a} \quad \text{for : } q < q_f \quad Eq. [136]$$

where

$$\begin{aligned} q_a &= \text{Asymptotic value of the shear strength.} \\ E_i &= \text{Initial stiffness.} \end{aligned}$$

$E_i$  is related to  $E_{50}$  by:

$$E_i = \frac{2E_{50}}{2 - R_f} \quad Eq. [137]$$

This relationship is plotted in [Figure 24](#) (on page 69). The parameter  $E_{50}$  is the confining stress dependent stiffness modulus for primary loading and is given by the equation:

$$E_{50} = E_{50}^{ref} \left( \frac{ccos(\varphi) - \sigma'_3 \sin(\varphi)}{ccos(\varphi) + p^{ref} \sin(\varphi)} \right)^m \quad Eq. [138]$$

where

$$E_{50}^{ref} = \text{Reference stiffness modulus corresponding to the reference confining pressure } p^{ref}.$$

In PLAXIS, a default setting  $p^{ref} = 100$  stress units is used. The actual stiffness depends on the minor principal stress,  $\sigma'_3$ , which is the confining pressure in a triaxial test. Please note that  $\sigma'_3$  is negative for compression. The amount of stress dependency is given by the power  $m$ . In order to simulate a logarithmic compression behaviour, as observed for soft clays, the power should be taken equal to 1.0. [Janbu \(1963\)](#) (on page 247) reports values of  $m$  around 0.5 for Norwegian sands and silts, whilst [von Soos \(1990\)](#) (on page 249) reports various different values in the range  $0.5 < m < 1.0$ .

The ultimate deviatoric stress,  $q_f$  and the quantity  $q_a$  in Eq. [136] are defined as:

$$q_f = (ccot(\varphi) - \sigma'_3) \frac{2\sin(\varphi)}{1 - \sin(\varphi)} \quad \text{and :} \quad q_a = \frac{q_f}{R_f} \quad Eq. [139]$$

Again it is remarked that  $\sigma'_3$  is usually negative. The above relationship for  $q_f$  is derived from the Mohr-Coulomb failure criterion, which involves the strength parameters  $c$  and  $\varphi$ . As soon as  $q = q_f$ , the failure criterion is satisfied and perfectly plastic yielding occurs as described by the Mohr-Coulomb model.

The ratio between  $q_f$  and  $q_a$  is given by the failure ratio  $R_f$ , which should obviously be smaller than or equal to 1. In PLAXIS,  $R_f = 0.9$  is chosen as a suitable default setting.

For unloading and reloading stress paths, another stress-dependent stiffness modulus is used:

## The Hardening Soil model (Isotropic hardening)

Approximation of hyperbola by the Hardening Soil model

$$E_{ur} = E_{ur}^{ref} \left( \frac{c \cos(\varphi) - \sigma'_3 \sin(\varphi)}{c \cos(\varphi) + p^{ref} \sin(\varphi)} \right)^m \quad Eq. [140]$$

where

$E_{ur}^{ref}$  = Reference Young's modulus and reloading, corresponding to the reference pressure  $p^{ref}$ .

**Note:** In many practical cases it is appropriate to set  $E_{ur}^{ref}$  equal to  $3E_{50}^{ref}$ ; this is the default setting used in PLAXIS.

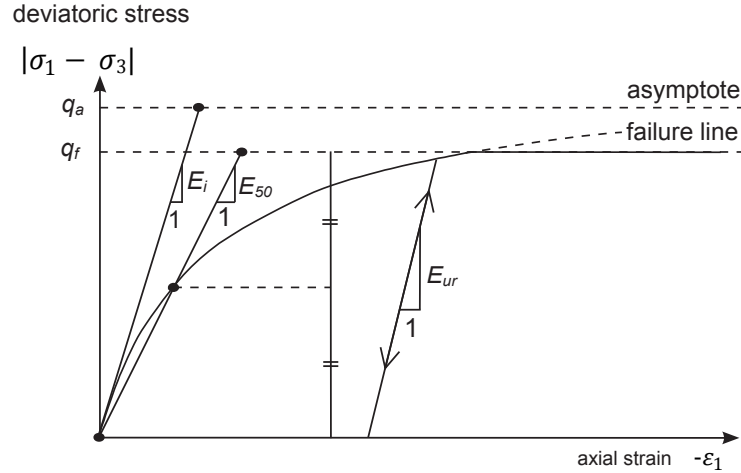


Figure 24: Hyperbolic stress-strain relation in primary loading for a standard drained triaxial test

## 6.2 Approximation of hyperbola by the Hardening Soil model

For the sake of convenience, restriction is made here to triaxial loading conditions with  $\sigma'_2 = \sigma'_3$  and  $\sigma'_1$  being the major compressive stress. In fact, for general states of stress,  $q$  can be replaced by  $\tilde{q}$  where:

$$\tilde{q} = \sigma'_1 + (\alpha - 1)\sigma'_2 - \alpha\sigma'_3 \quad \text{with} \quad \alpha = \frac{3 + \sin(\varphi)}{3 - \sin(\varphi)} \quad Eq. [141]$$

(refer to [On the cap yield surface in the Hardening Soil model](#) (on page 78) for more details). Moreover, it is assumed that  $q < q_f$ , as also indicated in [Figure 24](#) (on page 69). It should also be realised that compressive stress and strain are considered negative. For a more general presentation of the Hardening Soil model the reader is referred to [Schanz, Vermeer & Bonnier \(1999\)](#) (on page 248). In this section it will be shown that this model gives virtually the hyperbolic stress strain curve of Eq. [136] when considering stress paths of standard drained triaxial tests. Let us first consider the corresponding plastic strains. This stems from a shear hardening yield function of the form:

$$\bar{f} = \bar{f} - \gamma^p \quad Eq. [142]$$

where

$\bar{f}$  = Function of stress  
 $\gamma^p$  = Function of plastic strains:

## The Hardening Soil model (Isotropic hardening)

Approximation of hyperbola by the Hardening Soil model

$$\bar{f} = \frac{2}{E_i} \frac{q}{1 - q/q_a} - \frac{2q}{E_{ur}} \quad \gamma^p = - (2\varepsilon_1^p - \varepsilon_v^p) \approx - 2\varepsilon_1^p \quad \text{Eq. [143]}$$

with  $q$ ,  $q_a$ ,  $E_i$  and  $E_{ur}$  as defined by Eq. [136] to Eq. [139], whilst the superscript  $p$  is used to denote plastic strains. For hard soils, plastic volume changes ( $\varepsilon_v^p$ ) tend to be relatively small and this leads to the approximation  $\gamma^p \approx - 2\varepsilon_1^p$ . The above definition of the strain-hardening parameter  $\gamma^p$  will be referred to later.

An essential feature of the above definitions for  $\bar{f}$  is that it matches the well-known hyperbolic law Eq. [136]. For checking this statement, one has to consider primary loading, as this implies the yield condition  $f = 0$ . For primary loading, it thus yields  $\gamma^p = \bar{f}$  and it follows from Eq. [142] that:

$$\varepsilon_1^p \approx \frac{1}{2} \bar{f} = \frac{1}{E_i} \frac{q}{1 - q/q_a} - \frac{q}{E_{ur}} \quad \text{Eq. [144]}$$

In addition to the plastic strains, the model accounts for elastic strains. Plastic strains develop in primary loading alone, but elastic strains develop both in primary loading and unloading / reloading. For drained triaxial test stress paths with  $\sigma'_2 = \sigma'_3 = \text{constant}$ , the elastic Young's modulus  $E_{ur}$  remains constant and the elastic strains are given by the equations:

$$- \varepsilon_1^e = \frac{q}{E_{ur}} \quad - \varepsilon_2^e = - \varepsilon_3^e = - \nu_{ur} \frac{q}{E_{ur}} \quad \text{Eq. [145]}$$

where  $\nu_{ur}$  is the unloading / reloading Poisson's ratio. Here it should be realised that restriction is made to strains that develop during deviatoric loading, whilst the strains that develop during the very first stage of the test (isotropic compression with consolidation) are not considered.

For the deviatoric loading stage of the triaxial test, the axial strain is the sum of an elastic component given by Eq. [145] and a plastic component according to Eq. [144]. Hence, it follows that:

$$- \varepsilon_1 = - \varepsilon_1^e - \varepsilon_1^p \approx \frac{1}{E_i} \frac{q}{1 - q/q_a} \quad \text{Eq. [146]}$$

This relationship holds exactly in absence of plastic volume strains, i.e. when  $\varepsilon_v^p = 0$ .

In reality, plastic volumetric strains will never be precisely equal to zero, but for hard soils plastic volume changes tend to be small when compared with the axial strain so that this formulation yields a hyperbolic stress-strain curve under triaxial testing conditions.

For a given constant value of the hardening parameter,  $\gamma^p$ , the yield condition  $f = 0$ , can be visualised in  $p'$  -  $q$ -plane by means of a yield locus. Hence,  $\gamma^p$  is associated with mobilised friction. When plotting such yield loci, one has to use Eq. [143] as well as Eq. [140] and Eq. [139] for  $E_{50}$  and  $E_{ur}$  respectively. Because of the latter expressions, the shape of the yield loci depends on the exponent  $m$ . For  $m = 1$ , straight lines are obtained, but slightly curved yield loci correspond to lower values of the exponent. [Figure 25](#) (on page 71) shows the shape of yield loci for increasing values of  $\gamma^p$  considering  $m = 0.5$ , being typical for hard soils. Hence,  $\gamma^p$  can be regarded as the plastic shear strain related to the mobilised shear resistance.

**Note:** Note that there is approximately a factor 2 difference between the plastic shear strain parameter  $\gamma^p$  and the deviatoric plastic strain  $\varepsilon_q^p$  ( $\gamma^p \approx \varepsilon_q^p$ )

## The Hardening Soil model (Isotropic hardening)

Plastic volumetric strain for triaxial states of stress

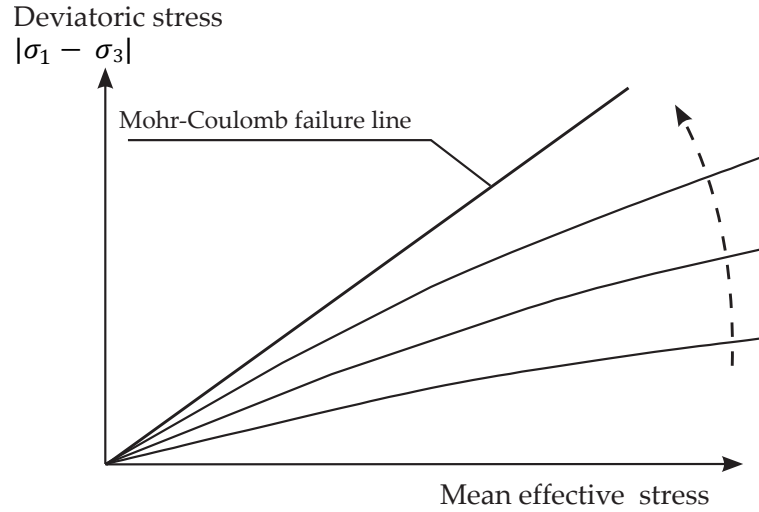


Figure 25: Successive yield loci for various constant values of the hardening parameter  $\gamma^p$

### 6.3 Plastic volumetric strain for triaxial states of stress

Having presented a relationship for the plastic shear strain,  $\gamma^p$ , attention is now focused on the plastic volumetric strain,  $\varepsilon_v^p$ . As for all plasticity models, the Hardening Soil model involves a relationship between rates of plastic strain, i.e. a relationship between  $\dot{\varepsilon}_v^p$  and  $\dot{\gamma}^p$ . This shear hardening flow rule has the linear form:

$$\dot{\varepsilon}_v^p = \sin(\psi_m) \dot{\gamma}^p \quad \text{Eq. [147]}$$

Clearly, further detail is needed by specifying the mobilised dilatancy angle  $\psi_m$ . For the present model, the following is considered (see also [Figure 26](#) (on page 71)):

$$\begin{aligned} \text{For } \sin(\varphi_m) < 3/4 \sin(\varphi) : & \quad \psi_m = 0 \\ \text{For } \sin(\varphi_m) \geq 3/4 \sin(\varphi) \text{ and } \psi > 0 & \quad \sin(\psi_m) = \max \left( \frac{\sin(\varphi_m) - \sin(\varphi_{cv})}{1 - \sin(\varphi_m) \sin(\varphi_{cv})}, 0 \right) \\ \text{For } \sin(\varphi_m) \geq 3/4 \sin(\varphi) \text{ and } \psi \leq 0 & \quad \psi_m = \psi \\ \text{If } \varphi = 0 & \quad \psi_m = 0 \end{aligned} \quad \text{Eq. [148]}$$

where

$$\begin{aligned} \varphi_{cv} &= \text{Critical state friction angle, being a material constant independent of density.} \\ \varphi_m &= \text{Mobilised friction angle:} \end{aligned}$$

$$\sin(\varphi_m) = \frac{\sigma'_1 - \sigma'_3}{\sigma'_1 + \sigma'_3 - 2c \cot(\varphi)} \quad \text{Eq. [149]}$$

## The Hardening Soil model (Isotropic hardening)

### Parameters of the Hardening Soil Model

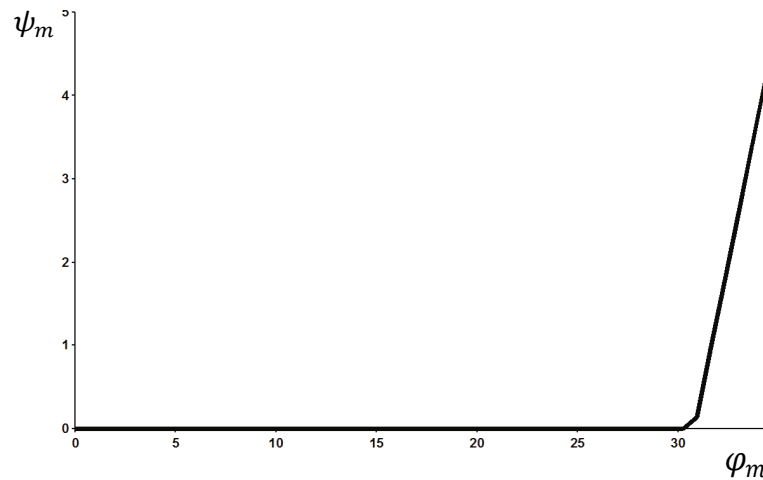


Figure 26: Plot of mobilized dilatancy angle  $\psi_m$  and mobilized friction angle  $\phi_m$  for Hardening Soil model

The above equations are a small adaptation from the well-known stress-dilatancy theory by [Rowe \(1962\)](#) (on page 248), as explained by [Schanz & Vermeer \(1966\)](#) (on page 248). The mobilised dilatancy angle,  $\psi_m$ , follows Rowe's theory for larger values of the mobilised friction angle, as long as this results in a positive value of  $\psi_m$ . For small mobilised friction angles and for negative values of  $\psi_m$ , as computed by Rowe's formula (as long as the dilatancy angle  $\psi$  is positive),  $\psi_m$  is taken zero. Furthermore, in all cases when  $\phi = 0$ ,  $\psi_m$  is set equal to zero.

The essential property of the stress-dilatancy theory is that the material contracts for small stress ratios  $\phi_m < \phi_{cv}$ , whilst dilatancy occurs for high stress ratios  $\phi_m > \phi_{cv}$ . At failure, when the mobilised friction angle equals the failure angle,  $\phi$ , it is found from Eq. [148] that:

$$\sin(\psi) = \frac{\sin(\phi) - \sin(\phi_{cv})}{1 - \sin(\phi)\sin(\phi_{cv})} \quad \text{Eq. [150]}$$

or equivalently:

$$\sin(\phi_{cv}) = \frac{\sin(\phi) - \sin(\psi)}{1 - \sin(\phi)\sin(\psi)} \quad \text{Eq. [151]}$$

Hence, the critical state angle can be computed from the failure angles  $\phi$  and  $\psi$ . PLAXIS performs this computation automatically and therefore users do not need to specify a value for  $\phi_{cv}$ . Instead, one has to provide input data on the peak friction angle,  $\phi$ , and the peak dilatancy angle,  $\psi$ .

The shear hardening process will continue with the mobilization of the shear strength, until the maximum shear strength according to the Mohr-Coulomb model failure criterion is reached.

## 6.4 Parameters of the Hardening Soil Model

Some parameters of the present hardening model coincide with those of the non-hardening Mohr-Coulomb model. These are the failure parameters  $c$ ,  $\phi$  and  $\psi$ .

# The Hardening Soil model (Isotropic hardening)

## Parameters of the Hardening Soil Model

Soil - Hardening Soil - <NoName>

General Mechanical Groundwater Thermal Interfaces \* Initial \*

Property	Unit	Value
<b>Stiffness</b>		
$E_{50}^{ref}$	kN/m <sup>2</sup>	0.000
$E_{oed}^{ref}$	kN/m <sup>2</sup>	0.000
$E_{ur}^{ref}$	kN/m <sup>2</sup>	0.000
$\nu_{ur}$		0.2000
<b>Alternatives</b>		
Use alternatives		<input type="checkbox"/>
$C_c$		10.00E9
$C_s$		10.00E9
$e_{init}$		0.5000
<b>Stress-dependency</b>		
power (m)		0.5000
$p_{ref}$	kN/m <sup>2</sup>	100.0
<b>Strength</b>		
<b>Shear</b>		
$c'_{ref}$	kN/m <sup>2</sup>	0.000
$\varphi'$ (phi)	°	0.000
$\psi$ (psi)	°	0.000
<b>Depth-dependency</b>		
$c'_{inc}$	kN/m <sup>2</sup> /m	0.000
$\gamma_{ref}$	m	0.000
<b>Dilatancy cutoff</b>		
Dilatancy-cutoff		<input type="checkbox"/>
$e_{min}$		1.000E-9
$e_{max}$		999.0
<b>Tension</b>		
Tension cut-off		<input checked="" type="checkbox"/>
Tensile strength	kN/m <sup>2</sup>	0.000
<b>Miscellaneous</b>		
Use defaults		<input checked="" type="checkbox"/>
$K_0^{nc}$		1.000
$R_f$		0.9000
<b>Excess pore pressure calculation</b>		
Determination	v-undrained definition	▼
$\nu_u$ definition method	Direct	▼
$\nu_{u,equivalent}$ (nu)		0.4950
Skempton B		0.9866
$K_{w,ref}/\eta$	kN/m <sup>2</sup>	0.000

Next OK Cancel

Figure 27: Parameters for the Hardening Soil model

Failure parameters as in Mohr-Coulomb model (see [Parameters of the Mohr-Coulomb model](#) (on page 34))

$c$	(Effective) cohesion	[kN/m <sup>2</sup> ]
$\varphi$	(Effective) angle of internal friction	[°]

## The Hardening Soil model (Isotropic hardening)

### Parameters of the Hardening Soil Model

$\psi$	Angle of dilatancy	[°]
$\sigma_t$	Tension cut-off and tensile strength	[kN/m <sup>2</sup> ]

Basic parameters for soil stiffness:

$E_{50}^{ref}$	Secant stiffness in standard drained triaxial test	[kN/m <sup>2</sup> ]
$E_{oed}^{ref}$	Tangent stiffness for primary oedometer loading	[kN/m <sup>2</sup> ]
$E_{ur}^{ref}$	Unloading / reloading stiffness (default $E_{ur}^{ref} = 3E_{50}^{ref}$ )	[kN/m <sup>2</sup> ]
$m$	Power for stress-level dependency of stiffness	[-]

Advanced parameters (it is advised to use the default setting):

$\nu_{ur}$	Poisson's ratio for unloading-reloading (default $\nu_{ur} = 0.2$ )	[-]
$p^{ref}$	Reference stress for stiffnesses (default $p^{ref} = 100$ kN/m <sup>2</sup> )	[kN/m <sup>2</sup> ]
$K_0^{nc}$	$K_0$ -value for normal consolidation (default $K_0^{nc} = 1 - \sin \varphi$ )	[-]
$R_f$	Failure ratio $q_f / q_a$ (default $R_f = 0.9$ ) (see <a href="#">Figure 24</a> (on page 69)).	[-]
$\sigma_{tension}$	Tensile strength (default $\sigma_{tension} = 0$ stress units)	[kN/m <sup>2</sup> ]
$c_{inc}$	As in Mohr-Coulomb model (default $c_{inc} = 0$ )	[kN/m <sup>3</sup> ]

Instead of entering the basic parameters for soil stiffness, alternative parameters can be entered. These parameters are listed below:

$C_c$	Compression index	[-]
$C_s$	Swelling index or reloading index	[-]
$e_{init}$	Initial void ratio	[-]

### 6.4.1 Stiffness moduli $E_{50}^{ref}$ , $E_{oed}^{ref}$ & $E_{ur}^{ref}$ and power $m$

The advantage of the Hardening Soil model over the Mohr-Coulomb model is not only the use of a hyperbolic stress-strain curve instead of a bi-linear curve, but also the control of stress level dependency. When using the Mohr-Coulomb model, the user has to select a fixed value of Young's modulus whereas for real soils this stiffness depends on the stress level. It is therefore necessary to estimate the stress levels within the soil and use these to obtain suitable values of stiffness. With the Hardening Soil model, however, this cumbersome selection of input parameters is not required.

## The Hardening Soil model (Isotropic hardening)

### Parameters of the Hardening Soil Model

Instead, a stiffness modulus  $E_{50}^{ref}$  is defined for a reference minor principal effective stress of  $-\sigma'_3 = p^{ref}$ . This is the secant stiffness at 50 % of the maximum deviatoric stress, at a cell pressure equal to the reference stress  $p^{ref}$  (Figure 28 (on page 75)). As a default value, the program uses  $p^{ref} = 100 \text{ kN/m}^2$ .

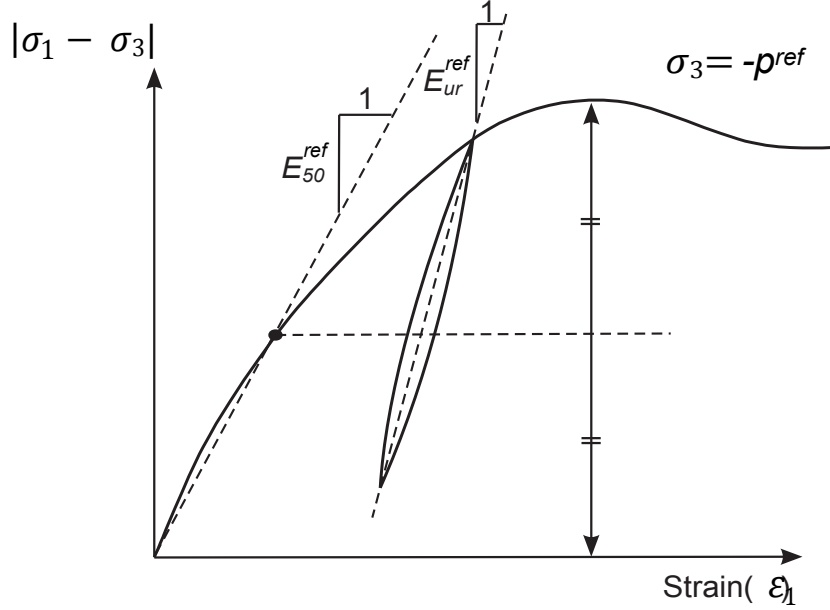


Figure 28: Definition of  $E_{50}^{ref}$  and  $E_{ur}^{ref}$  for drained triaxial test results

As some PLAXIS users are familiar with the input of shear moduli rather than the above stiffness moduli, shear moduli will now be discussed. Within Hooke's law of isotropic elasticity conversion between  $E$  and  $G$  goes by the equation  $E = 2(1 + \nu)G$ . As  $E_{ur}$  is a real elastic stiffness, one may thus write  $E_{ur} = 2(1 + \nu)G_{ur}$ , where  $G_{ur}$  is an elastic shear modulus.

**Note:** PLAXIS allows for the input of  $E_{ur}$  and  $\nu_{ur}$  but not for a direct input of  $G_{ur}$ . In contrast to  $E_{ur}$ , the secant modulus  $E_{50}$  is not used within a concept of elasticity. As a consequence, there is no simple conversion from  $E_{50}$  to  $G_{50}$ .

In contrast to elasticity based models, the elastoplastic Hardening Soil model does not involve a fixed relationship between the (drained) triaxial stiffness  $E_{50}$  and the oedometer stiffness  $E_{oed}$  for one-dimensional compression. Instead, these stiffnesses can be inputted independently. Having defined  $E_{50}$  by Eq. [138], it is now important to define the oedometer stiffness. Here we use the equation:

$$E_{oed} = E_{oed}^{ref} \left( \frac{c \cos(\varphi) - \frac{\sigma'_3}{K_0^{nc}} \sin(\varphi)}{c \cos(\varphi) + p^{ref} \sin(\varphi)} \right)^m \quad \text{Eq. [152]}$$

where  $E_{oed}$  is a tangent stiffness modulus obtained from an oedometer test, as indicated in Figure 29 (on page 76).

## The Hardening Soil model (Isotropic hardening)

### Parameters of the Hardening Soil Model

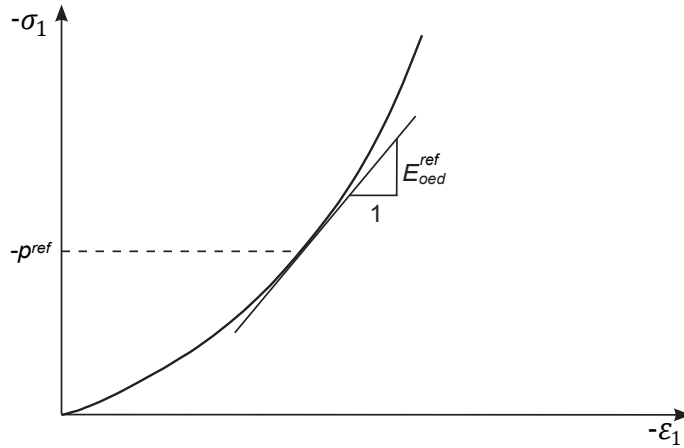


Figure 29: Definition of  $E_{oed}^{ref}$  and  $E_{ur}^{ref}$  in oedometer test results

Hence,  $E_{oed}^{ref}$  is a tangent stiffness at a vertical stress of  $-\sigma'_1 = \frac{\sigma'_3}{K_0^{nc}} = p^{ref}$ . Note that we basically use  $\sigma'_1$  rather than  $\sigma'_3$  and that we consider primary loading.

When undrained behaviour is considered in the Hardening Soil model the *Drainage type* should preferably be set to *Undrained (A)*. Alternatively, *Undrained (B)* can be used in case the effective strength properties are not known or the undrained shear strength is not properly captured using *Undrained (A)*. However, it should be noted that the material loses its stress-dependency of stiffness in that case. *Undrained (C)* is not possible since the model is essentially formulated as an effective stress model.

### 6.4.2 Alternative stiffness parameters

When soft soils are considered, the stiffness parameters can be calculated from the compression index, swelling index and the initial void ratio<sup>1</sup>. The relationship between these parameters and the compression index,  $C_c$ , is given by:

$$C_c = \frac{2.3(1 + e_{init})p_{red}}{E_{oed}^{ref}} \quad Eq. [153]$$

The relationship between the  $E_{ur}^{ref}$  and the swelling index,  $C_s$ , is given by:

$$C_s \approx \frac{2.3(1 + e_{init})(1 + \nu_{ur})(1 - 2\nu_{ur})p_{ref}}{(1 - \nu_{ur})E_{ur}^{ref}K_0} \quad Eq. [154]$$

**Note:** During unloading the  $K_0$ -value will increase, where values above 1.0 may be observed for significant unloading. By default, PLAXIS assumes that on average the horizontal stress is equal to the vertical stress ( $K_0=1$ ).

Regardless the previous value of  $E_{50}$ , a new value will be automatically assigned according to:

$$E_{50}^{ref} = 1.25E_{oed}^{ref} \quad Eq. [155]$$

<sup>1</sup> In the PLAXIS material database, these alternative parameters depend on the initial void ratio. In reality, these parameters depend on the actual void ratio, which is not a constant.

## The Hardening Soil model (Isotropic hardening)

### Parameters of the Hardening Soil Model

Although for *Soft soils*,  $E_{50}^{ref}$  could be as high as  $2E_{oed}^{ref}$ , this high value could lead to a limitation in the modeling; therefore a lower value is used. Changing the value of  $C_s$  will change the stiffness parameter  $E_{ur}$ .

Note that the value of the power for stress-level dependency of stiffness ( $m$ ) is automatically set to 1.

### 6.4.3 Advanced parameters

Realistic values of  $\nu_{ur}$  are about 0.2 and this value is thus used as a default setting, as indicated in [Figure 27](#) (on page 73). Note that in the Hardening Soil model,  $\nu_{ur}$  is a pure elastic parameter.

In contrast to the Mohr-Coulomb model,  $K_0^{nc}$  is not simply a function of Poisson's ratio, but an independent input parameter. As a default setting PLAXIS uses the correlation  $K_0^{nc} = 1 - \sin \varphi$ . It is suggested to maintain this value as the correlation is quite realistic. However, users do have the possibility to select different values. Not all possible input values for  $K_0^{nc}$  can be accommodated for. Depending on other parameters, such as  $E_{50}^{ref}$ ,  $E_{oed}^{ref}$ ,  $E_{ur}^{ref}$  and  $\nu_{ur}$ , there happens to be a certain range of valid  $K_0^{nc}$ -values.  $K_0^{nc}$  values outside this range are rejected by PLAXIS. On inputting values, the program shows the nearest possible value that will be used in the computations.

### 6.4.4 Dilatancy cut-off

After extensive shearing, dilating materials arrive in a state of critical density where dilatancy has come to an end, as indicated in [Figure 30](#) (on page 78). This phenomenon of soil behaviour can be included in the Hardening Soil model by means of a dilatancy cut-off. In order to specify this behaviour, the initial void ratio,  $e_{init}$ , and the maximum void ratio,  $e_{max}$ , of the material must be entered as general parameters. As soon as the volume change results in a state of maximum void, the mobilised dilatancy angle,  $\psi_m$ , is automatically set back to zero, as indicated in [Figure 30](#) (on page 78).

$$\text{for } e < e_{max} \quad \sin(\psi_m) = \frac{\sin(\varphi_m) - \sin(\varphi_{cv})}{1 - \sin(\varphi_m)\sin(\varphi_{cv})} \quad \text{Eq. [156]}$$

$$\text{where :} \quad \sin(\varphi_{cv}) = \frac{\sin(\varphi) - \sin(\psi)}{1 - \sin(\varphi)\sin(\psi)}$$

$$\text{for } e \geq e_{max} \quad \psi_m = 0 \quad \text{Eq. [157]}$$

The void ratio is related to the volumetric strain,  $\varepsilon_v$  by the relationship:

$$-(\varepsilon_v - \varepsilon_v^{init}) = \ln \left( \frac{1+e}{1+e_{init}} \right) \quad \text{Eq. [158]}$$

where an increment of  $\varepsilon_v$  is positive for dilatancy.

## The Hardening Soil model (Isotropic hardening)

On the cap yield surface in the Hardening Soil model

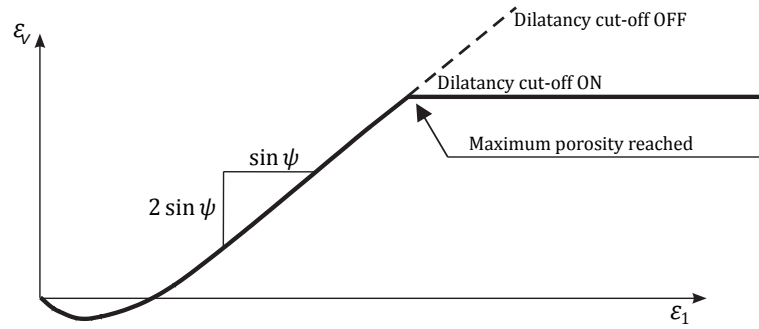


Figure 30: Resulting strain curve for a standard drained triaxial test when including dilatancy cut-off

The initial void ratio,  $e_{init}$ , is the in-situ void ratio of the soil body. The maximum void ratio is the void ratio of the material in a state of critical void (critical state). As soon as the maximum void ratio is reached, the dilatancy angle is set to zero. The minimum void ratio,  $e_{min}$ , of a soil can also be input, but this general soil parameter is not used within the context of the Hardening Soil model.

The selection of the *Dilatancy cut-off* is only available when the Hardening Soil model or the Hardening Soil model with small-strain stiffness has been selected. By default, the *Dilatancy cut-off* is not active. Note that the dilatancy cut-off does not help in limiting the shear strength when using the *Undrained A* drainage type with a positive dilatancy angle. This is because the void ratio remains constant for undrained materials. Therefore, it is strongly recommended to set  $\psi = 0$  for undrained material behaviour (*Undrained A*).

## 6.5 On the cap yield surface in the Hardening Soil model

Shear hardening yield surfaces as indicated in [Figure 25](#) (on page 71) do not explain the plastic volume strain that is measured in isotropic compression which is mostly observed in softer types of soil. A second type of yield surface must therefore be introduced to close the elastic region for compressive (compaction hardening) stress paths. Without such a cap type yield surface it would not be possible to formulate a model with independent input of both  $E_{50}^{ref}$  and  $E_{oed}^{ref}$ . The triaxial modulus largely controls the shear yield surface and the oedometer modulus controls the cap yield surface. In fact,  $E_{50}^{ref}$  largely controls the magnitude of the plastic strains that are associated with the shear yield surface. Similarly,  $E_{oed}^{ref}$  is used to control the magnitude of plastic strains that originate from the yield cap. In this section the yield cap will be described in detail. To this end we consider the definition of the cap yield surface:

$$f_c = \frac{\tilde{q}^2}{M^2} + (p')^2 - p_p^2 \quad Eq. [159]$$

where

$M$  = auxiliary model parameter that relates to  $K_0^{nc}$  (discussed later in section ).

Furthermore we have:

$p' = (\sigma'_1 + \sigma'_2 + \sigma'_3) / 3$  and  $q = \sigma'_1 + (\alpha - 1)\sigma'_2 - \alpha\sigma'_3$  with  $\alpha = (3 + \sin\phi) / (3 - \sin\phi)$ .  $q$  is a special stress measure for deviatoric stresses.

In the special case of triaxial compression ( $-\sigma'_1 > -\sigma'_2 = -\sigma'_3$ ) it yields  $q = -(\sigma'_1 - \sigma'_3)$  and for triaxial extension ( $-\sigma'_1 = -\sigma'_2 > -\sigma'_3$ )  $q$  reduces to  $q = -\alpha(\sigma'_1 - \sigma'_3)$ . The magnitude of the yield cap is determined by the isotropic pre-

## The Hardening Soil model (Isotropic hardening)

On the cap yield surface in the Hardening Soil model

consolidation stress  $p_p$ . In a  $(p', q)$  plane, the yield cap ( $f_c = 0$ ) is a part of an ellipse with its centre point in the origin ([Figure 31](#) (on page 80)). The hardening law relating  $\dot{p}$  to volumetric cap strain  $\dot{\epsilon}_v^{pc}$  is:

$$\dot{\epsilon}_v^{pc} = \frac{K_s / K_c - 1}{K_s^{ref}} \left[ \left( \frac{p_p + c \cot(\varphi)}{p^{ref} + c \cot(\varphi)} \right)^{-m} \right] \dot{p}_p \quad Eq. [160]$$

in which  $K_s^{ref}$  is the reference bulk modulus in unloading / reloading:

$$K_s^{ref} = \frac{E_{ur}^{ref}}{3(1 - 2\nu_{ur})} \quad Eq. [161]$$

and  $K_s/K_c$  is the ratio of bulk moduli in isotropic swelling and primary isotropic compression.

The volumetric cap strain is the plastic volumetric strain in isotropic compression. In addition to the well known constants  $m$  and  $p^{ref}$  there is another model constant  $K_s/K_c$ . Both  $M$  (Eq. [159]) and  $K_s/K_c$  (Eq. [160]) are cap parameters, but these are not used as direct input parameters. Instead, there is a relationship of the form:

$$M \leftrightarrow K_0^{nc} \quad (\text{default : } K_0^{nc} = 1 - \sin(\varphi)) \quad Eq. [162]$$

and the ratio  $K_s/K_c$  can be approximated as:

$$K_s / K_c \approx \frac{E_{ur}^{ref}}{E_{oed}^{ref}} \frac{K_0^{nc}}{(1 + 2K_0^{nc})(1 - 2\nu_{ur})} \quad Eq. [163]$$

such that  $K_0^{nc}$ ,  $E_{ur}^{ref}$  and  $E_{oed}^{ref}$  can be used as input parameters that determine the magnitude of  $M$  and  $K_s/K_c$  respectively.  $M$  is determined by finding the correct steepness of the cap for the  $K_0^{nc}$  path in the similar way as is done for the Soft Soil model [K0nc-parameter](#) (on page 117), see Eq. [234].

The ellipse on which the yield cap is located has length  $p_p$  on the  $p$ -axis and  $M p_p$  on the  $q$ -axis. Hence,  $p_p$  determines its magnitude and  $M$  its aspect ratio. High values of  $M$  lead to steep caps underneath the Mohr-Coulomb line and correspondingly small  $K_0^{nc}$ -values, whereas small  $M$ -values define caps that are much more pointed around the  $p$ -axis leading to large  $K_0^{nc}$ -values. The ellipse is used both as a yield surface and as a plastic potential (associated plasticity). Input data on initial  $p_p$ -values is provided by means of the PLAXIS procedure for initial stresses. Here,  $p_p$  is either computed from the input overconsolidation ratio (OCR) or the pre-overburden pressure (POP) (see [On the initial stresses](#) (on page 29)).

## The Hardening Soil model (Isotropic hardening)

State parameters in the Hardening Soil model

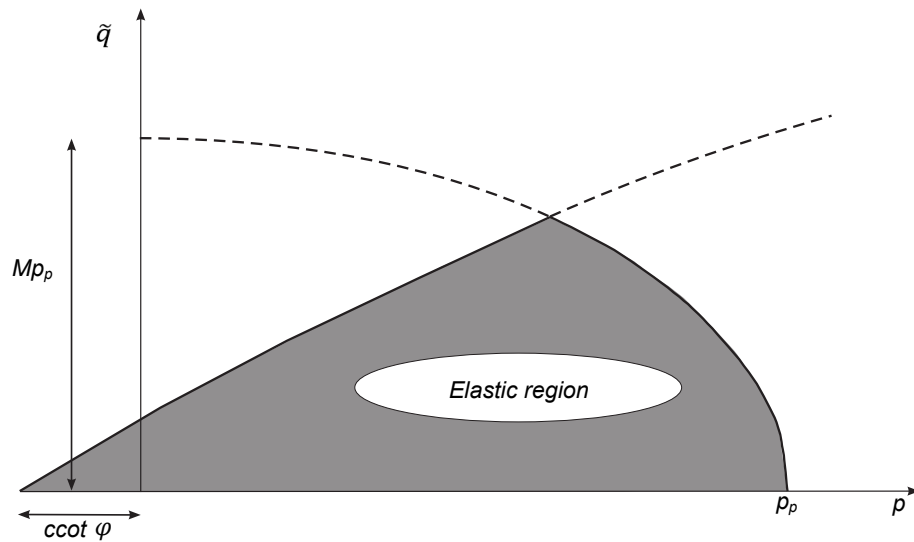


Figure 31: Yield surfaces of in  $p - q$  -plane. The elastic region can be further reduced by means of a tension cut-off

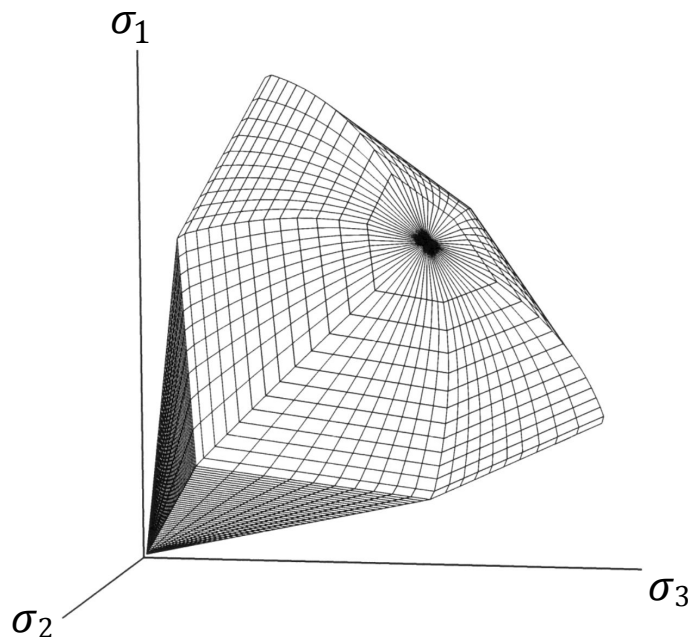


Figure 32: Representation of total yield contour of the Hardening Soil model in principal stress space for cohesionless soil

For understanding the yield surfaces in full detail, one should consider both [Figure 31](#) (on page 80) and [Figure 32](#) (on page 80). The first figure shows simple yield lines, whereas the second one depicts yield surfaces in principal stress space. Both the shear locus and the yield cap have the hexagonal shape of the classical Mohr-Coulomb failure criterion. In fact, the shear yield locus can expand up to the ultimate Mohr-Coulomb failure surface. The cap yield surface expands as a function of the pre-consolidation stress  $p_p$ .

## The Hardening Soil model (Isotropic hardening)

On the use of the Hardening Soil model in dynamics calculations

### 6.6 State parameters in the Hardening Soil model

In addition to the output of standard stress and strain quantities, the Hardening Soil model provides output (when being used) on state variables such as the hardening parameter  $\gamma^p$  and the isotropic pre-consolidation stress  $p_p$ . These parameters can be visualised by selecting the *State parameters* option from the *stresses* menu. An overview of available state parameters is given below:

$p_{eq}$	Equivalent isotropic stress $p_{eq} = \sqrt{\frac{\tilde{q}}{M^2} + (p' )^2}$	[kN/m <sup>2</sup> ]
$p_p$	Isotropic preconsolidation stress	[kN/m <sup>2</sup> ]
$OCR$	Isotropic overconsolidation ratio ( $OCR = p^p/p^{eq}$ )	[-]
$\gamma^p$	Hardening parameter (equivalent mobilised plastic shear strain)	[-]
$E_{ur}$	Current stress-dependent elastic Young's modulus	[kN/m <sup>2</sup> ]
$c$	Current depth-dependent cohesion	[kN/m <sup>2</sup> ]

### 6.7 On the use of the Hardening Soil model in dynamics calculations

When using the Hardening Soil model in dynamics calculations, the elastic stiffness parameter  $E_{ur}^{ref}$  needs to be selected such that the model correctly predicts wave velocities in the soil. This generally requires an even larger small strain stiffness rather than just an unloading-reloading stiffness to be entered for  $E_{ur}^{ref}$ . When subjected to dynamic or cyclic loading, the Hardening Soil model will generate plastic strains when mobilizing the soil's material strength (shear hardening) or increasing the soil's preconsolidation stress (compaction hardening). However, it should be noted that stress cycles within the current hardening contours will only generate elastic strains and no (hysteretic) damping, nor accumulation of strains or pore pressure nor liquefaction. In order to simulate the soil's damping characteristics in cyclic loading, Rayleigh damping may be defined. Note that some of the limitations of the Hardening Soil model in dynamic applications can be overcome by using the Hardening Soil model with small-strain stiffness ([The Hardening Soil model with small-strain stiffness \(HSsmall\)](#) (on page 82)).

# The Hardening Soil model with small-strain stiffness (HSsmall)

The original Hardening Soil model assumes elastic material behaviour during unloading and reloading. However, the strain range in which soils can be considered truly elastic, i.e. where they recover from applied straining almost completely, is very small. With increasing strain amplitude, soil stiffness decays nonlinearly. Plotting soil stiffness against  $\log(\text{strain})$  yields characteristic S-shaped stiffness reduction curves. [Figure 33](#) (on page 82) gives an example of such a stiffness reduction curve. It outlines also the characteristic shear strains that can be measured near geotechnical structures and the applicable strain ranges of laboratory tests. It turns out that at the minimum strain which can be reliably measured in classical laboratory tests, i.e. triaxial tests and oedometer tests without special instrumentation, soil stiffness is often decreased to less than half its initial value.

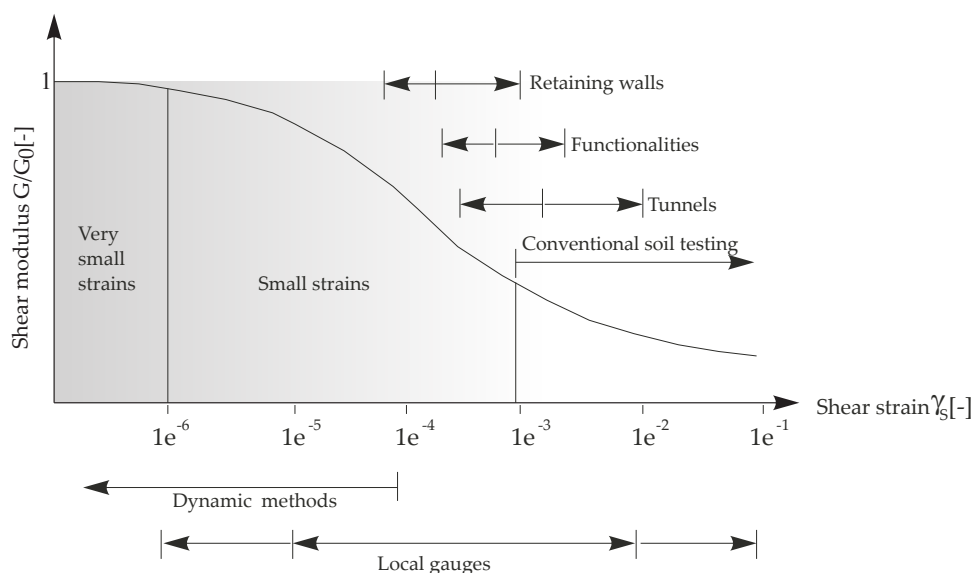


Figure 33: Characteristic stiffness-strain behaviour of soil with typical strain ranges for laboratory tests and structures (after Atkinson & Sallfors, 1991)

The soil stiffness that should be used in the analysis of geotechnical structures is not the one that relates to the strain range at the end of construction according to [Figure 33](#) (on page 82). Instead, very small-strain soil stiffness and its non-linear dependency on strain amplitude should be properly taken into account. In addition to all features of the Hardening Soil model, the Hardening Soil model with small-strain stiffness offers the possibility to do so.

## The Hardening Soil model with small-strain stiffness (HSsmall)

Describing small-strain stiffness with a Simple Hyperbolic Law

The Hardening Soil model with small-strain stiffness implemented in PLAXIS is based on the Hardening Soil model and uses almost entirely the same parameters (see [Parameters of the Hardening Soil Model](#) (on page 72)). In fact, only two additional parameters are needed to describe the variation of stiffness with strain:

- the initial or very small-strain shear modulus  $G_0$ .
- the shear strain level  $\gamma_{0.7}$  at which the secant shear modulus  $G_s$  is reduced to about 70% of  $G_0$ .

### 7.1 Describing small-strain stiffness with a Simple Hyperbolic Law

In soil dynamics, small-strain stiffness has been a well known phenomenon for a long time. In static analysis, the findings from soil dynamics have long been considered not to be applicable.

Seeming differences between static and dynamic soil stiffness have been attributed to the nature of loading (e.g. inertia forces and strain rate effects) rather than to the magnitude of applied strain which is generally small in dynamic conditions (earthquakes excluded). As inertia forces and strain rate have only little influence on the initial soil stiffness, dynamic soil stiffness and small-strain stiffness can in fact be considered as synonyms.

Probably the most frequently used model in soil dynamics is the Hardin-Drnevich relationship. From test data, sufficient agreement is found that the stress-strain curve for small strains can be adequately described by a simple hyperbolic law. The following analogy to the hyperbolic law for larger strains by [Konder \(1963\)](#) (on page 247) (see [The Hardening Soil model \(Isotropic hardening\)](#) (on page 67)) was proposed by [Hardin & Drnevich \(1972\)](#) (on page 247):

$$\frac{G_s}{G_0} = \frac{1}{1 + \left| \frac{\gamma}{\gamma_r} \right|} \quad \text{Eq. [164]}$$

where the threshold shear strain  $\gamma_r$  is quantified as:

$$\gamma_r = \frac{\tau_{\max}}{G_0} \quad \text{Eq. [165]}$$

with  $\tau_{\max}$  being the shear stress at failure. Essentially, Eq. [164] and Eq. [165] relate large (failure) strains to small-strain properties which often work well.

More straightforward and less prone to error is the use of a smaller threshold shear strain. [Santos & Correia \(2001\)](#) (on page 248), for example suggest to use the shear strain  $\gamma_r = \gamma_{0.7}$  at which the secant shear modulus  $G_s$  is reduced to about 70 % of its initial value. Eq. [164] can then be rewritten as:

$$\frac{G_s}{G_0} = \frac{1}{1 + a \left| \frac{\gamma}{\gamma_{0.7}} \right|} \quad \text{where } a = 0.385 \quad \text{Eq. [166]}$$

In fact, using  $a = 0.385$  and  $\gamma = \gamma_{0.7}$  gives  $G_s/G_0 = 0.722$ . Hence, the formulation "about 70%" should be interpreted more accurately as 72.2%.

[Figure 34](#) (on page 84) shows the fit of the modified Hardin-Drnevich relationship (Eq. [166]) to normalised test data.

## The Hardening Soil model with small-strain stiffness (HSsmall)

Applying the Hardin-Drnevich relationship in the HS Model

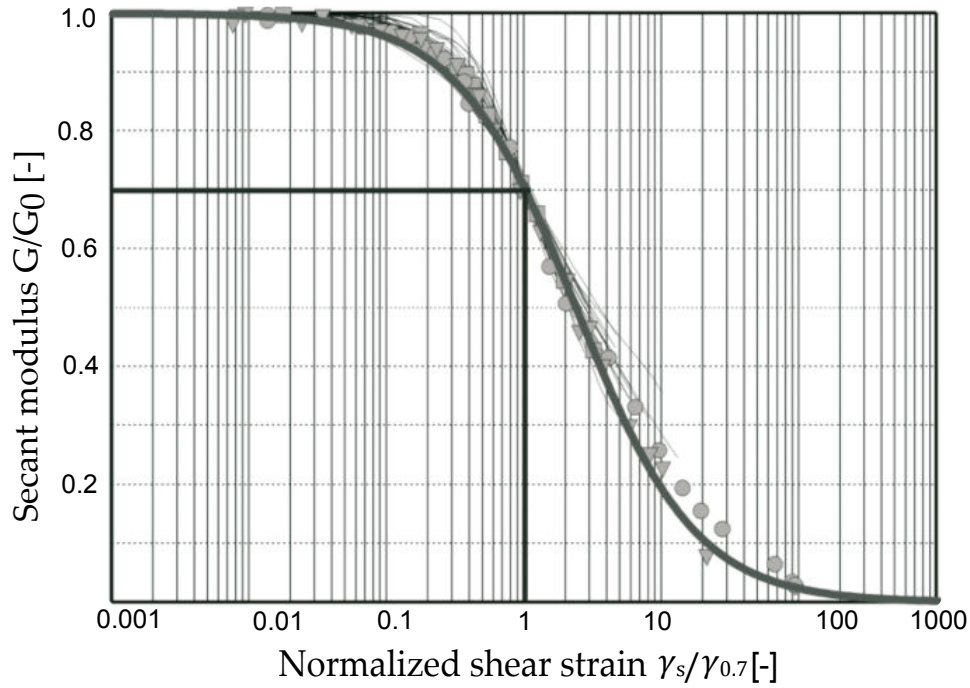


Figure 34: Results from the Hardin-Drnevich relationship compared to test data by Santos & Correia (2001)

## 7.2 Applying the Hardin-Drnevich relationship in the HS Model

The decay of soil stiffness from small strains to larger strains can be associated with loss of intermolecular and surface forces within the soil skeleton. Once the direction of loading is reversed, the stiffness regains a maximum recoverable value which is in the order of the initial soil stiffness. Then, while loading in the reversed direction is continued, the stiffness decreases again. A strain history dependent, multi-axial extension of the Hardin-Drnevich relationship is therefore needed in order to apply it in the Hardening Soil model. Such an extension has been proposed by [Benz \(2006\)](#) (on page 245) in the form of the small-strain overlay model. Benz derives a scalar valued shear strain  $\gamma_{hist}$  by the following projection:

$$\gamma_{hist} = \sqrt{3} \frac{\| \mathbf{H} \Delta \mathbf{e} \|}{\| \Delta \mathbf{e} \|} \quad \text{Eq. [167]}$$

where

$\Delta \mathbf{e}$  = Actual deviatoric strain increment.  
 $\mathbf{H}$  = Symmetric tensor that represents the deviatoric strain history of the material.

Whenever a strain reversal is detected the tensor  $\mathbf{H}$  is partially or fully reset before the actual strain increment  $\Delta \mathbf{e}$  is added.

As the criterion for strain reversals serves a criterion similar as in Simpson's brick model (1992): All three principal deviatoric strain directions are checked for strain reversals separately which resembles three independent brick models. When there is no principal strain rotation, the criterion reduces to two independent brick-models. For further details on the strain tensor  $\mathbf{H}$  and its transformation at changes in the load path it is referred to [Benz \(2006\)](#) (on page 245).

## The Hardening Soil model with small-strain stiffness (HSsmall)

Applying the Hardin-Drnevich relationship in the HS Model

The scalar valued shear strain  $\gamma = \gamma_{hist}$  calculated in Eq. [167] is applied subsequently used in Eq. [166]. Note that in both, Eq. [166] and Eq. [167], the scalar valued shear strain is defined as:

$$\gamma = \frac{3}{2} \varepsilon_q \quad \text{Eq. [168]}$$

where

$$\varepsilon_q = \text{Second deviatoric strain invariant}$$

In triaxial conditions  $\gamma$  can therefore be expressed as:

$$\gamma = \varepsilon_{axial} - \varepsilon_{lateral} \quad \text{Eq. [169]}$$

Within the Hardening Soil model with small-strain stiffness, the stress-strain relationship can be simply formulated from the secant shear modulus (Eq. [166]) as:

$$\tau = G_s \gamma = \frac{G_0 \gamma}{1 + 0.385 \frac{\gamma}{\gamma_{0.7}}} \quad \text{Eq. [170]}$$

Taking the derivative with respect to the shear strain gives the tangent shear modulus:

$$G_t = \frac{G_0}{\left(1 + 0.385 \frac{\gamma}{\gamma_{0.7}}\right)^2} \quad \text{Eq. [171]}$$

This stiffness reduction curve reaches far into the plastic material domain. In the Hardening Soil model and Hardening Soil model with small-strain stiffness, stiffness degradation due to plastic straining is simulated with strain hardening. In the Hardening Soil model with small-strain stiffness, the small-strain stiffness reduction curve is therefore bound by a certain lower limit, determined by conventional laboratory tests:

- The lower cut-off of the tangent shear modulus  $G_t$  is introduced at the unloading reloading stiffness  $G_{ur}$  which is defined by the material parameters  $E_{ur}$  and  $\nu_{ur}$ :

$$G_t \geq G_{ur} \quad \text{where} \quad G_{ur} = \frac{E_{ur}}{2(1 + \nu_{ur})} \quad \text{and} \quad G_t = \frac{E_t}{2(1 + \nu_{ur})} \quad \text{Eq. [172]}$$

- The cut-off shear strain  $\gamma_{cut-off}$  can be calculated as:

$$\gamma_{cut-off} = \frac{1}{0.385} \left( \sqrt{\frac{G_0}{G_{ur}}} - 1 \right) \gamma_{0.7} \quad \text{Eq. [173]}$$

Within the Hardening Soil model with small-strain stiffness, the quasi-elastic tangent shear modulus is calculated by integrating the secant stiffness modulus reduction curve over the actual shear strain increment. An example of a stiffness reduction curve used in the Hardening Soil model with small-strain stiffness is shown in [Figure 35](#) (on page 86).

## The Hardening Soil model with small-strain stiffness (HSsmall)

Virgin (initial) loading vs unloading/reloading

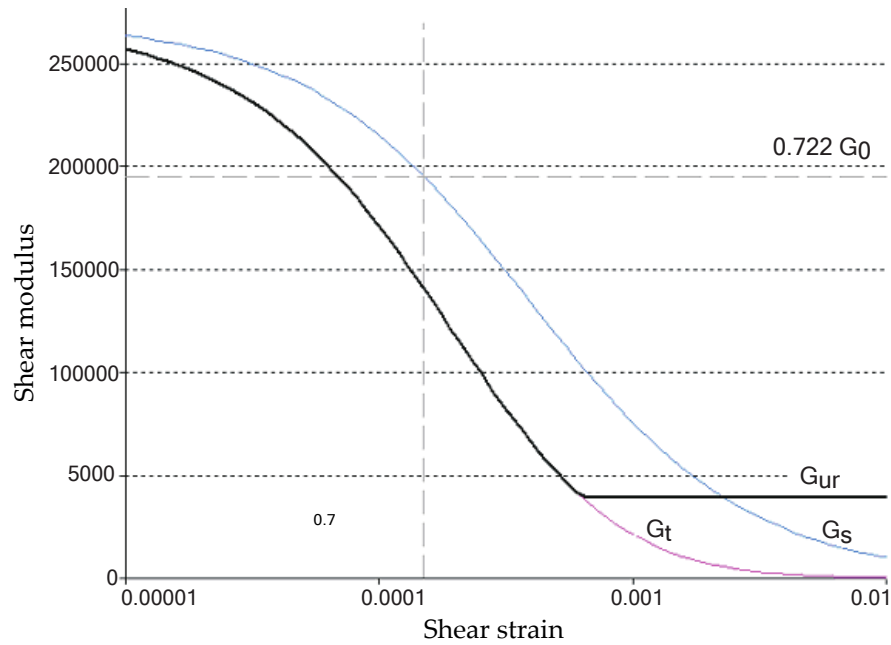


Figure 35: Secant and tangent shear modulus reduction curve

Moreover, the tangent shear modulus  $G_t$  and corresponding Young's modulus  $E_t$  (considering a constant Poisson's ratio  $\nu_{ur}$ ), is stress-dependent, and follows the same power law as formulated in Eq. [140]. For primary loading situations, the model uses the same hardening plasticity formulations as the Hardening Soil model, where  $E_{ur}$  is replaced by  $E_t$  as described above.

### 7.3 Virgin (initial) loading vs unloading/reloading

[Masing \(1926\)](#) (on page 247) described the hysteretic behaviour of materials in unloading / reloading cycles in the form of the following rules:

- The shear modulus in unloading is equal to the initial tangent modulus for the initial loading curve.
- The shape of the unloading and reloading curves is equal to the initial loading curve, but twice its size. In terms of the above introduced threshold shear strain  $\gamma_{0.7}$ , Masing's rule can be fulfilled by the following setting in the Hardin-Drnevich relation:

$$\gamma_{0.7 \text{ re-loading}} = 2\gamma_{0.7 \text{ virgin-loading}} \quad \text{Eq. [174]}$$

The Hardening Soil model with small-strain stiffness adopts Masing's rule. According to it, the threshold shear strain and the reloading curve are obtained by scaling the backbone curve (virgin loading) by a factor of 2. However, in the Hardening Soil model with small-strain stiffness, the hardening plasticity accounts for more rapidly decaying small-strain stiffness during virgin loading. [Figure 36](#) (on page 87) and [Figure 37](#) (on page 87) illustrate Masing's rule and the secant stiffness reduction in virgin loading and unloading / reloading.

## The Hardening Soil model with small-strain stiffness (HSsmall)

Model Parameters

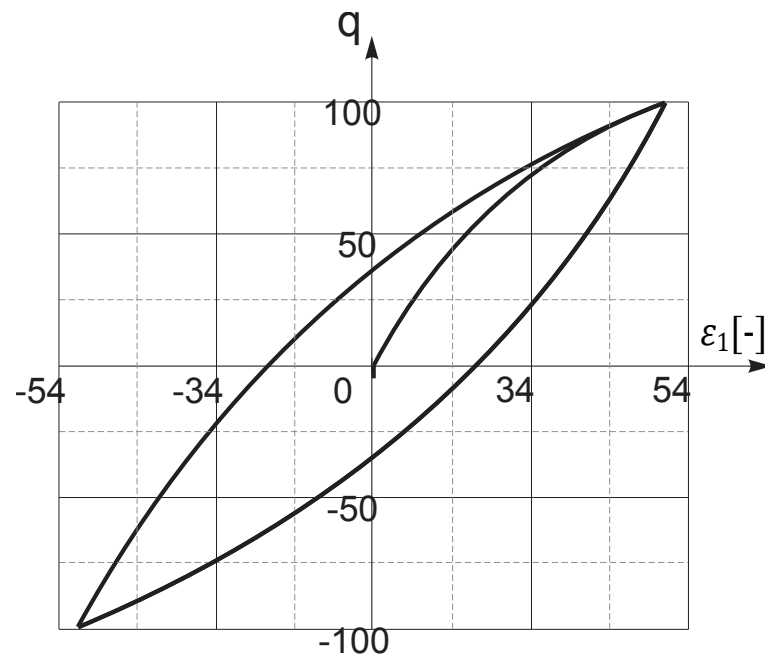


Figure 36: Hysteretic material behaviour

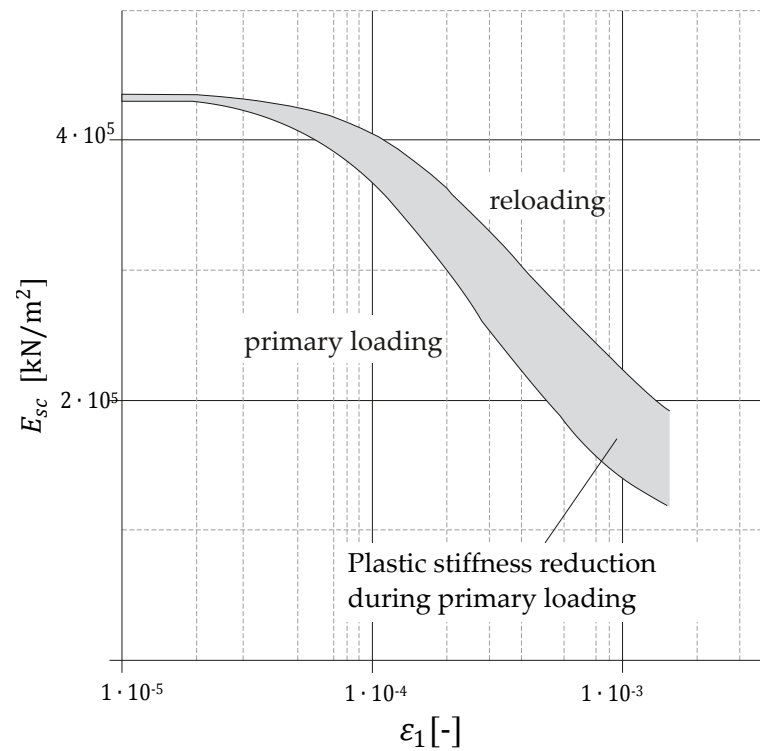


Figure 37: Stiffness reduction in initial -or primary loading and in unloading/reloading

## The Hardening Soil model with small-strain stiffness (HSsmall)

### Model Parameters

## 7.4 Model Parameters

Compared to the standard Hardening Soil model, the Hardening Soil model with small-strain stiffness requires two additional stiffness parameters as input:  $G_0^{ref}$  and  $\gamma_{0.7}$ . All other parameters, including the alternative stiffness parameters, remain the same as in the standard Hardening Soil model.  $G_0^{ref}$  defines the shear modulus at very small strains e.g.  $\varepsilon < 10^{-6}$  at a reference minor principal stress of  $\sigma'_3 = p^{ref}$ .

The Poisson's ratio  $\nu_{ur}$  is assumed a constant, as everywhere in PLAXIS, so that the shear modulus  $G_0^{ref}$  can also be calculated from the very small strain Young's modulus as:

$$G_0^{ref} = E_0^{ref} / (2(1 + \nu_{ur})) \quad Eq. [175]$$

The threshold shear strain  $\gamma_{0.7}$  is the shear strain at which the secant shear modulus  $G_s^{ref}$  is decayed to  $0.722G_0^{ref}$ . The threshold shear strain  $\gamma_{0.7}$  is to be supplied for virgin loading. In summary, the input stiffness parameters of the Hardening Soil model with small-strain stiffness are listed below:

$m$	Power for stress-level dependency of stiffness	[-]
$E_{50}^{ref}$	Secant stiffness in standard drained triaxial test	[KN/m <sup>2</sup> ]
$E_{oed}^{ref}$	Tangent stiffness for primary oedometer loading	[KN/m <sup>2</sup> ]
$E_{ur}^{ref}$	Unloading / reloading stiffness from drained triaxial test	[KN/m <sup>2</sup> ]
$\nu_{0.7}$	Poisson's ratio for unloading-reloading	[-]
$G_0^{ref}$	Reference shear modulus at very small strains ( $\varepsilon < 10^{-6}$ )	[KN/m <sup>2</sup> ]
$\gamma_{0.7}$	Threshold shear strain at which $G_s = 0.722G_0$	[-]

[Figure 38](#) (on page 89) illustrates the model's stiffness parameters in a drained triaxial test:  $E_{50}$ ,  $E_{ur}$ , and  $E_0 = 2G_0(1 + \nu_{ur})$ . For the order of strains at which  $E_{ur}$  and  $G_0$  are defined and determined, one may refer to e.g. [Figure 33](#) (on page 82) and [Figure 34](#) (on page 84).

## The Hardening Soil model with small-strain stiffness (HSsmall)

Model Parameters

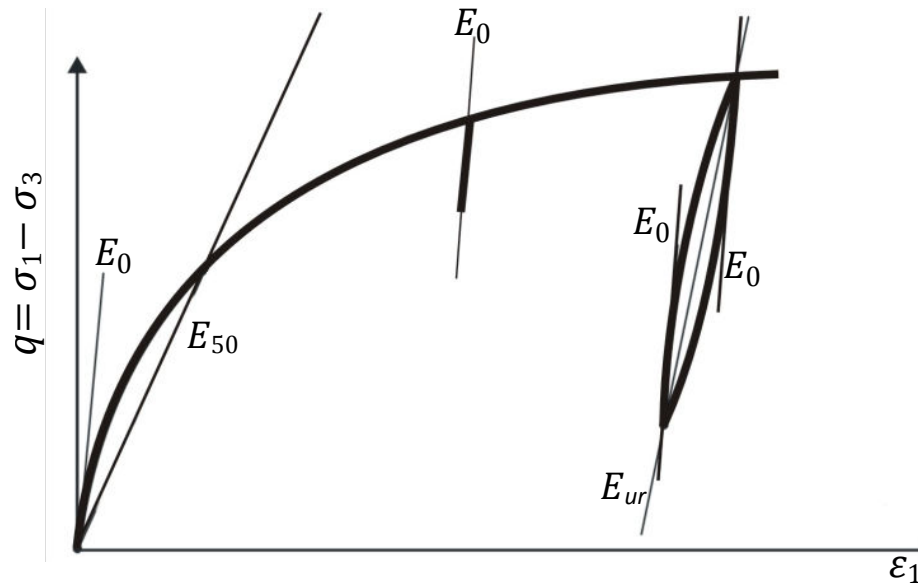


Figure 38: Stiffness parameters  $E_{50}$ ,  $E_{ur}$ , and  $E_0 = 2G_0(1 + \nu_{ur})$  of the Hardening Soil model with small-strain stiffness in a triaxial test

[Figure 39](#) (on page 89) illustrates the model's stiffness parameters in a stress-controlled drained cyclic shear test.

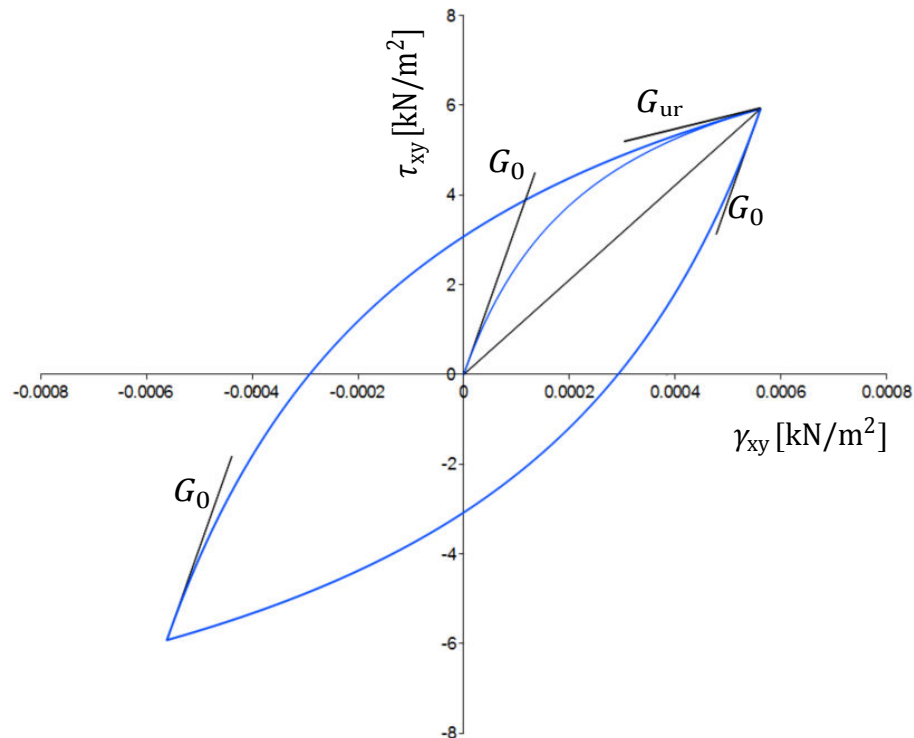


Figure 39: Stiffness parameters in cyclic shear test

A first estimation of the HSsmall parameters for quartz sand based on the relative density (RD) is given in [Brinkgreve, Engin & Engin \(2010\)](#) (on page 246).

## The Hardening Soil model with small-strain stiffness (HSsmall)

On the parameters  $G_0$  and  $\gamma_{0.7}$

### 7.5 On the parameters $G_0$ and $\gamma_{0.7}$

A number of factors influence the small-strain parameters  $G_0$  and  $\gamma_{0.7}$ . Most importantly they are influenced by the material's actual state of stress and void ratio  $e$ . In the Hardening Soil model with small-strain stiffness, the stress dependency of the shear modulus  $G_0$  is taken into account with the power law:

$$G_0 = G_0^{ref} \left( \frac{c \cos(\varphi) - \sigma'_3 \sin(\varphi)}{c \cos(\varphi) + p^{ref} \sin(\varphi)} \right)^m \quad Eq. [176]$$

which resembles the ones used for the other stiffness parameters. The threshold shear strain  $\gamma_{0.7}$  is taken independently of the mean stress.

Assuming that within a Hardening Soil model with small-strain stiffness (or HS) computation void ratio changes are rather small, the material parameters are not updated for changes in the void ratio. Knowledge of a material's initial void ratio can nevertheless be very helpful in deriving its small-strain shear stiffness  $G_0$ . Many correlations are offered in the literature ([Benz, 2006](#)) (on page 245). A good estimation for many soils is for example the relation given by [Hardin & Black \(1969\)](#) (on page 247):

$$G_0^{ref} = 33 \frac{(2.97 - e)^2}{1 + e} [MPa] \quad \text{for } p^{ref} = 100 [kPa] \quad Eq. [177]$$

[Alpan \(1970\)](#) (on page 245) empirically related dynamic soil stiffness to static soil stiffness ([Figure 40](#) (on page 90)). The dynamic soil stiffness in Alpan's chart is equivalent to the small-strain stiffness  $G_0$  or  $E_0$ . Considering that the static stiffness  $E_{static}$  defined by Alpan equals approximately the unloading / reloading stiffness  $E_{ur}$  in the Hardening Soil model with small-strain stiffness, Alpan's chart can be used to guess a soil's small-strain stiffness entirely based on its unloading / reloading stiffness  $E_{ur}$ . Although Alpan suggests that the ratio  $E_0 / E_{ur}$  can exceed 10 for very soft clays, the maximum ratio  $E_0 / E_{ur}$  or  $G_0 / G_{ur}$  permitted in the HSsmall model is limited to 20.

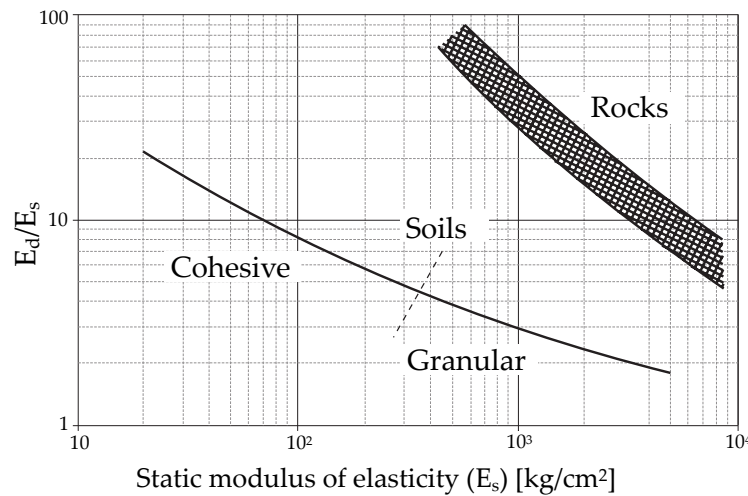


Figure 40: Relation between dynamic ( $E_d = E_0$ ) and static soil stiffness ( $E_s \approx E_{ur}$ ) after Alpan(1970)

## The Hardening Soil model with small-strain stiffness (HSsmall)

### Model Initialization

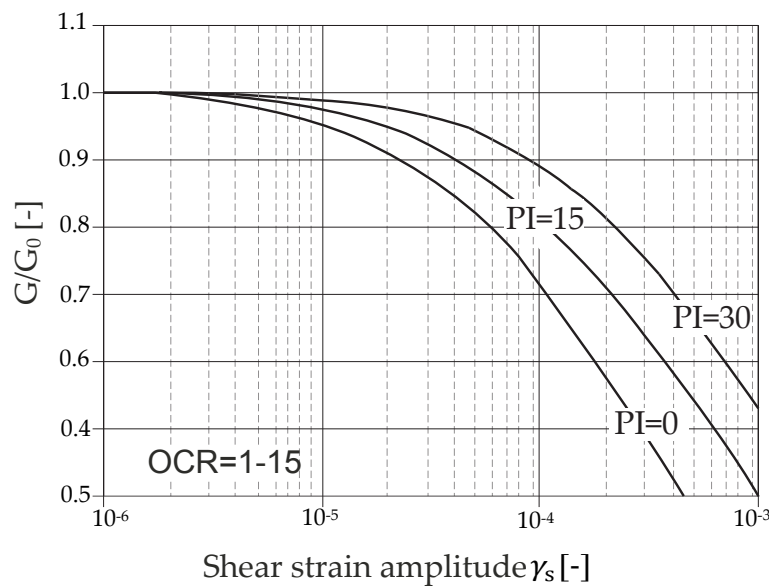


Figure 41: Influence of plasticity index (PI) on stiffness reduction after Vucetic & Dobry (1991)

In the absence of test data, correlations are also available for the threshold shear strain  $\gamma_{0.7}$ . Figure 41 (on page 91) for example gives a correlation between the threshold shear strain and the Plasticity Index. Using the original Hardin-Drnevich relationship, the threshold shear strain  $\gamma_{0.7}$  might be also related to the model's failure parameters. Applying the Mohr-Coulomb failure criterion in Eq. [165] and Eq. [166] yields:

$$\gamma_{0.7} \approx \frac{1}{9G_0} [2c'(1 + \cos(2\varphi')) - \sigma'_1(1 + K_0)\sin(2\varphi')] \quad \text{Eq. [178]}$$

where

$K_0$	=	The earth pressure coefficient at rest.
$\sigma'_1$	=	The effective vertical stress (pressure negative).

## 7.6 Model Initialization

Stress relaxation erases a soil's memory of previous applied stress. Soil aging in the form of particle (or assembly) reorganization during stress relaxation and formation of bonds between them can erase a soil's strain history. Considering that the second process in a naturally deposited soil develops relatively fast, the strain history should start from zero (**H**) in most boundary value problems. This is the default setting in the Hardening Soil model with small-strain stiffness.

However, sometimes an initial strain history may be desired. In this case the strain history can be adjusted by applying an extra load step before starting the actual analysis. Such an additional load step might also be used to model overconsolidated soils. Usually the overconsolidation's cause has vanished long before the start of calculation, so that the strain history should be reset afterwards. Unfortunately, strain history is already triggered by adding and removing a surcharge. In this case the strain history can be reset manually, by using the *Reset small strain* option in the calculation phases window. Also, when resetting displacements to zero, the strain history tensor is reset and the influence of strains from previous calculation phases is ignored.

## The Hardening Soil model with small-strain stiffness (HSsmall)

### State parameters in the Hardening Soil model with small-strain stiffness

When using the Hardening Soil model with small-strain stiffness, caution should be given to nil-steps. The strain increments in nil-steps are purely derived from the small numerical unbalance in the system which is due to the accepted tolerated error in the computation. The strain increment direction in nil-steps is therefore arbitrary. Hence, a nil-step may function as randomly reverse load step which is in most cases not desired.

## 7.7 State parameters in the Hardening Soil model with small-strain stiffness

In addition to the output of standard stress and strain quantities, the Hardening Soil model with small-strain stiffness provides output on *State variables*. These parameters can be visualised by selecting the *State parameters* option from the *stresses* menu. An overview of available state parameters in addition to those listed for the Hardening Soil model is given below:

$\varepsilon_{xx} - \varepsilon_v$	Strain history parameter used in strain-dependent stiffness formulation	[-]
$\varepsilon_{yy} - \varepsilon_v$	Strain history parameter used in strain-dependent stiffness formulation	[-]
$\varepsilon_{zz} - \varepsilon_v$	Strain history parameter used in strain-dependent stiffness formulation	[-]
$\varepsilon_{xy}$	Strain history parameter used in strain-dependent stiffness formulation	[-]
$\varepsilon_{yz}$	Strain history parameter used in strain-dependent stiffness formulation	[-]
$\varepsilon_{zx}$	Strain history parameter used in strain-dependent stiffness formulation	[-]
$G_s^{ref}$	Reference secant shear modulus at reference stress level	[kN/m <sup>2</sup> ]
$G/G_{ur}$	Ratio of elastic tangent shear modulus over unloading-reloading shear modulus	[-]

## 7.8 On the use of the Hardening Soil model with small-strain stiffness in dynamics calculations

In contrast to the Hardening Soil model, the Hardening Soil model with small-strain stiffness shows hysteresis in cyclic loading ([Figure 38](#) (on page 89)). The amount of hysteresis depends on the magnitude of the corresponding strain amplitude. However, note that the model does not generate accumulated strains with multiple loading cycles, nor does it generate accumulated pore pressures with undrained behaviour. When the Hardening Soil model with small-strain stiffness is used wave velocities are not shown because they vary due to the stress-dependent stiffness.

When applied in dynamics calculations, the hysteretic behaviour of the Hardening Soil model with small-strain stiffness leads to damping. The amount of hysteretic damping depends on the applied load amplitude and corresponding strain amplitudes. The maximum amount of hysteretic damping obtained with the Hardening Soil model with small-strain stiffness depend on the ratio of  $G_0$  and  $G_{ur} = E_{ur} / 2(1 + \nu_{ur})$ . A larger ratio leads to a

## The Hardening Soil model with small-strain stiffness (HSsmall)

Other differences with the Hardening Soil model

---

larger maximum amount of hysteretic damping. For more information about the hysteretic damping in the Hardening Soil model with small-strain stiffness reference is made to [Brinkgreve, Kappert & Bonnier](#) (on page 246).

## 7.9 Other differences with the Hardening Soil model

### 7.9.1 The mobilised dilatancy angle

The shear hardening flow rule of both the Hardening Soil model and the Hardening Soil model with small-strain stiffness have the linear form:

$$\dot{\varepsilon}_v^p = \sin(\psi_m) \dot{\gamma}^p \quad \text{Eq. [179]}$$

The mobilised dilatancy angle  $\psi_m$  in compression however, is defined differently. The HS model assumes the following:

$$\begin{aligned} \text{For } \sin(\phi_m) < \frac{3}{4}\sin(\phi) \quad & \psi_m = 0 \\ \text{For } \sin(\phi_m) < \frac{3}{4}\sin(\phi) \text{ and } \psi > 0 \quad & \sin(\psi_m) = \max\left(\frac{\sin(\phi_m) - \sin(\phi_{cv})}{1 - \sin(\phi_m)\sin(\phi_{cv})}, 0\right) \\ \text{For } \sin(\phi_m) < \frac{3}{4}\sin(\phi) \text{ and } \psi \leq 0 \quad & \psi_m = \psi \\ \text{If } \phi = 0 \quad & \psi_m = 0 \end{aligned} \quad \text{Eq. [180]}$$

where

$\phi_{cv}$  = Critical state friction angle, being a material constant independent of density.

$\phi_m$  = The mobilised friction angle.

$$\sin(\phi_m) = \frac{\sigma'_1 - \sigma'_3}{\sigma'_1 + \sigma'_3 - 2c \cot(\phi)} \quad \text{Eq. [181]}$$

## The Hardening Soil model with small-strain stiffness (HSsmall)

Other differences with the Hardening Soil model

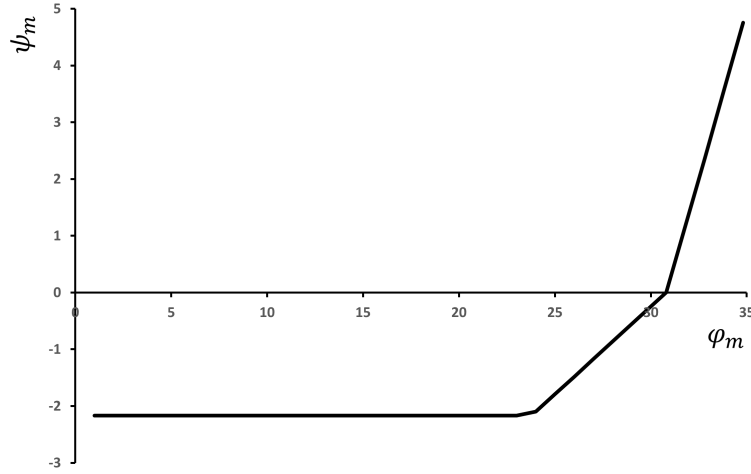


Figure 42: Plot of mobilised dilatancy angle  $\psi_m$  and mobilized friction angle  $\varphi_m$  for Hardening Soil model with small-strain stiffness

For small mobilised friction angles and for negative values of  $\psi_m$ , as computed by Rowe's formula,  $\psi_m$  in the Hardening Soil model is taken zero. Bounding the lower value of  $\psi_m$  may sometimes yield too little plastic volumetric strains though. Therefore, the Hardening Soil model with small-strain stiffness adapts an approach by [Li & Dafalias \(2000\)](#) (on page 247) whenever  $\psi_m$ , as computed by Rowe's formula, is negative. In that case, the mobilised dilatancy in the Hardening Soil model with small-strain stiffness is calculated by the following equation:

$$\sin(\psi_m) = \frac{1}{10} \left( -M_c \exp \left[ \frac{1}{15} \ln \left( \frac{M_c}{M_d} \frac{q}{q_a} \right) \right] + M_d \right) \quad \text{Eq. [182]}$$

where:

$$M_c = \frac{6 \sin(\varphi_{cv})}{3 - \sin(\varphi_{cv})} \quad \text{Eq. [183]}$$

$$M_d = \frac{6 \sin(\varphi_m)}{3 - \sin(\varphi_m)} \quad \text{Eq. [184]}$$

$$\frac{q}{q_a} = \max \left( \frac{1 - \sin(\varphi_{cv})}{\sin(\varphi_{cv})} \cdot \frac{\sin(\varphi_m)}{1 - \sin(\varphi_m)}, 10^{-4} \right) \quad \text{Eq. [185]}$$

And the mobilized friction angle is limited to:

$$\sin(\varphi_m) \geq \frac{\sin(\varphi_{cv})}{2 + \sin(\varphi_{cv})} \quad \text{Eq. [186]}$$

The mobilised dilatancy as a function of  $\varphi_m$  for the Hardening Soil model with small-strain stiffness is visualised in [Figure 42](#) (on page 94) for the specific case of  $\varphi=35^\circ$  and  $\psi=5^\circ$ .

# Modified Cam-Clay model

The Modified Cam-Clay model is described in several textbooks on critical state soil mechanics (for example [Muir Wood \(1990\)](#) (on page 248)). In this chapter a short overview is given of the basic equations.

## 8.1 Formulation of the Modified Cam-Clay model

In the Modified Cam-Clay model, a logarithmic relation is assumed between void ratio  $e$  and the mean effective stress  $p'$  in virgin isotropic compression, which can be formulated as:

$$e - e^0 = -\lambda \ln \left( \frac{p'}{p^0} \right) \quad (\text{virgin isotropic compression}) \quad \text{Eq. [187]}$$

The parameter  $\lambda$  is the Cam-Clay isotropic compression index, which determines the compressibility of the material in primary loading. When plotting relation (Eq. [187]) in a  $e - \ln p'$  diagram one obtains a straight line. During unloading and reloading, a different line is followed, which can be formulated as:

$$e - e^0 = -\kappa \ln \left( \frac{p'}{p^0} \right) \quad (\text{isotropic unloading and reloading}) \quad \text{Eq. [188]}$$

The parameter  $\kappa$  is the Cam-Clay isotropic swelling index, which determines the compressibility of material in unloading and reloading. In fact, an infinite number of unloading and reloading lines exists in  $p' - e$ -plane each corresponding to a particular value of the pre-consolidation stress  $p_p$ .

The yield function of the Modified Cam-Clay model is defined as:

$$f = \frac{q^2}{M^2} + p'(p' - p_p) \quad \text{Eq. [189]}$$

The yield surface ( $f = 0$ ) represents an ellipse in  $p' - q$ -plane as indicated in [Figure 43](#) (on page 96). The yield surface is the boundary of the elastic stress states. Stress paths within this boundary only give elastic strain increments, whereas stress paths that tend to cross the boundary generally give both elastic and plastic strain increments.

In  $p' - q$  - plane, the top of the ellipse intersects a line that we can be written as:

$$q = Mp' \quad \text{Eq. [190]}$$

This line is called the critical state line (CSL) and gives the relation between  $p'$  and  $q$  in a state of failure (i.e. the critical state). The constant  $M$  is the tangent of the critical state line and determines the extent to which the ultimate deviatoric stress,  $q$ , depends on the mean effective stress,  $p'$ . Hence,  $M$  can be regarded as a friction constant. Moreover,  $M$  determines the shape of the yield surface (height of the ellipse) and influences the

## Modified Cam-Clay model

### Parameters of the Modified Cam-Clay model

coefficient of lateral earth pressure  $K_0^{nc}$  in a normally consolidated stress state under conditions of one-dimensional compression.

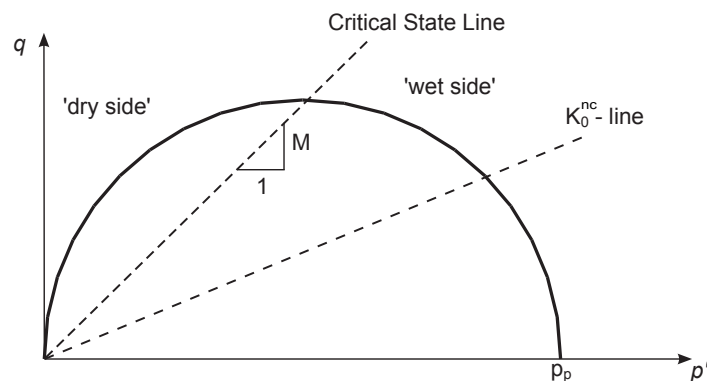


Figure 43: Yield surface of the of the Modified Cam-Clay model in  $p'$ - $q$  - plane

The preconsolidation stress,  $p_p$ , determines the size of the ellipse. In fact, an infinite number of ellipses exist, each corresponding to a particular value of  $p_p$ .

The left hand side of the yield ellipse (often described as the 'dry side' of the critical state line) may be thought of as a failure surface. In this region plastic yielding is associated with softening, and therefore failure. The values of  $q$  can become unrealistically large in this region.

For more detailed information on Cam-Clay type models, the reader is referred to [Muir Wood \(1990\)](#) (on page 248).

#### Note:

Note that the Modified Cam-Clay model model as implemented in PLAXIS gives a Drucker-Prager failure state instead of a Mohr-Coulomb model type of failure.

## 8.2 Parameters of the Modified Cam-Clay model

The Modified Cam-Clay model is based on the following parameters:

- Parameters for stiffness:

$\lambda$	Cam-Clay compression index	[-]
$\kappa$	Cam-Clay swelling index	[-]
$\nu_{ur}$	Poisson's ratio	[-]
$e_{init}$	Initial void ratio for loading/unloading	[-]

## Modified Cam-Clay model

### State parameters in the Modified Cam-Clay model

- Parameters for strength:

$M$	Tangent of the critical state line	[-]
$K_0^{nc}$	Coefficient of lateral stress in normal consolidation derived from $M$ . The relationship between $M$ and $K_0^{nc}$ is given in the <a href="#">Material Models Manual - Soft soil creep Model - Parameters of the soft soil creep model</a> .	[-]

### 8.2.1 Compression index and swelling index

These parameters can be obtained from an isotropic compression test including isotropic unloading. When plotting the natural logarithm of the mean stress as a function of the void ratio for clay-type materials, the plot can be approximated by two straight lines. The slope of the primary loading line gives the compression index and the slope of the unloading line gives the swelling index. These parameters can be obtained from a one-dimensional compression test, as discussed in [Parameters of the Soft Soil model](#) (on page 114).

### 8.2.2 Poisson's Ratio

Poisson's ratio  $\nu_{ur}$  is a real elastic parameter and not a pseudo-elasticity constant as used in the Mohr-Coulomb model. Its value will usually be in the range between 0.1 and 0.2.

### 8.2.3 Tangent of the critical state line

In order to obtain the correct shear strength, the parameter  $M$  should be based on the friction angle  $\varphi$ . The critical state line is comparable with the Drucker-Prager failure line, and represents a (circular) cone in principal stress space. Hence, the value of  $M$  can be obtained from  $\varphi$ :

$$M = \frac{6\sin\varphi}{3 - \sin\varphi} \quad (\text{for initial compression stress states}) \quad (\sigma'_1 \leq \sigma'_2 = \sigma'_3) \quad \text{Eq. [191]}$$

$$M = \frac{6\sin\varphi}{3 + \sin\varphi} \quad (\text{for initial compression stress states}) \quad (\sigma'_1 = \sigma'_2 \leq \sigma'_3) \quad \text{Eq. [192]}$$

$$M \approx \sqrt{3}\sin\varphi \quad (\text{for plane strain stress states}) \quad \text{Eq. [193]}$$

In addition to determining the shear strength, the parameter  $M$  has an important influence on the value of the coefficient of lateral earth pressure,  $K_0^{nc}$ , in a state of normal consolidation. In general, when  $M$  is chosen such that the model predicts the correct shearing strength, the resulting value of  $K_0^{nc}$  is too high.

## Modified Cam-Clay model

On the use of the Modified Cam-Clay model in dynamics calculations

---

### 8.3 State parameters in the Modified Cam-Clay model

In addition to the output of standard stress and strain, the Modified Cam-Clay model provides output (when being used) on state variables such as the isotropic pre-consolidation stress  $p_p$  and the isotropic overconsolidation ratio  $OCR$ . These parameters can be visualised by selecting the *State parameters* option from the *Stresses* menu. An overview of available state parameters is given below:

$p_{eq}$	Equivalent isotropic stress. $P_{eq} = p' + \frac{q^2}{M^2 p'}$	[kN/m <sup>2</sup> ]
$p_p$	Isotropic preconsolidation stress	[kN/m <sup>2</sup> ]
$OCR$	Isotropic overconsolidation ratio ( $OCR = p^p/p^{eq}$ )	[-]

### 8.4 On the use of the Modified Cam-Clay model in dynamics calculations

When using the Modified Cam-Clay model in dynamics calculations, the swelling index  $\kappa$  needs to be selected such that the model correctly predicts wave velocities in the soil. This generally requires a smaller value than just an unloading-reloading index.

When subjected to dynamic or cyclic loading, the Modified Cam-Clay model will generate plastic strains when the preconsolidation stress is increased. However, it should be noted that stress cycles within the current creep contour will only generate elastic strains and no (hysteretic) damping, nor accumulation of strains or pore pressure, nor liquefaction. In order to account for the soil damping in cyclic loading, Rayleigh damping may be defined.

### 8.5 Warning

The Modified Cam-Clay model may allow for extremely large shear stresses. This is particularly the case for stress paths that cross the critical state line. Furthermore, the Modified Cam-Clay model may give softening behaviour for particular stress paths. Without special regularization techniques, softening behaviour may lead to mesh dependency and convergence problems of iterative procedures. Moreover, the Modified Cam-Clay model cannot be used in combination with *Safety analysis* by means of phi-c reduction. The use of the Modified Cam-Clay model in practical applications is not recommended.

# The NGI-ADP model (anisotropic undrained shear strength)

The NGI-ADP model may be used for capacity, deformation and soil-structure interaction analyses involving undrained loading of clay. The basis of the material model is:

- Input parameters for (undrained) shear strength for three different stress paths/ states (Active, Direct Simple Shear, Passive).
- A yield criterion based on a translated approximated Tresca criterion.
- Elliptical interpolation functions for plastic failure strains and for shear strengths in arbitrary stress paths.
- Isotropic elasticity, given by the unloading/reloading shear modulus,  $G_{ur}$ .

## 9.1 Formulation of the NGI-ADP model

The NGI-ADP model is formulated for a general stress state, matching both undrained failure shear strengths and strains to that of selected design profiles ([Andresen & Jostad, 1999](#) (on page 245) ; [Andresen, 2002](#) (on page 245) ; [Grimstad, Andresen & Jostad, 2010](#) (on page 247) ). The model formulation is presented in steps, starting with 1D anisotropy in triaxial test condition. In [The NGI-ADP model in plane strain](#) (on page 100) a simplified expression for plane strain is presented. Thereafter the formulation is extended to full 3D stress state. In this formulation compressive stresses are positive.

In the NGI-ADP model the Tresca approximation after [Billington \(1988\)](#) (on page 246) together with a modified von Mises plastic potential function ([von Mises, 1913](#) (on page 249) ) is used to circumvent the possible corner problems. The yield and plastic potential function are independent of the mean stress hence zero plastic volume strain develops.

### 9.1.1 1D model presentation

Under triaxial tests condition two undrained shear strengths can be determined, i.e.  $s_u^C$  and  $s_u^E$ . The test measures the response in vertical stress  $\sigma'_v$  and horizontal stress  $\sigma'_h$  for applied shear strain  $\gamma$ . The Tresca yield criteria can be modified, Eq. [194], to account for the difference in undrained shear strength in compression and extension:

## The NGI-ADP model (anisotropic undrained shear strength)

Formulation of the NGI-ADP model

$$f = \left| \tau - (1 - \kappa)\tau_0 - \kappa \frac{s_u^C - s_u^E}{2} \right| - \kappa \frac{s_u^C + s_u^E}{2} = 0 \quad Eq. [194]$$

where

$$\begin{aligned} \tau &= \text{Shear stress defined as } \tau = 0.5(\sigma'_v - \sigma'_h) \\ \tau_0 &= \text{Initial in situ maximum shear stress. Defined as } \tau_0 = 0.5(\sigma'_{v0} - \sigma'_{h0}) = 0.5\sigma'_{v0}(1 - K_0) \end{aligned}$$

To account for difference in failure shear strain a stress path dependent hardening parameter is introduced. The stress path dependent hardening is made possible by different plastic failure shear strain  $\gamma_f^p$  in compression and extension. The hardening function is given by:

$$\kappa = 2 \frac{\sqrt{\gamma^p / \gamma_f^p}}{1 + \gamma^p / \gamma_f^p}; \text{ when } \gamma^p < \gamma_f^p; \text{ else } \kappa = 1 \quad Eq. [195]$$

where

$$\begin{aligned} \gamma^p &= \text{Plastic shear strain.} \\ \gamma_f^p &= \text{Failure (peak) plastic shear strain.} \end{aligned}$$

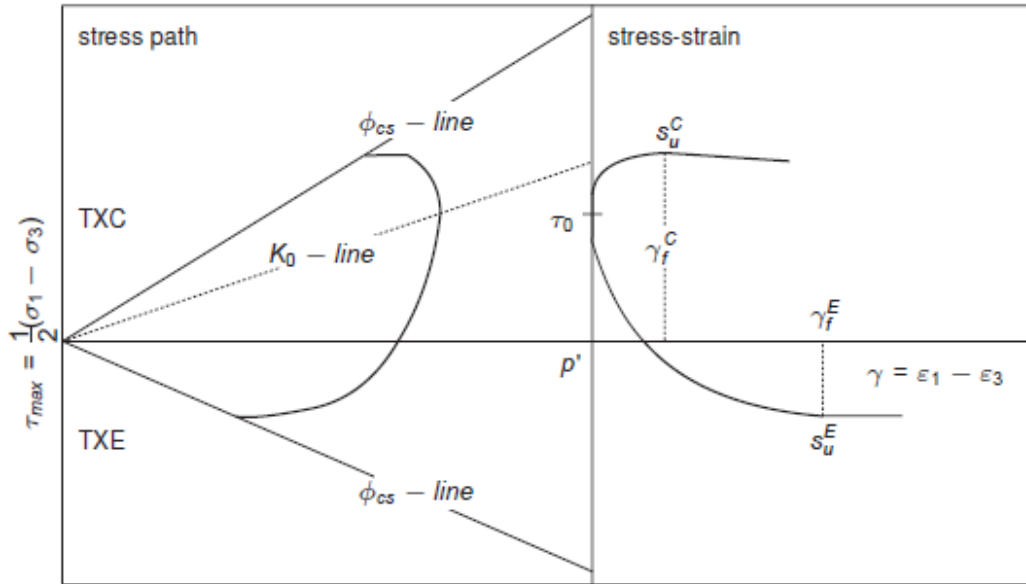


Figure 44: Typical stress paths and stress strain curves for triaxial compression and triaxial extension

### 9.1.2 The NGI-ADP model in plane strain

The yield criterion for the NGI-ADP model in plane strain is defined by:

$$f = \sqrt{\left( \frac{\sigma_{yy} - \sigma_{xx}}{2} - (1 - \kappa)\tau_0 - \kappa \frac{s_u^A - s_u^P}{2} \right)^2 + \left( \tau_{xy} - \frac{s_u^A + s_u^P}{2s_u^{DSS}} \right)^2} - \kappa \frac{s_u^A + s_u^P}{2} = 0 \quad Eq. [196]$$

## The NGI-ADP model (anisotropic undrained shear strength)

### Formulation of the NGI-ADP model

Restriction to clays with horizontal surfaces are made to simplify the presentation. Further  $y$  is taken as the vertical (depositional) direction. For isotropy in hardening (i.e.  $\kappa$  independent of stress orientation) Eq. [196] plots as an elliptical shaped curve in a plane strain deviatoric stress plot. When  $\kappa$  equals 1.0, the criterion in Eq. [196] reduces to the formulation given by [Davis & Christian \(1971\)](#) (on page 246). While hardening the yield curves are characterised by slightly distorted elliptical shapes. The shape is dependent on the interpolation function used and values of failure strain. The NGI-ADP model uses elliptical interpolation between failure strain in passive stress state, direct simple shear and active stress state. In the implementation of the NGI-ADP model the yield surface is ensured to remain convex by restricting the input.

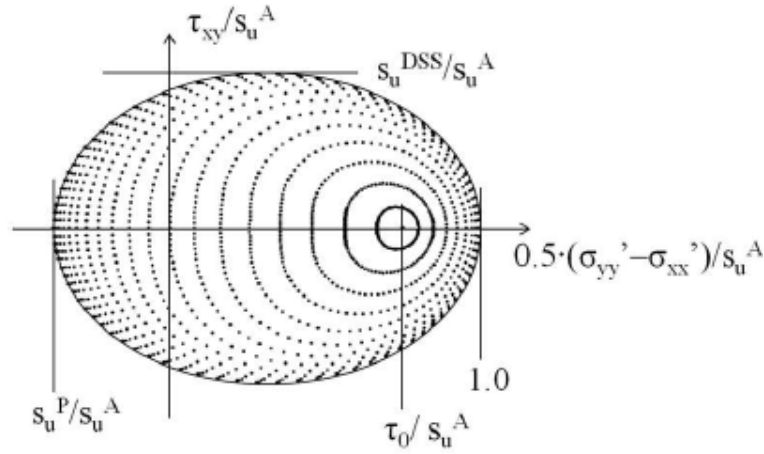


Figure 45: Typical deviatoric plane strain plot of equal shear strain contours for the NGI-ADP model

### 9.1.3 The NGI-ADP model in 3D stress space

This section describes the actual implementation of the NGI-ADP model in PLAXIS, whereas the previous sections should be regarded as an introduction using simplified formulation. For the general stress condition a modified deviatoric stress vector is defined as:

$$\begin{bmatrix} \hat{s}_{xx} \\ \hat{s}_{yy} \\ \hat{s}_{zz} \\ \hat{s}_{xy} \\ \hat{s}_{xz} \\ \hat{s}_{yz} \end{bmatrix} = \begin{bmatrix} \sigma'_{xx} - \sigma'_{xx0}(1 - \kappa) + \kappa \frac{1}{3}(s_u^A - s_u^P) - \hat{p} \\ \sigma'_{yy} - \sigma'_{yy0}(1 - \kappa) - \kappa \frac{2}{3}(s_u^A - s_u^P) - \hat{p} \\ \sigma'_{zz} - \sigma'_{zz0}(1 - \kappa) + \kappa \frac{1}{3}(s_u^A - s_u^P) - \hat{p} \\ \tau_{xy}s_u^A + \frac{s_u^P}{2s_u^{DSS}} \\ \tau_{xz} \\ \tau_{yz} \frac{s_u^A + s_u^P}{2s_u^{DSS}} \end{bmatrix} \quad \text{Eq. [197]}$$

where

$$\sigma'_{xx0}, \sigma'_{yy0} \text{ and } \sigma'_{zz0} = \text{Initial stresses.}$$

## The NGI-ADP model (anisotropic undrained shear strength)

Formulation of the NGI-ADP model

$\hat{p}$  = the modified mean stress. The modified mean stress is defined as:

$$\hat{p} = \frac{(\sigma'_{xx} - \sigma'_{xx0})(1 - \kappa) + (\sigma'_{yy} - \sigma'_{yy0})(1 - \kappa) + (\sigma'_{zz} - \sigma'_{zz0})(1 - \kappa)}{3} = p' - (1 - \kappa)p'_0 \quad \text{Eq. [198]}$$

where

$p'$  = Mean stress

Modified second and third deviatoric invariants are defined accordingly in Eq. [199] and Eq. [200].

$$\hat{J}_2 = -\hat{s}_{xx}\hat{s}_{yy} - \hat{s}_{xx}\hat{s}_{zz} - \hat{s}_{yy}\hat{s}_{zz} + \hat{s}_{xz}^2 + \hat{s}_{yz}^2 + \hat{s}_{xy}^2 \quad \text{Eq. [199]}$$

$$\hat{J}_3 = \hat{s}_{xx}\hat{s}_{yy}\hat{s}_{zz} + 2\hat{s}_{xy}\hat{s}_{yz}\hat{s}_{xz} - \hat{s}_{xx}\hat{s}_{yz}^2 - \hat{s}_{yy}\hat{s}_{xz}^2 - \hat{s}_{zz}\hat{s}_{xy}^2 \quad \text{Eq. [200]}$$

The yield criterion is expressed as:

$$f = \sqrt{H(\omega)\hat{J}_2} - \kappa \frac{s_u^A + s_u^P}{2} = 0 \quad \text{Eq. [201]}$$

where, to approximate the Tresca criterion, the term  $H(\omega)$  is defined as:

$$H(\omega) = \cos^2\left(\frac{1}{6}\arccos(1 - 2a_1\omega)\right) \quad \text{with} \quad \omega = \frac{27}{4} \frac{\hat{J}_3^2}{\hat{J}_2^3} \quad \text{Eq. [202]}$$

By letting the value of  $a_1$  go to 1.0 an exact Tresca criterion is obtained. The parameter  $a_1$  can be directly linked to the rounding ratio  $s_u^C/s_u^A$ . This ratio takes typically a value just below 1.0 and a value of 0.99 is chosen as an appropriate default. Figure 46 (on page 102) shows the failure criterion of the NGI-ADP model in the  $\sigma$ -plane (for Cartesian stresses) with default rounding ratio. This criterion is continuous and differentiable and it is described by a single function.

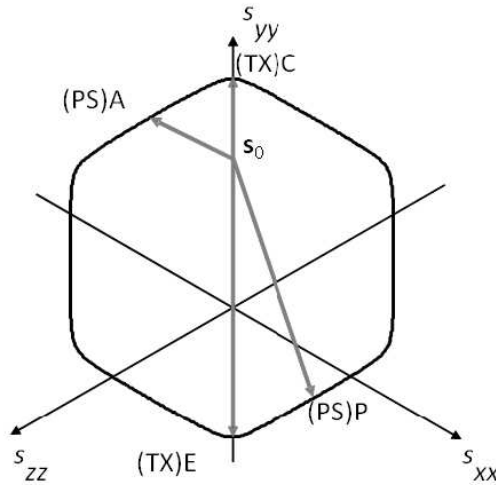


Figure 46: Failure criterion of the NGI-ADP model in the  $\sigma$ -plane

The combinations of strength ratios are limited by lower limit for combinations of  $s_u^C/s_u^A$  and  $s_u^P/s_u^A$ .

The value of  $\gamma^P$  is given by elliptical interpolation:

## The NGI-ADP model (anisotropic undrained shear strength)

Formulation of the NGI-ADP model

$$\gamma_f^p(\hat{\theta}) = \frac{\hat{R}_B \hat{R}_D \sqrt{(\hat{R}_D^2 - \hat{R}_C^2) \cos^2 \hat{\theta} + \hat{R}_C^2} \cdot \hat{R}_D^2 \hat{R}_A \cos(2\hat{\theta})}{\hat{R}_B^2 \cdot (\hat{R}_B^2 - \hat{R}_D^2) \cos^2(2\hat{\theta})} \quad \text{Eq. [203]}$$

where

$$\hat{R}_A = \frac{\gamma_{f,E}^p \cdot \gamma_{f,C}^p}{2} \quad \text{Eq. [204]}$$

$$\hat{R}_B = \frac{\gamma_{f,E}^p + \gamma_{f,C}^p}{2} \quad \text{Eq. [205]}$$

$$\hat{R}_C = \sqrt{\gamma_{f,E}^p \gamma_{f,C}^p} \quad \text{Eq. [206]}$$

$$\hat{R}_D = \frac{\gamma_{f,DSS}^p \hat{R}_B}{\hat{R}_C} \quad \text{Eq. [207]}$$

and  $\gamma_{f,C}^p$ ,  $\gamma_{f,DSS}^p$  and  $\gamma_{f,E}^p$  are the failure plastic maximum shear strain in triaxial compression, direct simple shear and triaxial extension respectively. Note that  $\hat{\theta}$  is not the Lode angle, but is defined as:

$$\cos(2\hat{\theta}) = \frac{\sqrt{3}}{2} \frac{\hat{s}_{xy}}{\sqrt{\hat{J}_2}} \quad \text{Eq. [208]}$$

A non-associated flow rule is used such that the derivative of the plastic potential  $g$  is:

$$\frac{\partial g}{\partial \sigma} = \frac{1}{2} \left( \hat{I} + \frac{\partial p}{\partial \sigma} \left( \frac{\partial \hat{s}}{\partial p} \right)^T \right) \frac{\partial \hat{J}_2}{\partial \hat{s}} \sqrt{\frac{1}{\hat{J}_2}} \quad \text{Eq. [209]}$$

where  $\hat{i}$  is a modified unit vector:

$$\hat{I} = \begin{bmatrix} 1 & & & & \\ & 1 & & & \\ & & 1 & & \\ & & & \frac{s_u^A + s_u^P}{2s_u^{DSS}} & \\ & & & & 1 \\ & & & & & \frac{s_u^A + s_u^P}{2s_u^{DSS}} \end{bmatrix} \quad \text{Eq. [210]}$$

The increment in plastic shear strain is defined as:

$$d\gamma^p = \sqrt{H(\omega)} \left( \frac{2}{3} \left( (d\varepsilon_{xx}^p - d\varepsilon_{yy}^p)^2 + (d\varepsilon_{xx}^p - d\varepsilon_{zz}^p)^2 + (d\varepsilon_{yy}^p - d\varepsilon_{zz}^p)^2 + (d\gamma_{xy}^p)^2 + (d\gamma_{xz}^p)^2 + (d\gamma_{yz}^p)^2 \right)^{1/2} \right) \quad \text{Eq. [211]}$$

where the plastic strains are defined as:

$$d\varepsilon^p = d\lambda \frac{\partial g}{\partial \sigma} \quad \text{Eq. [212]}$$

## The NGI-ADP model (anisotropic undrained shear strength)

Parameters of the NGI-ADP model

with  $d\lambda$  being the plastic multiplier. Hence, Eq. [211] gives the relation between the hardening parameter  $\gamma^p$  and the plastic multiplier  $d\lambda$ .

### 9.1.4 The NGI-ADP model traction criterion for interfaces in 2D

For plane strain conditions a traction criterion, corresponding to the plane strain failure criterion is formulated. This criterion is intended to be used on interface elements in finite element calculations. The interface strength is controlled by a lower and upper limit, which are dependent on the direction of the interface,  $\beta$ .

Let a plane being oriented by the direction  $\beta$  to the horizontal. The plane has a tangential direction  $t$  and a normal direction  $n$  and the adjacent continuum defines the stresses  $\sigma_{nn}$ ,  $\sigma_{tt}$  and  $\tau_n$  by:

$$\begin{bmatrix} \sigma_{tt} \\ \sigma_{nn} \\ \tau_{nn} \end{bmatrix} = A \begin{bmatrix} \sigma_{xx} \\ \sigma_{yy} \\ \tau_{xy} \end{bmatrix} \quad \text{Eq. [213]}$$

where

$$A = \text{Transformation matrix.}$$

In a local coordinate system three strains  $\varepsilon_{nn}$ ,  $\varepsilon_{tt}$  and  $\gamma_{tn}$  are defined in the plane strain condition. Due to the requirement of no volume change for a perfect plastic mechanism with shearing in tangential direction, will give that  $\varepsilon_{nn} = \varepsilon_{tt} = 0$ , resulting in:

$$\frac{\partial f}{\partial (\sigma_{nn} - \sigma_{tt})} = 0 \quad \text{Eq. [214]}$$

The plane strain formulation for the NGI-ADP model is defined as follows:

$$f = \sqrt{\left( \frac{\sigma_{nn} - \sigma_{tt}}{2} \cos(2\beta) - \tau_{tn} \sin(2\beta) - R_A \right)^2 + \left( \frac{R_B}{R_D} \left( \frac{\sigma_{nn} - \sigma_{tt}}{2} \sin(2\beta) + \tau_{tn} \cos(2\beta) \right) \right)^2} - R_B \quad \text{Eq. [215]}$$

where

$$R_A = \frac{s_u^A - s_u^P}{2} \quad \text{Eq. [216]}$$

$$R_B = \frac{s_u^A - s_u^P}{2} \quad \text{Eq. [217]}$$

$$R_D = s_u^{DSS} \quad \text{Eq. [218]}$$

## The NGI-ADP model (anisotropic undrained shear strength)

Parameters of the NGI-ADP model

### 9.2 Parameters of the NGI-ADP model

The NGI-ADP model requires a total of eleven parameters.

- Parameters for stiffness:

$G_{ur} / s_u^A$	Ratio unloading/reloading shear modulus over (plane strain) active shear strength	[-]
$\gamma_f^C$	Shear strain in triaxial compression ( $\gamma_f^C = 3 / 2 \varepsilon_1^C$ )	[%]
$\gamma_f^E$	Shear strain in triaxial extension	[%]
$\gamma_f^{DSS}$	Shear strain in direct simple shear	[%]

- Parameters for strength:

$s_u^{A, ref}$	Reference (plane strain) active shear strength	[kN/m <sup>2</sup> ]
$s_u^{C, TX} / s_u^A$	Ratio triaxial compressive shear strength over (plane strain) active shear strength (default = 0.99)	[-]
$y_{ref}$	Reference level	[m]
$s_{u, inc}^A$	Increase of shear strength with depth	[kN/m <sup>2</sup> /m]
$s_u^P / s_u^A$	Ratio of (plane strain) passive shear strength over (plane strain) active shear strength	[-]
$\tau_0 / s_u^A$	Initial mobilization (default = 0.7)	[-]
$s_u^{DSS} / s_u^A$	Ratio of direct simple shear strength over (plane strain) active shear strength	[-]

- Advanced parameters:

$\nu'$	Effective Poisson's ratio	[-]
$\nu_u$	Undrained Poisson's ratio	[-]

## The NGI-ADP model (anisotropic undrained shear strength)

Parameters of the NGI-ADP model

---

### 9.2.1 Ratio unloading / reloading shear modulus over plane strain active shear strength ( $G_{ur}/s_u^A$ )

Ratio unloading / reloading shear stiffness as a ratio of the plane strain active shear strength. If the shear strength is increasing with depth the constant ratio for  $G_{ur}/s_u^A$  gives a shear stiffness increasing linearly with depth.

### 9.2.2 Shear strain at failure in triaxial compression ( $\gamma_f^C$ )

This parameter  $\gamma_f^C$  (%) defines the shear strain at which failure is obtained in undrained triaxial compression mode of loading, i.e.  $\gamma_f^C = 3/2 \varepsilon_1^C$  from triaxial testing.

### 9.2.3 Shear strain at failure in triaxial extension ( $\gamma_f^E$ )

This parameter  $\gamma_f^E$  (%) defines the shear strain at which failure is obtained in undrained triaxial extension mode of loading, i.e.  $\gamma_f^E = 3/2 \varepsilon_1^E$  from triaxial testing.

### 9.2.4 Shear strain at failure in direct simple shear ( $\gamma_f^{DSS}$ )

This parameter  $\gamma_f^{DSS}$  (%) defines the shear strain at which failure is obtained in undrained direct simple shear mode of loading (DSS device).

For near normally consolidated clays, the failure strain in compression loading  $\gamma_f^C$  is generally the lowest value and the failure strain in extension loading  $\gamma_f^E$  is the highest value. The failure strain from direct simple shear loading takes an intermediate value, i.e.  $\gamma_f^C < \gamma_f^{DSS} < \gamma_f^E$ . From laboratory test results reported in literature one find typically  $\gamma_f^E$  in the range 3-8 %,  $\gamma_f^{DSS}$  in the range 2-8 % and  $\gamma_f^C$  in the range 0.5 - 4%.

If stress-strain curves from undrained triaxial and/or DSS laboratory tests are available it is recommended to choose the elastic shear modulus and failure strains such that a good fit to the curves are obtained. This is in particular important for deformation and SLS assessments. However, for pure capacity and stability (e.g. factor of safety) analyses the values for shear strains at failure is not important and one may set all three values equal to e.g. 5 % for simplicity.

Note that it is the failure strains from triaxial loading that is input because they are the most readily available. When the NGI-ADP model is used for plane strain conditions the failure strains will automatically be slightly adjusted for that loading condition. See [Grimstad, Andresen & Jostad \(2010\)](#) (on page 247) for more details.

### 9.2.5 Reference active shear strength ( $s_{u,ref}^A$ )

The reference active shear strength is the shear strength obtained in (plane strain) undrained active stress paths for the reference depth  $y_{ref}$  expressed in the unit of stress.

## The NGI-ADP model (anisotropic undrained shear strength)

Parameters of the NGI-ADP model

---

### 9.2.6 Ratio triaxial compressive shear strength over active shear strength ( $s_u^{C,TX}/s_u^A$ )

This ratio  $s_u^{C,TX} / s_u^A$  defines the shear strength in undrained triaxial compression mode of loading in relation to the shear strength in plane strain undrained active mode of loading. The value cannot be changed by the user and is predefined at 0.99 giving practically the same strengths in triaxial and plane strain conditions.

### 9.2.7 Reference depth ( $y_{ref}$ )

This is the reference depth  $y_{ref}$  at which the reference active shear strength  $s_{u,ref}^A$  is defined. Below this depth the shear strength and stiffness may increase linearly with increasing depth. Above the reference depth the shear strength is equal to  $s_{u,ref}^A$ .

### 9.2.8 Increase of shear strength with depth ( $s_{u,inc}^A$ )

This parameter  $s_{u,ref}^A$  defines the increase (positive) or decrease (negative) of the undrained active shear strength with depth, expressed in the unit of stress per unit of depth. Above the reference depth the shear strength is equal to  $s_{u,ref}^A$ , below the reference depth the shear strength is defined as:

$$s_u^A(y) = s_{u,ref}^A + (y_{ref} - y)s_{u,inc}^A \quad Eq. [219]$$

### 9.2.9 Ratio of passive shear strength over active shear strength ( $s_u^P/s_u^A$ )

This ratio  $s_u^P / s_u^A$  defines the undrained shear strength for (plane strain) passive mode of loading.

### 9.2.10 Ratio of direct simple shear strength over active shear strength ( $s_u^{DSS}/s_u^A$ )

This ratio  $s_u^{DSS} / s_u^A$  defines the undrained shear strength for direct simple shear mode of loading. Please note that active / passive strength input is defined for plane strain conditions. However, it is generally acceptable and only slightly conservative to use the strength obtained from a triaxial compression test as input for the active plane strain condition (i.e.  $s_u^A = s_u^{C,TX}$ ) and the strength obtained from a triaxial extension test as input for the passive plane strain condition (i.e.  $s_u^P = s_u^{E,TX}$ ). More control over the strength difference between triaxial and plane strain loading conditions can be obtained by using the advanced parameter  $s_u^{C,TX} / s_u^A$ .

For near normally consolidated clays, the passive strength  $s_u^P$  is generally the lowest strength value, while the direct simple shear strength takes an intermediate value, i.e.  $s_u^P < s_u^{DSS} < s_u^A$ . From laboratory results reported in literature one find typically  $s_u^P / s_u^A$  in the range 0.2 - 0.5 and  $s_u^{DSS} / s_u^A$  in the range 0.3 - 0.8. If direct simple shear strengths are not available  $s_u^{DSS}$  can be estimated from:

## The NGI-ADP model (anisotropic undrained shear strength)

Parameters of the NGI-ADP model

Shear strain at failure in direct simple shear ( $\gamma_f^{DSS}$ )

$$s_u^{DSS} / s_u^A = (1 + s_u^P / s_u^A) / 2 \quad Eq. [220]$$

### 9.2.11 Initial mobilization ( $\tau_0/s_u^A$ )

The initial mobilization  $\tau_0 / s_u^A$  is clearly defined for nearly horizontally deposited normally consolidated or lightly overconsolidated clay layers where the vertical stress is the major principle stress  $\sigma'_1$ . As defined in [Figure 47](#) (on page 108), the initial mobilization can be calculated from the earth pressure coefficient at rest  $K_0$  by the following equation:

$$\tau_0 / s_u^A = -0.5(1 - K_0)\sigma'_{yy0} \quad Eq. [221]$$

where

$$\sigma'_{yy0} = \text{Initial (in situ) vertical effective stress (compression negative)}$$

A default value 0.7 of  $s_u^P / s_u^A$  is given which represent a typical value for a near normally consolidated clay deposit (e.g.  $K_0 = 0.55$  and  $-\sigma'_{yy0} = s_u^P / s_u^A = 3.11$  or  $K_0 = 0.6$  and  $-\sigma'_{yy0} = s_u^P / s_u^A = 3.5$ ).

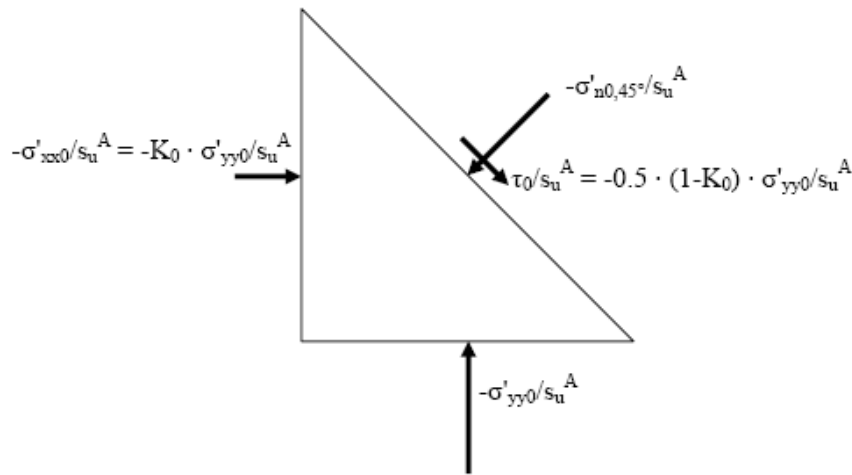


Figure 47: Definition of initial mobilised maximum shear stress  $\tau_0 = 1/2 |\sigma'_{yy0} - \sigma'_{xx0}|$  for a soil element in a horizontal deposited layer.

A more detailed evaluation of the initial (in situ) mobilization can be done by assessing the in situ  $K_0$  value and use the relationship:  $\tau_0/s_u^A = -0.5 (1-K_0) \sigma'_{v0}/s_u^A$ . Changing the default value for the initial mobilization should be considered in particular for overconsolidated materials where  $K_0$  generally is higher than 0.6, however the NGI-ADP model is not intended used for heavily overconsolidated clays and should be used with care for  $K_0 > 1.0$  (i.e. negative  $\tau_0/s_u^A$ ).

For non-horizontal layering (e.g. sloping ground) a  $K_0$  procedure is normally not recommended. In such cases it is recommended to establish the initial stress condition by gravity loading using a material model suited for such a purpose (e.g. drained behavior with the Mohr-Coulomb model or the Hardening Soil model). After the equilibrium initial stresses are established for gravity loading in the first phase, one should switch to the NGI-ADP model in the relevant clusters for the next phase and run a NIL step (i.e. without changing the external loads). The hardening parameter of the NGI-ADP model will then be adjusted such that equilibrium is obtained ( $f=0$ ). Then in the third phase the external loading can be applied.

## The NGI-ADP model (anisotropic undrained shear strength)

### State parameters in the NGI-ADP model

---

#### 9.2.12 Poisson's ratio ( $\nu'$ )

Similar as in the Mohr-Coulomb model, Poisson's ratio is generally between 0.3 and 0.4 for loading conditions considering effective stress analysis. For unloading conditions a lower value is more appropriate. For more information about the Poisson's ratio, see [Parameters of the Mohr-Coulomb model](#) (on page 34)

When the *Undrained (C)* drainage option is used a pure total stress analysis is carried out where no distinction between effective stresses and pore pressures is made and all stress changes should be considered as changes in total stress. A Poisson's ratio close to 0.5 should be entered.  $\nu = 0.495$  is given as default.

### 9.3 State parameters in the NGI-ADP model

In addition to the output of standard stress and strain quantities, the NGI-ADP model provides output (when being used) on state variables such as plastic shear strain  $\gamma^p$  and the hardening function  $r_k$ . These parameters can be visualised by selecting the *State parameters* option from the *Stresses* menu. An overview of available state parameters is given below:

$\gamma^p$	Plastic shear strain : $\gamma^p = \sum d\gamma^p$	[-]
$d\gamma^p$	Described in Eq. [211].	[-]
$r_k$	Hardening function: $r_k = 2 \frac{\sqrt{\gamma^p / \gamma_f^p}}{1 + \gamma^p / \gamma_f^p}$	[-]

## The Soft soil model [ADV]

As soft soils we consider near-normally consolidated clays, clayey silts and peat. A special feature of such materials is their high degree of compressibility. This is best demonstrated by oedometer test data as reported for instance by Janbu in his Rankine lecture (1985). Considering tangent stiffness moduli at a reference oedometer pressure of 100 kPa, he reports for normally consolidated clays  $E_{oed} = 1$  to 4 MPa, depending on the particular type of clay considered. The differences between these values and stiffnesses for NC-sands are considerable as here we have values in the range of 10 to 50 MPa, at least for non-cemented laboratory samples. Hence, in oedometer testing normally consolidated clays behave ten times softer than normally consolidated sands. This illustrates the extreme compressibility of soft soils.

A feature of soft soils is the linear stress-dependency of soil stiffness. According to the Hardening Soil model we have:

$$E_{oed} = E_{oed}^{ref} \left( \frac{-\sigma_1'}{p^{ref}} \right)^m \quad Eq. [222]$$

at least for  $c = 0$  and  $\sigma_3' = K_0^{nc} \sigma_1'$  and a linear relationship is obtained for  $m = 1$ . Indeed, on using an exponent equal to unity, the above stiffness law reduces to:

$$E_{oed} = \frac{-\sigma_1'}{\lambda^*} \quad Eq. [223]$$

where

$$\lambda^* = \frac{p^{ref}}{E_{oed}^{ref}} \quad Eq. [224]$$

For this special case of  $m = 1$ , the Hardening Soil model yields  $\dot{\epsilon} = \sigma^* \dot{\sigma}_1' / \sigma_1'$ , which can be integrated to obtain the well-known logarithmic compression law  $\epsilon = -\lambda^* \ln(-\sigma_1')$  for primary oedometer loading.

For many practical soft-soil studies, the modified compression index  $\lambda^*$  will be known and the PLAXIS 3D user can compute the oedometer modulus from the relationship:

$$E_{oed}^{ref} = \frac{p^{ref}}{\lambda^*} \quad Eq. [225]$$

From the above considerations it would seem that the Hardening Soil model is quite suitable for soft soils. Indeed, most soft soil problems can be analysed using this model, but the Hardening Soil model is not suitable when considering very soft soils with a high compressibility, i.e.  $E_{oed}^{ref}/E_{50}^{ref} < 0.5$ . For such soils, the Soft Soil model may be used.

Some features of the Soft Soil model are:

## The Soft soil model [ADV]

Isotropic states of stress and strain ( $\sigma'_1 = \sigma'_2 = \sigma'_3$ )

---

- Stress dependent stiffness (logarithmic compression behaviour).
- Distinction between primary loading and unloading-reloading.
- Memory for pre-consolidation stress.
- Failure behaviour according to the Mohr-Coulomb criterion.

### 10.1 Isotropic states of stress and strain ( $\sigma'_1 = \sigma'_2 = \sigma'_3$ )

In the Soft Soil model, it is assumed that there is a logarithmic relation between changes in volumetric strain,  $\varepsilon_v$ , and changes in mean effective stress,  $p'$ , which can be formulated as:

$$\varepsilon_v - \varepsilon_v^0 = -\lambda^* \ln \left( \frac{p' + c \cot(\varphi)}{p^0 + c \cot(\varphi)} \right) \quad (\text{virgin compression}) \quad \text{Eq. [226]}$$

In order to maintain the validity of Eq. [226] a minimum value of  $p'$  is set equal to a unit stress. The parameter  $\lambda^*$  is the modified compression index, which determines the compressibility of the material in primary loading. Note that  $\lambda^*$  differs from the index  $\lambda$  as used by [Burland \(1965\)](#) (on page 246). The difference is that Eq. [226] is a function of volumetric strain instead of void ratio. Plotting Eq. [226] gives a straight line as shown in [Figure 56](#) (on page 136).

During isotropic unloading and reloading a different path (line) is followed, which can be formulated as:

$$\varepsilon_v^e - \varepsilon_v^{e0} = -\kappa^* \ln \left( \frac{p' + c \cot(\varphi)}{p^0 + c \cot(\varphi)} \right) \quad (\text{unloading and reloading}) \quad \text{Eq. [227]}$$

Again, a minimum value of  $p'$  is set equal to a unit stress. The parameter  $\kappa^*$  is the modified swelling index, which determines the compressibility of the material in unloading and subsequent reloading. Note that  $\kappa^*$  differs from the index  $\kappa$  as used by Burland. The ratio  $\lambda^* / \kappa^*$  is, however, equal to Burland's ratio  $\lambda / \kappa$ . The soil response during unloading and reloading is assumed to be elastic as denoted by the superscript  $e$  in Eq. [227]. The elastic behaviour is described by Hooke's law. Eq. [227] implies linear stress dependency on the tangent bulk modulus such that:

$$K_{ur} = \frac{E_{ur}}{3(1 - 2\nu_{ur})} = \frac{p' + c \cot(\varphi)}{\kappa^*} \quad \text{Eq. [228]}$$

in which the subscript  $ur$  denotes unloading / reloading. Note that effective parameters are considered rather than undrained soil properties, as might be suggested by the subscripts  $ur$ . Neither the elastic bulk modulus,  $K_{ur}$ , nor the elastic Young's modulus,  $E_{ur}$ , is used as an input parameter. Instead,  $\nu_{ur}$  and  $\kappa^*$  are used as input constants for the part of the model that computes the elastic strains.

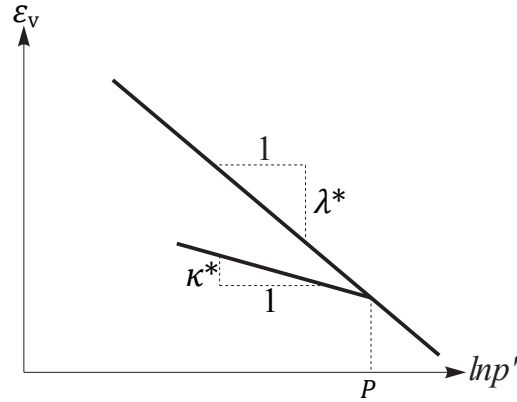


Figure 48: Logarithmic relation between volumetric strain and mean stress

An infinite number of unloading / reloading lines may exist in [Figure 48](#) (on page 112), each corresponding to a particular value of the isotropic pre-consolidation stress  $p_p$ . The pre-consolidation stress represents the largest stress level experienced by the soil. During unloading and reloading, this pre-consolidation stress remains constant. In primary loading, however, the pre-consolidation stress increases with the stress level, causing irreversible (plastic) volumetric strains.

## 10.2 Yield function

The yield function of the Soft Soil model is defined as:

$$f = \bar{f} - p_p \quad \text{Eq. [229]}$$

where

$$\begin{aligned} \bar{f} &= \text{Function of the stress state } (p', \tilde{q}) \\ p_p &= \text{The pre-consolidation stress which is a function of plastic strain.} \end{aligned}$$

$$\bar{f} = \frac{\tilde{q}^2}{M^2(p' + c \cot(\varphi))} + p' \quad \text{Eq. [230]}$$

$$p_p = p_p^0 \exp\left(\frac{-\varepsilon_v^p}{\lambda^* - \kappa^*}\right) \quad \text{Eq. [231]}$$

where

$$\tilde{q} = \text{similar deviatoric stress quantity as defined for the cap yield surface in the } \text{The Hardening Soil model (Isotropic hardening)} \text{ (on page 67):}$$

$$q = \sigma_1' + (\alpha - 1) \sigma_1' \quad \alpha = (3 + \sin(\varphi)) / (3 - \sin(\varphi)) \quad \text{Eq. [232]}$$

The yield function ( $f = 0$ ) describes an ellipse in the  $p'$  -  $\tilde{q}$ -plane, as illustrated in [Figure 49](#) (on page 113). The parameter  $M$  in Eq. [230] determines the height of the ellipse. The height of the ellipse is responsible for the ratio of horizontal to vertical stresses in primary one-dimensional compression.

## The Soft soil model [ADV]

### Yield function

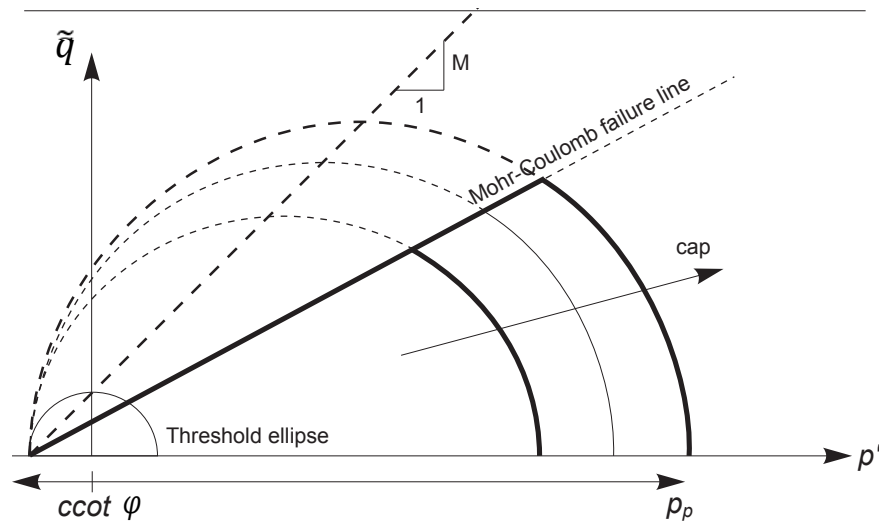


Figure 49: Yield surface of the Soft Soil model in  $p'$ - $q$ -plane

As a result, the parameter  $M$  determines largely the coefficient of lateral earth pressure  $K_0^{nc}$ . In view of this, the value of  $M$  can be chosen such that a known value of  $K_0^{nc}$  is matched in primary one-dimensional compression. Such an interpretation and use of  $M$  differs from the original critical state line idea, but it ensures a proper matching of  $K_0^{nc}$ .

The tops of all ellipses are located on a line with slope  $M$  in the  $p'$ - $\tilde{q}$ -plane. In [Burland \(1965\)](#) (on page 246) and [Burland \(1967\)](#) (on page 246) the  $M$ -line is referred to as the critical state line and represents stress states at post peak failure. The parameter  $M$  is then based on the critical state friction angle. In the Soft Soil model, however, failure is not necessarily related to critical state. The Mohr-Coulomb failure criterion is a function of the strength parameters  $\phi$  and  $c$ , which might not correspond to the  $M$ -line. The isotropic pre-consolidation stress  $p_p$  determines the extent of the ellipse along  $p'$  axis. During loading, an infinite number of ellipses may exist (see [Figure 49](#) (on page 113)) each corresponding to a particular value of  $p_p$ . In tension ( $p' < 0$ ), the ellipse extends to  $ccot \phi$  (Eq. [230] and [Figure 49](#) (on page 113)). In order to make sure that the right hand side of the ellipse (i.e. the 'cap') will remain in the 'compression' zone ( $p' > 0$ ) a minimum value of  $ccot \phi$  is adopted for  $p_p$ . For  $c = 0$ , a minimum value of  $p_p$  equal to a stress unit is adopted. Hence, there is a 'threshold' ellipse as illustrated in [Figure 49](#) (on page 113).

The value of  $p_p$  is determined by volumetric plastic strain following the hardening relation, Eq. [231]. This equation reflects the principle that the pre-consolidation stress increases exponentially with decreasing volumetric plastic strain (compaction).  $p_p^0$  can be regarded as the initial value of the pre-consolidation stress.

The determination of  $p_p^0$  is treated in [The initial pre-consolidation stress in advanced models](#) (on page 27). According to Eq. [231] the initial volumetric plastic strain is assumed to be zero.

In the Soft Soil model, the yield function, Eq. [229], describes the irreversible volumetric strain in primary compression, and forms the cap of the yield contour. To model the failure state, a perfectly-plastic Mohr-Coulomb type yield function is used. This yield function represents a straight line in  $p'$ - $\tilde{q}$ -plane as shown in [Figure 49](#) (on page 113). The slope of the failure line is smaller than the slope of the  $M$ -line.

## The Soft soil model [ADV]

### Parameters of the Soft Soil model

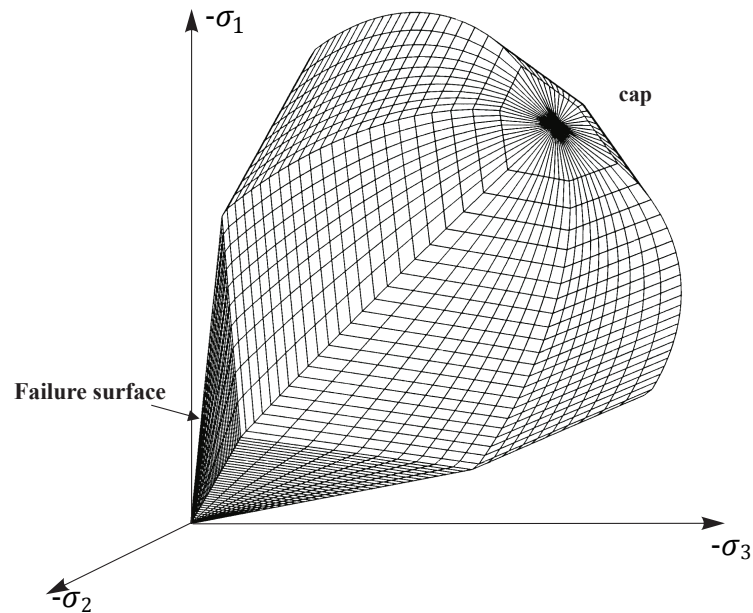


Figure 50: Representation of total yield contour of Soft Soil model in principal stress space

The total yield contour, as shown by the bold lines in [Figure 49](#) (on page 113), is the boundary of the elastic stress area. The failure line is fixed, but the cap may increase in primary compression. Stress paths within this boundary give only elastic strain increments, whereas stress paths that tend to cross the boundary generally give both elastic and plastic strain increments.

For general states of stress ( $p'$ ,  $\tilde{q}$ ), the plastic behaviour of the Soft Soil model is defined by the combination of the cap yield function and the Mohr-Coloumb yield functions. The total yield contour in principal stress space is indicated in [Figure 50](#) (on page 114).

## 10.3 Parameters of the Soft Soil model

The parameters of the Soft Soil model include compression and swelling indices, which are typical for soft soils, as well as the Mohr-Coulomb model failure parameters. In total, the Soft Soil model requires the following parameters to be determined:

Basic parameters:

$\lambda^*$	Modified compression index	[-]
$\kappa^*$	Modified swelling index	[-]
$\nu_{ur}$	Poisson's ratio for unloading / reloading	[-]
$c$	Effective cohesion	[kN/m <sup>2</sup> ]
$\varphi$	Friction angle	[°]

## The Soft soil model [ADV]

Parameters of the Soft Soil model

$\psi$	Dilatancy angle	[°]
$\sigma_t$	Tensile strength	[kN/m <sup>2</sup> ]

Miscellaneous parameters (use default settings):

$K_0^{nc}$	Coefficient of lateral stress in normal consolidation	[-]
$M$	$K_0^{nc}$ -parameter	[-]

Soil - Soft Soil - <NoName>

General Mechanical Groundwater Thermal Interfaces Initial

Property	Unit	Value
<b>Stiffness</b>		
$\lambda^*$ (lambda*)		0.000
$\kappa^*$ (kappa*)		0.000
$\nu_{ur}$		0.1500
<b>Alternatives</b>		
Use alternatives		<input type="checkbox"/>
$C_c$		0.000
$C_s$		0.000
$e_{init}$		0.5000
<b>Strength</b>		
<b>Shear</b>		
$c'_{ref}$	kN/m <sup>2</sup>	5.000
$\phi'$ (phi)	°	25.00
$\psi$ (psi)	°	0.000
<b>Tension</b>		
Tension cut-off		<input checked="" type="checkbox"/>
Tensile strength	kN/m <sup>2</sup>	0.000
<b>Miscellaneous</b>		
Use defaults		<input checked="" type="checkbox"/>
$K_0^{nc}$		0.5774
$M$		2.413

Next OK Cancel

Figure 51: Mechanical tabsheet for the Soft Soil model

## The Soft soil model [ADV]

### Parameters of the Soft Soil model

[Figure 51](#) (on page 115) shows the PLAXIS 3D window for inputting the values of the model parameters for mechanical behaviour.  $M$  is calculated automatically from the coefficient of the lateral earth pressure,  $K_0^{nc}$ , by means of Eq. [234]. Note that, physically, in the current model  $M$  differs from the similar parameter in the Modified Cam-Clay model where it is related to the material friction.

### 10.3.1 Modified swelling index and modified compression index

These parameters can be obtained from an isotropic compression test including isotropic unloading. When plotting the logarithm of the mean stress as a function of the volumetric strain for clay-type materials, the plot can be approximated by two straight lines (see [Figure 48](#) (on page 112)). The slope of the primary loading line gives the modified compression index, and the slope of the unloading (or swelling) line gives the modified swelling index. Note that there is a difference between the modified indices  $\kappa^*$  and  $\lambda^*$  and the original Cam-Clay parameters  $\kappa$  and  $\lambda$ . The latter parameters are defined in terms of the void ratio  $e$  instead of the volumetric strain  $\varepsilon_v$ .

Apart from the isotropic compression test, the parameters  $\kappa^*$  and  $\lambda^*$  can be obtained from a one-dimensional compression test. Here a relationship exists with the internationally recognised parameters for one-dimensional compression and swelling,  $C_c$  and  $C_s$ . These relationships are summarised in [Table 2](#) (on page 116) and [Table 3](#) (on page 116).

**Table 2: Relationship to Cam-Clay parameters**

1. $\lambda^* = \frac{\lambda}{1+e}$	2. $\kappa^* = \frac{\kappa}{1+e}$
--------------------------------------	------------------------------------

**Table 3: Relationship to internationally normalised parameters**

3. $\lambda^* = \frac{C_c}{2.3(1+e)}$	3. $\kappa^* \approx \frac{2C_s}{2.3(1+e)}$
---------------------------------------	---

**Note:** Remarks on [Table 2](#) (on page 116) and [Table 3](#) (on page 116)

- In relations 1 and 2, the void ratio,  $e$ , is assumed to be constant. In fact,  $e$  will change during a compression test, but this will give a relatively small difference in void ratio. For  $e$  one can use the average void ratio that occurs during the test or just the initial value.
- In relation 4 there is no exact relation between  $\kappa^*$  and the one-dimensional swelling index  $C_s$ , because the ratio of horizontal and vertical stresses changes during one-dimensional unloading. For this approximation it is assumed that the average stress state during unloading is an isotropic stress state, hence  $K_0=1$ . This assumption is reasonable for moderately overconsolidated clays with friction angles in the range of 20°-30°.
- In practice, swelling is often assumed to be equivalent to recompression behaviour, which, may not be right. Hence  $\kappa^*$  should be based on  $C_s$  rather than the recompression index  $C_r$ .
- The factor 2.3 in relation 3 is obtained from the ratio between the logarithm of base 10 and the natural logarithm.
- The ratio  $\lambda^*/\kappa^*$  ( $=\lambda/\kappa$ ) ranges, in general, between 2.5 and 7.

### 10.3.2 Cohesion

The cohesion has the dimension of stresses. A small effective cohesion may be used, including a cohesion of zero. Entering a cohesion will result in an elastic region that is partly located in the 'tension' zone, as illustrated in [Figure 49](#) (on page 113). The left hand side of the ellipse crosses the  $p'$ -axis at a value of  $ccot \varphi$ . In order to maintain the right hand side of the ellipse (i.e. the cap) in the 'pressure' zone of the stress space, the isotropic pre-consolidation stress  $p_p$  has a minimum value of  $ccot \varphi$ . This means that entering a cohesion larger than zero may result in a state of 'overconsolidation', depending on the magnitude of the cohesion and the initial stress state. As a result, a stiffer behaviour is obtained during the onset of loading. It is not possible to specify undrained shear strength by means of high cohesion and a friction angle of zero. Input of model parameters should always be based on effective values. The PLAXIS option to model undrained behaviour using effective parameters may be used (*Undrained (A)*). Please note that the resulting effective stress path may not be accurate, which may lead to an unrealistic undrained shear strength. Hence, when using *Undrained (A)* as drainage type, the resulting stress state must be checked against a known undrained shear strength profile.

### 10.3.3 Friction angle

The effective angle of internal friction represents the increase of shear strength with effective stress level. It is specified in degrees. Zero friction angle is not allowed. On the other hand, care should be taken with the use of high friction angles. It is often recommended to use  $\varphi_{cv}$ , i.e. the critical state friction angle, rather than a higher value based on small strains. Moreover, using a high friction angle will substantially increase the computational requirements.

### 10.3.4 Dilatancy angle

For the type of materials, which can be described by the Soft Soil model, the dilatancy can generally be neglected. A dilatancy angle of zero degrees is considered in the standard settings of the Soft Soil model.

### 10.3.5 Poisson's ratio

In the Soft Soil model, the Poisson's ratio  $\nu$  is the well known pure elastic constant rather than the pseudo-elasticity constant as used in the linear elastic perfectly-plastic model. Its value will usually be in the range between 0.1 and 0.2. If the standard setting for the Soft Soil model parameters is selected, then  $\nu_{ur} = 0.15$  is automatically used. For loading of normally consolidated materials, Poisson's ratio plays a minor role, but it becomes important in unloading problems. For example, for unloading in a one-dimensional compression test (oedometer), the relatively small Poisson's ratio will result in a small decrease of the lateral stress compared with the decrease in vertical stress. As a result, the ratio of horizontal and vertical stress increases, which is a well-known phenomenon in overconsolidated materials. Hence, Poisson's ratio should not be based on the normally consolidated  $K_0^{nc}$ -value, but on the ratio of the horizontal stress increment to the vertical stress increment in oedometer unloading and reloading test such that:

$$\frac{\nu_{ur}}{1 - \nu_{ur}} = \frac{\Delta\sigma_{xx}}{\Delta\sigma_{yy}} \quad (\text{unloading and reloading}) \quad \text{Eq. [233]}$$

## The Soft soil model [ADV]

State parameters in the Soft Soil model

### 10.3.6 $K_0^{nc}$ -parameter

The parameter  $M$  is automatically determined based on the coefficient of lateral earth pressure in normally consolidated condition,  $K_0^{nc}$ , as entered by the user. The exact relation between  $M$  and  $K_0^{nc}$  gives [\(Brinkgreve, 1994\)](#) (on page 246):

$$M = 3 \sqrt{\frac{(1 - K_0^{nc})^2}{(1 + 2K_0^{nc})^2} + \frac{(1 - K_0^{nc})(1 - 2\nu_{ur})(\lambda^* / \kappa^* - 1)}{(1 + 2K_0^{nc})(1 - 2\nu_{ur})\frac{\lambda^*}{\kappa^*} - (1 - K_0^{nc})(1 + \nu_{ur})}} \quad \text{Eq. [234]}$$

The value of  $M$  is indicated in the input window. As can be seen from Eq. [235],  $M$  is also influenced by the Poisson's ratio  $\nu_{ur}$  and by the ratio  $\lambda^* / \kappa^*$ . However, the influence of  $K_0^{nc}$  is dominant. Eq. [235] can be approximated by:

$$M \approx 3.0 - 2.8K_0^{nc} \quad \text{Eq. [235]}$$

## 10.4 State parameters in the Soft Soil model

In addition to the output of standard stress and strain, the Soft Soil model provides output (when being used) on state variables such as the hardening parameter  $\gamma^p$  and the isotropic pre-consolidation stress  $p_p$ . These parameters can be visualised by selecting the *State parameters* option from the *stresses* menu. An overview of available state parameters is given below:

$p_{eq}$	Equivalent isotropic stress	[kN/m <sup>2</sup> ]
$p_p$	Isotropic preconsolidation stress $p_{eq} = p' + \frac{q^2}{M^2(p' - c \cot(\varphi))}$	[kN/m <sup>2</sup> ]
$OCR$	Isotropic overconsolidation ratio $OCR = p_p / p^{eq}$	[-]
$\gamma^p$	Hardening parameter (equivalent mobilised plastic shear strain)	[-]
$E_{ur}$	Current stress-dependent elastic Young's modulus	[kN/m <sup>2</sup> ]
$c$	Current depth-dependent cohesion	[kN/m <sup>2</sup> ]

## 10.5 On the use of the Soft Soil model in dynamics calculations

## The Soft soil model [ADV]

On the use of the Soft Soil model in dynamics calculations

---

When using the Soft Soil model in dynamics calculations, the modified swelling index  $\kappa^*$  needs to be selected such that the model correctly predicts wave velocities in the soil. This generally requires a smaller value than just an unloading-reloading index.

When subjected to dynamic or cyclic loading, the Soft Soil model will generate plastic strains when the preconsolidation stress is increased. However, it should be noted that stress cycles within the current hardening contour will only generate elastic strains and no (hysteretic) damping, nor accumulation of strains or pore pressure, nor liquefaction. In order to account for the soil damping in cyclic loading, Rayleigh damping may be defined.

# Soft Soil Creep model (time dependent behaviour)

## [ADV]

---

### 11.1 Introduction

Both the Hardening Soil model and the Soft Soil model can be used to model the behaviour of compressible soft soils, but none of these models are suitable when considering creep, i.e. secondary compression. All soils exhibit some creep, and primary compression is thus always followed by a certain amount of secondary compression. Assuming the secondary compression (for instance during a period of 10 or 30 years) to be a certain percentage of the primary compression, it is clear that creep is important for problems involving large primary compression. This is for instance the case when constructing embankments on soft soils. Indeed, large primary settlements of footings and embankments are usually followed by substantial creep settlements in later years. In such cases it is desirable to estimate the creep from FEM-computations.

Foundations may also be founded on initially overconsolidated soil layers that yield relatively small primary settlements. Then, as a consequence of the loading, a state of normal consolidation may be reached and significant creep may follow. This is a treacherous situation as considerable secondary compression is not preceded by the warning sign of large primary compression. Again, computations with a creep model are desirable.

[Buisman \(1936\)](#) (on page 246) was probably the first to propose a creep law for clay after observing that soft-soil settlements could not be fully explained by classical consolidation theory. This work on 1D-secondary compression was continued by other researchers including, for example, [Bjerrum \(1967\)](#) (on page 246), [Garlanger \(1972\)](#) (on page 247), [Mesri & Godlewski \(1977\)](#) (on page 248) and [Leroueil \(1977\)](#) (on page 247). More mathematical lines of research on creep were followed by, for example, [Sekiguchi \(1977\)](#) (on page 249), [Adachi & Oka \(1982\)](#) (on page 245) and [Borja & Kavazanjian \(1985\)](#) (on page 246). This mathematical 3D-creep modelling was influenced by the more experimental line of 1D-creep modelling, but conflicts exist.

3D-creep should be a straight forward extension of 1D-creep, but this is hampered by the fact that present 1D-models have not been formulated as differential equations. For the presentation of the Soft Soil Creep model we will first complete the line of 1D-modelling by conversion to a differential form. From this 1D differential equation an extension was made to a 3D-model. This chapter gives a full description of the formulation of the Soft Soil Creep model. In addition, attention is focused on the model parameters. Finally, a validation of the 3D model is presented by considering both model predictions and data from triaxial tests. Here, attention is focused on constant strain rate triaxial tests and undrained triaxial creep tests. For more applications of the model the reader is referred to [Vermeer, Stolle & Bonnier \(1998\)](#) (on page 249), [Vermeer & Neher \(1999\)](#) (on page 249) and [Brinkgreve \(2004\)](#) (on page 246).

## Soft Soil Creep model (time dependent behaviour) [ADV]

### Basics of one-dimensional creep

Some basic characteristics of the Soft Soil Creep model are:

- Stress-dependent stiffness (logarithmic compression behaviour)
- Distinction between primary loading and unloading-reloading
- Secondary (time-dependent) compression
- Ageing of pre-consolidation stress
- Failure behaviour according to the Mohr-Coulomb criterion

## 11.2 Basics of one-dimensional creep

When reviewing previous literature on secondary compression in oedometer tests, one is struck by the fact that it concentrates on behaviour related to step loading, even though natural loading processes tend to be continuous or transient in nature. [Buisman \(1936\)](#) (on page 246) was probably the first to consider such a classical creep test. He proposed the following equation to describe creep behaviour under constant effective stress:

$$\varepsilon = \varepsilon_c - C_B \log\left(\frac{t}{t_c}\right) \quad \text{for} \quad t > t_c \quad \text{Eq. [236]}$$

where

$\varepsilon_c$	=	The strain up to the end of consolidation.
$t$	=	Time measured from the beginning of loading.
$t_c$	=	Time to the end of primary consolidation and $C_B$ is a material constant.

Please note that we do not follow the soil mechanics convention that compression is considered positive. Instead, compressive stresses and strains are taken to be negative. For further consideration, it is convenient to rewrite this equation as:

$$\varepsilon = \varepsilon_c - C_B \log\left(\frac{t_c + t'}{t_c}\right) \quad \text{for} \quad t' > 0 \quad \text{Eq. [237]}$$

with  $t' = t - t_c$  being the effective creep time.

Based on the work by Bjerrum on creep, as published for instance in 1967, [Garlanger \(1972\)](#) (on page 247) proposed a creep equation of the form:

$$e = e_c - C_a \log\left(\frac{\tau_c + t'}{\tau_c}\right) \quad \text{with} \quad C_a = C_B(1 + e_0) \quad \text{for} : \quad t' > 0 \quad \text{Eq. [238]}$$

Differences between Garlanger's and Buisman's forms are modest. The engineering strain  $\varepsilon$  is replaced by void ratio  $e$  and the consolidation time  $t_c$  is replaced by the parameter  $\tau_c$ . Eq. [237] and Eq. [238] are identical when choosing  $\tau_c = t_c$ . For the case that  $\tau_c = t_c$ , differences between both formulations will vanish when the effective creep time  $t'$  increases.

For practical consulting, oedometer tests are usually interpreted by assuming  $t_c = 24h$ . Indeed, the standard oedometer test is a *Multiple Stage Loading Test* with loading periods of precisely one day. Due to the special assumption that this loading period coincides to the consolidation time  $t_c$ , it follows that such tests have no effective creep time.

Hence one obtains  $t' = 0$  and the log-term drops out of Eq. [238]. It would thus seem that there is no creep in this standard oedometer test, but this suggestion is false. Even highly impermeable oedometer samples need less than one hour for primary consolidation. Then all excess pore pressures are zero and one observes pure creep

## Soft Soil Creep model (time dependent behaviour) [ADV]

On the variables  $\tau_c$  and  $\varepsilon_c$

---

for the other 23 hours of the day. Therefore we will not make any assumptions about the precise values of  $\tau_c$  and  $t_c$ .

Another slightly different possibility to describe secondary compression is the form adopted by [Butterfield \(1979\)](#) (on page 246):

$$\varepsilon^H = \varepsilon_c^H - c \ln \left( \frac{\tau_c + t'}{\tau_c} \right) \quad \text{for} \quad t' > 0 \quad \text{Eq. [239]}$$

where  $\varepsilon^H$  is the logarithmic strain defined as:

$$\varepsilon^H = \ln \left( \frac{V}{V_0} \right) = \ln \left( \frac{1+e}{1+e_0} \right) \quad \text{Eq. [240]}$$

with the subscript '0' denoting the initial values. The superscript 'H' is used to denote logarithmic strain, as the logarithmic strain measure was originally used by Hencky. For small strains it is possible to show that:

$$c = \frac{C_a}{(1+e_0) \cdot \ln 10} = \frac{C_B}{\ln 10} \quad \text{Eq. [241]}$$

because then logarithmic strain is approximately equal to the engineering strain. Both [Butterfield \(1979\)](#) (on page 246) and [den Haan \(1994\)](#) (on page 246) showed that for cases involving large strain, the logarithmic small strain supersedes the traditional engineering strain.

### 11.3 On the variables $\tau_c$ and $\varepsilon_c$

In this section attention will first be focused on the variable  $\tau_c$ . Here a procedure is to be described for an experimental determination of this variable. In order to do so we depart from Eq. [239]. By differentiating this equation with respect to time and dropping the superscript 'H' to simplify the notation, one finds:

$$-\dot{\varepsilon} = \frac{c}{\tau_c + t'} \quad \text{or inversely:} \quad \frac{-1}{\dot{\varepsilon}} = \frac{\tau_c + t'}{c} \quad \text{Eq. [242]}$$

which allows one to make use of the construction developed by [Janbu \(1969\)](#) (on page 247) for evaluating the parameters  $c$  and  $\tau_c$  from experimental data. Both the traditional way, being indicated in [Figure 52](#) (on page 123) a), as well as the Janbu method of [Figure 52](#) (on page 123) b) can be used to determine the parameter  $c$  from an oedometer test with constant load.

## Soft Soil Creep model (time dependent behaviour) [ADV]

On the variables  $\tau_c$  and  $\varepsilon_c$

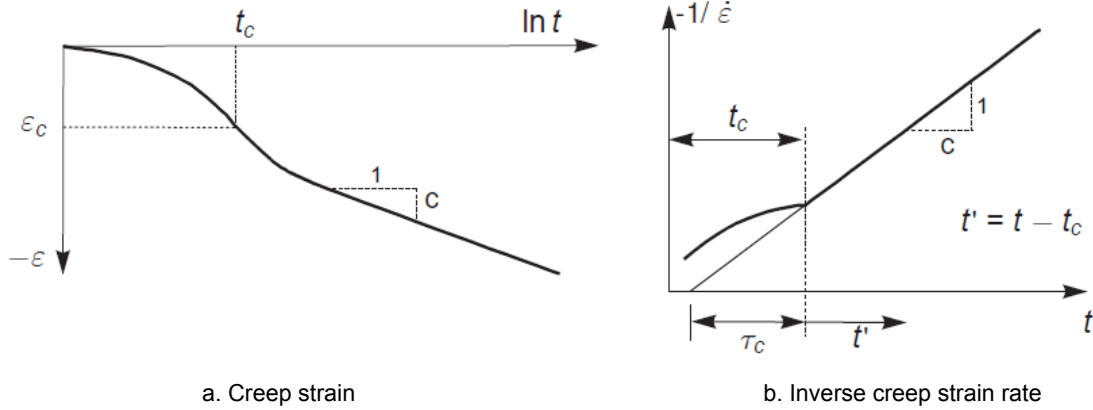


Figure 52: Standard oedometer test

The use of the Janbu method is attractive, because both  $\tau_c$  and  $c$  follow directly when fitting a straight line through the data. In Janbu's representation of [Figure 52](#) (on page 123) b),  $\tau_c$  is the intercept with the (non-logarithmic) time axis of the straight creep line. The deviation from a linear relation for  $t < t_c$  is due to consolidation.

Considering the classical literature it is possible to describe the end-of-consolidation strain  $\varepsilon_c$ , by an equation of the form:

$$\varepsilon_c = \varepsilon_c^e + \varepsilon_c^c = -a \ln \left( \frac{\sigma'}{\sigma'_0} \right) - (b - a) \ln \left( \frac{\sigma_{pc}}{\sigma_{p0}} \right) \quad \text{Eq. [243]}$$

Note that  $\varepsilon$  is a logarithmic strain, rather than a classical small strain although we conveniently omit the subscript 'H'. In the above equation  $\sigma'_0$  represents the initial effective pressure before loading and  $\sigma'$  is the final effective loading pressure. The values  $\sigma_{p0}$  and  $\sigma_{pc}$  represent the pre-consolidation pressure corresponding to before-loading and end-of-consolidation states respectively. In most literature on oedometer testing, one adopts the void ratio  $e$  instead of  $\varepsilon$ , and  $\log$  instead of  $\ln$ , the swelling (recompression) index  $C_s$  instead of  $a$ , and the compression index  $C_c$  instead of  $b$ . The above constants  $a$  and  $b$  relate to  $C_s$  and  $C_c$  as:

$$a = \frac{C_s}{(1 + e_0) \cdot \ln 10} \quad b = \frac{C_c}{(1 + e_0) \cdot \ln 10} \quad \text{Eq. [244]}$$

Combining Eq. [239] and Eq. [243] it follows that:

$$\varepsilon = \varepsilon^e + \varepsilon^c = -a \ln \left( \frac{\sigma'}{\sigma'_0} \right) - (b - a) \ln \left( \frac{\sigma_{pc}}{\sigma_{p0}} \right) - c \ln \left( \frac{\tau_c + t'}{\tau_c} \right) \quad \text{Eq. [245]}$$

where  $\varepsilon$  is the total logarithmic strain due to an increase in effective stress from  $\sigma'_0$  to  $\sigma'$  and a time period of  $t_c + t'$ .

In [Figure 53](#) (on page 124) the terms of Eq. [245] are depicted in an  $\varepsilon - \ln \sigma$  diagram. Notice that this figure has a division of strain increments into an elastic and a creep component. Also, for  $t' + t_c = 1$  day, one arrives precisely on the NC-line.

## Soft Soil Creep model (time dependent behaviour) [ADV]

Differential law for 1D-creep

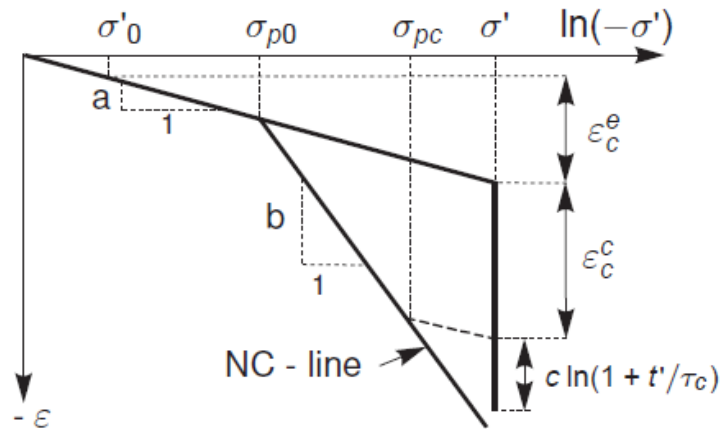


Figure 53: Idealised stress-strain curve from oedometer test with division of strain increments into an elastic and a creep component.

Up to this point, the more general problem of creep under transient loading conditions has not yet been addressed, as it should be recalled that restrictions have been made to creep under constant load. For generalising the model, a differential form of the creep model is needed. No doubt, such a general equation may not contain  $t'$  and neither  $\tau_c$  as the consolidation time is not clearly defined for transient loading conditions.

### 11.4 Differential law for 1D-creep

The previous equations emphasize the relation between accumulated creep and time, for a given constant effective stress. For solving transient or continuous loading problems, it is necessary to formulate a constitutive law in differential form, as will be described in this section. In a first step we will derive an equation for  $\tau_c$ . Indeed, despite the use of logarithmic strain and  $\ln$  instead of  $\log$ , equation (Eq. [245]) is classical without adding new knowledge. Moreover, the question on the physical meaning of  $\tau_c$  is still open. In fact, we have not been able to find precise information on  $\tau_c$  in the literature, apart from Janbu's method of experimental determination.

In order to find an analytical expression for the quantity  $\tau_c$ , we adopt the basic idea that all inelastic strains are time dependent. Hence total strain is the sum of an elastic part  $\varepsilon^e$  and a time-dependent creep part  $\varepsilon^c$ . For non-failure situations as met in oedometer loading conditions, we do not assume an instantaneous plastic strain component, as used in traditional elastoplastic modelling. In addition to this basic concept, we adopt Bjerrum's idea that the pre-consolidation stress depends entirely on the amount of creep strain being accumulated in the course of time. In addition to Eq. [245] we therefore introduce the expression:

$$\varepsilon = \varepsilon^e + \varepsilon^c = -a \ln\left(\frac{\sigma'}{\sigma_0}\right) - (b-a) \ln\left(\frac{\sigma_{pc}}{\sigma_{p0}}\right) \quad \text{Eq. [246]}$$

where

$$\sigma_p = \sigma_{p0} \exp\left(\frac{-\varepsilon^c}{b-a}\right) \quad \text{Eq. [247]}$$

Please note that  $\varepsilon^c$  is negative, so that  $\sigma_p$  exceeds  $\sigma_{p0}$ . The longer a soil sample is left to creep the larger  $\sigma_p$  grows. The time-dependency of the pre-consolidation pressure  $\sigma_p$  is now found by combining Eq. [245] and Eq. [246] to obtain:

## Soft Soil Creep model (time dependent behaviour) [ADV]

Three-dimensional-model

$$\varepsilon^c - \varepsilon_c^c = -(b-a) \ln \left( \frac{\sigma_p}{\sigma_{pc}} \right) = -c \left( \frac{\tau_c + t'}{\tau_c} \right) \quad \text{Eq. [248]}$$

This equation can now be used for a better understanding of  $\tau_c$ , at least when adding knowledge from standard oedometer loading. In conventional oedometer testing the load is stepwise increased and each load step is maintained for a constant period of  $t_c + t' = \tau$ , where  $\tau$  is precisely one day.

In this way of stepwise loading the so-called normal consolidation line (NC-line) with  $\sigma_p = \sigma'$  is obtained. On entering  $\sigma_p = \sigma'$  and  $t' = \tau - t_c$  into Eq. [248] it is found that:

$$(b-a) \ln \left( \frac{\sigma'}{\sigma_{pc}} \right) = c \left( \frac{\tau_c + \tau - t_c}{\tau_c} \right) \quad \text{for : } OCR = 1 \quad \text{Eq. [249]}$$

It is now assumed that  $(\tau_c - t_c) \ll \tau$ . This quantity can thus be disregarded with respect to  $\tau$  and it follows that:

$$\frac{\tau}{\tau_c} = \left( \frac{\sigma'}{\sigma_{pc}} \right)^{\frac{b-a}{c}} \quad \text{or : } \tau_c = \tau \left( \frac{\sigma_{pc}}{\sigma'} \right)^{\frac{b-a}{c}} \quad \text{Eq. [250]}$$

Hence  $\tau_c$  depends both on the effective stress  $\sigma'$  and the end-of-consolidation pre-consolidation stress  $\sigma_{pc}$ . In order to verify the assumption  $(\tau_c - t_c) \ll \tau$ , it should be realised that usual oedometer samples consolidate for relatively short periods of less than one hour. Considering load steps on the normal consolidation line, we have  $OCR=1$  both in the beginning and at the end of the load step. During such a load step  $\sigma_p$  increases from  $\sigma_{p0}$  up to  $\sigma_{pc}$  during the short period of (primary) consolidation. Hereafter  $\sigma_p$  increases further from  $\sigma_{pc}$  up to  $\sigma'$  during a relatively long creep period. Hence, at the end of the day the sample is again in a state of normal consolidation, but directly after the short consolidation period the sample is under-consolidated with  $\sigma_p < \sigma'$ . For the usually very high ratios of  $(b-a)/c \geq 15$ , we thus find very small  $\tau_c$ -values from Eq. [250]. Hence not only  $t_c$  but also  $\tau_c$  tends to be small with respect to  $\tau$ . It thus follows that the assumption  $(\tau_c - t_c) \ll \tau$  is certainly correct.

Having derived the simple expression Eq. [250] for  $\tau_c$ , it is now possible to formulate the differential creep equation. To this end Eq. [245] is differentiated to obtain:

$$\dot{\varepsilon} = \dot{\varepsilon}^e + \dot{\varepsilon}^c = -a \frac{\dot{\sigma}'}{\sigma'} - \frac{c}{\tau_c} \left( \frac{\sigma_{pc}}{\sigma_p} \right)^{\frac{b-a}{c}} \quad \text{Eq. [251]}$$

where  $\tau_c + t'$  can be eliminated by means of Eq. [248] to obtain:

$$\dot{\varepsilon} = \dot{\varepsilon}^e + \dot{\varepsilon}^c = -a \frac{\dot{\sigma}'}{\sigma'} - \frac{c}{\tau_c} \left( \frac{\sigma_{pc}}{\sigma_p} \right)^{\frac{b-a}{c}} \quad \text{Eq. [252]}$$

with:

$$\sigma_p = \sigma_{p0} \exp \left( \frac{-\varepsilon^c}{b-a} \right) \quad \text{Eq. [253]}$$

Again it is recalled that  $\varepsilon^c$  is a compressive strain, being considered negative in this manual. Eq. [250] can now be introduced to eliminate  $\tau_c$  and  $\sigma_{pc}$  and to obtain:

$$\dot{\varepsilon} = \dot{\varepsilon}^e + \dot{\varepsilon}^c = -a \frac{\dot{\sigma}'}{\sigma'} - \frac{c}{\tau_c} \left( \frac{\sigma'}{\sigma_p} \right)^{\frac{b-a}{c}} \quad \text{Eq. [254]}$$

## 11.5 Three-dimensional-model

On extending the 1D-model to general states of stress and strain, the well-known stress invariants for isotropic stress  $p$  and deviatoric stress  $q$  are adopted. These invariants are used to define a new stress measure named  $p^{eq}$ :

$$p^{eq} = p' + \frac{\tilde{q}^2}{M^2(p' + c \cot(\varphi))} \quad Eq. [255]$$

and  $q$  is a similar deviatoric stress quantity as defined in the Hardening Soil model and Soft Soil model. In [Figure 54](#) (on page 126) it is shown that the stress measure  $p^{eq}$  is constant on ellipses in  $p - \tilde{q}$ -plane. In fact we have the ellipses from the Modified Cam-Clay model as introduced by [Roscoe & Burland \(1968\)](#) (on page 248).

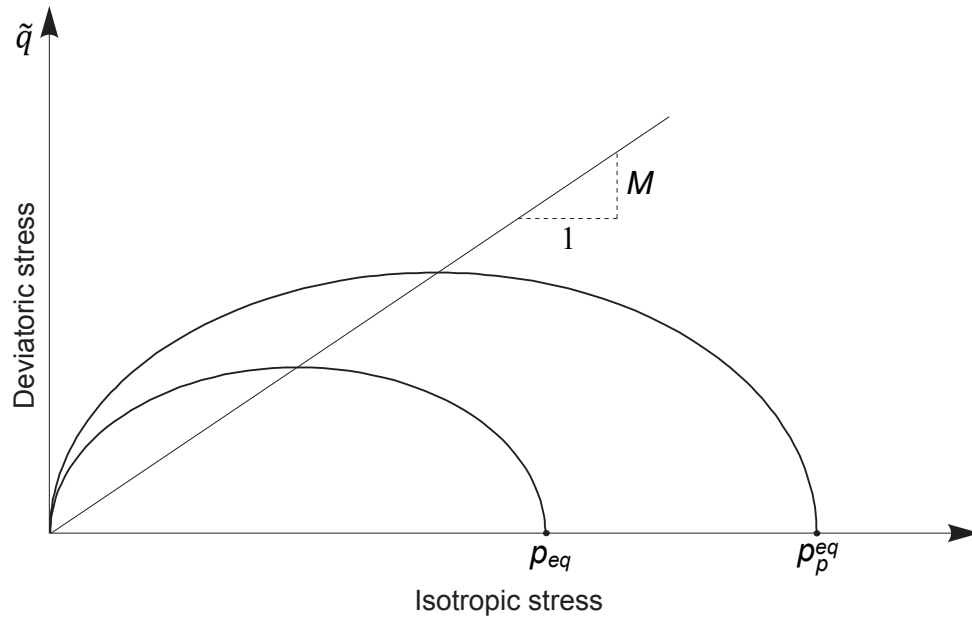


Figure 54: Diagram of  $p^{eq}$ -ellipse in a  $p - \tilde{q}$ -plane

The soil parameter  $M$  represents the slope of the so-called 'critical state line' as also indicated in [Figure 54](#) (on page 126). We use:

$$M = \frac{6 \sin(\varphi_{cv})}{3 - \sin(\varphi_{cv})} \quad Eq. [256]$$

where

$\varphi_{cv}$  = Critical-void friction angle, also referred to as critical-state friction angle.  
 $p^{eq}$  = The equivalent pressure is constant along ellipsoids in principal stress space.

To extend the 1D-theory to a general 3D-theory, attention is now focused on normally consolidated states of stress and strain as met in oedometer testing. In such situations it yields  $\sigma'_2 = \sigma'_3 = K_0^{nc} \sigma'_1$ , and it follows from Eq. [255] that:

## Soft Soil Creep model (time dependent behaviour) [ADV]

Three-dimensional-model

$$p_p^{eq} = \sigma_p \left[ \frac{1 + 2K_0^{nc}}{3} + \frac{3(1 - K_0^{nc})^2}{M^2(1 + 2K_0^{nc})} \right] \quad Eq. [257]$$

where

$$p_p^{eq} = \text{Generalised pre-consolidation pressure, being simply proportional to the one-dimensional one } \sigma_p.$$

For a known stress state in p'-q stress space,  $p^{eq}$  can thus be computed from  $\sigma'_1$ , and with known values of  $K_0^{nc}$ ,  $p_p^{eq}$  can thus be computed from  $\sigma_p$ . Omitting the elastic strain in the 1D-equation (Eq. [254]), introducing the above expressions for  $p^{eq}$  and  $p_p^{eq}$  and writing  $\varepsilon_v$  instead of  $\varepsilon$  it is found that:

$$-\dot{\varepsilon}_v^c = \frac{\mu^*}{\tau} \left( \frac{p^{eq}}{p_p^{eq}} \right)^{\frac{\lambda^* - \kappa^*}{\mu^*}} \quad \text{where} \quad p_p^{eq} = p_{p0}^{eq} \exp \left( \frac{-\varepsilon_v^c}{\lambda^* - \kappa^*} \right) \quad Eq. [258]$$

For one-dimensional oedometer conditions, this equation reduces to Eq. [254], so that one has a true extension of the 1D-creep model. It should be noted that the subscript '0' is once again used in the equations to denote initial conditions and that  $\varepsilon_v^c = 0$  for time  $t = 0$ .

Instead of the parameters  $a$ ,  $b$  and  $c$  of the 1D-model, the 3D-model uses the material parameters  $\kappa^*$ ,  $\lambda^*$  and  $\mu^*$ , who fit into the framework of critical-state soil mechanics. Conversion between constants follows the rules:

$$\kappa^* \approx \frac{2}{3}(1 + 2K_0)a \quad b = \lambda^* \quad \mu^* = c \quad Eq. [259]$$

The expression for  $\kappa^*$  is an approximation under the assumption that  $v_{ur} \approx 0.2$ . There is no constant relation between  $\kappa^*$  and  $a$ , this is a result of the fact that during unloading and reloading under oedometer conditions the ratio of normal stress components changes and therefore the ratio between changes of  $p'$  and  $\sigma'_1$  deviates.

As yet the 3D-creep model is incomplete, as we have only considered a volumetric creep strain  $\varepsilon_v^c$ , whilst soft soils also exhibit deviatoric creep strains.

To introduce general creep strains, we adopt the view that creep strain is simply a time-dependent plastic strain. It is thus logic to assume a flow rule for the rate of creep strain, as usually done in plasticity theory. For formulating such a flow rule, it is convenient to adopt the vector notation and considering principal directions:

$$\underline{\sigma} = (\sigma_1 \quad \sigma_2 \quad \sigma_3)^T \quad \text{and} \quad \underline{\varepsilon} = (\varepsilon_1 \quad \varepsilon_2 \quad \varepsilon_3)^T \quad Eq. [260]$$

where  $T$  is used to denote a transpose. Similar to the 1D-model we have both elastic and creep strains in the 3D-model. Using Hooke's law for the elastic part, and a flow rule for the creep part, one obtains:

$$\dot{\underline{\varepsilon}} = \dot{\underline{\varepsilon}}^e + \dot{\underline{\varepsilon}}^c = \mathbf{D}^{-1} \dot{\underline{\sigma}} + \lambda \frac{\partial g^c}{\partial \underline{\sigma}} \quad Eq. [261]$$

where the elasticity matrix and the plastic potential function are defined as:

$$\mathbf{D}^{-1} = \frac{1}{E_{ur}} \begin{bmatrix} 1 & -v_{ur} & -v_{ur} \\ -v_{ur} & 1 & -v_{ur} \\ -v_{ur} & -v_{ur} & 1 \end{bmatrix} \quad \text{and} \quad g^c = p^{eq} \quad Eq. [262]$$

where  $E_{ur}$  relates to the modified swelling index (Eq. [267]). Hence we use the equivalent pressure  $p^{eq}$  as a plastic potential function for deriving the individual creep strain-rate components. The subscripts 'ur' are introduced to emphasize that both the elasticity modulus and Poisson's ratio will determine unloading-reloading behaviour. Now it follows from the above equations that:

## Soft Soil Creep model (time dependent behaviour) [ADV]

Formulation of elastic 3D-strains

$$\dot{\varepsilon}_v^c = \dot{\varepsilon}_1^c + \dot{\varepsilon}_2^c + \dot{\varepsilon}_3^c = \lambda \cdot \left( \frac{\partial p^{eq}}{\partial \sigma_1} + \frac{\partial p^{eq}}{\partial \sigma_2} + \frac{\partial p^{eq}}{\partial \sigma_3} \right) = \frac{\partial p^{eq}}{\partial p} = \lambda \cdot \alpha \quad Eq. [263]$$

Hence we define  $\alpha = \partial p^{eq} / \partial p$ . Together with Eq. [260] and Eq. [261] this leads to:

$$\dot{\varepsilon} = \mathbf{D}^{-1} \dot{q} + \frac{\varepsilon_v^c}{a} \frac{\partial p^{eq}}{\partial q} = \mathbf{D}^{-1} \dot{q} + \frac{1}{a} \frac{\mu^*}{\mu} \left( \frac{p^{eq}}{p} \right)^{\frac{\lambda^* - \kappa^*}{\mu^*}} \frac{\partial p^{eq}}{\partial q} \quad Eq. [264]$$

where:

$$p_p^{eq} = p_{p0}^{eq} \exp \left( \frac{-\varepsilon_v^c}{\lambda^* - \kappa^*} \right) \quad Eq. [265]$$

or inversely:

$$-\varepsilon_v^c = (\lambda^* - \kappa^*) \ln \left( \frac{p_p^{eq}}{p_{p0}^{eq}} \right) \quad Eq. [266]$$

## 11.6 Formulation of elastic 3D-strains

Considering creep strains, it has been shown that the 1D-model can be extended to obtain the 3D-model, but as yet this has not been done for the elastic strains.

To get a proper 3D-model for the elastic strains as well, the elastic modulus  $E_{ur}$  has to be defined as a stress-dependent tangent stiffness according to:

$$E_{ur} = 3(1 - 2\nu_{ur})K_{ur} = -3(1 - 2\nu_{ur}) \left( \frac{p' + c \cot(\varphi)}{k^*} \right) \quad Eq. [267]$$

Hence,  $E_{ur}$  is not a new input parameter, but simply a variable quantity that relates to the input parameter  $\kappa^*$ . On the other hand  $\nu_{ur}$  is an additional true material constant.

Hence similar to  $E_{ur}$ , the bulk modulus  $K_{ur}$  is stress dependent according to the rule  $K_{ur} = -(p' + c \cot(\varphi))^* / \kappa^*$  where in this context  $c$  is again the effective cohesion rather than the creep parameter. Now it can be derived for the volumetric elastic strain that:

$$\begin{aligned} \dot{\varepsilon}_v^e &= \frac{\dot{p}'}{K_{ur}} = -\kappa^* \frac{\dot{p}'}{p' + c \cot(\varphi)} \\ \text{or by integration :} & \quad Eq. [268] \\ -\varepsilon_v^e &= \kappa^* \ln \left( \frac{p' + c \cot(\varphi)}{p_0' + c \cot(\varphi)} \right) \end{aligned}$$

Hence in the 3D-model the elastic strain is controlled by the mean stress  $p'$ , rather than by principal stress  $\sigma'$  as in the 1D-model. However mean stress can be converted into principal stress. For one-dimensional compression on the normal consolidation line, we have both  $3p' = (1 + 2 K_0^{nc}) \sigma'$  and  $3p'_0 = (1 + 2 K_0^{nc}) \sigma'_0$  and it follows that  $p'/p'_0 = \sigma'/\sigma'_0$ . As a consequence, for  $c = 0$ , we derive the simple rule  $-\varepsilon_v^e = \kappa^* \ln \sigma'/\sigma'_0$ , whereas the 1D-model involves  $-\varepsilon_v^e = a \ln \sigma'/\sigma'_0$ . It would thus seem that  $\kappa^*$  coincides with  $a$ . Unfortunately this line of thinking cannot be extended toward overconsolidated states of stress and strain. For such situations, it can be derived that:

## Soft Soil Creep model (time dependent behaviour) [ADV]

### Formulation of failure condition

---

$$\frac{\dot{p}'}{p'} = \frac{1 + v_{ur}}{1 - v_{ur}} \frac{1}{1 + 2K_0} \frac{\dot{\sigma}'}{\sigma'} \quad Eq. [269]$$

and it follows that:

$$-\dot{\varepsilon}_v^e = \kappa^* \frac{\dot{p}'}{p'} = \frac{1 + v_{ur}}{1 - v_{ur}} \frac{\kappa^*}{1 + 2K_0} \frac{\dot{\sigma}'}{\sigma'} \quad Eq. [270]$$

where  $K_0$  depends to a great extent on the degree of over-consolidation. Assuming that for soft clay the friction angle  $\varphi$  is in the order of 20-30° and OCR is in the order of 2-3, it is reasonable to assume  $K_0 \approx 1$  and together with  $v_{ur} \approx 0.2$  one obtains  $-2\varepsilon_v^c \approx \kappa^* \ln(\sigma'/\sigma'_0)$ . Good agreement with the 1D-model is then thus found by taking  $\kappa^* \approx 2a$ . Note that for clays with significantly different friction angles and/or degrees of consolidation good agreement with practical results may be found for values of both  $\kappa^* < 2a$  or  $\kappa^* > 2a$ .

## 11.7 Formulation of failure condition

The creep formulation does not include failure. Therefore, a Mohr-Coulomb type failure criterion, formulated in a perfect-plasticity framework, is added to the Soft Soil Creep model, generating plastic strains as soon as the failure condition is met. As soon as the Mohr-Coulomb failure yield criterion  $f(\sigma', c, \varphi) = 0$  is met, instantaneous plastic strain rates develop according to the flow rule  $\dot{\varepsilon}^P = \lambda \partial g / \partial \sigma'$  with  $g = g(\sigma', \psi)$ . For details see [Linear Elastic Perfectly Plastic Model \(Mohr-Coulomb Model\)](#) (on page 31).

In each stress point, the stresses are calculated according to the creep formulation before considering the failure criterion. Subsequently, the new stress state is checked against the failure criterion and corrected, if applicable.

## 11.8 Parameters of the Soft Soil Creep model

In addition to the parameters of the Soft Soil Creep model, the Soft Soil Creep model involves a creep parameter in the form of the *Modified Creep index*  $\mu^*$ . In total, the Soft Soil Creep model requires the following parameters to be determined:

## Soft Soil Creep model (time dependent behaviour) [ADV]

Parameters of the Soft Soil Creep model

Soil - Soft Soil Creep - <NoName>

General Mechanical Groundwater Thermal Interfaces Initial

Property	Unit	Value
<b>Stiffness</b>		
$\lambda^*$ (lambda*)		0.000
$\kappa^*$ (kappa*)		0.000
$\mu^*$		0.000
$v_{ur}$		0.1500
<b>Alternatives</b>		
Use alternatives		<input type="checkbox"/>
$C_c$		0.000
$C_s$		0.000
$C_a$		0.000
$e_{init}$		0.5000
<b>Strength</b>		
<b>Shear</b>		
$c'_{ref}$	kN/m <sup>2</sup>	5.000
$\varphi'$ (phi)	°	25.00
$\psi$ (psi)	°	0.000
<b>Tension</b>		
Tension cut-off		<input checked="" type="checkbox"/>
Tensile strength	kN/m <sup>2</sup>	0.000
<b>Miscellaneous</b>		
Use defaults		<input checked="" type="checkbox"/>
$K_{0\ nc}$		0.5774
$M$		2.413

Next OK Cancel

Figure 55: Mechanical tabsheet for the Soft Soil Creep model

In conclusion, the Soft Soil Creep model requires the following material constants:

Failure parameters as in the Mohr-Coulomb model:

$c'_{ref}$	Effective cohesion	[kN/m <sup>2</sup> ]
$\varphi'$	Friction angle	[°]
$\psi$	Dilatancy angle	[°]

Basic stiffness parameters

$\kappa^*$	Modified swelling index	[-]
------------	-------------------------	-----

## Soft Soil Creep model (time dependent behaviour) [ADV]

Parameters of the Soft Soil Creep model

$\lambda^*$	Modified compression index	[-]
$\mu^*$	Modified creep index	[-]

Advanced parameters (it is advised to use the default setting):

$\nu_{ur}$	Poisson's ratio for unloading - reloading (default 0.15)	[-]
$K_0^{nc}$	$\sigma'_{xx} / \sigma'_{yy}$ stress ratio in a state of normal consolidation	[-]
$M$	$K_0^{nc}$ -related parameter (see below)	[-]

Instead of defining the stiffness by the basic stiffness parameters, alternative stiffness parameters can be used. These material constants are given by:

$C_c$	Compression index	[-]
$C_s$	Swelling index	[-]
$C_\alpha$	Creep index for secondary compression	[-]
$e_{init}$	Initial void ratio	[-]

### 11.8.1 *Modified swelling index, modified compression index and modified creep index*

These parameters can be obtained from an isotropic compression test including isotropic unloading. When plotting the logarithm of the mean stress as a function of the volumetric strain for clay-type materials, the plot can be approximated by two straight lines (see [Figure 48](#) (on page 112)). The slope of the primary loading line gives the modified compression index, and the slope of the unloading (or swelling) line gives the modified swelling index. Note that there is a difference between the modified indices  $\kappa^*$  and  $\lambda^*$  and the original Cam-Clay parameters  $\kappa$  and  $\lambda$ . The latter parameters are defined in terms of the void ratio  $e$  instead of the volumetric strain  $\varepsilon_v$ . The parameter  $\mu^*$  ([Table 5](#) (on page 132)) can be obtained by measuring the volumetric strain on the long term and plotting it against the logarithm of time (see [Figure 52](#) (on page 123)).

In [Table 6](#) (on page 132), the value 2.3 is in fact  $\ln 10$  and stems from the conversion from  $^{10}\log$  to natural logarithm. The alternative stiffness parameters can also be calculated from this table. Since the void ratio  $e$  is not a constant, in the conversion from the alternative parameters to the original model parameters in PLAXIS the void ratio  $e$  is defined as the initial void ratio  $e_{init}$ . Entering a particular value for one of the alternatives  $C_c$ ,  $C_s$  or  $C_\alpha$  results in a change of  $\lambda^*$ ,  $\kappa^*$  or  $\mu^*$  respectively.

For a rough estimate of the model parameters, one might use the correlation  $\lambda^* \approx I_p(\%)/500$ , the fact that  $\lambda^* / \mu^*$  is in the range between 15 to 25 and the general observation  $\lambda^* / \kappa^*$  is between 2.5 and 7.

**Table 4: Relationship to Cam-Clay parameters**

$\lambda^* = \frac{\lambda}{1+e}$	$\kappa^* = \frac{\kappa}{1+e}$	---
-----------------------------------	---------------------------------	-----

## Soft Soil Creep model (time dependent behaviour) [ADV]

Parameters of the Soft Soil Creep model

**Table 5: Relationship to a,b,c parameters**

$\lambda^* = b$	$\kappa^* \approx \frac{2}{3} (1 + 2K_0) a \approx 2a$	$\mu^* = c$
-----------------	--	-------------

**Table 6: Relationship to internationally normalised parameters**

$\lambda^* = \frac{C_c}{2.3(1+e)}$	$\kappa^* \approx \frac{2}{2.3} \frac{C_s}{(1+e)}$	$\mu^* \approx \frac{1}{2.3} \frac{C_a}{(1+e)}$
------------------------------------	--	---

**Note:**

As already indicated in [Formulation of elastic 3D-strains](#) (on page 128), there is no exact relation between the isotropic compression index  $\kappa^*$  and the one-dimensional swelling indices  $A$  and  $C_s$ , because the ratio of horizontal and vertical stress changes during one-dimensional unloading. For the approximation it is assumed that the average stress state during unloading is an isotropic stress state, hence  $K_0=1$ . This is a reasonable assumption for moderately overconsolidated clays with a friction angle in the range of 20°-30°.

For characterising a particular layer of soft soil, it is also necessary to know the initial pre-consolidation pressure  $\sigma_{p0}$ . This pressure may, for example, be computed from a given value of the overconsolidation ratio (OCR). Subsequently  $\sigma_{p0}$  can be used to compute the initial value of the generalised pre-consolidation pressure  $p^{eq}_p$  (see [The initial pre-consolidation stress in advanced models](#) (on page 27)).

### 11.8.2 Poisson's ratio

In the case of the Soft Soil Creep model, Poisson's ratio is purely an elasticity constant rather than a pseudo-elasticity constant as used in the Mohr-Coulomb model. Its value will usually be in the range between 0.1 and 0.2. If the standard setting for the Soft Soil Creep model parameters is selected, then the value  $\nu_{ur} = 0.15$  is automatically adopted. For loading of normally consolidated materials, Poisson's ratio plays a minor role, but it becomes important in unloading problems. For example, for unloading in a one-dimensional compression test (oedometer), the relatively small Poisson's ratio will result in a small decrease of the lateral stress compared with the decrease in vertical stress. As a result, the ratio of horizontal and vertical stress increases, which is a well-known phenomenon for overconsolidated materials. Hence, Poisson's ratio should not be based on the normally consolidated  $K_0^{nc}$ -value, but on the ratio of difference in horizontal stress to difference in vertical stress in oedometer unloading and reloading:

$$\frac{\nu_{ur}}{1 - \nu_{ur}} = \frac{\Delta\sigma_{xx}}{\Delta\sigma_{yy}} \quad (\text{Unloading and reloading}) \quad \text{Eq. [271]}$$

### 11.8.3 $K_0^{nc}$ - parameter

By default,  $M$  is automatically determined based on the coefficient of lateral earth pressure in normally consolidated condition,  $K_0^{nc}$ , as entered by the user. The exact relationship between  $M$  and  $K_0^{nc}$  can be formulated as [Brinkgreve \(1994\)](#) (on page 246):

## Soft Soil Creep model (time dependent behaviour) [ADV]

State parameters in the Soft Soil Creep model

$$M = \sqrt{\frac{(1 - K_0^{nc})^2}{(1 + 2K_0^{nc})^2} + \frac{(1 - K_0^{nc})(1 - 2\nu_{ur})(\lambda^* / \kappa^* - 1)}{(1 - 2K_0^{nc})(1 - 2\nu_{ur})\lambda^* / \kappa^* - (1 - K_0^{nc})(1 + \nu_{ur})}} \quad Eq. [272]$$

Hence the user cannot enter directly a particular value of  $M$ . Instead he can choose values for  $K_0^{nc}$ . Note that the particular selection of  $M$  has an influence on lateral deformation of pseudo-vertical loading problems. For details, see [Brinkgreve \(2004\)](#) (on page 246).

$$M \approx 3.0 - 2.8K_0^{nc} \quad Eq. [273]$$

### 11.9 State parameters in the Soft Soil Creep model

In addition to the output of standard stress and strain quantities, the Soft Soil Creep model provides output (when being used) on state variables such as the isotropic pre-consolidation stress  $p_p$ . These parameters can be viewed by selecting the *State parameters* option from the *Stresses* menu. An overview of available state parameters is given below:

$p_{eq}$	Equivalent isotropic stress $p_{eq} = p' + q^2 / M^2 (p' + c \cot(\varphi))$	[-]
$p_p$	Isotropic pre-consolidation stress	[-]
OCR	Isotropic overconsolidation $OCR = p_p / p_{eq}$	[-]

### 11.10 On the use of the Soft Soil Creep model in dynamics calculations

When using the Soft Soil Creep model in dynamics calculations, the modified swelling index  $\kappa^*$  needs to be selected such that the model correctly predicts wave velocities in the soil. This generally requires a smaller value than just an unloading-reloading index.

When subjected to dynamic or cyclic loading, the Soft Soil Creep model will generate plastic strains when the preconsolidation stress is increased. However, it should be noted that stress cycles within the current creep contour will only generate elastic strains and no (hysteretic) damping, nor accumulation of strains or pore pressure, nor liquefaction. In order to account for the soil damping in cyclic loading, Rayleigh damping may be defined.

### 11.11 On the use of the Soft Soil Creep model in practical applications

## Soft Soil Creep model (time dependent behaviour) [ADV]

On the use of the Soft Soil Creep model in practical applications

---

In the Soft Soil Creep model, creep strains are generated as long as there is effective stress. In oedometer tests and other lab tests, self-weight stresses of the soil sample are negligible and the effective stress in the sample is dominated by external loading conditions. However, when it comes to practical applications, the effective stress in the soil is generally dominated by the initial self-weight stresses. As a consequence, creep will occur without additional loading.

Following the formulation of the model, the rate at which creep strains occur highly depends on the overconsolidation ratio as well as the ratio of the (modified) compression index over the (modified) creep index. Regarding the latter, it should be considered that natural clays may involve structure (bonding) whilst the Soft Soil Creep model does not include such effects. This requires the effective stress range in the application to be taken into account when determining the compression and creep indices from one-dimensional compression tests. This may also have an effect on the pre-consolidation stress to be used in the application. Moreover, considering 'normally-consolidated' soft soil deposits in practice, it would seem logical to set the initial *OCR*-value equal to 1.0. However, this would lead to unrealistic large creep strain rates due to the initial stresses, without even considering additional loading.

In order to avoid these unrealistic creep strain rates, it is recommended to set the initial *OCR*-value larger than 1.0. A value in the order of 1.2-1.4 will generally work, but in some cases even higher values might be needed. Please keep in mind that this changes the pre-consolidation pressure, such that the material becomes lightly overconsolidated and the pre-consolidation stress may not correspond anymore to what is observed in compression tests.

The above may be validated from a practical viewpoint by considering that the layer has aged since its deposition in geological history. Moreover, in particular the top few metres of an existing soft soil layer have been subjected to various possible external influences (traffic, weather, temperature changes, changes in saturation, etc.). Accurate measurements of the pre-consolidation pressure on soil samples that are assumed to be 'normally-consolidated' would typically show a pre-consolidation pressure that is noticeably larger than the initial effective stress. However, lab tests are often performed on soil samples that have been disturbed to a certain extent, and therefore the measurement of the pre-consolidation stress in practice is often inaccurate.

In conclusion, the determination of model parameters for the Soft Soil Creep model requires a cautious interpretation of test data, in view of the envisioned practical application. It is recommended, before commencing any 2D or 3D analysis, to perform a careful calibration of model parameters. This can be done by performing simulations using the PLAXIS Soil Test facility in combination with an analysis of a one-dimensional soil column (based on the in-situ soil layering), in which a realistic time interval is considered.

## The Sekiguchi-Ohta model [ADV]

The Sekiguchi-Ohta model has been developed to formulate a constitutive law for normally consolidated clay. Particular emphasis is placed on taking the effect of time and stress-induced anisotropy into consideration. A complete description of the model has been presented in [Sekiguchi & Ohta \(1977\)](#) (on page 249) and [Iizuka & Ohta \(1987\)](#) (on page 247).

### 12.1 Formulation of the Sekiguchi-Ohta model

The Sekiguchi-Ohta model combines the concepts lying behind the well known Cam Clay model ([Roscoe, Schofield & Thurairajah \(1963\)](#) (on page 248)) and the rheological model developed by [Murayama & Shibata \(1966\)](#) (on page 248). The Cam Clay model was further developed by [Ohta & Hata \(1973\)](#) (on page 248) counting for the stress induced anisotropy for anisotropically consolidated clays. However due to the fact that this model deals with the stress-strain behaviour of the soil in equilibrium, the time effect is not considered. The rheological model is further developed by [Sekiguchi \(1977\)](#) (on page 249) to describe the time-dependent and elastoplastic behaviour for normally consolidated clays.

#### 12.1.1 Isotropic states of stress and strain ( $\sigma'_1 = \sigma'_2 = \sigma'_3$ )

In the Sekiguchi-Ohta model, it is assumed that there is a logarithmic relation between changes in volumetric strain,  $\varepsilon_v$ , and changes in mean effective stress,  $p'$ , which can be formulated as:

$$\varepsilon_v - \varepsilon_v^0 = -\lambda^* \ln \left( \frac{p'}{p^0} \right) \quad (\text{virgin compression}) \quad \text{Eq. [274]}$$

The parameter  $\lambda^*$  is the modified compression index, which determines the compressibility of the material in primary loading. Note that  $\lambda^*$  differs from the index  $\lambda$  as used by [Burland \(1965\)](#) (on page 246). The difference is that Eq. [274] is a function of volumetric strain instead of void ratio. Plotting Eq. [274] gives a straight line as shown in [Figure 56](#) (on page 136).

During isotropic unloading and reloading a different path (line) is followed, which can be formulated as:

$$\varepsilon_v^e - \varepsilon_v^{e0} = -\kappa^* \ln \left( \frac{p'}{p^0} \right) \quad (\text{unloading and reloading}) \quad \text{Eq. [275]}$$

The parameter  $\kappa^*$  is the modified swelling index, which determines the compressibility of the material in unloading and subsequent reloading. Note that  $\kappa^*$  differs from the index  $\kappa$  as used in the Cam-Clay models. The

## The Sekiguchi-Ohta model [ADV]

### Formulation of the Sekiguchi-Ohta model

ratio  $\lambda^*/\kappa^*$  is, however, equal to the ratio  $\lambda/\kappa$ . The soil response during unloading and reloading is assumed to be elastic as denoted by the superscript  $e$  in Eq. [275]. The elastic behaviour is described by Hooke's law. Eq. [275] implies linear stress dependency on the tangent bulk modulus such that:

$$K_{ur} \equiv \frac{E_{ur}}{3(1 - 2\nu_{ur})} = \frac{p'}{\kappa^*} \quad \text{Eq. [276]}$$

in which the subscript  $ur$  denotes unloading/reloading. Neither the elastic bulk modulus,  $K_{ur}$ , nor the elastic Young's modulus,  $E_{ur}$ , is used as an input parameter. Instead,  $\nu_{ur}$  and  $\kappa^*$  are used as input constants for the part of the model that computes the elastic strains.

An infinite number of unloading/reloading lines may exist in [Figure 56](#) (on page 136), each corresponding to a particular value of the isotropic pre-consolidation stress  $p_p$ . The pre-consolidation stress represents the largest stress level experienced by the soil. During unloading and reloading, this pre-consolidation stress remains constant. In primary loading, however, the pre-consolidation stress increases with the stress level, causing irreversible (plastic) volumetric strains.

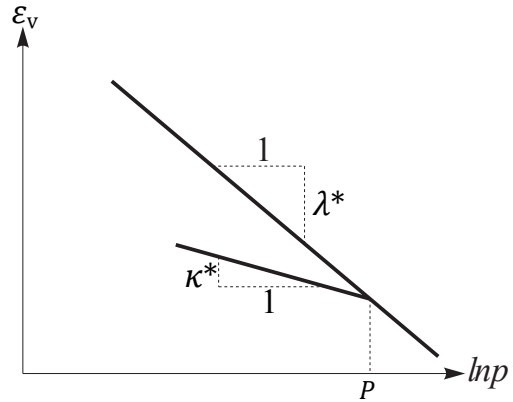


Figure 56: Logarithmic relation between volumetric strain and mean stress

### 12.1.2 Inviscid (time-independent) formulation

The yield function of the inviscid model in triaxial space is expressed by the following equation:

$$f = MD \ln \left( \frac{p'}{p_p} \right) + D \frac{\bar{q}}{p} \quad \text{Eq. [277]}$$

where

$M$	=	Critical state frictional parameter.
$D$	=	Coefficient of dilatancy.
$p'$	=	Mean effective stress.
$p_p$	=	Isotropic hardening stress parameter.
$\bar{q}$	=	Relative deviatoric stress

The isotropic hardening stress parameter of the model is defined as:

$$p_p = p_{p0} e^{\frac{(\varepsilon_v^p - \varepsilon_{v0}^p)}{MD}} \quad \text{Eq. [278]}$$

## The Sekiguchi-Ohta model [ADV]

Parameters of the Sekiguchi-Ohta model

---

where

$$\begin{aligned} MD &= \lambda^* - \kappa^* \\ \varepsilon_{v0}^p &= \text{Initial plastic volumetric strain} \end{aligned}$$

Hence, the parameter  $D$  is an auxiliary parameter implicitly defined as  $D = (\lambda^* - \kappa^*)/M$ .

### 12.1.3 Viscid (time-dependent) formulation

The flow function of the visco-plastic (viscid) model is written as:

$$F = \alpha^* \ln \left( 1 + \frac{\dot{\varepsilon}_0 t}{\alpha^*} \exp \left( \frac{f(\sigma)}{\alpha^*} \right) \right) - \varepsilon_v^{vp} = 0 \quad \text{Eq. [279]}$$

where

$$f(\sigma) = MD \ln \frac{p'}{p_0} + D \frac{\dot{q}}{p'} \quad \text{Eq. [280]}$$

The flow function  $F$  can be transformed to a function of stress and hardening parameter  $g$  as follows:

$$g(\sigma', h) = f(\sigma') - h(\varepsilon_v^{vp}, t) = 0 \quad \text{Eq. [281]}$$

where the hardening parameter  $h$  is defined as:

$$h(\varepsilon_v^{vp}, t) = \alpha^* \ln \left\{ \frac{\alpha^*}{\dot{\varepsilon}_0 t} \left[ \exp \left( \frac{\varepsilon_v^{vp}}{\alpha^*} \right) - 1 \right] \right\} \quad \text{Eq. [282]}$$

The initial time to calculate the hardening parameter  $h$  should not be zero, because it is not determined due to  $1/t$  in Eq. [282]. To be able to calculate the initial volumetric visco-plastic strain, it is assumed that the hardening parameter  $h$  is equal to zero. Hence, the initial visco-plastic volumetric strain can be calculated as follows:

$$h(\varepsilon_v^{vp}, t) = \alpha^* \ln \left\{ \frac{\alpha^*}{\dot{\varepsilon}_0 t} \left[ \exp \left( \frac{\varepsilon_v^{vp}}{\alpha^*} \right) - 1 \right] \right\} = 0 \quad \text{Eq. [283]}$$

$$\varepsilon_{v0}^{vp} = \alpha^* \ln \left\{ \frac{\dot{\varepsilon}_0 t}{\alpha^*} + 1 \right\} = 0 \quad \text{Eq. [284]}$$

$\varepsilon_{v0}^{vp}$  is used as the initial visco-plastic volumetric strain to calculate the current visco-plastic volumetric strain.

## The Sekiguchi-Ohta model [ADV]

Parameters of the Sekiguchi-Ohta model

---

### 12.2 Parameters of the Sekiguchi-Ohta model

#### 12.2.1 Model parameters of the inviscid model

- *Basic parameters for soil stiffness:*

$\lambda^*$	Modified compression index	[-]
$\kappa^*$	Modified swelling index	[-]

- *Alternative parameters can be used to define soil stiffness:*

$C_c$	Compression index	[-]
$C_s$	Swelling index or reloading index	[-]
$e_{init}$	Initial void ratio	[-]

- *Advanced parameters for soil stiffness:*

$\nu_{ur}$	Poisson's ratio for unloading-reloading	[-]
$K_0^{nc}$	Coefficient of lateral stress in normal consolidation	[-]

- *Parameters for soil strength:*

$M$	Tangent of the critical state line	[-]
-----	------------------------------------	-----

#### Modified compression index and modified swelling index ( $\lambda^*$ and $\kappa^*$ )

These parameters can be obtained from an isotropic compression test including isotropic unloading. When plotting the logarithm of the mean effective stress as a function of the volumetric strain for clay type materials, the plot can be approximated by two straight lines, see [Figure 57](#) (on page 139). The slope of the primary loading line gives the modified compression index  $\lambda^*$ , and the slope of the unloading (or swelling) line gives the modified swelling index  $\kappa^*$ .

## The Sekiguchi-Ohta model [ADV]

Parameters of the Sekiguchi-Ohta model

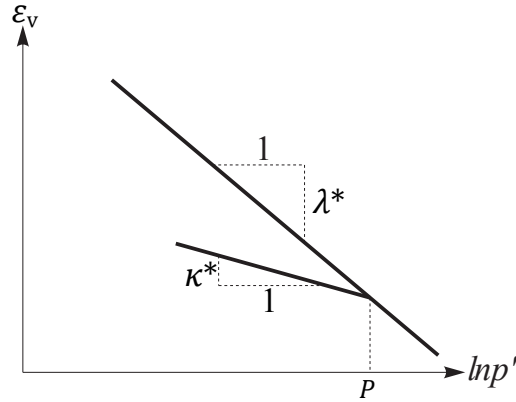


Figure 57: Logarithmic relation between volumetric strain and mean stress

### Poisson's ratio ( $\nu_{ur}$ )

The poisson's ratio  $\nu_{ur}$  is a real elastic parameter and not a pseudo-elasticity constant as used in the Mohr-Coulomb model. Its value will usually be in the range between 0.1 and 0.2.

### Earth pressure coefficient at rest ( $K_0^{nc}$ )

The  $K_0^{nc}$  parameter is defined as the stress ratio in one-dimensional compression in a state of normal consolidation:

$$K_0^{nc} = \frac{\sigma'_{xx}}{\sigma'_{yy}}$$

The  $K_0^{nc}$  -parameter determines the singular point in the Sekiguchi-Ohta model yield contour. Hence,  $K_0^{nc}$  relates to the inclination of the stress path in one-dimensional compression where  $\alpha$ , as described in the Eq. [285] is the slope of the  $K_0^{nc}$  line in the  $p$  -  $q$  plane.

$$\alpha = \frac{3(1 - K_0^{nc})}{1 + 2K_0^{nc}} \quad \text{Eq. [285]}$$

## The Sekiguchi-Ohta model [ADV]

Parameters of the Sekiguchi-Ohta model

---

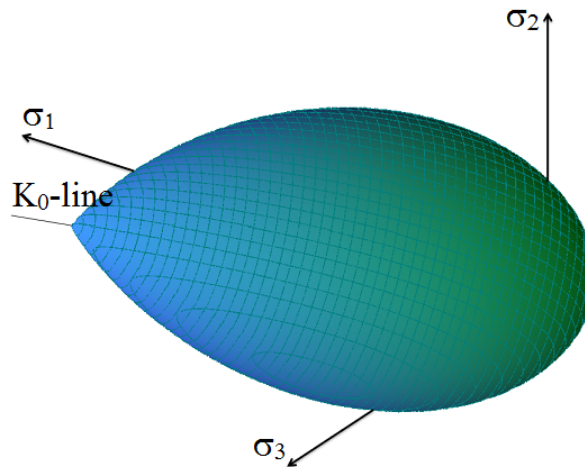


Figure 58: The Sekiguchi-Ohta model yield surface in triaxial stress space

### Slope of the critical state line ( $M$ )

In order to obtain the correct shear strength, the parameter  $M$  should be based on the friction angle  $\varphi$ . The critical state line is comparable with the Drucker-Prager failure criteria, and represents a (circular) cone in the principal stress space. Hence, the value of  $M$  can be obtained from  $\varphi$  in a similar way as the Drucker-Prager friction constant  $\alpha$  is obtained from  $\varphi$ . For details see also the [Modified Cam-Clay model](#) (on page 95).

### Initial overconsolidation ratio ( $OCR_0$ )

The initial overconsolidation ratio  $OCR_0$  is defined as the highest vertical effective stress experienced in the past,  $\sigma'_p$ , divided by the current stress  $\sigma'_{yy}$ . A soil which is currently experiencing its highest stress is said to be normally consolidated and to have an  $OCR$  of 1.

### Initial pre-overburden pressure ( $POP_0$ )

The initial pre-overburden pressure  $POP_0$ , expressed in the unit of stress, is defined as:

$$POP_0 = \sigma'_p - \sigma'_{yy}$$

where

$\sigma'_p$	=	vertical pre-consolidation stress (the greatest vertical stress reached previously)
$\sigma'_{yy}$	=	In-situ effective vertical stress.

## 12.2.2 Model parameters of the viscid model

Compared to the inviscid Sekiguchi-Ohta model, the viscid Sekiguchi-Ohta model requires the coefficient of secondary compression  $\alpha^*$  and the initial volumetric strain rate  $\dot{v}_0$  as two additional parameters of input. All other parameters remain the same as in the inviscid Sekiguchi-Ohta model.

- *Basic parameters for soil stiffness:*

## The Sekiguchi-Ohta model [ADV]

Parameters of the Sekiguchi-Ohta model

$\lambda^*$	Modified compression index	[-]
$\kappa^*$	Modified swelling index	[-]
$\alpha^*$	Coefficient of secondary compression	[-]
$\dot{v}_0$	Initial volumetric strain rate	[day <sup>-1</sup> ]

- Alternative parameters can be used to define soil stiffness:

$C_C$	Compression index	[-]
$C_s$	Swelling index or reloading index	[-]
$C_{\alpha^*}$	Secondary compression index	[-]
$e_{init}$	Initial void ratio	[-]

- Parameters for soil strength:

$M$	Tangent of the critical state line	[-]
-----	------------------------------------	-----

- Advanced parameters for soil stiffness:

$\nu_{ur}$	Poisson's ratio for unloading-reloading	[-]
$K_0^{nc}$	Coefficient of lateral stress in normal consolidation	[-]

### Coefficient of secondary compression ( $\alpha^*$ )

The coefficient of secondary compression  $\alpha^*$  is defined as:

$$\alpha^* = \frac{d\varepsilon_v}{d(\ln t)} \quad Eq. [286]$$

at time  $t_c$  (the end of primary consolidation).

### Initial volumetric strain rate ( $\dot{v}_0$ )

The initial volumetric strain rate  $\dot{v}_0$  at reference state is expressed as:

$$\dot{v}_0 = \frac{\alpha^*}{t_c} \quad Eq. [287]$$

## The Sekiguchi-Ohta model [ADV]

State parameters in the Sekiguchi-Ohta model

---

### 12.3 State parameters in the Sekiguchi-Ohta model

In addition to the output of standard stress and strain, the Sekiguchi-Ohta model provides output (when being used) on state variables such as the isotropic pre-consolidation stress  $p_p$  and the isotropic overconsolidation ratio  $OCR$ . These parameters can be visualised by selecting from the *Stresses* menu in the *State parameters* option. An overview of available state parameters is given below:

$p_{eq}$	Equivalent isotropic stress $P_{eq} = \frac{p'}{\exp\left(-\frac{\tilde{q}}{Mp'}\right)}$	[kN/m <sup>2</sup> ]
$p_p$	Isotropic preconsolidation stress	[kN/m <sup>2</sup> ]
$OCR$	Isotropic over-consolidation ratio ( $OCR = p^p/p^{eq}$ )	[-]

For the design of offshore structures under a design storm (i.e. a combination of wave, wind and current loading), the stiffness and the bearing capacity of the foundation have to be calculated accounting for the effect of cyclic loading. The response of saturated soils under cyclic loading is different from the case of the static loading. It may be increased due to strain rate effects and reduced due to the degradation process, pore pressure build-up and destructuration.

The soil strength in static undrained conditions can be described by the undrained shear strength of the soil  $s_u$ , which is dependent on the effective stress level, stress path and the material. However, by cyclic loading of the soil, the soil strength depends in addition on the value of the combination of the average and cyclic stresses in the soil. The shear strength is therefore written as  $\tau_{f,cy}$  instead of the static undrained shear strength  $s_u$ . The undrained cyclic shear strength is described by [Andersen, Kleven & Heien \(1988\)](#) (on page 245), as:

$$\tau_{f,cy} = (\tau_a + \tau_{cy})_f \quad Eq. [288]$$

where

$\tau_a$	=	Average shear stress at failure.
$\tau_{f,cy}$	=	The cyclic undrained shear strength.

The two aforementioned stress components are shown in [Figure 59](#) (on page 144)([Andersen & Jostad, 2009](#) (on page 245)), where the process of excess pore pressure build-up in cyclic loading is depicted. The shear stress, the pore pressure and the shear strain are divided into two components: the average component and the cyclic component. In a cyclic triaxial test the stress is varying with the cyclic shear stress  $\tau_{cy}$  with respect to the average shear stress  $\tau_a$ . The effective stress decreases due to the increase in pore pressure and the stress paths move to the left, generally defined as either 15% average shear strain or 15% cyclic shear strain. After a certain number of cycles  $N$  the soil reaches a failure strength. The same soil can thus fail at a lower shear stress in cyclic loading than in monotonic loading.

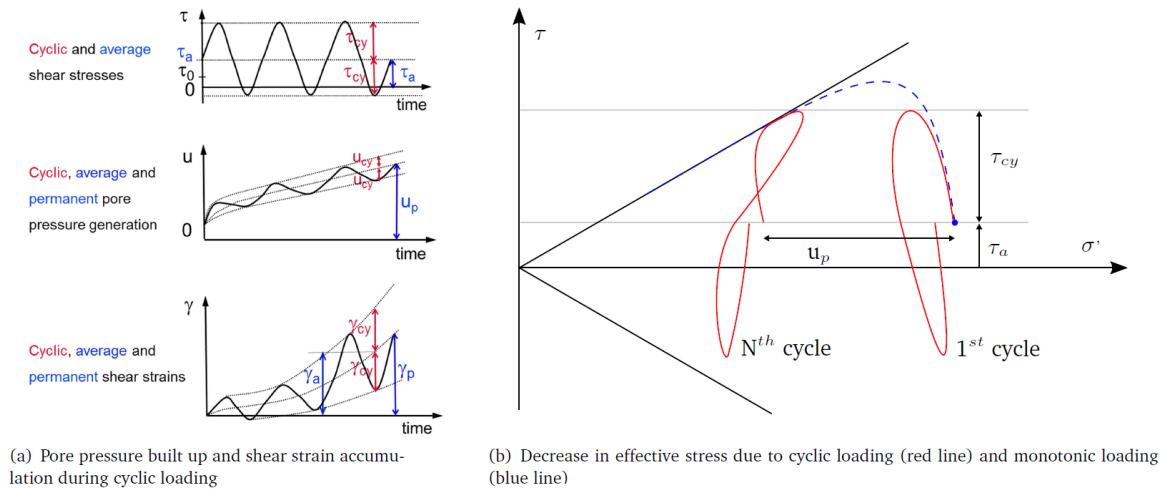


Figure 59: Generation of pore pressures and strains in a cyclic triaxial test

Stress anisotropy (or stress path dependent behaviour) is an important aspect regarding the stability of a system. This means that the stress state is varying in the soil, and thus have to be accounted for. As shown in [Figure 60](#) (on page 144) ([Andersen, 2015](#) (on page 245)), the soil behaviour along a potential failure surface, indicated by the dashed line, can be interpolated between by three undrained cyclic laboratory tests:

- Direct Simple Shear test (DSS).
  - Symmetric loading ( $\tau_a = 0$ ).
  - Asymmetric loading ( $\tau_a \neq 0$ ).
- Anisotropically consolidated Triaxial Compression test (TXC).
- Anisotropically consolidated Triaxial Extension test (TXE).

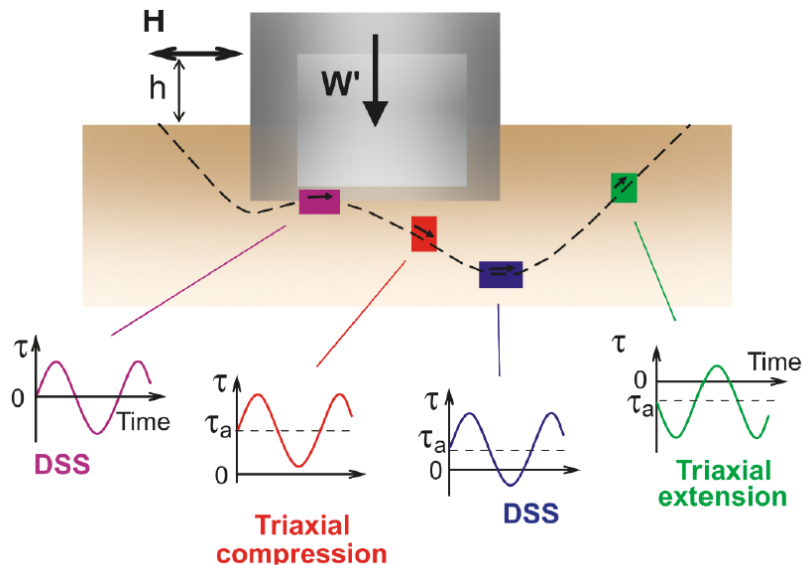


Figure 60: Ideal stress conditions along a potential failure surface in the soil beneath a gravity base structure under cyclic loading

## The UDCAM-S model [ADV]

### Parameters of the UDCAM-S model

The Simplified UnDrained Cyclic Accumulation Model (UDCAM-S) is an advanced model to deal with undrained soil behaviour and degradation of the strength and stiffness in cyclic loading of clay or low permeable silty soils. The UDCAM-S model is derived from the UDCAM model by NGI ([Andresen & Jostad, 2009](#) (on page 245)) with simplifications in order to be more suitable for engineering practice. The material model is based on the NGI-ADP model ([Andresen & Jostad, 1999](#) (on page 245)) for the undrained behavior of clays, implementing a pre-processing procedure called cyclic accumulation tool (Reference Manual - Chapter 6 - *Cyclic accumulation and optimisation tool*) to obtain the adjusted parameter set based on the type of analysis the user has to perform:

- Cyclic: to calculate cyclic displacements or stiffness to be used in dynamics analysis of the structure.
- Average: to calculate accumulated (permanent) displacements of the foundation.
- Total: to calculate total (*average + cyclic*) displacements, capacity or stiffnesses to be used in pseudo-static analysis of the structure.

Except from the calculation of the degraded parameter set with the cyclic accumulation tool, the UDCAM-S model inherits the same formulation and implementation of the NGI-ADP model. For more information about the formulation of the NGI-ADP model, reference is made to [The NGI-ADP model \(anisotropic undrained shear strength\)](#) (on page 99).

## 13.1 Parameters of the UDCAM-S model

The UDCAM-S model requires a total of ten parameters.

The actual components can be cyclic, average or total (average + cyclic):

- *Parameters for stiffness:*

$G_{max}/\tau^C$	Ratio unloading/reloading shear modulus over (plane strain) active shear strength	[-]
$\gamma_f^C$	Shear strain in triaxial compression	[%]
$\gamma_f^E$	Shear strain at failure in triaxial extension	[%]
$\gamma_f^{DSS}$	Shear strain at failure in direct simple shear	[%]

- *Parameters for strength:*

$\tau_{ref}^C$	Degraded reference shear strength in triaxial compression	[kN/m <sup>2</sup> ]
$z_{ref}$	Reference level	[m]
$\tau_{inc}^C$	Increase of degraded triaxial compression shear strength with depth	[kN/m <sup>2</sup> /m]
$\tau^E/\tau^C$	Ratio of degraded triaxial compression shear strength triaxial extension over degraded triaxial compression shear strength	[-]
$\tau_0/\tau^C$	Initial mobilisation	[-]
$\tau^{DSS}/\tau^C$	Ratio of degraded direct simple shear strength over degraded triaxial compression shear strength	[-]

## The UDCAM-S model [ADV]

### Parameters of the UDCAM-S model

- Advanced parameters:

$\nu'$	Effective Poisson's ratio	[-]
$\nu_u$	Undrained Poisson's ratio	[-]

**Note:**

The model should be only used for undrained conditions.

#### 13.1.1 Ratio of the initial shear modulus to the degraded TXC shear strength ( $G_{max}/\tau^C$ )

Ratio of the initial shear modulus to the degraded shear strength at failure in the triaxial compression test. If the shear strength is increasing with depth the constant ratio for  $G_{max}/\tau^C$  gives a shear stiffness increasing linearly with depth.

#### 13.1.2 Shear strain at failure in triaxial compression ( $\gamma_f^C$ )

This parameter  $\gamma_f^C$  (%) defines the shear strain at which failure is obtained in undrained triaxial compression mode of loading.

#### 13.1.3 Shear strain at failure in triaxial extension ( $\gamma_f^E$ )

This parameter  $\gamma_f^E$  (%) defines the shear strain at which failure is obtained in undrained triaxial extension mode of loading.

#### 13.1.4 Shear strain at failure in direct simple shear ( $\gamma_f^{DSS}$ )

This parameter  $\gamma_f^{DSS}$  (%) defines the shear strain at which failure is obtained in undrained simple shear mode of loading.

#### 13.1.5 Reference degraded TXC shear strength ( $\tau_{ref}^C$ )

The reference degraded TxC shear strength at failure in the triaxial compression test is the shear strength obtained in triaxial compression stress paths at the reference depth  $y_{ref}$  expressed in the unit of stress.

### 13.1.6 Reference depth ( $y_{ref}$ )

This is the reference depth  $y_{ref}$  at which the reference TXC shear strength  $\tau^C$  is defined. Below this depth the shear strength and stiffness may increase linearly with increasing depth. Above the reference depth the shear strength is equal to  $\tau^C$ .

### 13.1.7 Increase of degraded TXC shear strength with depth ( $\tau_{inc}^C$ )

The parameter  $\tau_{inc}^C$  defines the increase (positive) or decrease (negative) of the undrained TXC shear strength with depth, expressed in the unit of stress per unit of depth. Above the reference depth the shear strength is equal to  $\tau_{ref}^C$ , below the reference depth the shear strength is defined as:

$$\tau^C(y) = \tau_{ref}^C + (y_{ref} - y)\tau_{inc}^C \quad Eq. [289]$$

### 13.1.8 Ratio of the degraded TXE shear strength to the undrained TXC shear strength ( $\tau^E/\tau^C$ )

The ratio  $\tau^E/\tau^C$  defines the degraded undrained shear strength for triaxial extension mode of loading in relation to the degraded undrained shear strength in triaxial compression mode of loading. Please note that active / passive strength input is defined for plane strain conditions. However, it is generally acceptable and only slightly conservative to use the strength obtained from a triaxial compression test as input for the active plane strain condition (i.e.  $\tau^A = \tau^C$ ) and the strength obtained from a triaxial extension test as input for the passive plane strain condition (i.e.  $\tau^P = \tau^E$ ).

### 13.1.9 Ratio of the degraded DSS shear strength to the undrained TXC shear strength ( $\tau^{DSS} / \tau^C$ )

The ratio  $\tau^{DSS}/\tau^C$  defines the degraded undrained shear strength in direct simple shear mode of loading in relation to the degraded undrained shear strength in triaxial compression mode of loading.

### 13.1.10 Initial mobilization ( $\tau_0/\tau^C$ )

The initial mobilization  $\tau_0/\tau^C$  is clearly defined for nearly horizontally deposited normally consolidated or lightly overconsolidated clay layers where the vertical stress is the major principle stress  $\sigma'_1$ . As defined in [Figure 61](#) (on page 148), the initial mobilization can be calculated from the earth pressure coefficient at rest  $K_0$  by the following equation:

## The UDCAM-S model [ADV]

State parameters in the UDCAM-S model

$$\tau_0/\tau^C = -0.5(1 - K_0)\sigma'_{yy0}/\tau^C \quad \text{Eq. [290]}$$

where

$\sigma'_{yy0}$  = initial (in situ) vertical effective stress (compression negative).

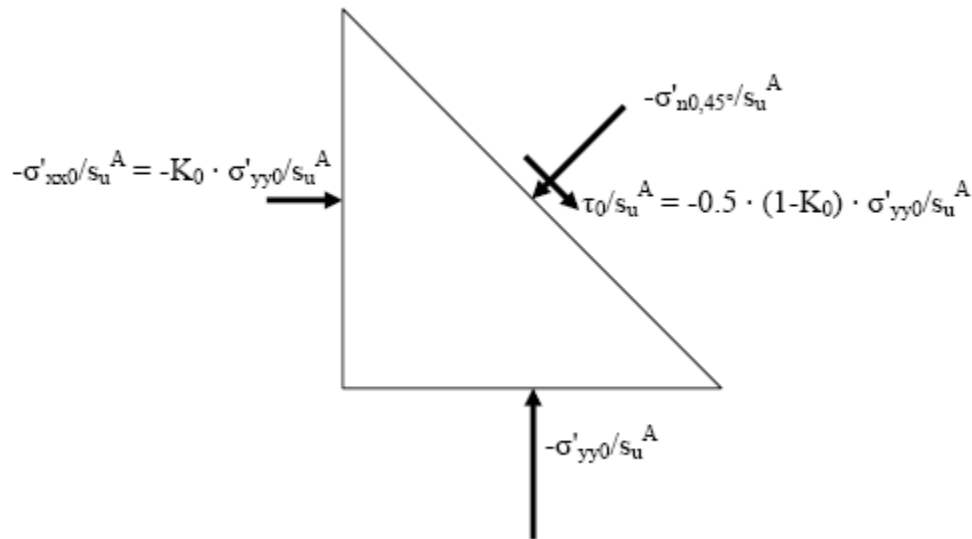


Figure 61: Definition of initial mobilised maximum shear stress  $\tau_0 = 1/2 |\sigma'_{yy0} - \sigma'_{xx0}|$  for a soil element in a horizontal deposited layer.

Changing the default value for the initial mobilization should be considered in particular for overconsolidated materials where  $K_0$  generally is higher than 0.6, however the UDCAM-S model (like NGI-ADP model) is not intended used for heavily overconsolidated clays and should be used with care for  $K_0 > 1.0$  (i.e. negative  $\tau_0/\tau^C$ ).

### 13.1.11 Poisson's ratio ( $\nu$ )

Only *Undrained (C)* drainage option should be used as a pure total stress analysis is carried out where no distinction between effective stresses and pore pressures is made and all stress changes should be considered as changes in total stress. A Poisson's ratio of  $\nu = 0.495$  should be used for the calculation.

## 13.2 State parameters in the UDCAM-S model

$\gamma_p$	Plastic shear strain	[-]
$r_k$	Hardening function	[-]

$$r_k = 2 \frac{\sqrt{\gamma^p / \gamma_f^p}}{1 + \gamma^p / \gamma_f^p} \quad \text{Eq. [291]}$$

## The UDCAM-S model [ADV]

On the use of the UDCAM-S model in dynamics calculations

---

### 13.3 On the use of the UDCAM-S model in dynamics calculations

The model should not be used in dynamics calculations.

## The Concrete model [ADV]

Generally, for concrete structure elements, a linear elastic material model is adopted due to their strength compared to the one of the soil. However, in some kind of geotechnical problems, the complex non-linear behaviour of the concrete structures must be inspected for a reliable redistribution of stress-strain in the continuum and a correct design. Distinction can be made between the main features of the complex concrete behaviour: limited strength in compression and tension, time-dependent strength and stiffness, strain hardening/softening, creep and shrinkage.

The Concrete model was originally developed to model the behaviour of shotcrete, but it is also useful for soil reinforcement (e.g. concrete columns), soil improvements (e.g. jet grouting columns) and concrete structures (e.g. beams). The current engineering approach to model shotcrete linings in numerical simulations assumes a linear elastic material with a stepwise increase of the (artificially low) Young's modulus in subsequent excavation stages. While realistic lining deformations may be obtained with this method, lining stresses are usually too high, in particular if the lining is subjected to significant bending. With the Concrete model more realistic stress distributions can be obtained, as the non-linearity of the material behaviour is taken into account. Furthermore, the stability of the tunnel can be checked at all intermediate stages without the need for additional capacity checks of the lining cross section.

The Concrete model is an elastoplastic model for simulating the time-dependent strength and stiffness of concrete, strain hardening-softening in compression and tension as well as creep and shrinkage ([Schadlich & Schweiger, 2014](#) (on page 248)). Hence, differently from what is seen in Eq. [70], the total strain  $\varepsilon$  is not only decomposed into elastic strain  $\varepsilon^e$  and plastic strain  $\varepsilon^p$  but also considers creep strain  $\varepsilon^{cr}$  and shrinkage strain  $\varepsilon^{shr}$ :

$$\varepsilon = \varepsilon^e + \varepsilon^p + \varepsilon^{cr} + \varepsilon^{shr} \quad \text{Eq. [292]}$$

When subjected to deviatoric loading, concrete shows different behaviours: in compression, the strength increases non-linearly up to a peak value and then softens to a residual one; in tension, it's considered linear elastic until reaching the tensile strength and then softens to the residual value. The Concrete model employs a Mohr-Coulomb yield surface for deviatoric loading, combined with a Rankine yield surface in the tensile regime.

Most of the input parameters for the Concrete model can be derived from standard uniaxial tension and compression tests. Some basic characteristics of the Concrete model and their relevant input parameters are:

Limited strength in compression and tension.	$f_{c,28}, f_{t,28}$
Time-dependent strength and stiffness.	$f_{c,1} / f_{c,28}, E_1 / E_{28}, \varepsilon_{cp}^p, t_{hydr}$
Strain hardening in compression	$f_{c0n}$
Strain softening in compression and tension	$f_{cfn}, f_{cun}, G_{c,28}, f_{tun}, G_{t,28}$
Stress- and stiffness-dependent creep strains	$\varphi^{cr}, t_{50}^{cr}$

## The Concrete model [ADV]

### Formulation of the Concrete model

Stress-independent shrinkage strains	$\varepsilon_{\infty}^{shr}, t_{50}^{shr}$
--------------------------------------	--

The stress-strain approach for hardening and softening is proposed by [Schütz, Potts & Zdravković \(2011\)](#) (on page 248), involving mobilised compression and tensile strength through the uniaxial plastic peak strain  $\varepsilon_{cp}^p$  at 1h, 8h, 24h and the fracture energy of the material both in compression,  $G_c$ , and in tension,  $G_t$ . Furthermore, thanks to the time-dependent internal laws of the Concrete model for  $f_c, f_t, G_c$  and  $G_t$ , the hardening-softening of the yield surfaces completely follows the evolution of the material in time. The time-dependency of elastic stiffness, compressive and tensile strength is taken into account following an approach similar to the recommendation of CEB-FIP model code (1990) as well as EN 14487-1. The ability of young concrete to withstand large deformations at early age, thanks to its initial high plastic ductility, is represented by a time-dependent plastic peak strain  $\varepsilon_{cp}^p$  ([Meschke, Kropik & Mang, 1996](#) (on page 248)).

## 14.1 Formulation of the Concrete model

The Concrete model employs a composite yield surface; Mohr-Coulomb surface for deviatoric loading and Rankine surface in the tensile regime with isotropic compression softening ([Figure 62](#) (on page 151)). In the Concrete model formulation, the yield function is named with capital  $F$  in order to distinguish it from the yield stress  $f$ . The sign convention is strictly tension-positive and  $\sigma_1$  is the major (tensile) principle stress and  $\sigma_3$  is the minor (compressive) principle stress.

The yield functions can be formulated in terms of principal stresses in relation to the uniaxial compressive and tensile yield stresses,  $f_{cy}$  and  $f_t$ , as:

$$F_c = \frac{\sigma_1 \cdot \sigma_3}{2} + \frac{\sigma_1 + \sigma_3}{2} \sigma_{rot} - \frac{f_{cy}}{2} \sigma_{rot} + f_{cy} \quad Eq. [293]$$

$$F_t = \sigma_1 - f_t \quad Eq. [294]$$

where

$$\sigma_{rot} = \text{Intersection of the Mohr-Coulomb failure envelope and the isotropic axis.}$$

For a given maximum inclination of the Mohr-Coulomb envelope,  $\sigma_{rot}$  can be written as:

$$\sigma_{rot} = \frac{f_c}{2} \left( \frac{1}{\sin(\varphi_{max})} - 1 \right) \quad Eq. [295]$$

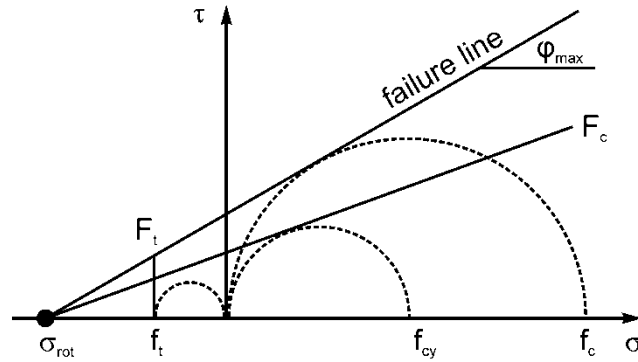


Figure 62: Yield surfaces and failure envelope for Concrete model

## 14.2 Strain hardening and softening

### 14.2.1 Compression

In compression, the Concrete model follows the approach proposed by [Schütz, Potts & Zdravković \(2011\)](#) (on page 248). The stress-strain curve is divided in four parts ([Figure 63](#) (on page 152)):

- Part I - quadratic strain hardening
- Part II - linear strain softening
- Part III - linear strain softening
- Part IV - constant residual strength

Due to the time-dependency of the involved material parameters, a normalised hardening/softening parameter  $H_c = \varepsilon_{p3}^p / \varepsilon_{cp}^p$  is used, with  $\varepsilon_{p3}^p$  = minor plastic strain (calculated from  $F_c$ ) and  $\varepsilon_{cp}^p$  = plastic peak strain in uniaxial compression.

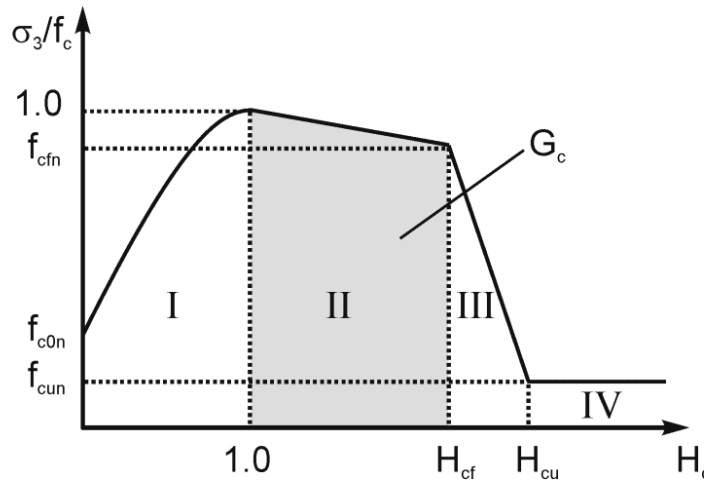


Figure 63: Normalised stress-strain curve in compression

In part I, the uniaxial yield stress  $f_{cy}$  is mobilised with  $H_c$  according to a quadratic function:

$$f_{cy,I} = f_c \left( f_{c0n} + (1 - f_{c0n}) (2H_c - H_c^2) \right) \quad \text{Eq. [296]}$$

where  $f_{c0n}$  is the initial ratio  $f_{cy} / f_c$ . During mobilisation the yield surface  $F_c$  rotates around the anchor point  $\sigma_{rot}$  on the isotropic axis, activating the shear isotropic hardening.

Full mobilisation of  $f_c$  coincides with  $H_c = 1$ , after which (i.e. part II) linear softening takes place, until the failure strength  $f_{cf} = f_{cfn} f_c$  is reached at  $H_{cf} = \varepsilon_{cf}^p / \varepsilon_{cp}^p$ . Strength reduction is assumed to be caused by the destruction of inter-particle bonds, and consequently a parallel shift of the fully mobilised Mohr-Coulomb failure envelope:

## The Concrete model [ADV]

### Strain hardening and softening

$$f_{cy,II} = f_c \left( 1 + (f_{cfn} - 1) \left( \frac{H_c - 1}{H_{cf} - 1} \right) \right) \quad \text{Eq. [297]}$$

where  $\varepsilon_{cf}^p$  is derived from the fracture energy in compression,  $G_c$ , and the characteristic length of the finite element,  $L_{eq}$ , which provides the necessary regularisation to avoid mesh dependent numerical results:

$$\varepsilon_{cf}^p = \varepsilon_{cp}^p - \frac{2G_c}{(1 + f_{cfn}) f_c L_{eq}} \quad \text{Eq. [298]}$$

$L_{eq}$  is calculated by PLAXIS from the size of the finite element,  $A_{el}$ , and the number of stress points per element  $n_{GP}$ , ([Polling, 2000](#) (on page 248)):

$$L_{eq} = 2\sqrt{\frac{A_{el}}{\sqrt{3} n_{GP}}} \quad \text{Eq. [299]}$$

**Note:** When using the **SoilTest** with the Concrete Model, since there is no mesh,  $L_{eq} = 1$ .

In part III the linear strain softening is governed by the condition that the energy in elastic unloading must not be greater than the plastic strain energy absorbed by the crack (no span-back of stress-strain curve on stress point level). That delivers the plastic ultimate strain  $\varepsilon_{cu}^p$  as:

$$\varepsilon_{cu}^p = \varepsilon_{cf}^p - \frac{2f_c (f_{cfn} - f_{cun})}{E} \quad \text{Eq. [300]}$$

with  $f_{cun}$  = residual strength level =  $f_{cu}/f_c$  and  $E$  = elastic Young's modulus. The yield stress  $F_{cy}$  follows as:

$$f_{cy,III} = f_c \left( f_{cfn} + (f_{cun} - f_{cfn}) \left( \frac{H_c - H_{cf}}{H_{cu} - H_{cf}} \right) \right) \quad \text{Eq. [301]}$$

where  $H_{cu} = \varepsilon_{cu}^p / \varepsilon_{cp}^p$ . In part IV, there is no further softening of the stress-strain curve, which yields:

$$f_{cy,IV} = f_c f_{cun} \quad \text{Eq. [302]}$$

To account for the increasing ductility with increasing confining pressure, the total peak strain  $\varepsilon_{cp} = \varepsilon_{cp}^p + \varepsilon_{cp}^e$  increases with the confining pressure,  $\sigma_1$ , as in a triaxial compression test, governed by the input parameter  $a$ :

$$\varepsilon_{cp} = \varepsilon_{cp,UC} \left( 1 + a \frac{\sigma_1}{-f_c} \right) \quad \text{Eq. [303]}$$

For instance,  $a = 1$  and  $\sigma_1 = -f_c$  yield a 100% increase of total peak strain  $\varepsilon_{cp}$  compared to the uniaxial compression test. Internally, the increase of  $\varepsilon_{cp}$  is translated into an increase of  $\varepsilon_{cp}^p$ , which is assumed to be governed by the mean stress  $p = (\sigma_1 + \sigma_2 + \sigma_3) / 3$  according to:

$$\varepsilon_{cp}^p = \varepsilon_{cp,UC}^p \left( 1 + b \frac{p + f_c/3}{-f_c} \right) \quad \text{Eq. [304]}$$

$$b = \frac{2\sin(\varphi_{max}) \frac{f_c}{E} + a(1 - \sin(\varphi_{max})) \left( \varepsilon_{cp}^p - \frac{f_c}{E} \right)}{\varepsilon_{cp}^p (1 - \sin(\varphi_{max})/3)} \quad \text{Eq. [305]}$$

### 14.2.2 Tension

The Concrete model behaviour in tension is linear elastic until the tensile strength  $f_t$  is reached, then softens with a linear strain softening (Figure 64 (on page 154)). The strain softening is governed by the normalised tension softening parameter  $H_t = \varepsilon_1^p / \varepsilon_{tu}^p$  with  $\varepsilon_1^p$  = major principal plastic strain (calculated from  $F_t$ ) and  $\varepsilon_{tu}^p$  = Plastic ultimate strain in uniaxial tension as:

$$f_{ty} = f_t (1 + (f_{tun} - 1) H_t) \quad \text{Eq. [306]}$$

Similar to softening in compression,  $\varepsilon_{tu}^p$  is derived from the fracture energy in tension,  $G_t$ :

$$\varepsilon_{tu}^p = \varepsilon_{tp} + \frac{2G_t}{(1 + f_{tun})f_t L_{eq}} \quad \text{Eq. [307]}$$

where

$$\varepsilon_{tp} = \text{Elastic peak strain in uniaxial extension.}$$

Once the residual strength  $f_{tu} = f_{tun} f_t$  is reached, no further softening takes place.

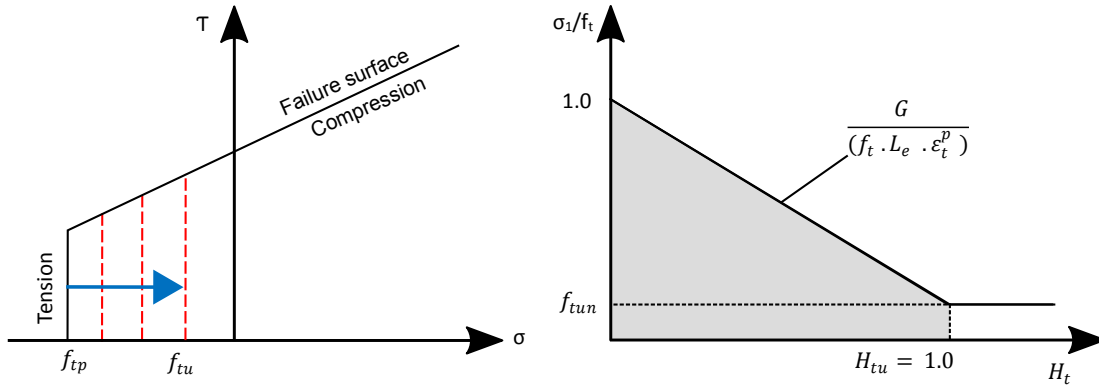


Figure 64: Tension softening

## 14.3 Time-dependency of the Concrete model

### 14.3.1 Strength and Stiffness

The Concrete model takes into account the time-dependent behaviour of material parameters. The stiffness and strength of concrete increase rapidly with time due to the hydration of the cement paste. The increase of Young's

## The Concrete model [ADV]

### Time-dependency of the Concrete model

modulus  $E$  in the model follows an approach similar to the recommendation of [CEB-FIP model code \(1990\)](#) (on page 245):

$$E(t) = E_{28} e^{s_{stiff} (1 - \sqrt{t_{hydr}/t})} \quad \text{Eq. [308]}$$

where

$$\begin{aligned} E_{28} &= \text{Young's modulus of cured concrete.} \\ t_{hydr} &= \text{Time until full curing (e.g. usually taken as 28 days).} \\ t &= \text{time (days).} \\ s_{stiff} &= \text{Parameter governing stiffness evolution with time.} \end{aligned}$$

$s_{stiff}$  is related to the stiffness ratio at 1 day,  $E_1 / E_{28}$ , and  $t_{hydr}$ , as:

$$s_{stiff} = - \frac{\ln(E_1 / E_{28})}{\sqrt{t_{hydr} / t_{1d}} - 1} \quad \text{Eq. [309]}$$

where  $t_{1d}$  is the duration of one day in the unit time. The Young's modulus is constant for  $t < 1h$  and for  $t > t_{hydr}$ .

For the uniaxial compressive strength  $f_c$ , the Concrete model implements two different approaches. The first, as for  $E$ , is similar to the recommendation of CEB-FIP model code (1990) for concrete. The relations are the same as before but exchanging  $s_{stiff}$  with  $s_{strength}$ , which depends now on the strength ratio at 1 day,  $f_{c,1} / f_{c,28}$ , and  $t_{hydr}$  (equations Eq. [310] and Eq. [311]). A lower limit of  $f_c = 0.005 f_{c,28}$  is used at very early age. The CEB-FIP type approach yields very low concrete strength at ages  $< 2h$ .

$$f_c(t) = f_{c,28} e^{s_{strength} (1 - \sqrt{t_{hydr}/t})} \quad \text{Eq. [310]}$$

$$s_{strength} = - \frac{\ln(f_{c,1} / f_{c,28})}{\sqrt{t_{hydr} / t_{1d}} - 1} \quad \text{Eq. [311]}$$

Alternatively, the strength evolution can be modelled in accordance to the shotcrete strength classes J1, J2 and J3 of EN 14497-1, which define ranges of shotcrete strength at different shotcrete ages up to 24h. Mean values of these ranges have been assumed for class J1 and J2 in the Concrete model with class J3 lying 50% above the boundary between classes J2 and J3 ([Table 7](#) (on page 155)). Between 24h and  $t_{hydr}$ , an approach proposed by [Oluokun, Burdette & Deatherage \(1991\)](#) (on page 248) is adopted:

$$f_c = \alpha_c e^{-b_c/t} \quad \text{Eq. [312]}$$

$$\alpha_c = \frac{f_{c,28}}{\ln(\kappa) / (t_{hydr} - t_{1d})} b_c = (-t_{hydr} / (t_{hydr} - t_{1d})) \ln(\kappa) \kappa = f_{c,24h} / f_{c,28} \quad \text{Eq. [313]}$$

where  $f_c$  is the time-dependent compressive strength and  $f_{c,24h}$  is the compressive strength at 24h ([Table 7](#) (on page 155)).

**Table 7: Mean uniaxial compressive strength of J1, J2 and J3 strength classes**

Time[hr]	J1[MPa]	J2[MPa]	J3[MPa]
<0.1	0.15	0.35	0.75
0.5	0.23	0.715	1.65
12	2.0	5.5	12.0

## The Concrete model [ADV]

Time-dependency of the Concrete model

Time[hr]	J1[MPa]	J2[MPa]	J3[MPa]
24	3.5	12.0	28.5

The ratio of  $f_t/f_c$  and the values of  $f_{cf}$ ,  $f_{cun}$  and  $f_{tun}$  are assumed to be constant in curing for both approaches.

### 14.3.2 Plastic Deformability

The ability of young concrete to withstand large deformations is not only a result of its low elastic modulus at this age, but also due to its high plastic ductility. With concrete aging this ductile behaviour decreases.

In the Concrete model this behaviour is represented by a time-dependent plastic peak strain  $\varepsilon_{cp}^p$ . Similar to the approach proposed by [Meschke, Kropik & Mang \(1996\)](#) (on page 248), a tri-linear function in time is adopted. Input values are the plastic peak strains at  $t = 1$ h, 8h and 24h. Beyond 24h,  $\varepsilon_{cp}^p$  is assumed to be constant ([Figure 65](#) (on page 156)).

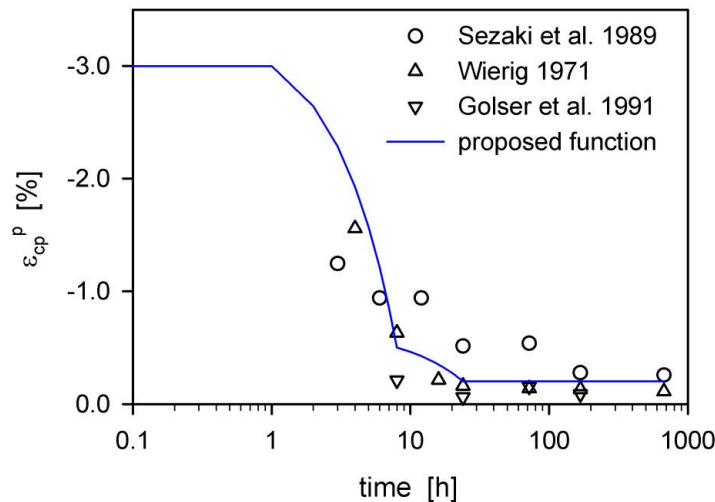


Figure 65: Reduction of  $\varepsilon_{cp}^p$  with aging in the Concrete model compared to experimental data from uniaxial compression tests. The chosen  $\varepsilon_{cp}^p$  values are -3%, -0.5% and -0.2%.

### 14.3.3 Fracture energy

The plastic time-dependency during softening is taken into account with the change of fracture energies with time, which is automatically computed by PLAXIS. In tension, the tensile failure strain  $\varepsilon_{tu}^p$  is derived from the tensile fracture energy and tensile strength of the cured concrete, regardless of the current concrete age. Since the tensile strength  $f_t$  increases with time, but  $\varepsilon_{tu}^p$  remains constant, the current fracture  $G_t$  increases proportionally with the increase of  $f_t$ .

The plastic failure strain in compression,  $\varepsilon_{cf}^p$ , is coupled to the plastic peak strain  $\varepsilon_{cp}^p$  such that the ratio  $\varepsilon_{cf}^p/\varepsilon_{cp}^p$  remains constant. As  $\varepsilon_{cp}^p$  decreases with time ([Figure 65](#) (on page 156)),  $\varepsilon_{cf}^p$  and hence  $G_c$  reduce. On the

## The Concrete model [ADV]

### Time-dependency of the Concrete model

other hand, the compressive strength  $f_c$  increases with time, which results in higher values of  $G_c$ . The influence of these counteracting trends brings high values of the fracture energy at early age, a sharp drop at  $\approx 12$ h and a linear increase of  $G_c$  with  $f_c$  afterward (Figure 66 (on page 157)). The high fracture energy at very early age is a consequence of the desired ductile behaviour at this stage. As very young concrete effectively does not fail at all in compression, the fracture energy theoretically should be infinite.

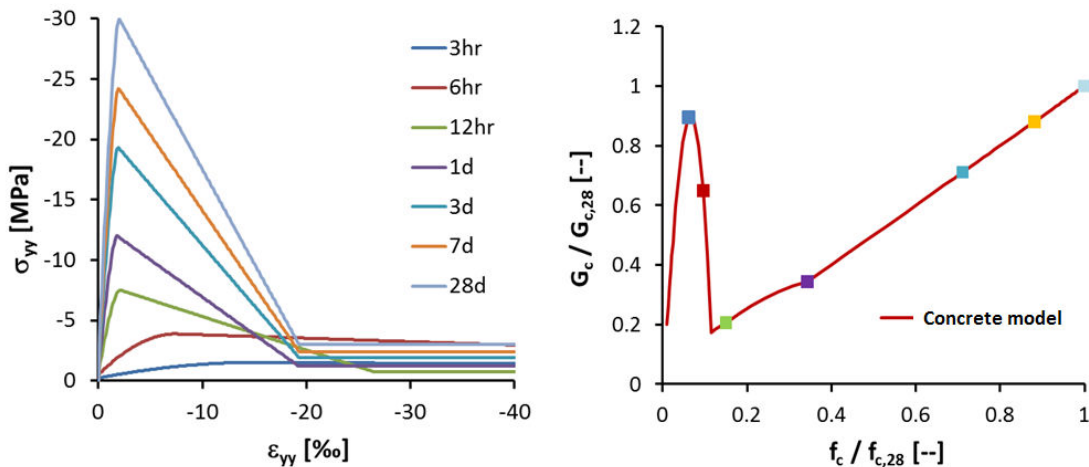


Figure 66: Stress-strain curves in uniaxial compression at different ages and development of compressive fracture energy with compressive strength

### 14.3.4 Viscoelastic Creep

The Concrete model employs a viscoelastic approach for creep. Creep strains,  $\epsilon^{cr}$ , increase linearly with stress  $\sigma$  and are related to elastic strains via the creep factor  $\varphi^{cr}$ :

$$\epsilon^{cr}(t) = \frac{\varphi^{cr}}{\mathbf{D}^e} \frac{t - t_0}{t + t_{50}^{cr}} \quad Eq. [314]$$

The evolution of creep with time  $t$  is governed by the start of loading at time  $t_0$  and the parameter  $t_{50}^{cr}$ . For instantaneous loading ( $t_0 = 0$ ),  $t_{50}^{cr}$  equals the time until 50% of the creep strains have evolved. For concrete utilization higher than 45% of  $f_c$ , non-linear creep effects are accounted for by replacing  $\varphi^{cr}$  with the following equation from Eurocode 2:

$$\varphi_k^{cr} = \varphi^{cr} e^{1.5(k_\sigma - 0.45)} \quad Eq. [315]$$

with  $k_\sigma = \sigma_c / f_{cm}$  being the degree of concrete utilisation in compression. Due to the time-dependency of the linear elastic stiffness matrix  $\mathbf{D}^e$ , the creep history is stored as normalised values of  $\epsilon^{cr}(t) \cdot E(t)$ .

#### Note:

The creep history is adjusted for the stress state at first activation of the concrete cluster, such that no creep strains are produced by initial stresses. The state variables are taken over if the previous material was also defined with the Concrete model, in which case creep will also continue. If a reset of state variables is desired, a nil step with a different material (e.g. linear elastic) is required.

## The Concrete model [ADV]

### Parameters of the Concrete model

#### 14.3.5 Shrinkage

The Concrete model refers to shrinkage as the isotropic loss of volume with time, which is independent of the stress state. Shrinkage strains  $\varepsilon^{shr}$  are calculated according to the recommendation of [ACI \(1992\)](#) (on page 245) as:

$$\varepsilon^{shr}(t) = \varepsilon_{\infty}^{shr} \frac{t}{t + t_{50}^{shr}} \quad Eq. [316]$$

with  $\varepsilon_{\infty}^{shr}$  being the final axial shrinkage strain and  $t_{50}^{shr}$  the time when 50% of shrinkage has occurred.

#### 14.4 Parameters of the Concrete model

The Concrete model involves a number of parameters which are generally familiar to structural engineers. These parameters with their standard units are listed below.

- Parameters for stiffness:

$E_{28}$	Young's modulus of cured concrete at $t_{hydr}$	[kN/m <sup>2</sup> ]
$\nu$	Poisson's ratio	[-]

- Parameters for strength:

<i>Compression parameters</i>		
$f_{c,28}$	Uniaxial compressive strength of cured concrete at $t_{hydr}$	[kN/m <sup>2</sup> ]
$f_{c0n}$	Normalised failure strength	[-]
$f_{cfn}$	Normalised initially mobilised strength	[-]
$f_{cun}$	Normalised residual strength	[-]
$G_{c,28}$	Compressive fracture energy of cured concrete at $t_{hydr}$	[kN/m]
$\varphi_{max}$	Maximum friction angle	[°]
$\psi$	Dilatancy angle	[°]

## The Concrete model [ADV]

### Parameters of the Concrete model

$\gamma_{fc}$	Safety factor for compressive strength	[-]
---------------	--	-----

#### *Tension parameters*

$f_{t,28}$	Uniaxial tensile strength of cured concrete at $t_{hydr}$	[kN/m <sup>2</sup> ]
$f_{tun}$	Ratio of residual vs. peak tensile strength	[-]
$G_{t,28}$	Tensile fracture energy of cured concrete at $t_{hydr}$	[kN/m]
$\gamma_{ft}$	Safety factor for tensile strength	[-]

- Parameters for ductility:*

$\varepsilon_{cp}^p$	Uniaxial plastic failure strain	[-]
$a$	Increase $\varepsilon_{cp}$ with increase of p	[-]

- Time-dependent parameters:*

$t_{hydr}$	Time for full hydration	[day]
------------	-------------------------	-------

#### *Stiffness parameters*

$E_1 / E_{28}$	Time-dependency ratio of elastic stiffness	[-]
----------------	--	-----

#### *Strength parameters*

$f_{c,1} / f_{c,28}$	Time-dependency of compressive strength	[-]
----------------------	---	-----

#### *Ductility*

$\varepsilon_{cp,1h}^p$	Uniaxial plastic failure strain at 1h (negative value)	[-]
$\varepsilon_{cp,8h}^p$	Uniaxial plastic failure strain at 8h (negative value)	[-]
$\varepsilon_{cp,24h}^p$	Uniaxial plastic failure strain at 24h (negative value)	[-]

#### *Shrinkage*

$\varepsilon_{\infty}^{shr}$	Final shrinkage strain (negative value)	[-]
$t_{50}^{shr}$	Time for 50% of shrinkage strains	[day]

#### *Creep*

$\phi^{cr}$	Ratio between creep and elastic strains	[-]
$t_{50}^{cr}$	Time for 50% of creep strains	[day]

## The Concrete model [ADV]

### Parameters of the Concrete model

---

The Concrete model allows two drainage types: non-porous, which is the general approach for concrete structural elements, and drained, in case of semi-permeable walls or tunnel linings.

#### 14.4.1 Recommended values for the parameters of the Concrete model

##### *Elastic parameters*

Differently from the Mohr-Coulomb model, the Concrete model employs time-dependent stiffness. If *Time dependent strength and stiffness* is turned off then the editing of  $E_1 / E_{28}$  is disabled and it's set to 1. If *Time dependent strength and stiffness* is turned on, a  $E_1 / E_{28}$  is defined, generally a range of 0.5 - 0.7 is recommended with  $E_{28}$  between 25 GPa and 30 GPa.

##### *Strength in compression*

The uniaxial compressive strength of cured concrete  $f_{c,28}$  can be derived from uniaxial compressive test results. The time-dependency of compressive strength expressed as  $f_{c,1} / f_{c,28}$  is recommended in the range of 0.2-0.3 for cast concrete, whilst it depends on the strength class (i.e. J1, J2 and J3) for shotcrete. The stress-strain curve in compression ([Figure 63](#) (on page 152)) is defined through the normalised strength values. The normalised mobilised strength  $f_{con}$  contributes to the part I hardening, a value in the range of 0.1 - 0.25 is recommended. The normalised failure strength  $f_{cfn}$  rules the part II softening, a value of 0.1 is recommended. The normalised residual strength  $f_{cun}$  rules the part III softening and the residual strength, a value of 0.1 is recommended.  $f_{cfn}$  must be greater or almost equal to  $f_{cun}$  in order to avoid input error.  $f_{cfn}$  or  $f_{cun} = 1$  implies no softening in the respective regions.

##### *Time-dependency of compressive strength*

The uniaxial compressive strength is defined at the time  $t_{hydr}$ , time for full hydration (usually 28 days). If *Time dependent strength and stiffness* is turned off then  $f_{c,1} / f_{c,28}$  is set automatically equal to 1 and the editing is disabled. If *Time dependent behaviour* is turned on, then the user can choose in the combo box *Strength functions* among:

- *CEB-FIP model code (1990)*: the user can define  $f_{c,1} / f_{c,28}$ . The default value = 1 corresponds to no time-dependency. For cast concrete a value of [0.2, 0.3] is recommended.
- *Shotcrete strength class J1*:  $f_{c,1} / f_{c,28}$  is automatically computed in accordance with the selected strength class ([Table 7](#) (on page 155)).
- *Shotcrete strength class J3*:  $f_{c,1} / f_{c,28}$  is automatically computed in accordance with the selected strength class ([Table 7](#) (on page 155)).

##### *Strength in tension*

The tensile strength  $f_{t,28}$  can in principle be derived from uniaxial tensile test results. Due to the experimental difficulties involved in these tests, however, indirect tests or direct correlations with the compressive strength are more common. Both for concrete and shotcrete, a value of  $f_{t,28} = 0.1 f_c$  is recommended. The ratio of residual vs. peak tensile strength  $f_{tun}$  is recommended to be 0.

##### **Note:**

In shotcrete linings the tensile strength is essential for tunnel stability. Neglecting or considering low values of it could result in unrealistic failure.

## The Concrete model [ADV]

### Parameters of the Concrete model

#### Parameters $\varphi_{max}$ , $\psi$ and $a$

Determination of  $\varphi_{max}$ ,  $\psi$  and  $a$  requires triaxial tests on cured concrete. The impact of these parameters in typical tunnelling calculations, however, is small, as at least one of the major principal stresses in the lining is close to 0. Furthermore, not all of these will be typically available, so values in the range of 35°- 43°, 0°- 10° and 16 - 20 are respectively suggested for  $\varphi_{max}$ ,  $\psi$  and  $a$ .

#### Fracture energy

The compressive fracture energy of cured concrete  $G_{c,28}$  can be estimated from the stress-strain curve of uniaxial compression tests. However a value in the range of 30kN/m - 70kN/m is recommended. The tensile fracture energy of cured concrete  $G_{t,28}$  can be estimated from the stress-strain curve of uniaxial tensile tests. Due to the experimental difficulties involved in these tests, the fracture energy can be estimated as following. For plain shotcrete, a value in the range of 0.05kN/m - 0.15kN/m is recommended. However, the shotcrete can be reinforced using steel fibres, in this case  $G_{t,28}$  can be estimated with the correlation proposed by [Barros & Figueiras \(1999\)](#) (on page 245):

$$G_{t,28} = (1 + 13.159W_f^{1.827})G_{t0} \quad \text{Eq. [317]}$$

where

$$\begin{aligned} G_{t0} &= \text{The fracture energy of plain shotcrete} \\ W_t &= \text{fibre percentage in weigh [kg/m}^3\text{]} \end{aligned}$$

For plain concrete, the value is strictly dependent on the strength class and the maximum aggregate size  $d_{max}$  ([Table 8](#) (on page 161), [CEB-FIP model code \(1990\)](#) (on page 245)).

**Table 8: Fracture energy  $G_{t,28}$  for plain concrete**

$d_{max}(mm)$	$G_{t,28} (N/m)$							
	C12	C20	C30	C40	C50	C60	C70	C80
8	26.91	34.06	42.18	49.67	56.71	63.39	69.78	75.93
16	32.30	40.87	50.61	59.61	68.05	76.07	83.73	91.11
32	62.44	79.02	97.86	115.24	131.56	147.06	161.88	176.15

#### Ductility

If *Time dependent behaviour* is turned off then a single peak parameter  $\varepsilon_{cp}^p$  is available instead of  $\varepsilon_{cp1,h}^p$ ,  $\varepsilon_{cp8,h}^p$  and  $\varepsilon_{cp24,h}^p$  and no-dependency of ductility in time is considered. If *Time dependent behaviour* is turned on, then the user can define  $\varepsilon_{cp,1h}^p$ ,  $\varepsilon_{cp,8h}^p$  and  $\varepsilon_{cp,24h}^p$ . Values in the range of -0.03 - -0.01, -0.0015 - -0.001 and -0.0012 - -0.0007 are respectively suggested for  $\varepsilon_{cp,1h}^p$ ,  $\varepsilon_{cp,8h}^p$  and  $\varepsilon_{cp,24h}^p$ .

#### Creep

Creep properties of concrete can be derived from uniaxial multistage creep tests. Deriving creep properties from such a test requires additional information about strength, stiffness and ductility development with time. The user can follow the recommendation of Eurocode 2 for cast concrete, instead values in the range of 2 - 3 for  $\varphi^{cr}$  are suggested for shotcrete tunnel linings.  $t_{50}^{cr}$  is recommended in a range of 1d - 5d. If *Creep behaviour* is

## The Concrete model [ADV]

### Parameters of the Concrete model

inactive,  $\varphi^{cr}$  and  $t^{cr}_{50}$  are disabled for editing and both set to 0. If *Creep behaviour* is active, the parameters can be defined.

### Shrinkage

Concrete shrinkage is strongly influenced by environmental conditions and water-cement-ratio, such that low air humidity and high water-cement ratios amplify it. Due to less aggregate content and higher water-cement ratio, shrinkage of shotcrete is more pronounced than for conventional cast concrete ([Austin & Robins, 1995](#) (on page 245)). If *Shrinkage behaviour* is inactive,  $\varepsilon^{shr}_{\infty}$  and  $t^{shr}_{50}$  are disabled. If *Shrinkage behaviour* is active, the user can set the parameters.

Eurocode 2 recommends final shrinkage strains,  $\varepsilon^{shr}_{\infty}$ , for cast concrete of -0.0002 to -0.0006 depending on air humidity, concrete class and the effective size of the structural element. For tunnel linings values in the range of -0.0015 - -0.0005 for  $\varepsilon^{shr}_{\infty}$  and of 28d - 100d for  $t^{shr}_{50}$  are suggested.

### Safety factors

To facilitate calculations based on design values of concrete strength, the Concrete model implements the possibility to use separate safety factors  $\gamma_{fc}$  and  $\gamma_{ft}$  for compressive and tensile strength. In fact PLAXIS design approach is not advisable for these two parameters, because:

- In case the user defines the time-dependency of strength through the classes J1, J2 and J3, the shotcrete strength values at 0.5h, 12h and 24h are not related to  $f_{c,28}$ . Using a lower value of  $f_{c,28}$  therefore does not affect the shotcrete strength at early age, if the early strength classes are used.
- If lower concrete strength is used due to safety considerations, also the fracture energy should be reduced to obtain similar stress-strain curves.
- The creep factor increases for concrete utilisation  $>0.45 f_c$ . Using design values for  $f_c$  would therefore overestimate creep effects.

For these reasons input safety factors  $\gamma_{fc}$  and  $\gamma_{ft}$  have been introduced. The characteristic, time-dependent compressive and tensile strengths  $f_c$  and  $f_t$  as well as the corresponding fracture energies  $G_c$  and  $G_b$ , are divided by  $\gamma_{fc}$  and  $\gamma_{ft}$  in each calculation step, but concrete utilization always refers to the characteristic values of  $f_c$  and  $f_t$ .

## 14.4.2 Summary of recommended parameters for Concrete model

[Table 9](#) (on page 162) groups the Concrete model parameters as a function of the material properties and the time dependency.

**Table 9: Recommended parameters and values for the Concrete model**

Parameter	Recommended values	Unit
<b>1. Stiffness parameters (non-time dependent)</b>		
$E_{28}$	[25, 30]	[GPa]
$\nu$	[0.15, 0.25]	[-]
<b>2. Strength parameters</b>		

## The Concrete model [ADV]

Parameters of the Concrete model

Parameter	Recommended values	Unit
<i>a) Strength in compression</i>		
$f_{c,28}$	Depending on strength class	[kN/m <sup>2</sup> ]
$f_{c0n}$	[0.10, 0.25]	[-]
$f_{cfn}$	[0.1]	[-]
$f_{cun}$	[0.1]	[-]
$G_{c,28}$	[30, 70]	[kN/m]
$\varphi_{max}$	[35, 43]	[°]
$\psi$	[0, 10]	[°]
$\gamma_{fc}$	Safety factor depending on design standard	[-]
<i>b) Strength in tension</i>		
$f_{t,28}$	Depending on strength class	[kN/m <sup>2</sup> ]
$f_{tun}$	[0]	-
$G_{t,28}$	[0.05, 0.15] plain shotcrete, <a href="#">[Table 8</a> (on page 161)] cast concrete	[kN/m]
$\gamma_{ft}$	Safety factor depending on design standard	[-]
<i>c) Ductility</i>		
$\varepsilon_{cp}^p$		[-]
$a$	[16, 20]	[-]
<b>3. Time dependent parameters</b>		
$t_{hydr}$	[28]	[day]
<i>a) Stiffness</i>		
$E_1 / E_{28}$	[0.5, 0.7]	[-]
<i>b) Strength</i>		
$f_{c,1} / f_{c,28}$	[J1, J2, J3] shotcrete, [0.2, 0.3] cast concrete	[-]

## The Concrete model [ADV]

State parameters in the Concrete model

Parameter	Recommended values	Unit
<i>c) Ductility</i>		
$\varepsilon_{cp,1h}^p$	[-0.01, -0.03]	[-]
$\varepsilon_{cp,8h}^p$	[-0.001, -0.0015]	[-]
$\varepsilon_{cp,24h}^p$	[-0.0007, -0.0012]	[-]
$a$	[16, 20]	[-]
<i>d) Shrinkage</i>		
$\varepsilon_{\infty}^{shr}$	[-0.0005, -0.0015] shotcrete tunnel lining, [-0.0002, -0.0006] cast concrete	[-]
$t_{50}^{shr}$	[28, 100]	[day]
<i>e) Creep</i>		
$\varphi^{cr}$	[2, 3] shotcrete tunnel lining, [Eurocode 2] cast concrete	[°]
$t_{50}^{cr}$	[1, 5]	[day]

## 14.5 State parameters in the Concrete model

In addition to the output of standard stress and strain, the Concrete model provides an output on state variables such as the current elastic modulus  $E(t)$  and the current compressive yield stress  $f_{cy}$ . These parameters can be visualised by selecting the **State parameters** option from the **Stresses** menu. An overview of available state parameters is given below:

$\Delta t$	Age of concrete	day
$E$	Average Young's modulus in current step	[kN/m <sup>2</sup> ]
$f_c$	Uniaxial compressive strength at the end of the current step	[kN/m <sup>2</sup> ]
$f_{cy}$	Current compressive yield stress	[kN/m <sup>2</sup> ]
$H_c$	Normalised compressive strain hardening parameter	[-]
$H_t$	Normalised tensile strain hardening parameter	[-]
$UtilFC$	Concrete utilisation factor in compression	[-]

## The Concrete model [ADV]

On the use of the Concrete model in dynamics calculations

$UtilFT$	Concrete utilisation factor in tension	[-]
$\varepsilon_{xx}^{cr} \cdot E(t)$	Normalised creep history strain in xx direction	[-]
$\varepsilon_{yy}^{cr} \cdot E(t)$	Normalised creep history strain in yy direction	[-]
$\varepsilon_{zz}^{cr} \cdot E(t)$	Normalised creep history strain in zz direction	[-]
$\varepsilon_{xy}^{cr} \cdot E(t)$	Normalised creep history strain in xy direction	[-]
$\varepsilon_{yz}^{cr} \cdot E(t)$	Normalised creep history strain in yz direction	[-]
$\varepsilon_{xz}^{cr} \cdot E(t)$	Normalised creep history strain in xz direction	[-]

Some parameters are further explained in the following two sections:

### 14.5.1 Concrete utilisation factor in compression $UtilFC$

The concrete utilisation factor in compression  $UtilFC$  is defined as:

$$UtilFC = \sigma_{rot} \left( \frac{\sigma_3 - \sigma_1}{\sigma_1 - \sigma_{rot}} \right) \bigg| (Y_{fc} f_c) \quad (Hardening) \quad Eq. [318]$$

$$UtilFC = \sigma_{rot} \left( \frac{\sigma_3 - \sigma_1}{\sigma_1 - \sigma_{rot}} \right) \bigg| (Y_{fc} f_{cy}) \quad (Softening) \quad Eq. [319]$$

The utilisation factor is constant in hardening and is related to the maximum uniaxial compressive strength at the end of the current step  $f_c$ . After the peak value is reached and the softening is taking place, the utilisation factor is related to the current compressive yield stress  $f_{cy}$  and follows the stress-strain curve in softening ([Figure 63](#) (on page 152)).

### 14.5.2 Concrete utilisation factor in tension $UtilFT$

The concrete utilisation factor in tension  $UtilFT$  is defined as:

$$UtilFT = \frac{\sigma_1}{f_t Y_{ft}} \quad (Softening) \quad Eq. [320]$$

The utilisation factor is constant during the linear softening in tension and is related to the maximum uniaxial tensile strength at the end of the current step  $f_t$ . When the residual value is reached, then  $f_t = f_{tun}$ .

## 14.6 On the use of the Concrete model in dynamics calculations

Generally the time steps and the time interval for the usual dynamics calculations are in the range of seconds. However, the time scale in concrete hardening is in the range of hours to days. For this reason, in dynamics analysis, the use of the Concrete model with time-dependency of the parameters is not recommended unless the concrete elements are not totally cured in the previous construction stages. Otherwise, in dynamics analysis the

## The Concrete model [ADV]

### Warning

---

***Time dependent strength and stiffness***, the ***Creep behaviour*** and the ***Shrinkage behaviour*** should be disabled, nevertheless the Concrete model continues to take into account the stress-strain hardening and softening.

## 14.7 Warning

The problems involving tension softening with low fracture energy could affect the convergence of the FE-calculation, even though the model itself can never fail physically. The crack initiation massively increases the global error, even though the step size is gradually reduced by the global iteration procedure.

A structure made of strain softening material behaves in a brittle or ductile manner, not only depending on the material behaviour formulated at stress point level, but also on the size of the structure, with the response becoming ever more brittle the larger the structure is. This is due to the increase of energy released by the unloading part of the structure compared to the fracture energy dissipated in the crack. If the energy in unloading is larger than the fracture energy of the crack, both forces and displacements need to decrease in order to reach equilibrium.

However, in tunnelling the shotcrete never involves failure with low fracture energy. The problem could occur in other applications regarding rigid inclusions in the ground.

## The UBC3D-PLM model [ULT]

During an earthquake, the seismic waves propagate from the source till the ground surface, causing ground shaking. The soil deposit acts as a filter causing the variation of the seismic waves in terms of amplitude, duration and frequency content at any depth of the soil deposit. The effects of an earthquake can be different, such as structural damages, landslides and soil liquefaction.

The term liquefaction is used to describe a variety of phenomena that occurs in saturated cohesionless soils under undrained conditions. Under static and cyclic loading, dry cohesionless soils tend to densify. If these soils are saturated and the applied load acts in a short time, as in the case of an earthquake, the tendency to densify causes an increase in excess pore pressures that cannot rapidly be dissipated and consequently a decrease in the effective stresses occurs. When this happens, the soil behaves as a fluid.

This phenomenon can be explained considering that the shear resistance  $\tau$  for cohesionless soils is given by Coulomb's formula:

$$\tau = \sigma'_{vo} \tan(\varphi) \quad \text{Eq. [321]}$$

where

$$\begin{aligned} \sigma'_{vo} &= \text{The initial effective stress} \\ \varphi &= \text{The friction angle.} \end{aligned}$$

According to Terzaghi's formula, the effective stress is given by:

$$\sigma'_{vo} = \sigma_{vo} - p_w \quad \text{Eq. [322]}$$

where

$$\begin{aligned} \sigma_{vo} &= \text{The total vertical stress.} \\ p_w &= \text{The pore pressure.} \end{aligned}$$

When the excess pore pressures  $\Delta p_w$  develop during an earthquake, the equation can be written as:

$$\sigma'_{vo} = \sigma_{vo} - (p_w + \Delta p_w) \quad \text{Eq. [323]}$$

which means that the effective stress state tends to decrease and, when it reaches zero, also the shear resistance is null.

In order to evaluate the potential liquefaction hazard of a site, it is necessary to identify the predisposing and triggering factors for liquefaction. The predisposing factors are the characteristics of the soil deposit such as particle size and shape, gradation and plasticity characteristics. The triggering factors depend on the earthquake magnitude, duration and peak ground acceleration. To establish if liquefaction can occur in a specific site subjected to a selected earthquake semi-empirical procedures or nonlinear dynamic analyses can be used.

The UBC3D-PLM model<sup>2</sup> is an effective stress elasto-plastic model which is capable of simulating the liquefaction behaviour of sands and silty sands under seismic loading ([Tsegaye \(2010\)](#) (on page 249), [Petalas & Galavi](#)

<sup>2</sup> PLM = PLAXIS Liquefaction Model

## The UBC3D-PLM model [ULT]

### Elasto-plastic behaviour and hardening rule

(2012) (on page 248)). The UBC3D-PLM model formulation is based on the original UBCSAND (University of British Columbia Sand) model introduced by [Puebla, Byrne & Phillips \(1997\)](#) (on page 248) and [Beatty & Byrne \(1988\)](#) (on page 245). The original UBCSAND is a 2D model formulated in the classical plasticity theory with a hyperbolic strain hardening rule, based on the original Duncan-Chang model. The hardening rule relates the mobilised friction angle to the plastic shear strain at a given stress. The UBCSAND model contains a 2D Mohr-Coulomb yield surface and a corresponding non-associated plastic potential function. The flow rule in the model is based on the stress-dilatancy theory developed by [Rowe \(1962\)](#) (on page 248), linearised and simplified according to energy considerations.

The main difference between the UBCSAND model and the UBC3D-PLM model is the generalized 3D formulation of the latter. The UBC3D-PLM model uses the Mohr-Coulomb yield condition in a 3D principal stress space for primary loading, and a yield surface with a simplified kinematic hardening rule for secondary loading. Moreover, a modified non-associated plastic potential function based on Drucker-Prager's criterion is used for the primary yield surface, in order to maintain the assumption of stress-strain coaxiality in the deviatoric plane for a stress path beginning from the isotropic line [Tsegaye \(2010\)](#) (on page 249).

The assessment of the liquefaction potential of a soil deposit can be done by performing a dynamic site response analysis. Generally the following steps are needed to perform such an analysis ([Laera & Brinkgreve, 2015](#) (on page 247)):

- Definition of the geotechnical model of the soil deposit, in terms of soil layer distribution, water table depth, appropriate dynamic boundary conditions and soil mechanical properties to describe its behaviour under static and cyclic loading.
- Definition of the seismic input motion, according to the specific site and the probabilistic study as reported in the current regulations (i.e. Eurocode 8, NTC 2008, etc.).
- Definition of the numerical model to perform the analysis including the appropriate dynamic boundary conditions.

A site response analysis requires a deep and extended investigation of the soil deposit to identify the soil layer distribution and hydraulic conditions as well as the mechanical properties of the soil. When possible, the investigation should be extended until the depth of a rock or rock-like formation. In situ and laboratory tests should be performed to evaluate index properties, stiffness and strength of the soil layers with regard to their behaviour under cyclic loading (Cross-hole and Down-hole in situ tests, among others, and cyclic triaxial, cyclic direct simple shear and resonant column laboratory tests). However, in many cases only data from drained triaxial tests (CD TxC) or in situ tests like SPT or CPT are available. For this reason the UBC3D-PLM model implements a specific formulation with input parameters based on these tests.

Main characteristics of the UBC3D-PLM model and the corresponding input parameters are given below:

- Stress dependent stiffness according to a power law  $k_B^{*e}, k_G^{*e}, m_e, n_e, n_p$ .
- Plastic straining due to primary deviatoric loading  $k_G^{*p}$ .
- Densification due to the number of cycles during secondary loading  $f_{dens}$ .
- Post-liquefaction stiffness degradation  $f_{Epost}$ .
- Failure according to the Mohr-Coulomb failure criterion  $\phi_{cv}, \phi_p$  and  $c$ .

## 15.1 Elasto-plastic behaviour and hardening rule

The UBC3D-PLM model incorporates a non-linear, isotropic law for the elastic behaviour that is defined in terms of the elastic bulk modulus  $K$  and the elastic shear modulus  $G$ , which are defined by the following equations:

## The UBC3D-PLM model [ULT]

Elasto-plastic behaviour and hardening rule

$$K = k_B^{*e} p_{ref} \left( \frac{p'}{p_{ref}} \right)^{me} \quad Eq. [324]$$

$$G = k_G^{*e} p_{ref} \left( \frac{p'}{p_{ref}} \right)^{ne} \quad Eq. [325]$$

where

$k_B^{*e}$	=	Bulk modulus factor.
$k_G^{*e}$	=	Shear modulus factor.
$p_{ref}$	=	Reference pressure
Factors $me$ and $ne$	=	parameters that define the rate of stress dependency of stiffness

Pure elastic behaviour with  $G_{max}$  is predicted by the model during the unloading process. Once the stress state reaches the yield surface, plastic behaviour is taken into account as long as the stress point is not going immediately back into the elastic zone.

**Note:** The implicit Poisson's ratio calculated from elastic bulk and shear modulus from Eq. [324] and Eq. [325] is suitable for dynamics calculation, but using it for gravity loading may give improper initial stress state. Therefore, the user is advised to use another material for the stress initialization.

The first yield surface is defined from a set of Mohr-Coulomb functions. The position and size of the yield surface is defined based on the hardening law. More specifically, plastic hardening based on the principle of strain hardening is used in the model (similar to the Hardening Soil model). The hardening rule governs the amount of plastic strain as a result of mobilisation of the shear strength ( $\sin \phi_{mob}$ ). The mobilised friction angle derived from the Mohr-Coulomb yield criterion, is given as:

$$\sin(\phi_{mob}) = \frac{\sigma'_1 - \sigma'_3}{\sigma'_1 + \sigma'_3 - 2c \cot(\phi_p)} \quad Eq. [326]$$

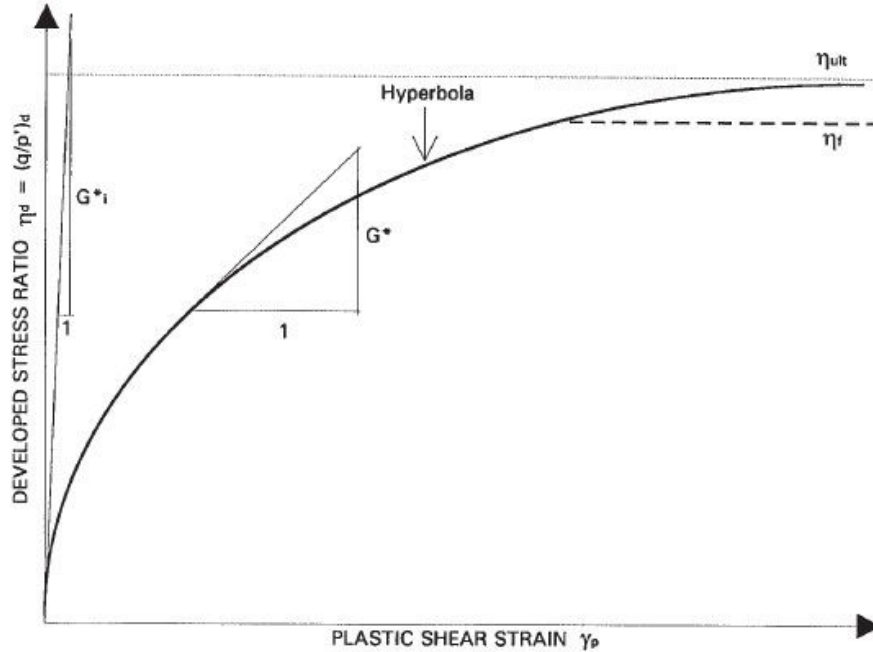


Figure 67: The original UBCSAND hardening rule

## The UBC3D-PLM model [ULT]

### Flow rule

The hyperbolic hardening rule (Beatty & Byrne, 1988 (on page 245)) is presented schematically in Figure 67 (on page 169). It relates the increment of the sine of the mobilised friction angle (calculated according to Eq. [326]) to the plastic shear strain increment as follows (Puebla, Byrne & Phillips, 19997 (on page 248)):

$$d\gamma_p = \left(\frac{1}{G^*}\right) d\sin(\varphi_{mob}) \quad Eq. [327]$$

$$G^* = k_G^{*p} \left(\frac{p'}{p_{ref}}\right)^{np} \left(1 - \left(\frac{\sin(\varphi_{mob}')}{\sin(\varphi_p)}\right) R_f\right)^2 \quad Eq. [328]$$

where  $k_G^{*p}$  is the plastic shear modulus factor;  $np$  is the plastic shear modulus exponent;  $\varphi_{mob}$  is the mobilised friction angle, which is defined by the stress ratio;  $\varphi_p$  is the peak friction angle; and  $R_f$  is the failure ratio  $\eta_f / \eta_{ult}$  ranging from 0.5 to 1.0, where  $\eta_f$  is the stress ratio at failure and  $\eta_{ult}$  is the asymptotic stress ratio from the best fit hyperbola. The hardening rule as reformulated by Tsegaye (2010) (on page 249) in UBC3D-PLM model is given as:

$$d\sin(\varphi_{mob}) = 1.5 k_G^{*p} \left(\frac{p'}{p_{ref}}\right)^{np} \frac{p_{ref}}{p'} \left(1 - \left(\frac{\sin(\varphi_{mob}')}{\sin(\varphi_p)}\right) R_f\right)^2 d\lambda \quad Eq. [329]$$

where  $d\lambda$  is the plastic strain increment multiplier.

## 15.2 Flow rule

The plastic potential function specifies the direction of the plastic strain. A non-associated flow rule based on the Drucker-Prager plastic potential function is used in the UBC3D-PLM model (Tsegaye, 2010 (on page 249)). The plastic potential function  $g$  is formulated as:

$$g = q - M(p' + c \cot(\varphi_p)) \quad Eq. [330]$$

$$M = \frac{6 \sin(\psi_M)}{3 - \sin(\psi_M)} \quad Eq. [331]$$

where the Drucker-Prager surface is fixed in the compression point.

In the UBC3D-PLM model the flow rule of the original UBSCAND model is used, which is derived from energy considerations by Puebla, Byrne & Phillips (1997) (on page 248). Similar to the Hardening Soil model it is based on three observations (Figure 68 (on page 171)):

- There is a unique stress ratio, defined by the constant volume friction angle  $\varphi_{cv}$ , for which plastic shear strains do not cause plastic volumetric strains.
- Stress ratios which lie below  $\sin \varphi_{cv}$  exhibit contractive behaviour, while stress ratios above  $\sin \varphi_{cv}$  lead to a dilative response. This means that the constant volume friction angle works as the phase transformation angle.
- The amount of contraction or dilatancy depends on the difference between the current stress ratio and the stress ratio at  $\sin \varphi_{cv}$ .

The increment of plastic volumetric strain  $d\varepsilon_v^p$  is calculated as follows:

$$d\varepsilon_v^p = \sin(\psi_m) d\gamma^p \quad Eq. [332]$$

$$\sin(\psi_m) = \sin(\varphi_m) - \sin(\varphi_{cv}) \quad Eq. [333]$$

where,  $\varphi_{cv}$  is the constant volume friction angle.

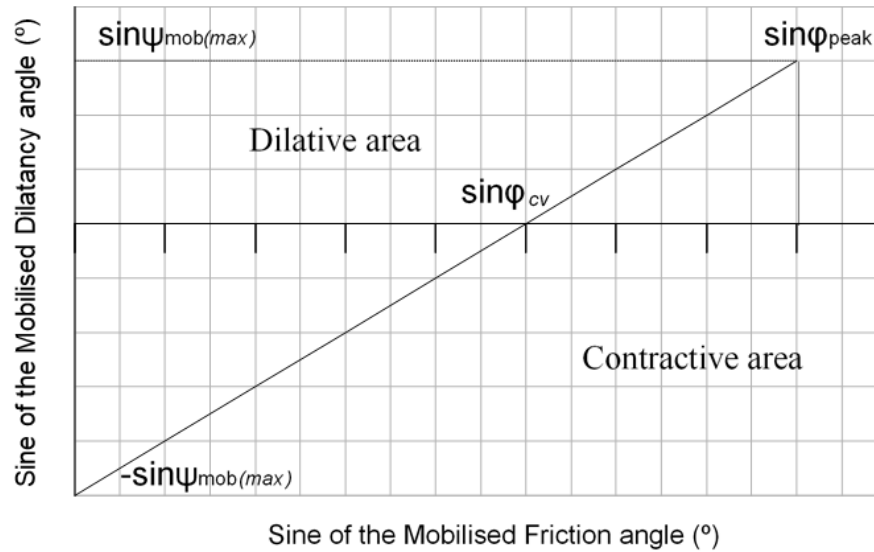


Figure 68: Graphical representation of the modified Rowe's flow rule as used in UBC3D-PLM model

Based on the mobilised friction angle an unloading-reloading criterion is defined in the model as follows:

$$\sin(\varphi_{mob}^e) < \sin(\varphi_{mob}^0) \text{ (unloading; elastic behaviour)} \quad \text{Eq. [334]}$$

$$\sin(\varphi_{mob}^e) > \sin(\varphi_{mob}^0) \text{ (Loading or reloading; plastic behaviour)} \quad \text{Eq. [335]}$$

The previous mobilised friction angle  $\sin(\varphi_{mob}^0)$  is memorised from the previous calculation step, while the current one  $\sin(\varphi_{mob}^e)$  is calculated based on the current stresses. During loading, the friction angle is mobilised, and hardening plasticity occurs. During unloading, pure elastic behaviour is predicted until the stress point reaches the  $p'$  axis.

## 15.3 Load state during liquefaction

The UBC3D-PLM model employs two yield surfaces to guarantee a smooth transition into the liquefied state of the soil and to enable the distinction between primary and secondary loading (Figure 69 (on page 172)). The UBC3D-PLM model incorporates a densification law through a secondary yield surface with a kinematic hardening rule that improves the precision of the evolution of the excess pore pressure. This surface generates lower plastic deformations compared to the primary yield surface.

## The UBC3D-PLM model [ULT]

Load state during liquefaction

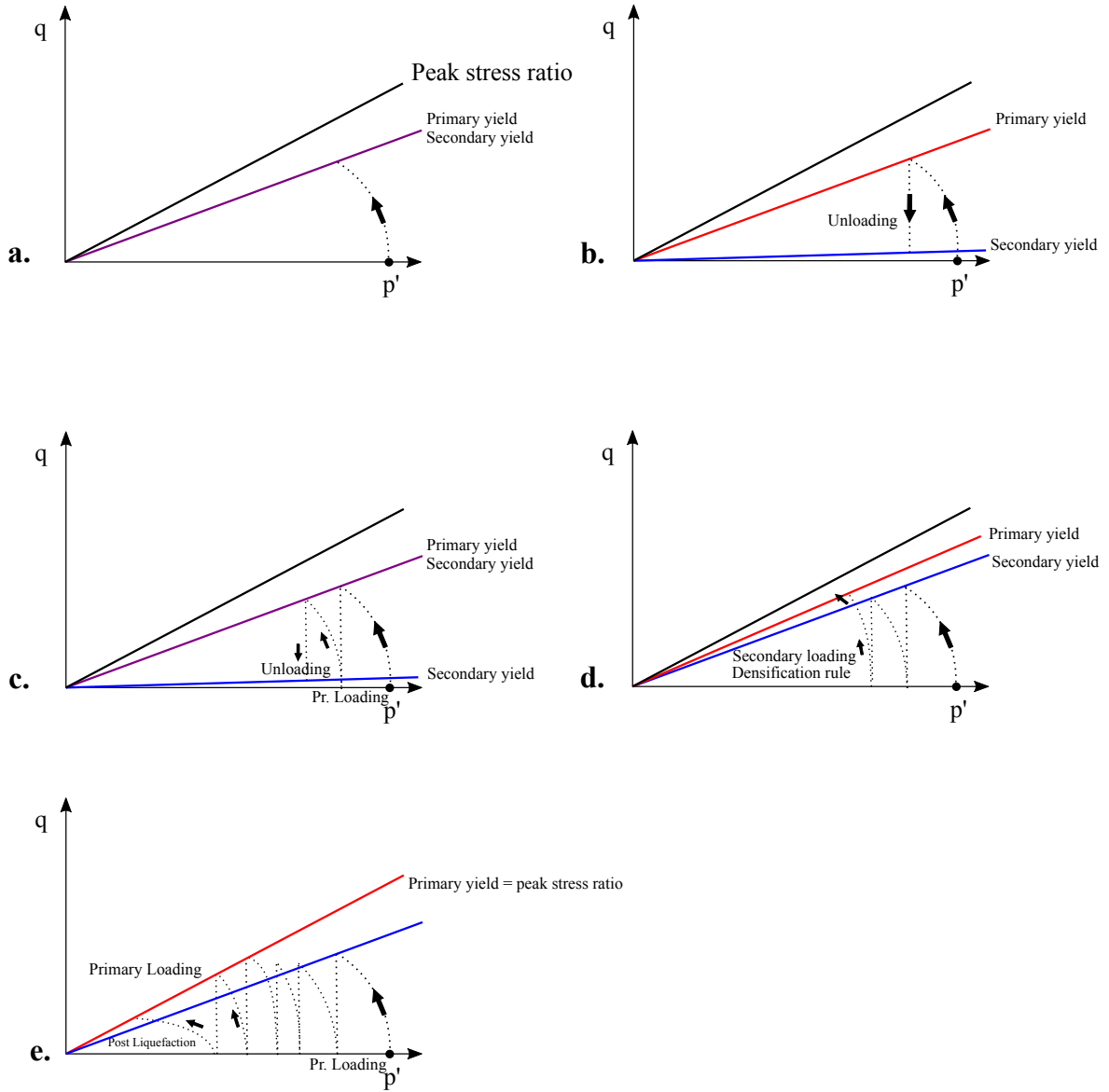


Figure 69: Introduction of two yield surfaces in order to include soil densification, smooth transition in liquefaction and post-liquefaction behaviour

The plastic shear modulus factor  $k_G^{*p}$  during primary loading is identical with the one entered as input parameter by the user and is used in the hardening rule governing the hardening of the primary yield surface. The plastic shear modulus factor  $k_G^{*p}$  during the secondary loading is a function of the number of cycles followed during the loading process. A simple rule based on stress reversals of loading to unloading and vice versa is used to define the counting of cycles. This leads to an increase of the excess pore pressure during undrained cyclic loading with a decreasing rate until the liquefied state is approached. The modification of the plastic shear modulus factor during the secondary loading is calculated as follows:

$$K_{G, \text{secondary}}^{*p} = k_G^{*p} \left( 4 + \frac{n_{rew}}{2} \right)_{hard} f_{dense} \quad Eq. [336]$$

## The UBC3D-PLM model [ULT]

### Post-liquefaction rule and cyclic mobility

where

$k_G^{*p}$	=	Input plastic shear modulus factor.
$k_{G,secondary}^{*p}$	=	Secondary plastic shear modulus factor.
$n_{rev}$	=	Number of shear stress reversals from loading to unloading or vice versa.
$hard$	=	Factor which is correcting the densification rule for loose soils.
$f_{dens}$	=	Multiplier which is a user input parameter to adjust the densification rule.

A correction is made in the densification rule for loose sands ( $5 \leq (N_1)_{60} \leq 9$ ) according to the experimental observations and following the formulation of the UBCSAND model proposed by [Beatty & Byrne \(2011\)](#) (on page 245) and reported by [Naesgaard \(2011\)](#) (on page 248). The correction rule is as follows:

$$hard = \min(1; \max(0.5; 0.1(N_1)_{60})) \quad Eq. [337]$$

**Note:** The corrected penetration resistance  $(N_1)_{60}$  from SPT tests is an input parameter to define only the *hard* factor. However, the user can correlate the other input parameters of the UBC3D-PLM model using  $(N_1)_{60}$  ([Parameters of the UBC3D-PLM model](#) (on page 174)).

The plastic shear modulus is limited according to the maximum corrected SPT value ( $\max(N_1)_{60}$ ) of corresponding dense soils defined as 60.

$$K_{G,max}^{*p} = K_G^{*p} (K_G^{*e} (\max N_{1,60})^2 0.003 + 100) \quad Eq. [338]$$

This rule is the result of calibrating a number of direct simple shear tests. Thus, the calibration factor plays a key role when the user wants to model different stress paths (i.e. cyclic triaxial tests, etc.) and the final value is a matter of judgement according to the most critical stress path for a specific problem. It finally leads to an increase of the excess pore pressure during undrained cyclic loading until the liquefied state is approached. The rate of generation of excess pore pressure decreases by increasing number of cycles.

## 15.4 Post-liquefaction rule and cyclic mobility

An important issue during the modelling of cyclic liquefaction in sands is the volumetric locking. The evolution of the plastic volumetric strains, after the stress path reaches the yield surface defined by the peak friction angle, becomes constant due to the formulation of the flow rule (in Eq. [332]). In the case  $\sin \varphi_{mob}$  becomes  $\sin \varphi_p$  and remains constant meaning that  $\sin \psi_m$  is also constant.

Consequently the stiffness degradation of loose non-cohesive soils due to the post liquefaction behaviour as well as dense non-cohesive soils due to the cyclic mobility cannot be modelled. This limitation is overcome in the formulation of the UBC3D-PLM model with the equation which gradually decreases the plastic shear modulus as a function of the generated plastic deviatoric strain during dilation, due to the deconstruction of the soil skeleton which occurs during dilative behaviour. This leads to the decreased soil stiffness during the contraction phase which follows after the unloading phase. This behaviour is presented in [Figure 70](#) (on page 174) picturing the process of cyclic mobility of a dense sand. The aforementioned stiffness degradation is computed as follows:

$$K_{G, post-liquefaction}^{*p} = k_G^{*p} E_{dil} \quad Eq. [339]$$

$$E_{dil} = \max \left( e^{-110 \varepsilon_{dil}}; f_{Epost} \right) \quad Eq. [340]$$

## The UBC3D-PLM model [ULT]

Parameters of the UBC3D-PLM model

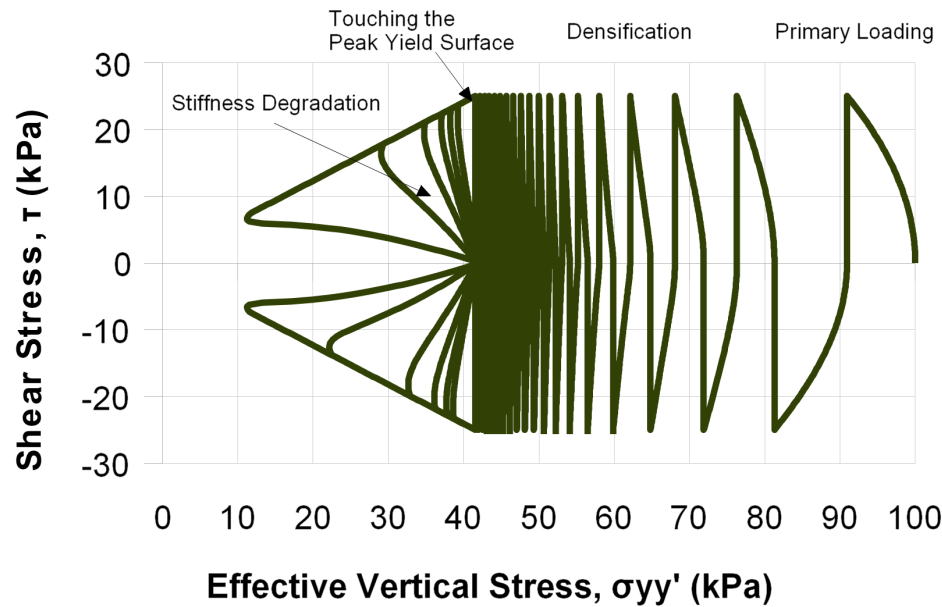


Figure 70: Undrained cyclic shear stress path reproduced with UBC3D-PLM model for a dense sand. Cyclic mobility, stiffness degradation and soil densification are indicated on the graph

where  $k^{*p}_G$  is the input plastic shear modulus factor,  $k^{*p}_{G,post-liquefaction}$  is the plastic shear modulus factor during liquefaction,  $\varepsilon_{dil}$  is the accumulation of the plastic deviatoric strain which is generated during dilation of the soil element. The minimum value of  $E_{dil}$  term in the above mentioned equation is limited by the input parameter  $f_{Epost}$

## 15.5 Parameters of the UBC3D-PLM model

Usually, in earthquake engineering, when the onset of liquefaction is the modelling target a cyclic triaxial or a cyclic direct simple shear test is the proper way to extract all the parameters for the UBC3D-PLM model. However, in many cases only data from drained triaxial tests (CD TxC) or in situ tests (SPT) are available. For this reason the UBC3D-PLM model implements a specific formulation with input parameters based on these tests. However, some of the equations based on SPT values proposed by [Beatty & Byrne \(2011\)](#) (on page 245) for the generic calibration of the UBCSAND model should be used with careful consideration for the calibration of the UBC3D-PLM model.

The parameters with their standard units are listed below.

Stiffness parameters:		
$k^{*e}_B$	Elastic bulk modulus factor	[-]
$k^{*e}_G$	Elastic shear modulus factor	[-]
$k^{*p}_G$	Plastic shear modulus factor	[-]

## The UBC3D-PLM model [ULT]

Parameters of the UBC3D-PLM model

$me$	Rate of stress-dependency of elastic bulk modulus	[-]
$ne$	Rate of stress-dependency of elastic bulk modulus	[-]
$np$	Rate of stress-dependency of plastic shear modulus	[-]
$p_{ref}$	Reference pressure	[kN/m <sup>2</sup> ]
<i>Strength parameters:</i>		
$\varphi_{cv}$	Constant volume friction angle	[°]
$\varphi_p$	Peak friction angle	[°]
$c$	Cohesion	[kN/m <sup>2</sup> ]
$\sigma_t$	Tension cut-off and tensile strength	[kN/m <sup>2</sup> ]
<i>Field data</i>		
$(N_1)_{60}$	Corrected SPT value	[-]
<i>Advanced parameters:</i>		
$R_f$	Failure ratio	[-]
$f_{dens}$	Densification factor	[-]
$f_{Epost}$	Post-liquefaction factor	[-]

The UBC3D-PLM model allows two drainage types: Drained and Undrained A. The other undrained calculations are not available due to the effective stress nature of the model.

## The UBC3D-PLM model [ULT]

Parameters of the UBC3D-PLM model

Property	Unit	Value
<b>Stiffness</b>		
$k_B^*$		0.000
$k_G^*$		0.000
$k_G^p$		0.000
<b>Stress-dependency</b>		
$m_e$		0.000
$n_e$		0.000
$n_p$		0.000
$p_{ref}$	kN/m²	100.0
<b>Strength</b>		
<b>Shear</b>		
$c$	kN/m²	0.000
$\varphi_{cv}$	°	0.000
$\varphi_p$	°	0.000
<b>Tension</b>		
$\sigma_t$	kN/m²	0.000
<b>Field data</b>		
$(N_1)_{60}$		0.000
<b>Advanced</b>		
Use defaults		<input checked="" type="checkbox"/>
<b>Stiffness</b>		
$f_{dens}$		1.000
$f_{Epost}$		1.000
<b>Strength</b>		
$R_f$		0.9000

Figure 71: Parameters of the UBC3D-PLM model

### 15.5.1 Stiffness modulus factors $k_B^*$ , $k_G^*$ & $k_G^p$ and indexes $m_e$ , $n_e$ and $n_p$

Beatty & Byrne (2011) (on page 245) proposed a set of equations based on the normalised  $N_{SPT}$  value,  $(N_1)_{60}$  for the initial generic calibration of the UBCSAND 904aR model. Makra (2013) revised the proposed equations and highlighted the differences between the original UBCSAND 2D formulation and the UBC3D-PLM model, as implemented in PLAXIS. The proposed equations for the generic initial calibration are the following:

$$k_G^* = 21.7 \times 20 \times (N_1)_{60}^{0.3333} \quad Eq. [341]$$

## The UBC3D-PLM model [ULT]

Parameters of the UBC3D-PLM model

$$k_B^{*e} = 0.7 \times k_G^{*e} \quad \text{Eq. [342]}$$

$$k_B^{*p} = k_G^{*e} \times (N_1)_{60}^2 \times 0.003 + 100 \quad \text{Eq. [343]}$$

The index parameters  $me$ ,  $ne$  and  $np$  should be calibrated by curve fitting. The range of these values is 0-1. The suggested default values are  $me = ne = 0.5$  and  $np = 0.4$ . Alternatively the relative density correlations can be used to calibrate the above mentioned parameters as suggested by [Souliotis & Gerolymos \(2016\)](#) (on page 249).

**Note:** The implicit Poisson's ratio that is defined based on  $k_B^{*e}$  and  $k_G^{*e}$  is suitable for dynamics calculation, but it does not generate a proper initial stress state if the initial stress condition is established by gravity loading procedure. In such a case the user should define another material set for the stress initialization step with proper characteristics.

### 15.5.2 Strength parameters $\varphi_{cv}$ , $\varphi_p$ and $c$

The strength parameters of the primary yield surface  $\varphi_{cv}$ ,  $\varphi_p$  and  $c$  can be derived directly from CD TxC or DSS tests. The default value for the cohesion  $c$  is 0, as in most cases for granular soils without relevant fine component. The peak friction angle  $\varphi_p$  can be calculated from SPT test as:

$$\varphi_p = \varphi_{cv} + \frac{(N_1)_{60}}{10} + \max\left(0; \frac{(N_1)_{60} - 15}{5}\right) \quad \text{Eq. [344]}$$

The constant volume friction angle  $\varphi_{cv}$  can be derived directly from SPT test using one of the correlations available in literature ([Bolton, 1986](#) (on page 246); [Mayne, 2001](#) (on page 247)).

**Note:** In the UBC3D-PLM model, the constant volume friction angle  $\varphi_{cv}$  plays the role of the phase transformation angle  $\varphi_{pt}$ .

### 15.5.3 Advanced parameters $R_f$ , $f_{dens}$ and $f_{Epost}$

The densification factor  $f_{dens}$  is a multiplier that controls the scaling of the plastic shear modulus factor during secondary loading. The acceptable range is 0 - 1, when a value below 1 means the  $k_G^{*p}$  becomes lower and the behaviour softer. It is recommended to use  $f_{dens} = 1.0$  ([Petalas & Galavi, 2012](#) (on page 248)) because the variation of the densification does not significantly affect liquefaction triggering.

$f_{Epost}$  is the parameter to adjust post-liquefaction behaviour. The acceptable range of  $f_{Epost}$  is 0.1 - 1 and a value of 0.2 - 1 is recommended. Resistance is underestimated for very dense sands, which can be counterbalanced by an increase of the  $f_{Epost}$  parameter.

The failure ratio  $R_f$  has a default value of 0.9, but it can be also estimated from the SPT test based on the original UBCSAND ([Beatty & Byrne, 2011](#) (on page 245)):

$$R_f \approx 1.1((N_1)_{60})^{-0.15} < 0.99 \quad \text{Eq. [345]}$$

### 15.5.4 Corrected SPT value $(N_1)_{60}$

The SPT blow count  $N_{SPT}$  is affected by a number of procedural details such as rod lengths, hammer energy, sampler details and borehole size which are accounted using correction factors. In addition, if the  $N_{SPT}$  is corrected by the overburden stress effects one obtains the *corrected penetration resistance*  $(N_1)_{60}$ , expressed as:

## The UBC3D-PLM model [ULT]

State parameters in the UBC3D-PLM model

$$(N_1)_{60} = C_N C_E C_R C_B C_S N_{SPT} \quad \text{Eq. [346]}$$

where

$C_N$	=	overburden correction factor.
$C_E$	=	$ER_m/60$ .
$ER_m$	=	Measured value of the delivered energy as a percentage (%) of the theoretical free-fall hammer energy.
$C_R$	=	Correction factor to account for different rod lengths.
$C_B$	=	Correction factor for nonstandard borehole diameters.
$C_S$	=	Correction factor that depends on the sampler.
$N_{SPT}$	=	Calculated as $N_2 + N_3$ considering that $N_1$ , $N_2$ and $N_3$ are the number of blows needed for the tube to penetrate each 15 cm.

The suggested values for  $C_B$ ,  $C_R$  and  $C_S$  are given in [Table 10](#) (on page 178).

**Table 10: List of values of the different coefficient for the correction of the SPT test**

Coefficient	Condition	Value
General		
Borehole diameter, $C_B$	65÷115 mm (standard)	1.00
	150 mm	1.05
	200 mm	1.15
Rod length, $C_R$	3÷4 m	0.75
	4÷6 m	0.85
	6÷10 m	0.95
	10÷30 m	1.00
	>30 m	1.00
Type of sampler, $C_S$	Standard	1.00
	Non standard	1.1÷1.3

If  $(N_1)_{60}$  is not known, the following approximation (adapted from [Beaty & Byrne \(2011\)](#) (on page 245) ) with relative density RD (expressed in %) can be used:

$$(N_1)_{60} \approx \frac{RD^2}{15^2} \quad \text{Eq. [347]}$$

## 15.6 State parameters in the UBC3D-PLM model

## The UBC3D-PLM model [ULT]

### State parameters in the UBC3D-PLM model

In addition to the output of standard stress and strain, the UBC3D-PLM model provides output of state variables, such as the excess pore pressure ratio in terms of vertical effective stresses  $r_{u,\sigma'v}$  and the mobilised peak friction angle  $\phi_{p, reached}$ . These parameters can be visualised by selecting the *State parameters* option from the *Stresses* menu. An overview of available state parameters is given below:

$\sin \phi_{mob}$	Sine of the mobilised friction angle (Eq. [326])	[-]
$\sin \phi_{mob, max}$	Sine of the maximum mobilised friction angle	[-]
$\phi_{p, reached}$	Flag indicating whether peak friction angle has been reached (0/1)	[-]
$n_{rev}$	Number of half cycles	[-]
$r_{u,\sigma'v}$	Excess pore pressure ratio in terms of vertical effective stress (Eq. [348])	[-]
$r_{u,\sigma'v, max}$	Maximum excess pore pressure ratio in terms of vertical effective stress	[-]
$r_{u,p'}$	Excess pore pressure ratio in terms of mean effective stress (Eq. [349])	[-]
$r_{u,p', max}$	Maximum excess pore pressure ratio in terms of mean effective stresses	[-]
$\epsilon_{dil, total}$	Accumulated dilative plastic deviatoric strain	[-]

$r_{u,\sigma'v}$ ,  $r_{u,p'}$ ,  $\phi_{p, reached}$  are further explained in the following subsections:

#### 15.6.1 Excess pore pressure ratio in terms of vertical effective stresses $r_{u,\sigma'v}$

The liquefaction potential in terms of vertical effective stress can be expressed by means of the excess pore pressure ratio  $r_{u,\sigma'v}$  given by:

$$r_{u,\sigma'v} = \frac{\sigma'_{v0} - \sigma'_v}{\sigma'_{v0}} = 1 - \frac{\sigma'_v}{\sigma'_{v0}} \quad \text{Eq. [348]}$$

where  $\sigma'_v$  is the current vertical effective stress during the dynamics calculation and  $\sigma'_{v0}$  is the initial effective vertical stress prior to the seismic motion. When  $r_{u,\sigma'v}$  is equal to 1, the corresponding layer is in a complete liquefied state. consider zones with a maximum  $r_{u,\sigma'v}$  greater than 0.7 to be liquefied.

#### 15.6.2 Excess pore pressure ratio in terms of mean effective stress $r_{u,p'}$

The state variable  $r_{u,\sigma'v}$  gives similar information as  $r_{u,p'}$  but instead of the vertical effective stress the mean effective stress is used:

$$r_{u,p'} = \frac{p'_0 - p'}{p'_0} = 1 - \frac{p'}{p'_0} \quad \text{Eq. [349]}$$

where  $p'$  is the current mean effective stress during the dynamics calculation and  $p'_0$  is the initial mean effective stress prior to the seismic motion. When  $r_{u,p'}$  equals 1, the soil is in a liquified state.

## The UBC3D-PLM model [ULT]

On the use of the UBC3D-PLM model in dynamics calculations

---

### 15.6.3 Reached peak friction angle $\varphi_{p, reached}$

The reached peak friction angle  $\varphi_{p, reached}$  is a flag indicating if  $\varphi_p$  has been reached (0 = no, 1 = yes).

## 15.7 On the use of the UBC3D-PLM model in dynamics calculations

When subjected to dynamic or cyclic loading, the UBC3D-PLM model generates plastic strains when mobilising the soil's material strength (shear hardening). A Rayleigh damping can be defined to simulate the initial soil's damping characteristics.

The UBC3D-PLM model has been developed for simulating the dynamic behaviour of non-cohesive soils and it is particularly suitable for analysing the problems involving generation of pore pressure in undrained behaviour and liquefaction. For the same reason, it is less suitable for use in static analysis. This limitation can be overcome by using Hardening Soil model ([The Hardening Soil model \(Isotropic hardening\)](#) (on page 67)) or Hardening Soil model with small-strain stiffness ([The Hardening Soil model with small-strain stiffness \(HSsmall\)](#) (on page 82)) instead.

The UBC3D-PLM model develops overdamping due to use of  $G_{max}$  in elastic unloading. In the problems not involving generation of pore pressure in undrained behaviour, liquefaction or softening due to dilatancy, this limitation can be overcome by using the Hardening Soil model with small-strain stiffness ([The Hardening Soil model with small-strain stiffness \(HSsmall\)](#) (on page 82)) instead.

## User-defined soil models [ADV]/[ULT] + [GSE]

---

### 16.1 Introduction

PLAXIS has a facility for User-defined Soil Models (UDSM). This facility allows users to implement a wide range of constitutive soil models (stress-strain-time relationship) in PLAXIS. Such models must be programmed in FORTRAN (or another programming language), then compiled as a Dynamic Link Library (DLL) and then added to the UDSM sub-folder of the PLAXIS program directory.

In principle the user provides information about the current stresses and state variables and PLAXIS provides information about the previous ones and also the strain and time increments. In the material data base of the PLAXIS input program, the required model parameters can be entered in the material data sets.

$\sigma_{ij}^{t+\Delta t}, \kappa^{t+\Delta t}$

Current stresses and state variables.

$\sigma_{ij}^t, \kappa^t$

Previous stresses and state variables.

$\Delta \varepsilon_{ij}, \Delta t$

Strain and time increments.

**Note:**

- Please note that the PLAXIS organization cannot be held responsible for any malfunctioning or wrong results due to the implementation and/or use of user-defined soil models.
- For a detailed view of the UDSMs offered in PLAXIS please check [Bentley Communities website](#).

## 16.2 Implementation of User Defined (UD) soil Models in calculations program

### 16.2.1 Main Functionalities UD Models

The PLAXIS calculations program has been designed to allow for UDSM. There are mainly six tasks (functionalities) to be performed in the calculations program:

- *Initialization of state variables*
- *Calculation of constitutive stresses (stresses computed from the material model at certain step)*
- *Return of the state variables*
- *Return of attributes matrix*
- *Creation of effective material stiffness matrix*
- *Creation of elastic material stiffness matrix*

These main tasks (and other tasks) have to be defined by the user in a subroutine called 'User\_Mod'. In this subroutine more than one user-defined soil model can be defined. If a UD soil model is used in an application, the calculation program calls the corresponding task from the subroutine *User\_Mod*. To create a UD soil model, the *User\_Mod* subroutine must have the following structure:

```
Subroutine      (IDTask, iMod, IsUndr, iStep, iTer, Iel,Int, X, Y, Z, Time0, dTime,  
User_mod        Props, Sig0, Swp0, StVar0, dEps, D, Bulk_W, Sig, Swp, StVar, ipl,  
                  nStat, NonSym, iStrsDep, iTimeDep, iTang, iPrjDir, iPrjLen, iAbort)
```

where

<b>IDTask</b>	=	Identification of the task (1 = Initialise state variables; 2 = Calculate constitutive stresses; 3 = Create effective material stiffness matrix; 4 = Return the number of state variables; 5 = Return matrix attributes (NonSym, iStrsDep, iTimeDep, iTang); 6 = Create elastic material stiffness matrix).
<b>iMod</b>	=	User-defined soil model number (This option allows for more than one UD model, up to 10).
<b>IsUndr</b>	=	Drained condition (IsUndr = 0) or undrained condition (IsUndr = 1). In the latter case, PLAXIS will add a large bulk stiffness for water.
<b>iStep</b>	=	Current calculation step number
<b>iter</b>	=	Current iteration number
<b>Iel</b>	=	Current element number
<b>Int</b>	=	Current local stress point number (1..3 for 6-noded elements, or 1..12 for 15-noded elements)
<b>X,Y,Z</b>	=	Global coordinates of current stress point
<b>Time0</b>	=	Time at the start of the current step
<b>dTime</b>	=	Time increment of current step
<b>Props</b>	=	Array(1..50) with User-defined model parameters for the current stress point

## User-defined soil models [ADV]/[ULT] + [GSE]

Implementation of User Defined (UD) soil Models in calculations program

<b>Sig0</b>	=	Array(1..20) with previous (= at the start of the current step) effective stress components of the current stress point and some other variables ( $\sigma_{xx}^0, \sigma_{yy}^0, \sigma_{zz}^0, \sigma_{xy}^0, \sigma_{yz}^0, \sigma_{zx}^0, p_{steady}, \Sigma Mstage^0, \Sigma Mstage, Sat, Sat^0, Suc, Suc^0, \Sigma Msf^0, \Sigma Msf, SatEff, SatRes, Temp, Temp0$ ). Where: SatEff is the effective saturation. Temp0 is the temperature at the beginning of the current step and Temp is the updated temperature during the step calculation. In 2D calculations $\sigma_{yz}$ and $\sigma_{zx}$ should be zero.
<b>Swp0</b>	=	Previous excess pore pressure of the current stress point}
<b>StVar0</b>	=	Array(1..nStat) with previous values of state variables of the current stress point
<b>dEps</b>	=	Array(1..12) with strain increments of the current stress point in the current step ( $\Delta \varepsilon_{xx}, \Delta \varepsilon_{yy}, \Delta \varepsilon_{zz}, \Delta \gamma_{xy}, \Delta \gamma_{yz}, \Delta \gamma_{zx}, \varepsilon_{xx}^0, \varepsilon_{yy}^0, \varepsilon_{zz}^0, \gamma_{xy}^0, \gamma_{yz}^0, \gamma_{zx}^0$ ). In 2D calculations $\Delta \gamma_{yz}, \Delta \gamma_{zx}, \gamma_{yz}^0$ and $\gamma_{zx}^0$ should be zero. In PLAXIS 2D this array may also contain non-local strains. Contact PLAXIS for more details.
<b>D</b>	=	Effective material stiffness matrix of the current stress point (1..6, 1..6)
<b>Bulk_W</b>	=	Bulk modulus of water for the current stress point (for undrained calculations and consolidation)
<b>Sig</b>	=	Array (1..6) with resulting constitutive stresses of the current stress point ( $\sigma'_{xx}, \sigma'_{yy}, \sigma'_{zz}, \sigma'_{xy}, \sigma'_{yz}, \sigma'_{zx}$ )
<b>Swp</b>	=	Resulting excess pore pressure of the current stress point
<b>StVar</b>	=	Array(1..nStat) with resulting values of state variables for the current stress point
<b>ipl</b>	=	Plasticity indicator: 0 = no plasticity, 1 = Mohr-Coulomb (failure) point; 2 = Tension cut-off point, 3 = Cap hardening point, 4 = Cap friction point, 5 = Friction hardening point, 6 = Plotting liquefaction indicators.
<b>nStat</b>	=	Number of state variables (unlimited)
<b>NonSym</b>	=	Parameter indicating whether the material stiffness matrix is non-symmetric (NonSym = 1) or not (NonSym = 0) (required for matrix storage and solution).
<b>iStrsDep</b>	=	Parameter indicating whether the material stiffness matrix is stress-dependent (iStrsDep = 1) or not (iStrsDep = 0).
<b>iTimeDep</b>	=	Parameter indicating whether the material stiffness matrix is time-dependent (iTimeDep = 1) or not (iTimeDep = 0).
<b>iTang</b>	=	Parameter indicating whether the material stiffness matrix is a tangent stiffness matrix, to be used in a full Newton-Raphson iteration process (iTang = 1) or not (iTang = 0).
<b>iPrjDir</b>	=	Project directory (for debugging purposes)
<b>iPrjLen</b>	=	Length of project directory name (for debugging purposes)
<b>iAbort</b>	=	Parameter forcing the calculation to stop (iAbort = 1).

In the above, 'increment' means 'the total contribution within the current step' and *not* per iteration. 'Previous' means 'at the start of the current step', which is equal to the value at the end of the previous step.

In the terminology of the above parameters it is assumed that the standard type of parameters is used, i.e. parameters beginning with the characters A-H and O-Z are double (8-byte) floating point values and the remaining parameters are 4-byte integer values.

The parameters IDTask to dEps and iPrjDir and iPrjLen are input parameters; The values of these parameters are provided by PLAXIS and can be used within the subroutine. These input parameters should not

## User-defined soil models [ADV]/[ULT] + [GSE]

Implementation of User Defined (UD) soil Models in calculations program

be modified (except for `StVar0` in case `IDTask= 1`). The parameters `D` to `iTang` and `iAbort` are output parameters. The values of these parameters are to be determined by the user. In case `IDTask = 1`, `StVar0` becomes output parameter.

The user subroutine should contain program code for listing the tasks and output parameters `IDTask= 1` to `6`). After the declaration of variables, the `User_Mod` subroutine must have the following structure (here specified in pseudo code):

```
Case IDTask of
  1 Begin
      { Initialise state Variable StVar }
  End
  2 Begin
      { Calculate constitutive stresses Sig (and Swp) }
  End
  3 Begin
      { Create effective material stiffness matrix D }
  End
  4 Begin
      { Return the number of state variables nStat }
  End
  5 Begin
      { Return matrix attributes NonSym, iStrsDep, iTimeDep }
  End
  6 Begin
      { Create elastic material stiffness matrix De }
  End
End Case
```

If more than one UD model is considered, distinction should be made between different models, indicated by the UD model number `iMod`.

### *Initialise state variables (IDTask = 1)*

State variables (also called the hardening parameters) are, for example, used in hardening models to indicate the current position of the yield loci. The update of state variables is considered in the calculation of constitutive stresses based on the previous value of the state variables and the new stress state. Hence, it is necessary to know about the initial value of the state variables, i.e. the value at the beginning of the calculation step. Within a continuous calculation phase, state variables are automatically transferred from one calculation step to another. The resulting value of the state variable in the previous step, `StVar`, is stored in the output files and automatically used as the initial value in the current step, `StVar0`. When starting a new calculation phase, the initial value of the state variables is read from the output file of the previous calculation step and put in the `StVar0` array. In this case it is not necessary to modify the `StVar0` array.

However, if the previous calculation step does not contain information on the state variables (for example in the very first calculation step), the `StVar0` array would contain zeros. For this case the initial value has to be calculated based on the actual conditions (actual stress state) at the beginning of the step. Consider, for example, the situation where the first state variable is the minimum mean effective stress,  $p'$  (considering that compression is negative). If the initial stresses have been generated using the  $K_0$ -procedure, then the initial effective stresses are non-zero, but the initial value of the state variable is zero, because the initialization of this user-defined variable is not considered in the  $K_0$ -procedure. In this case, part 1 of the user subroutine may look like:

```
1 Begin
  { Initialise stage variables StVar() }
```

## User-defined soil models [ADV]/[ULT] + [GSE]

Implementation of User Defined (UD) soil Models in calculations program

```
p = (Sig0[1] + Sig0[2] + Sig0[3]) / 3.0
StVar0[1] = Min(StVar0[1], p)
End
```

### *Calculate constitutive stresses (IDTask = 2)*

This task constitutes the main part of the user subroutine in which the stress integration and correction are performed according to the user-defined soil model formulation. Let us consider a simple example using a linear elastic  $D$ -matrix as created under IDTask = 3.

In this case the stress components, Sig, can directly be calculated from the initial stresses, Sig0, the material stiffness matrix,  $D$ , and the strain increments, dEps:  $\text{Sig}[i] = \text{Sig0}[i] + \sum (D[i, j] * d\text{Eps}[j])$ . In this case, part 2 of the user subroutine may look like:

```
2 Begin
  { Calculate constitutive stresses Sig (and Swp) }
  For i=1 to 6 do
    Sig[i] = Sig0[i]
    For j=1 to 6 do
      Sig[i] = Sig[i] + D[i,j]*dEps[j]
    End for{j}
  End for {i}
End
```

### *Create effective material stiffness matrix (IDTask = 3)*

The material stiffness matrix,  $D$ , may be a matrix containing only the elastic components of the stress-strain relationship (as it is the case for the existing soil models in PLAXIS), or the full elastoplastic material stiffness matrix (tangent stiffness matrix). Let us consider the very simple example of Hooke's law of isotropic linear elasticity. There are only two model parameters involved: Young's modulus,  $E$ , and Poisson's ratio,  $\nu$ . These parameters are stored, respectively, in position 1 and 2 of the model parameters array, Props(1..50). In this case, part 3 of the user subroutine may look like:

```
3 Begin
  { Calculate effective material stiffness matrix D }
  E = Props[1]
  v = Props[2]
  G = 0.5*E/(1.0+v)
  Fac = 2*G/(1.0-2*v){ make sure that v<0.5!!}
  Term1 = Fac*(1-v)
  Term2 = Fac*v
  D[1,1] = Term1
  D[1,2] = Term2
  D[1,3] = Term2
  D[2,1] = Term2
  D[2,2] = Term1
  D[2,3] = Term2
  D[3,1] = Term2
  D[3,2] = Term2
  D[3,3] = Term1
  D[4,4] = G
  D[5,5] = G
  D[6,6] = G
End
```

## User-defined soil models [ADV]/[ULT] + [GSE]

Implementation of User Defined (UD) soil Models in calculations program

---

(By default, D will be initialised to zero, so the remaining terms are still zero; however, it is a good habit to explicitly define zero terms as well.)

If undrained behaviour is considered ( $IsUndr = 1$ ), then a bulk stiffness for water ( $Bulk\_W$ ) must be specified at the end of part 3. After calling the user subroutine with  $IDTask = 3$  and  $IsUndr = 1$ , PLAXIS will automatically add the stiffness of the water to the material stiffness matrix D such that:  $D[i=1..3, j=1..3] = D[i, j] + Bulk\_W$ . If  $Bulk\_W$  is not specified, PLAXIS will give it a default value of  $100 * Avg(D[i=1..3, j=1..3])$ .

### *Return the number of state variables ( $IDTask = 4$ )*

This part of the user subroutine returns the parameter  $nStat$ , i.e. the number of state variables. In the case of just a single state parameter, the user subroutine should look like:

```
4  Begin
    { Return the number of state variables nStat }
    nStat = 1
End
```

### *Return matrix attributes ( $IDTask = 5$ )*

The material stiffness matrix may be stress-dependent (such as in the Hardening Soil model) or time-dependent (such as in the Soft Soil Creep model). When using a tangent stiffness matrix, the matrix may even be non-symmetric, for example in the case of non-associated plasticity. The last part of the user subroutine is used to initialize the matrix attributes in order to update and store the global stiffness matrix properly during the calculation process. For the simple example of Hooke's law, as described earlier, the matrix is symmetric and neither stress- nor time-dependent. In this case the user subroutine may be written as:

```
5  Begin
    { Return the matrix attributes NonSym, IStrsDep,      }
    {   iTimeDep, iTang      }
    NonSym      = 0
    iStrsDep     = 0
    iTimeDep     = 0
    iTang        = 0
End
```

For  $NonSym = 0$  only half of the global stiffness matrix is stored using a profile structure, whereas for  $NonSym = 1$  the full matrix profile is stored.

For  $iStrsDep = 1$  the global stiffness matrix is created and decomposed at the beginning of each calculation step based on the actual stress state (modified Newton-Raphson procedure).

For  $iTimeDep = 1$  the global stiffness matrix is created and decomposed every time when the time step changes.

For  $iTang = 1$  the global stiffness matrix is created and decomposed at the beginning of each iteration based on the actual stress state (full Newton-Raphson procedure; to be used in combination with  $iStrsDep=1$ ).

### *Create elastic material stiffness matrix ( $IDTask = 6$ )*

The elastic material stiffness matrix,  $D^e$ , is the elastic part of the effective material stiffness matrix as described earlier.

## User-defined soil models [ADV]/[ULT] + [GSE]

### Implementation of User Defined (UD) soil Models in calculations program

In the case that the effective material stiffness matrix was taken to be the elastic stiffness matrix, this matrix may just be adopted here. However in the case that an elastoplastic or tangent matrix was used for the effective stiffness matrix, then the matrix to be created here should only contain the elastic components.

The reason that an elastic material stiffness matrix is required is because PLAXIS calculates the current relative global stiffness of the finite element model as a whole (CSP = Current Stiffness Parameter). The CSP parameter is defined as:

$$CSP = \frac{\text{Total work}}{\text{Total elastic work}} \quad \text{Eq. [350]}$$

The elastic material stiffness matrix is required to calculate the total elastic work in the definition of the CSP. The CSP equals unity if all the material is elastic whereas it gradually reduces to zero when failure is approached.

The CSP parameter is used in the calculation of the global error. The global error is defined as:

$$\text{Global error} = \frac{|\text{unbalance force}|}{|\text{currently activated load}| + CSP \cdot |\text{previously activated load}|} \quad \text{Eq. [351]}$$

The unbalance force is the difference between the external forces and the internal reactions. The currently activated load is the load that is being activated in the current calculation phase, whereas the previously activated load is the load that has been activated in previous calculation phases and that is still active in the current phase.

Using the above definition for the global error in combination with a fixed tolerated error results in an improved equilibrium situation when plasticity increases or failure is approached. The idea is that a small out-of-balance is not a problem when a situation is mostly elastic, but in order to accurately calculate failure state, safety factor or bearing capacity, a stricter equilibrium condition must be adopted.

Part 6 of the user subroutine looks very similar to part 3, except that only elastic components are considered here. It should be noted that the same variable D is used to store the elastic material stiffness matrix, whereas in Part 3 this variable is used to store the effective material stiffness matrix.

```
6   Begin
    {   Create elastic material stiffness matrix D   }
      D[1,1]
      D[1,2]
      D[1,3]
      ...
      D[6,6]
End
```

## 16.2.2 Using predefined subroutines from the source code

In order to simplify the creation of user subroutines, a number of FORTRAN subroutines and functions for vector and matrix operations are available in the source code (to be included in the file with the user subroutine). The available subroutines may be called by User\_Mod subroutine to shorten the code. An overview of the available subroutines is given in [Modelling of embedded structures](#) (on page 261).

## 16.2.3 Definition of user-interface functions

## User-defined soil models [ADV]/[ULT] + [GSE]

### Implementation of User Defined (UD) soil Models in calculations program

---

In addition to the user-defined model itself it is possible to define functions that will facilitate its use within the PLAXIS user-interface. If available, PLAXIS Input will retrieve information about the model and its parameters using the procedures described hereafter.

```
procedure GetModelCount(var C:longint) ;
```

where

**C** = number of models (return parameter)

This procedure retrieves the number of models that have been defined in the DLL. PLAXIS assumes that model IDs are successive starting at model ID = 1.

```
procedure GetModelName(var iModel : longint;
                        var Name : shortstring) ;
```

where

**iModel** = User-defined soil model number to retrieve the name for (input parameter)}

**Name** = Model name (return parameter)

This procedure retrieves the names of the models defined in the DLL.

```
procedure GetParamCount(var iModel : longint; var C: longint) ;
```

where

**iModel** = User-defined soil model number (input parameter)

**C** = number of parameters for the specified model (return parameter)

This procedure retrieves the parameter name of a specific model.

```
Procedure GetParamName(var iModel,iParam : longint;
                        var Name : shortstring);
```

where

**iModel** = User-defined soil model number (input parameter)

**iParam** = Parameter number (input parameter)

**Name** = parameter name (return parameter)

This procedure retrieves the parameter name of a specific parameter.

```
Procedure GetParamUnit(var iModel,iParam : longint;
                        var Units : shortstring)
```

where

**iModel** = User-defined soil model number (input parameter)

**iParam** = Parameter number (input parameter)

**Units** = Parameter units (return parameter)

This procedure retrieves the parameter units of a specific parameter. Since the chosen units are dependent on the units of length, force and time chosen by the user the following characters should be used for defining parameter units:

'L' or 'l' for units of length 'F' or 'f' for units of force 'T' or 't' for units of time.

For model names, model parameter names and model parameter units special characters can be used for indicating subscript, superscript or symbol font (for instance for Greek characters).

## User-defined soil models [ADV]/[ULT] + [GSE]

Implementation of User Defined (UD) soil Models in calculations program

---

- ^ From here characters will be superscript
- \_ From here characters will be subscript
- @ From here characters will be in symbol font
- # Ends the current superscript or subscript.

Pairs of '^..#','\_...#' and '@...#' can be nested.

For example:

A UD model parameter uses the oedometer stiffness as parameter. The parameter name can be defined as 'E\_oed#' and its units as 'F/L^2#'.

When defining a unit containing one of the letters 'l', 'f' or 't', like 'cal/mol', these letters will be replaced by the unit of length, the unit of force or the unit of time respectively. To avoid this, these letters should be preceded by a backslash. For example 'cal/mol' should be defined as 'ca\l/mo\l' to avoid getting 'cam/mom'.

The state variables to be displayed in the Output program can be defined.

```
procedure GetStateVarCount(var iModel : longint; var C :longint) ;
```

where

<b>iModel</b>	=	User-defined soil model number (input parameter)
<b>C</b>	=	number of state variables for the specified model (return parameter)

This procedure retrieves the number of state variables of a specific model.

```
procedure GetStateVarName(var iModel,iParam : longint;  
var Name : shortstring);
```

where

<b>iModel</b>	=	Used-defined soil model number (input parameter)
<b>iParam</b>	=	Parameter number (input parameter)
<b>Name</b>	=	Parameter name (return parameter)

This procedure retrieves the state parameter name of a specific parameter.

```
Procedure GetStateVarUnit(var iModel,iParam : longint;  
var Units : shortstring) ;
```

where

<b>iModel</b>	=	User-defined soil model number (input parameter)
<b>iParam</b>	=	Parameter number (input parameter)
<b>Units</b>	=	Parameter units (return parameter)

This procedure retrieves the state parameter units of a specific parameter.

All procedures are defined in Pascal but equivalent procedures can be created, for instance in a Fortran programming language. Please make sure that the data format of the parameters in the subroutine headers is identical to those formulated before. For instance, the procedures mentioned above use a "shortstring" type; a "shortstring" is an array of 256 characters where the first character contains the actual length of the shortstring contents. Some programming languages only have null-terminated strings; in this case it may be necessary to use an array of 256 bytes representing the ASCII values of the characters to return names and units. An example of Fortran subroutines is included in the software package.

### 16.2.4 UDSM additional information

To allow the use of some specific options as required and passed by the PLAXIS calculation program, the following subroutine can optionally be defined within the UDSM implementation:

```
Subroutine setDLLExtraInfo( iInfo, rInfo )
```

where

<b>iInfo</b>	=	array of integers containing the following data:
		<ul style="list-style-type: none"><li>• iInfo(1): "Special option" specified value (see <i>Special option for User Defined Soil Models</i> [ADV] of the <a href="#">Reference manual</a>).</li><li>• iInfo(2): temperature measure unit, being 1: K, 2: °C, 3: °F.</li><li>• iInfo(3): length measure unit, being 1: mm, 2: cm, 3: m, 4: km, 5: in, 6: ft, 7: yd.</li><li>• iInfo(4): force measure unit, being 1: N, 2: KN, 3: MN, 4: lbf, 5: kip.</li><li>• iInfo(5): time measure unit, being 1: sec, 2: min, 3: hour, 4: day.</li></ul>
<b>rInfo</b>	=	array of floating points, currently not used.

The main purpose of this subroutine is to offer to users implementing a UDSM a way to retrieve and store (e.g. in a module) the measure units adopted at the same time by the PLAXIS calculation kernel and therefore comply with these or transform to and from these within the UDSM implementation.

### 16.2.5 Compiling the user subroutine

The user subroutine `User_Mod` has to be compiled into a DLL file using an appropriate compiler. Note that the compiler must have the option for compiling DLL files. Below are examples for two different FORTRAN compilers. It is supposed that the user subroutine `User_Mod` is contained in the file `USRMOD.FOR`.

After creating the user subroutine `User_Mod`, a command must be included to export data to the DLL. 64-bit compiler must be used.

The following statement has to be inserted in the subroutine just after the declaration of variables:

- Using GNU Fortran:  

```
!DEC$ATTRIBUTES DLLEXPORT :: User_Mod
```
- Using Intel Visual Fortran:  

```
!DEC$ ATTRIBUTES DLLEXPORT,StdCall,Reference :: User_Mod
```

In order to compile the `USRMOD.FOR` into a DLL file, the following command must be executed:

- Using GNU Fortran:  

```
gfortran USRMOD.FOR -o usermod64.dll -shared -fno-underscoring -static
```
- Using Intel Visual Fortran:  

```
ifort /winapp USRMOD.FOR DFusrLib.lib /dll
```

## User-defined soil models [ADV]/[ULT] + [GSE]

Input of UD model parameters via user-interface

---

In all cases USRMOD64.DLL file will be created. It can be renamed to 'any64'.dll. This file should be placed in the **usdm** folder under the PLAXIS program directory, thereafter it can be used together with the existing PLAXIS calculations program (PLASW.EXE in PLAXIS 2D or PLASW3DF.EXE in PLAXIS 3D). Once the User-defined Soil Model is used, PLAXIS will execute the commands as listed in the USRMOD64.DLL file.

### 16.2.6 Debugging possibilities

When making computer programs, usually some time is spent to 'debug' earlier written source code. In order to be able to effectively debug the user subroutine, there should be a possibility for the user to write any kind of data to a file. Such a 'debug-file' is not automatically available and has to be created in the user subroutine.

After the debug-file is created, data can be written to this file from within the user subroutine. This can be done by using, for example, the available written subroutines ( [Fortran subroutines for User-defined soil models](#) (on page 263)).

## 16.3 Input of UD model parameters via user-interface

Input of the model parameters for user-defined soil models can be done using the PLAXIS material data base. In fact, the procedure is very similar to the input of parameters for the existing PLAXIS models.

When creating a new material data set for soil and interfaces in the material data base, a window appears with six tabsheets: **General**, **Mechanical**, **Groundwater**, **Thermal**, **Interfaces**, **Initial** [Figure 72](#) (on page 192). A user-defined model can be selected from the *Material model* combo box in the **General** tabsheet.

# User-defined soil models [ADV]/[ULT] + [GSE]

Input of UD model parameters via user-interface

Soil - UBC3D-PLM - <NoName>

General Mechanical Groundwater Thermal Interfaces Initial

Property	Unit	Value
<b>Material set</b>		
Identification		<NoName>
Soil model		UBC3D-PLM
Drainage type		Linear Elastic
Colour		Mohr-Coulomb
Comments		Hardening Soil
		HS small
		Soft Soil
		Soft Soil Creep
		Jointed Rock
		Modified Cam-clay
		NGI-ADP
		Hoek-Brown
		Sekiguchi-Ohta Inviscid
		Sekiguchi-Ohta Viscid
		Concrete
		UBC3D-PLM
		UDCAM-S
		User-defined
		Color equivalent
<b>Unit weights</b>		
$\gamma_{unsat}$	kN/m <sup>3</sup>	
$\gamma_{sat}$	kN/m <sup>3</sup>	
<b>Void ratio</b>		
$e_{init}$		
$n_{init}$		
<b>Rayleigh damping</b>		
Input method		
Rayleigh $\alpha$		0.000
Rayleigh $\beta$		0.000
$\xi_1$	%	0.000
$\xi_2$	%	0.000
$f_1$	Hz	0.1000
$f_2$	Hz	1.000

Next OK Cancel

Figure 72: Selection Window. Selection of user-defined soil models

## User-defined soil models [ADV]/[ULT] + [GSE]

Input of UD model parameters via user-interface

Property	Unit	Value
<b>User-defined model</b>		
DLL file		pm4sand64.dll
Model in DLL		PM4Sand
<b>User-defined parameters</b>		
DR0		0.000
G0		0.000
hp0		0.000
pA	kN/m <sup>2</sup>	0.000
emax		0.000
emin		0.000
nb		0.000
nd		0.000
phi <sub>cv</sub>	°	0.000
nu		0.000
Q		0.000
R		0.000
PostShake		0.000
<b>Excess pore pressure calcula</b>		
Determination		v-undrained definition
v <sub>w, equivalent</sub> (nu)		0.4950

Figure 73: Selection window. Input of parameters

After inputting general properties, the appropriate UD model can be chosen from the available models that have been found by PLAXIS Input.

The **Mechanical** tabsheet shows two combo boxes; the top combo box lists all the DLLs that contain valid UD models and the next combo box shows the models defined in the selected DLL. Each UD model has its own set of model parameters, defined in the same DLL that contains the model definition.

When an available model is chosen PLAXIS will automatically read its parameter names and units from the DLL and fill the parameter table below.

### 16.3.1 Interfaces

The **Interfaces** tabsheet, [Figure 74](#) (on page 194), contains the material data for interfaces.

Normally, this tabsheet contains the  $R_{inter}$  parameter. For user-defined soil models the interface tabsheet is slightly different as for a user-defined soil model the interface properties cannot be taken from the material set, but should be explicitly defined. The stiffness can be specified in 2 ways through the *Stiffness determination* parameter: either a *Direct* specification of the interface stiffness parameters  $k_n$  and  $k_s$ , or by specification of the interface stiffness from the oedometer stiffness modulus,  $E_{oed}^{ref}$ . Additionally, the interface strength parameters  $c_{inter}$ ,  $\phi_{inter}$  and  $\psi_{inter}$  must be specified. Hence, the interface shear strength is directly given in strength

## User-defined soil models [ADV]/[ULT] + [GSE]

Input of UD model parameters via user-interface

parameters instead of using a factor relating the interface shear strength to the soil shear strength, as it is the case in PLAXIS models.

Property	Unit	Value
<b>Stiffness</b>		
Stiffness determination		From Eoed
$E_{oed}^{ref}$	kN/m <sup>2</sup>	0.000
UD-Power		0.000
$UD-P^{ref}$	kN/m <sup>2</sup>	100.0
<b>Strength</b>		
$c_{ref,inter}$	kN/m <sup>2</sup>	0.000
$\phi_{inter}$ (phi)	°	0.000
$\psi_{inter}$ (psi)	°	0.000
Consider gap closure		<input checked="" type="checkbox"/>
<b>Groundwater</b>		
Cross permeability		Impermeable
Drainage conductivity, dk	m <sup>3</sup> /day/m	0.000
<b>Thermal</b>		
$R_{thermal}$	m <sup>2</sup> K/kW	0.000

Figure 74: Interface tabsheet

In addition, two parameters are included to enable stress-dependency of the interface stiffness according to a power law formulation:

$$E_{oed}(\sigma'_n) = E_{oed}^{ref} \left( \frac{\sigma'_n}{UD-P^{ref}} \right)^{UD-Power} \quad Eq. [352]$$

where

$UD-Power$	=	Rate of stress dependency of the interface stiffness
$UD-P^{ref}$	=	Reference stress level (usually 100 kN/m <sup>2</sup> )
$\sigma'_n$	=	Effective normal stress in the interface stress point.

After having entered values for all parameters, the data sets can be assigned to the corresponding soil clusters, in a similar way as for the existing material models in PLAXIS. The user-defined parameters are transmitted to the calculation program and appear for the appropriate stress points as Props(1..50) in the User\_Mod subroutine.

## Application of advanced soil models

In this chapter, advanced soil models will be utilised in various applications in order to illustrate the particular features of these models.

### 17.1 Hardening Soil model: Response in drained and undrained triaxial tests

In this section, the Hardening Soil model is utilised for the simulations of drained and undrained triaxial tests. Arbitrary sets of model parameters, [Table 11](#) (on page 195), representing sands of different properties, are considered.

**Table 11: Arbitrary Hardening Soil parameters for sands of different densities**

Parameter	Loose	Medium	Dense	Unit
$E_{50}^{ref}$ (for $p_{ref} = 100$ kPa)	20000	30000	40000	[kN/m <sup>2</sup> ]
$E_{ur}^{ref}$ (for $p_{ref} = 100$ kPa)	60000	90000	120000	[kN/m <sup>2</sup> ]
$E_{oed}^{ref}$ (for $p_{ref} = 100$ kPa)	20000	30000	40000	[kN/m <sup>2</sup> ]
Cohesion $c$	0.0	0.0	0.0	[kN/m <sup>2</sup> ]
Friction angle $\varphi$	30	35	40	°
Dilatancy angle $\psi$	0	5	10	°
Poisson's ratio $\nu_{ur}$	0.2	0.2	0.2	-
Power $m$	0.5	0.5	0.5	-
$K_0^{nc}$ (using Cap)	0.5	0.43	0.36	-
Tensile strength	0.0	0.0	0.0	[kN/m <sup>2</sup> ]

## Application of advanced soil models

Hardening Soil model: Response in drained and undrained triaxial tests

Parameter	Loose	Medium	Dense	Unit
Failure ratio	0.9	0.9	0.9	-

A triaxial test can simply be modelled by means of an axisymmetric geometry of unit dimensions (1m x 1m), that represent a quarter of the soil specimen, [Figure 75](#) (on page 196). These dimensions are not realistic, but they are selected for simplicity. The dimension of the model does not influence the results, provided that the soil weight is not taken into account. In this configuration the stresses and strains are uniformly distributed over the geometry. The deformation magnitudes in  $x$ - and  $y$ -direction of the top right hand corner correspond to the horizontal and vertical strains respectively.

The left hand side and the bottom of the geometry are axes of symmetry. At these boundaries the displacements normal to the boundary are fixed and the tangential displacements are kept free to allow for 'smooth' movements. The remaining boundaries are fully free to move.

The value of the applied loads can be controlled by the load multipliers such as  $\Sigma MloadA$  and  $\Sigma MloadB$ . However, in PLAXIS 2D, and as described in the *Reference Manual*, the load configurations and magnitudes can be specified in the Input program. Then in the calculation program these loads can be activated or deactivated by means of the **Staged construction** option. For this case, and to simulate the confining pressure  $p'$ , distributed loads of -100 kN/m<sup>2</sup> representing the principal stresses  $\sigma'_1$  (load A) and  $\sigma'_3$  (load B) are applied in the **Input**, as shown in [Figure 75](#) (on page 196).

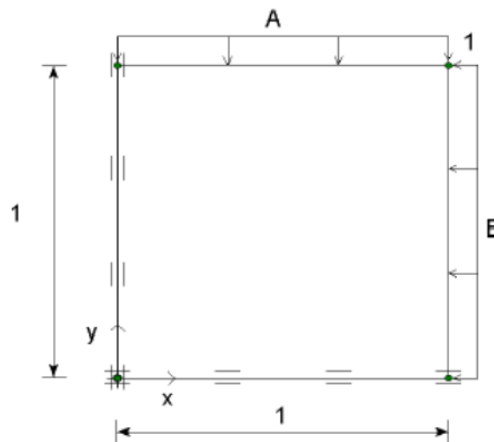


Figure 75: Simplified configuration of a triaxial test

A very coarse mesh is sufficient for this simple geometry. Initial stresses and steady pore pressures are not taken into account.

In the calculation program, the calculation of all phases can be done by means of the **Staged construction** process. In the first phase, the confinement pressure  $p'$  is applied by activating load A and B. In the second phase the displacements are reset to zero and the sample is vertically loaded up to failure while the horizontal load is kept constant. This implies modification of load A by double clicking the load in the geometry model. As a result a **load** window appears in which the input values of the load can be changed. (Details of the procedure can be found in the *Reference* and *Tutorial manuals*) The latter phase is carried out for drained as well as undrained conditions.

These calculations are performed for the three different sets of material parameters, [Table 11](#) (on page 195). The computational results are presented in the figures on the following pages.

## Application of advanced soil models

Hardening Soil model: Response in drained and undrained triaxial tests

[Figure 76](#) (on page 197) shows the principal stress difference versus the axial strain for the drained condition. This shows a hyperbolic relationship between the stress and the strain, which is typical for the Hardening Soil model. Obviously, the failure level is higher when the sand is denser. The Hardening Soil model does not include softening behaviour, so after reaching failure the stress level does not reduce, at least in the drained tests.

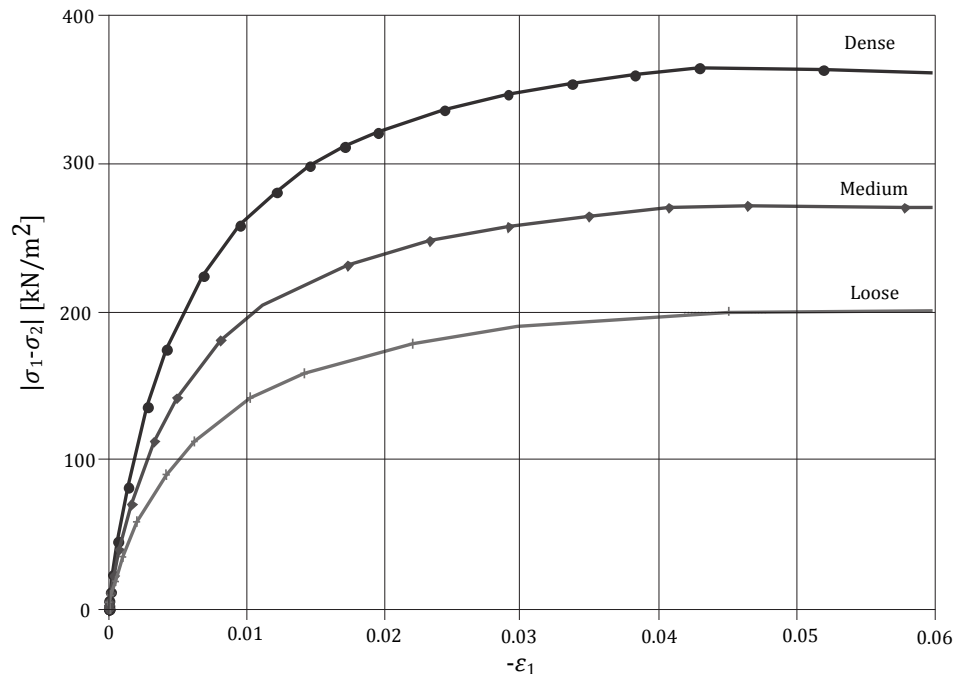


Figure 76: Results of drained triaxial tests using the Hardening Soil model, Principal stress difference versus axial strain.

[Figure 77](#) (on page 197) shows the axial strain versus the volumetric strain for the drained test. This graph clearly shows the influence of dilatancy in the denser sands. In contrast to the Mohr-Coulomb model, the transition from elastic behaviour to failure is much more gradual when using the Hardening Soil model. In fact, in the Hardening Soil model, plastic strain occurs immediately after load application.

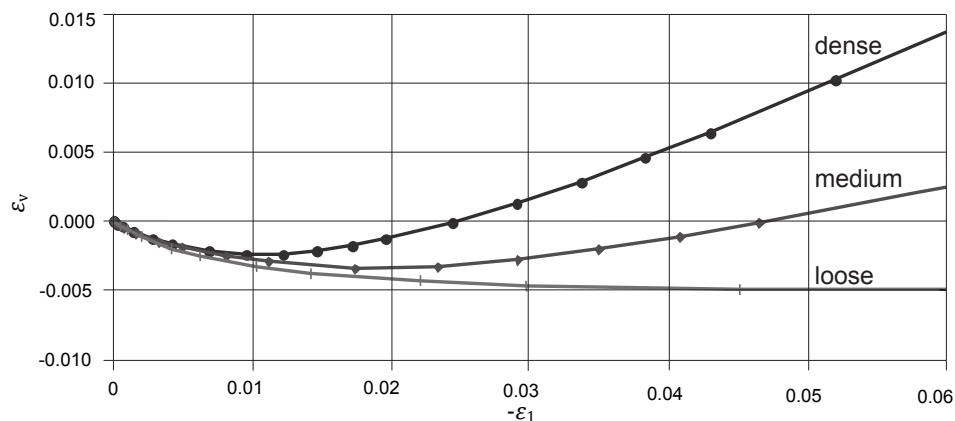


Figure 77: Results of drained triaxial tests using the Hardening Soil model, Volumetric strain versus axial strain

## Application of advanced soil models

### Hardening Soil model: Response in drained and undrained triaxial tests

In the undrained tests, [Figure 78](#) (on page 198), the failure level is, in principle, lower than that of the drained tests. However, for the medium and dense sands the stress level continues to increase after reaching the failure level due to the fact that dilatancy occurs which causes reduction of excess pore pressures and thus increase of the effective stresses. This can be seen in [Figure 79](#) (on page 198).

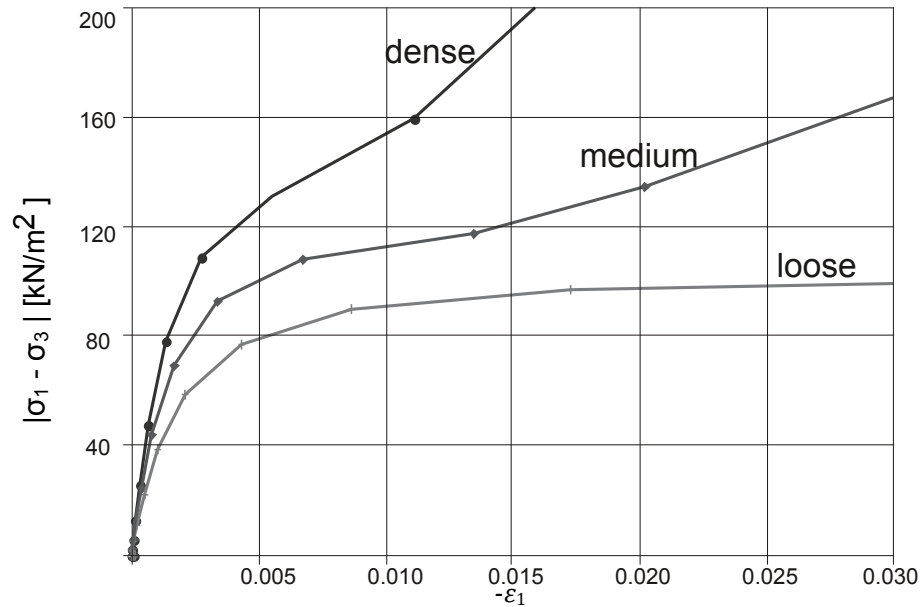


Figure 78: Results of undrained triaxial tests using the Hardening Soil model, Principal stress difference versus axial strain

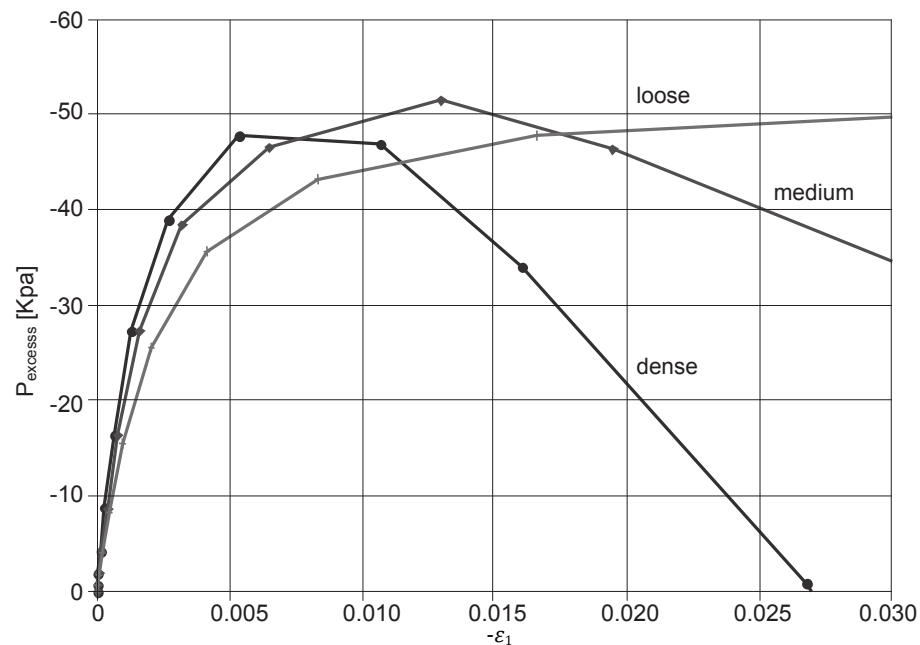


Figure 79: Results of undrained triaxial tests using the Hardening Soil model, Excess pore pressure vs axial strain

## Application of advanced soil models

### Application of the Hardening Soil model on real soil tests

[Figure 80](#) (on page 199) shows the effective stress paths, for the medium sand, during both the drained and undrained tests. During first phase (isotropic loading), both tests were drained. In the second phase there is a clear distinction between the two tests. In the undrained test the effective horizontal stress reduces while the vertical stress increases due to the development of excess pore pressures. The decrease in horizontal effective stress is more than when if the Mohr-Coulomb model would have been used. This is attributed to the plastic compaction (Cap hardening) that occurs in the Hardening Soil model.

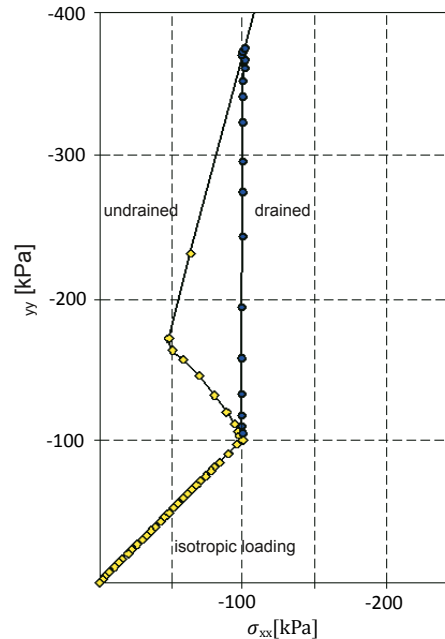


Figure 80: Stress paths for drained and undrained triaxial tests using the Hardening Soil model

## 17.2 Application of the Hardening Soil model on real soil tests

In this section the ability of the Hardening Soil model to simulate laboratory tests on sand is examined by comparing PLAXIS calculation results with those obtained from laboratory tests provided by Prof. J. Desrues (University Joseph Fourier, Grenoble, France). Extensive laboratory tests were conducted on loose and dense Hostun sand. On the basis of these tests the model parameters for the Hardening Soil model were determined and they are presented in [Table 12](#) (on page 199).

Table 12: Hardening Soil parameters for loose and dense Hostun sand

Parameter	Loose sand	Dense sand	Unit
Unit weight $\gamma$	17	17.5	kN/m <sup>3</sup>
$E_{50}^{ref} (p_{ref} = 100 \text{ kPa})$	20000	37000	kN/m <sup>2</sup>
$E_{ur}^{ref} (p_{ref} = 100 \text{ kPa})$	60000	90000	kN/m <sup>2</sup>

## Application of advanced soil models

Application of the Hardening Soil model on real soil tests

Parameter	Loose sand	Dense sand	Unit
$E_{oed}^{ref} (p_{ref} = 100 \text{ kPa})$	16000	29600	kN/m <sup>2</sup>
Cohesion $c'$	0.0	0.0	kN/m <sup>2</sup>
Friction angle $\varphi'$	34.0	41.0	°
Dilatancy angle $\psi$	0.0	14.0	°
Poisson's ratio $\nu_{ur}$	0.2	0.2	-
Power $m$	0.65	0.5	-
$K_0^{nc}$	0.44	0.34	-
Tensile strength	0.00	0.00	kN/m <sup>2</sup>
Failure ratio	0.9	0.9	-

### 17.2.1 Triaxial Test

Standard drained triaxial tests were performed on loose and dense sand specimens. The procedure for the simulation of the triaxial tests in PLAXIS has been described in [Hardening Soil model: Response in drained and undrained triaxial tests](#) (on page 195). In the first phase the sample is isotropically compressed up to a confining pressure of  $p' = -300 \text{ kN/m}^2$ . In the second phase the sample is vertically loaded up to failure while the horizontal stress (confining pressure) is kept constant. The computational results and the measured data are presented in [Figure 81](#) (on page 200) to [Figure 84](#) (on page 202).

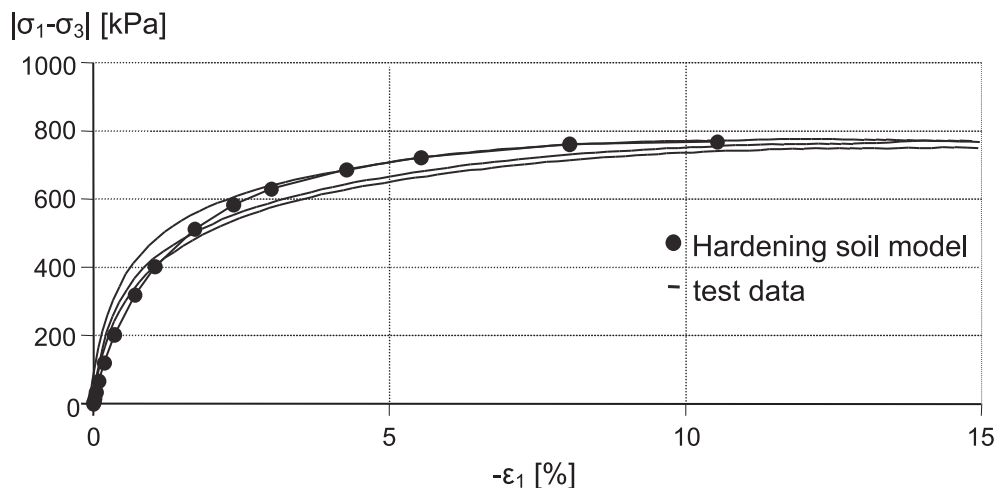


Figure 81: Results of drained triaxial tests on loose Hostun sand, deviatoric stress versus axial strain

## Application of advanced soil models

Application of the Hardening Soil model on real soil tests

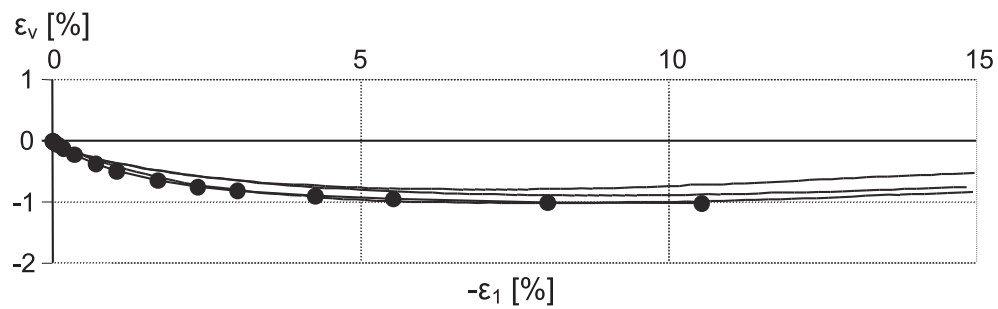


Figure 82: Results of drained triaxial tests on loose Hostun sand, volumetric strain versus axial strain

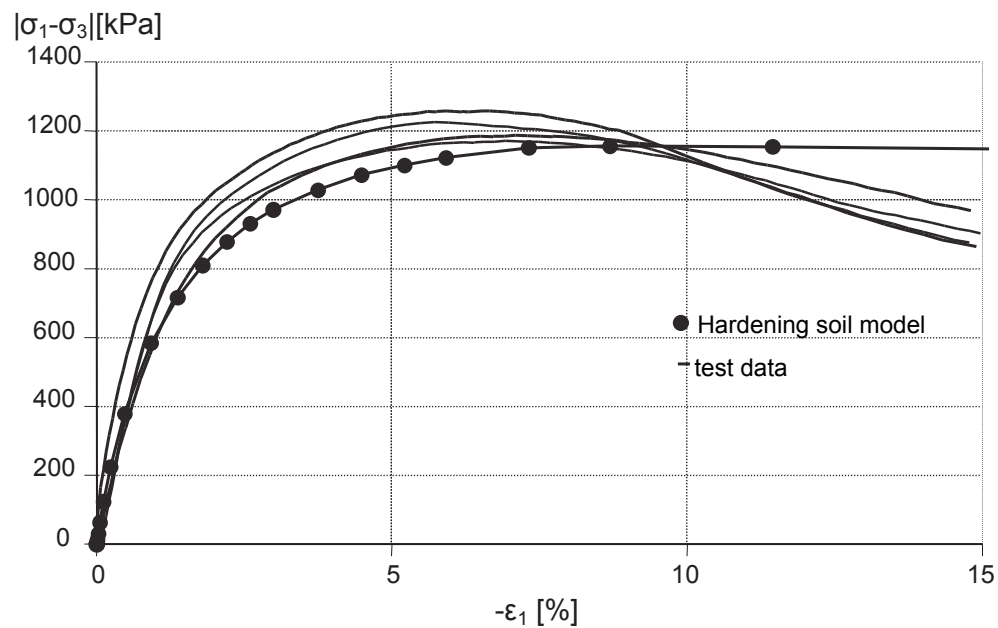


Figure 83: Results of drained triaxial tests on dense Hostun sand, deviatoric stress versus axial strain

## Application of advanced soil models

### Application of the Hardening Soil model on real soil tests

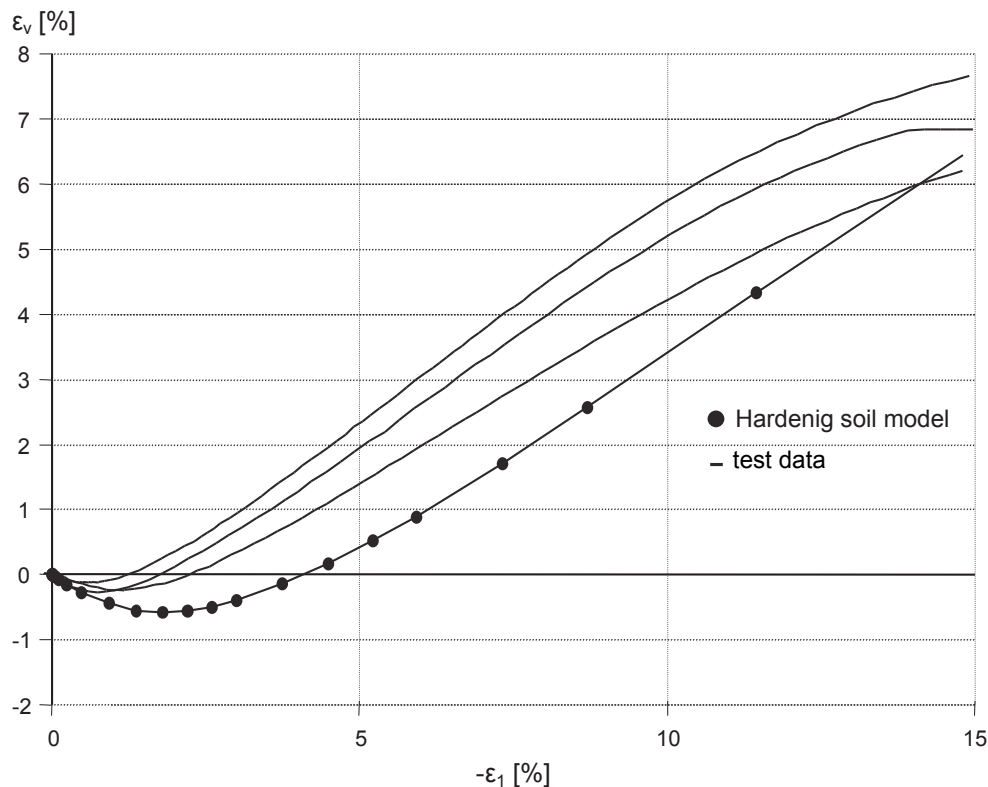


Figure 84: Results of drained triaxial tests on dense Hostun sand, volumetric strain versus axial strain

The figures show that the computational results match reasonably with the test data. It can be seen that the material response (measured and computed) show gradual transition from elastic to plastic behaviour. As such the relation between the deviatoric stress and the axial strain can be approximated by a hyperbola.

The failure level is fully controlled by the friction angle (the cohesion is zero). The test results on dense sand show softening behaviour after the peak load has been reached. Modelling of the softening behaviour, however, is not incorporated in the Hardening Soil model, and thus, the deviatoric stress remains constant. It can also be seen from the test data that the dilatancy reduces during softening. However, in the Hardening Soil model the dilatancy continues to infinity, unless the dilatancy cut-off option has been used.

### 17.2.2 Oedometer test

As for the triaxial tests, a set of oedometer tests on both loose and dense sands ([Table 12](#) (on page 199)) was conducted. In PLAXIS the oedometer test is simulated as an axisymmetric geometry with unit dimensions ([Figure 85](#) (on page 203)). A coarse mesh is sufficient for this case.

## Application of advanced soil models

Application of the Hardening Soil model on real soil tests

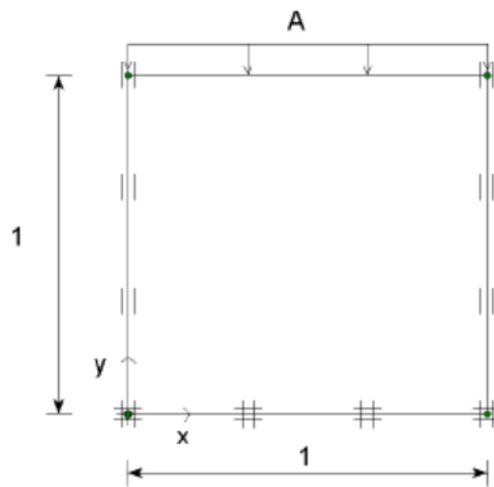


Figure 85: Simplified configuration of an oedometer test

The computational results as compared with those obtained from the laboratory tests are shown in [Figure 86](#) (on page 203) and [Figure 87](#) (on page 204).

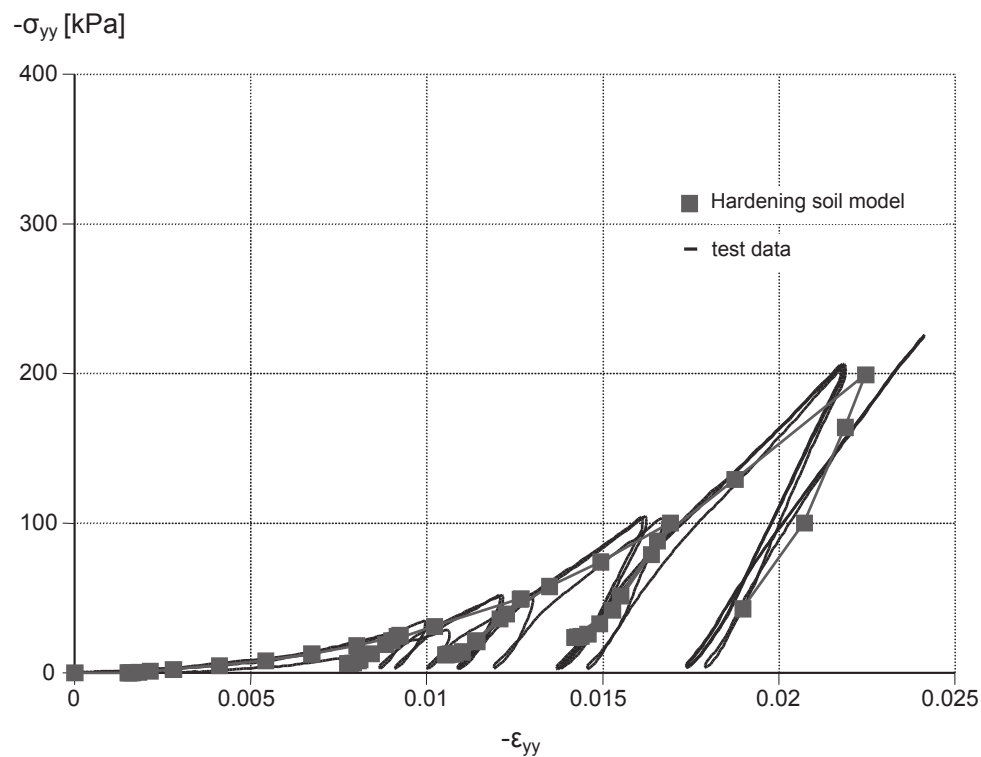


Figure 86: Results of oedometer test on loose Hostun sand, axial stress versus axial strain

## Application of advanced soil models

### Application of the Hardening Soil model on real soil tests

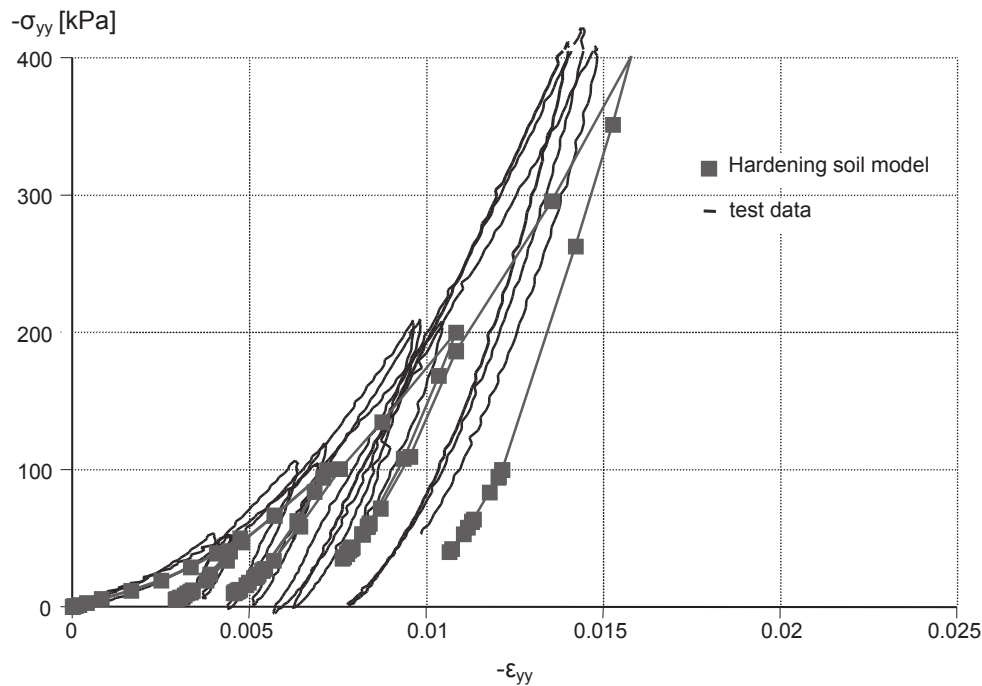


Figure 87: Results of oedometer test on dense Hostun sand, axial stress versus axial strain

From a stress free state the loose sand sample is loaded consecutively to 25 kPa, 50 kPa, 100 kPa and 200 kPa with intermediate unloading. The dense sand sample is loaded to 50 kPa, 100 kPa, 200 kPa and 400 kPa with intermediate unloading.

As it can be seen, the computational results show a reasonable agreement with the test data. No doubt, distinction should be made between loose and dense soil, but it seems that for a soil with a certain density the stiffness behaviour under different stress paths can be well captured with a single set of model parameters. (A small offset of 0.15% has been applied to the computational results of the loose sample in order to account for the relative soft response at the beginning of the test.)

### 17.2.3 Pressiometer test

In this section the Pressiometer test is simulated and results from PLAXIS 2D and laboratory tests ([Branque, 1997](#) (on page 246)) are compared. Laboratory testing results on dense sand with material parameters listed in [Table 12](#) (on page 199) are used.

In the field, the pressiometer of 0.044 m diameter covered with a membrane of 0.16 m height is attached to the Cone penetration shaft. In the laboratory, the pressiometer is attached to a 0.044 m pipe ( $r_0 = 0.022$  m) and placed in a circular calibration chamber with a diameter of 1.2 m and a height of 1.50 m. A high overburden pressure of 500 kPa is applied to the surface to simulate the stress state at larger depths.

In PLAXIS 2D a quarter of the geometry is simulated by an axisymmetric model ([Figure 88](#) (on page 205)). The left boundary is placed 0.022 m away from the vertical axis of symmetry. A line displacement is generated at the left model boundary, set to be *free* in vertical direction and *fixed* in horizontal direction. The overburden pressure is simulated by the load A, and the volumetric expansion of the pressiometer is simulated by imposing

## Application of advanced soil models

### Application of the Hardening Soil model on real soil tests

a horizontally distributed load, load B (Figure 88 (on page 205)). Therefore the initial boundary conditions have to be changed at the level of the pressiometer in order to allow for horizontal displacements.

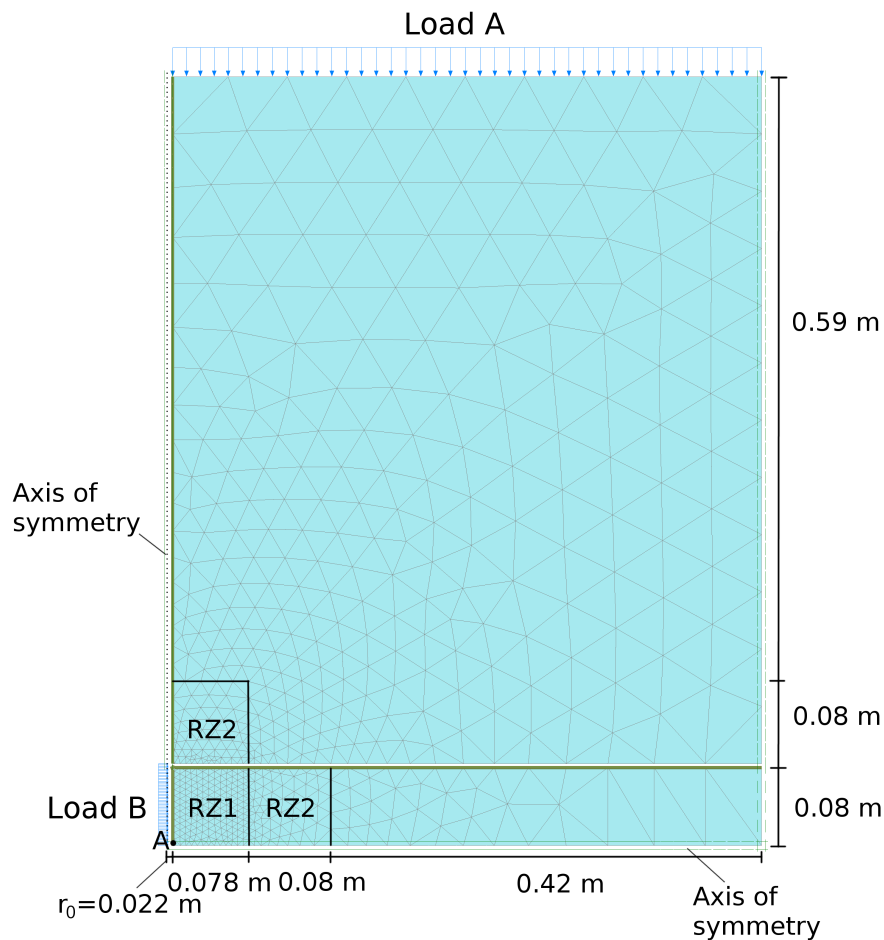


Figure 88: Model geometry and generated mesh

To allow for a discontinuity in horizontal displacements, a vertical interface along the shaft of the pressiometer borehole and a horizontal interface just above the pressiometer are introduced. Both interfaces are set rigid ( $R_{inter} = 1.0$ ). Extra geometry lines are created around the pressiometer to locally generate a finer mesh (Figure 88 (on page 205)). A *Coarseness factor* equal to 0.1 is used for the refinement zone 1 (RZ1) and a *Coarseness factor* of 0.3 is used for the refinement zone 2 (RZ2). For the **Element distribution** the **Medium** option is selected.

After the generation of initial stresses in the Initial Phase, the vertical overburden load (load A) is applied in **Phase 1**. The left model boundary is horizontally fixed via the line displacement as discussed above, while the bottom and right model boundaries are set to **Normally fixed** via the Deformations option in the **Model explorer** window. A plastic calculation is performed. For the subsequent calculation phases, the left model boundary should be set to **Free** via the **Deformations** option in the **Model explorer** window.

In **Phase 2**, the line displacement which is placed at the level of the pressiometer, at the left boundary, is deactivated. The Load B is activated in order to maintain equilibrium, i.e. zero deformation. The magnitude of this load increases linearly with depth and it is calculated based on the vertical stress and Jaky's formula (for normally consolidated soils). Thus the horizontal load acting on the node located at the top of the pressiometer

## Application of advanced soil models

### Application of the Hardening Soil model on real soil tests

equals 176.0 kPa and the horizontal load acting on the node located at the bottom model boundary equals 176.5 kPa. A plastic calculation is performed in Phase 2 as well.

In both Phases 1 and 2, the **Tolerated error** is set equal to 0.0001 and the **Max load fraction per step** is set to 0.01 to increase the accuracy of the numerical calculation. This is important in order to meticulously replace the horizontal fixity with the horizontal load at the level of the pressiometer in Phase 2.

#### Note:

Note that the values at the edges of the horizontal load mentioned above are calculated analytically and may slightly differ from the numerical results at the corresponding nodes, at the end of Phase 1. This is because the numerically obtained values depend on the selected number of mesh elements (mesh discretization) and on the used numerical settings for the plastic calculation in Phase 1. The user may check this discrepancy and if necessary use the numerical values to maintain equilibrium.

In the following calculation **Phase 3**, the pressure (load B) is further increased by use of *Staged construction*. Thus the load B is set equal to 2500 kPa. An *Updated mesh analysis* is used. The *Tolerated error* is 0.01 (default value) and the **Max load fraction per step** is set to 0.1. The results of this calculation are presented in [Figure 89](#) (on page 206) and [Figure 90](#) (on page 207).

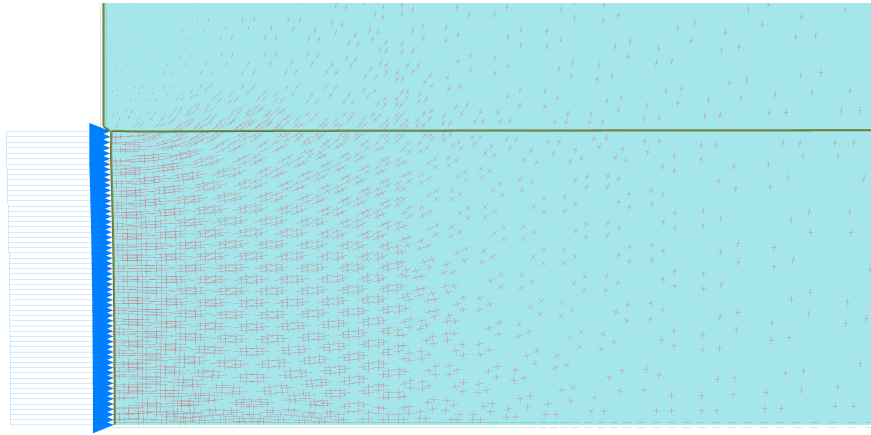


Figure 89: Effective principal stress distribution at the vicinity of the pressiometer, for a pressure of 2427 kPa (scaled up  $4 \times 10^{-6}$  times)<sup>-6</sup> times)

[Figure 89](#) (on page 206) shows details of effective principal stress distribution when the pressure in the pressiometer is 2427 kPa. The high passive stresses appear very locally near the pressiometer. Just above the pressiometer the vertical stress is very low due to arching effects. Away from the pressiometer, a  $K_0$ -like stress state exists.

[Figure 90](#) (on page 207) depicts a comparison of the numerical results with those obtained from the laboratory test. A Node A at the interface, at the bottom left corner of the model, is selected to illustrate the results ([Figure 88](#) (on page 205)). In [Figure 90](#) (on page 207) the pressiometer pressure  $P$  is plot against volumetric deformation  $\Delta V/V_0$ . Because the calculation in Phase 3 was run by accounting for large deformations (updated mesh analysis), the pressure  $P$  in the pressiometer is calculated by  $\backslash eqnref{PressiometerPressureP}$ , based on the output quantity  $\Sigma Mstage$ , the value of the applied Load B in Phase 2 ( $LoadB_2 = 176.5$  kPa), the value of the applied Load B in Phase 3 ( $LoadB_3 = 2500$  kPa) and a correction factor to account for large deformations:

$$P = [Load B_2 + \Sigma Mstage (Load B_3 - Load B_2)] \frac{r_0}{r_0 + u_{rr}} \quad Eq. [353]$$

## Application of advanced soil models

### Application of the Hardening Soil model on real soil tests

where

$$\begin{aligned} r_0 &= \text{Initial radius (0.022 m)} \\ u_{rr} &= \text{Radial deformation of the Node A} \end{aligned}$$

#### Note:

By considering updated mesh analysis, the area  $E$  upon which pressure  $P$  acts, should be adjusted to the increasing radius, from  $r_0$  to  $r_0 + u_{rr}$ . Assuming an angle  $\theta$  of 1 rad, the length of the corresponding arc is  $s = r \theta$ . The area  $E$  is equal to the length  $s$  times the height of the membrane  $H$  (0.08 m). Force equilibrium between the initial state ( $r_0$ ) and every next step of the calculation ( $r_0 + u_{rr}$ ) results in the correction factor  $\frac{r_0}{r_0 + u_{rr}}$ . The latter is taken into account in Eq. [353].

The volumetric deformation  $\Delta V/V_0$  cannot be directly obtained from PLAXIS and it is calculated by Eq. [354], based on the initial radius  $r_0$  and the lateral expansion  $u_{rr}$  of the pressiometer at the Node A:

$$\frac{\Delta V}{V_0} = \frac{(r_0 + u_{rr})^2 - r_0^2}{r_0^2} \quad \text{Eq. [354]}$$

Based on [Figure 90](#) (on page 207) it is concluded that the agreement between the numerical results and the experimental data is very good, both for the initial part of the loading curve and for larger volumetric deformations up to 30%. The original set of parameters for the dense sand that were derived from triaxial testing seem to match the pressiometer data quite well.

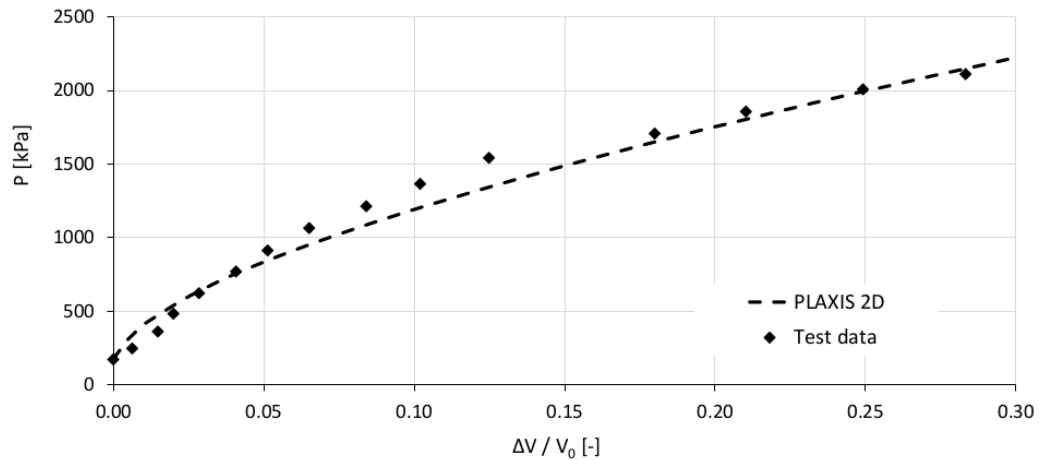


Figure 90: Comparison of numerical results and pressiometer test data

## 17.2.4 Conclusions of the Application of the Hardening Soil model on real soil tests

The test results indicate that by using the Hardening Soil model it is possible to simulate different laboratory tests with different stress paths. This cannot be obtained with simple models such as the Mohr-Coulomb model without changing input parameters. Hence, the parameters in the Hardening Soil model are consistent and more

## Application of advanced soil models

### Application of the Hardening Soil model with small-strain stiffness on real soil tests

---

or less independent from the particular stress path. This makes the Hardening Soil model a powerful and an accurate model, which can be used in many applications.

## 17.3 Application of the Hardening Soil model with small-strain stiffness on real soil tests

In this section, the ability of the Hardening Soil model with small-strain stiffness (*HS small model*) to simulate laboratory tests is examined. Both, the laboratory test data and the basic HS parameters are identical to those presented in the previous section. The two additional small strain parameters used in the Hardening Soil model are quantified in [Table 13](#) (on page 208).

**Table 13: Additional HSsmall model parameter for loose and dense Hostun sand**

Parameter	Loose sand	Dense sand	Unit
$G_0^{ref} (p_{ref} = 100 \text{ kPa})$	70000	112500	[kN/m <sup>2</sup> ]
$\gamma_{0.7}$	0.0001	0.0002	[-]

Triaxial tests on loose and dense Hostun sand are presented in [Figure 91](#) (on page 209) and [Figure 92](#) (on page 210) respectively. As a reference, the previously obtained results from the Hardening Soil model are plotted as well.

## Application of advanced soil models

Application of the Hardening Soil model with small-strain stiffness on real soil tests

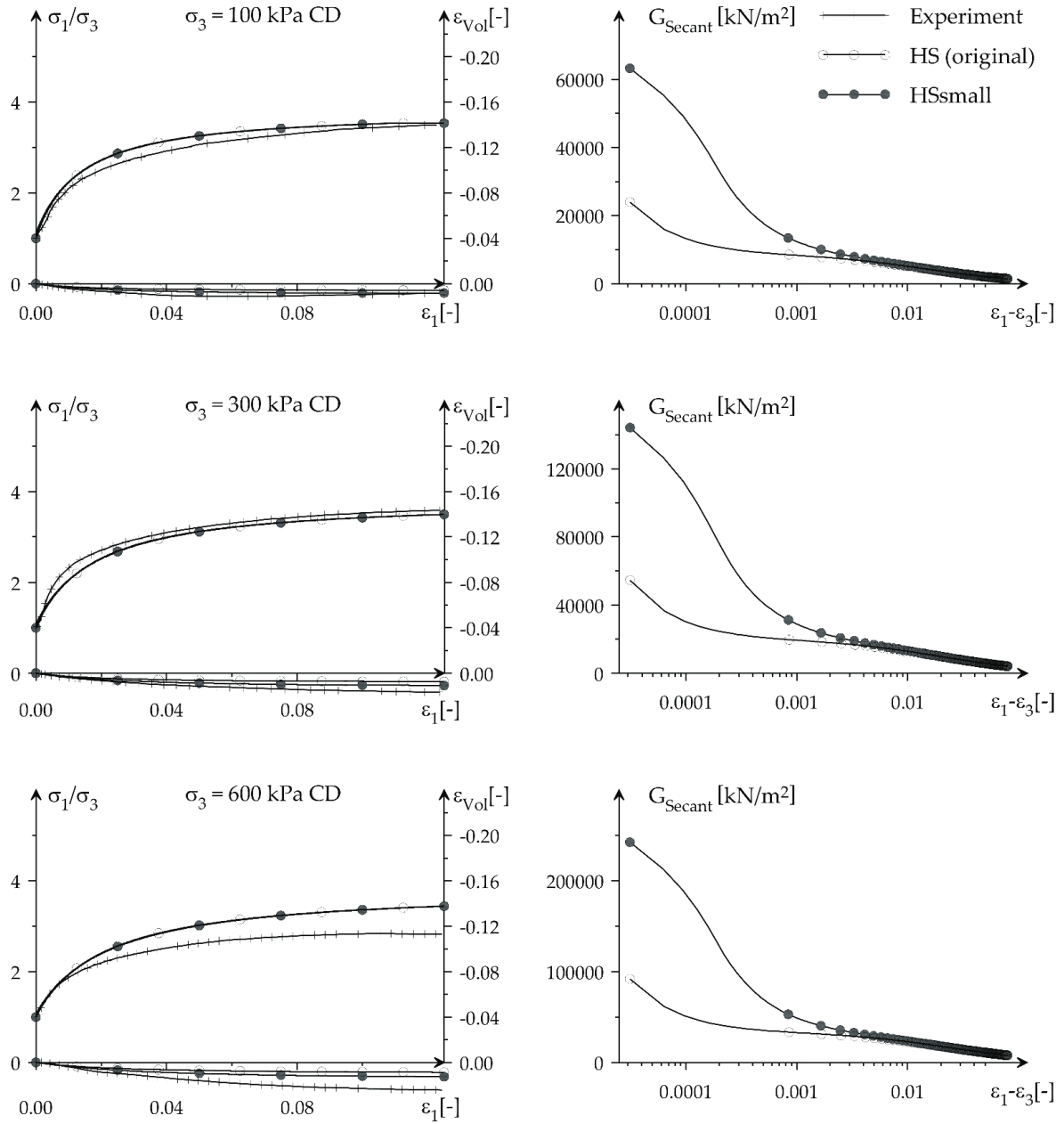


Figure 91: Excavation Drained triaxial tests on loose Hostun sand at confining pressures of 100, 300, and 600 kPa.  
Left: Stress-strain data. Right: Shear modulus reduction

## Application of advanced soil models

### Application of the Hardening Soil model with small-strain stiffness on real soil tests

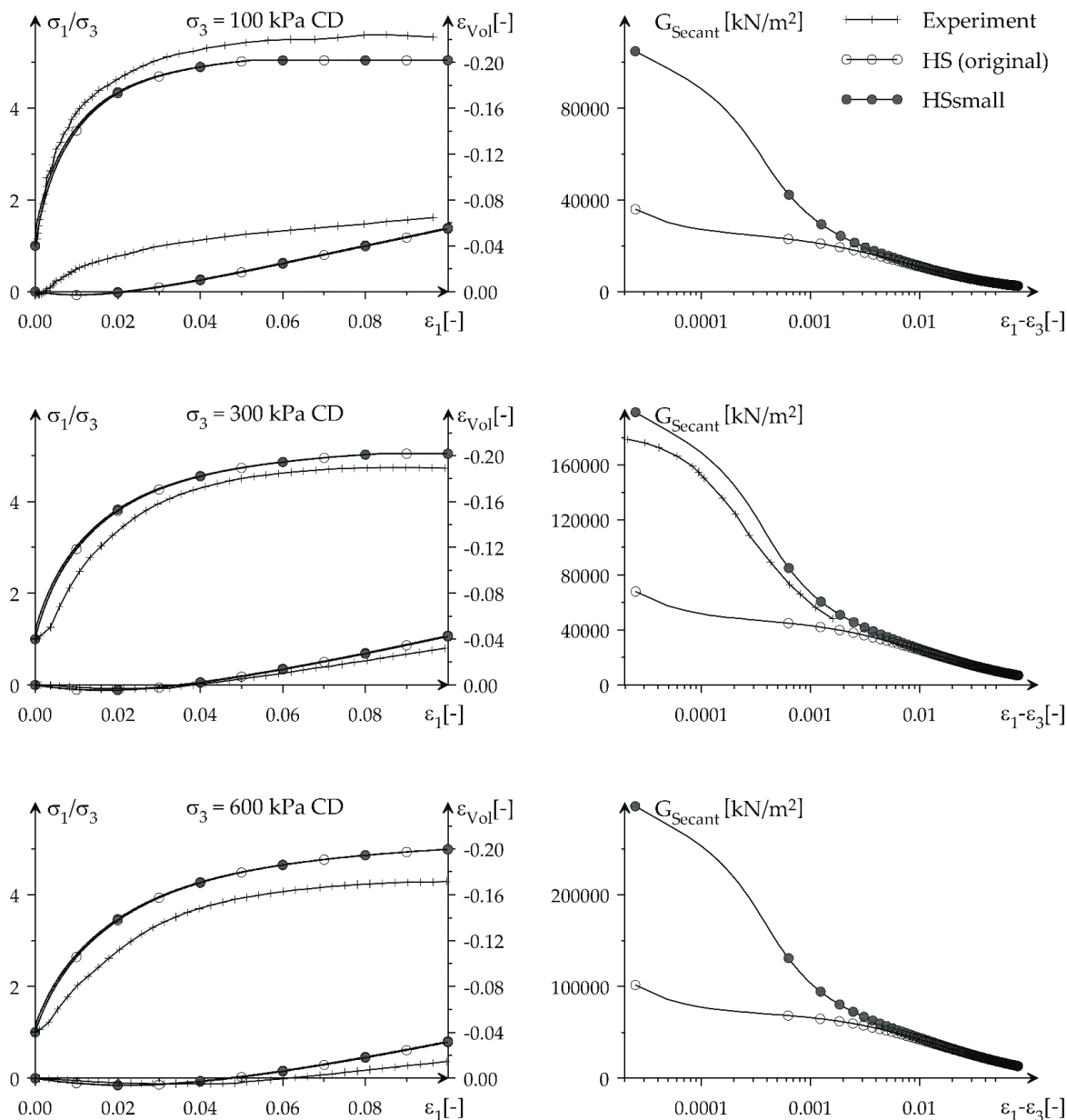


Figure 92: Drained triaxial tests on dense Hostun sand at confining pressures of 100, 300, and 600 kPa. Left: Stress-strain data. Right: Shear modulus reduction

The overall stress-strain data obtained from both models seems almost identical. Only a closer look at the small-strain domain shows a clear difference: The Hardening Soil model with small-strain stiffness follows a S-shaped stiffness reduction curve with much higher initial stiffness than the one of the Hardening Soil model. Generally, both models match the test data at different confining pressures reasonably well.

Figure 93 (on page 211) presents results from a cyclic triaxial test by Rivera & Bard on dense sand. The Hardening Soil model with small-strain stiffness simulation of the test shows material damping which could not be obtained when simulating the test with the Hardening Soil model. As virgin loading is conducted in

## Application of advanced soil models

### Soft Soil Creep model : Undrained triaxial tests at different loading rates

triaxial compression, the unloading sequence in triaxial extension gives some plasticity. Therefore the first unloading / reloading loop is not closed.

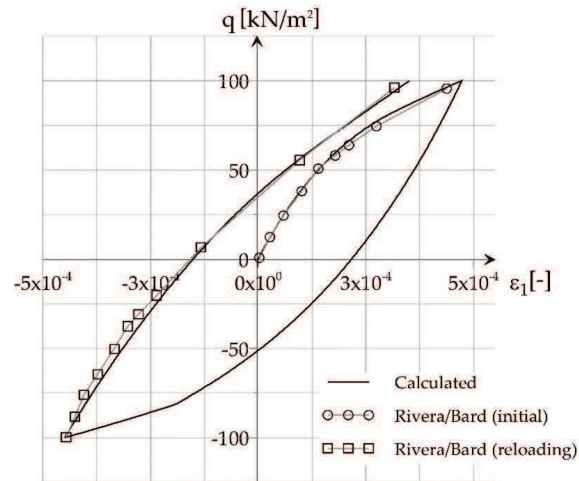


Figure 93: Hysteresis loop in a drained triaxial test on dense Hostun sand. Test data published in Biarez & Hicher (1994).

## 17.4 Soft Soil Creep model : Undrained triaxial tests at different loading rates

In this section the Soft Soil Creep model (see [Soft Soil Creep model \(time dependent behaviour\) \[ADV\]](#) (on page 120)) is utilised for the simulation of clay in an undrained triaxial test, at various strain rates. The model parameters are obtained from test results on Haney Clay and are listed in [Table 14](#) (on page 211) .

The initial isotropic preconsolidation pressure  $P_p = 373 \text{ kN/m}^2$ , as reported in the literature, is obtained by specifying a POP of  $433 \text{ kN/m}^2$  in the initial conditions.

**Table 14: Soft Soil Creep model parameters for Haney clay**

Parameter	Symbol	Value	Unit
Modified compression index	$\lambda^*$	0.105	-
Modified swelling index	$\kappa^*$	0.016	-
Secondary compression index	$\mu^*$	0.004	-
Poisson's ratio	$\nu_{ur}$	0.15	-
Cohesion	$c$	0.0	[kN/m²]

## Application of advanced soil models

Soft Soil Creep model : Undrained triaxial tests at different loading rates

Parameter	Symbol	Value	Unit
Friction angle	$\varphi$	32	[°]
Dilatancy angle	$\psi$	0.0	[°]
Coefficient of lateral stress	$K_0^{nc}$	0.61	[-]
Permeability	$k_x, k_y$	0.0001	[m/day]
Pre overburden pressure	$POP$	433	[kN/m <sup>2</sup> ]

Modelling of the triaxial test is as described in [Hardening Soil model: Response in drained and undrained triaxial tests](#) (on page 195). However, here, a quarter of the real dimension of the test set-up is simulated (17.5 x 17.5 mm<sup>2</sup>). [Figure 94](#) (on page 212) illustrates the model geometry. The specimen surfaces (top and right hand side in [Figure 94](#) (on page 212)) are assumed drained whereas the other boundaries are assumed closed.

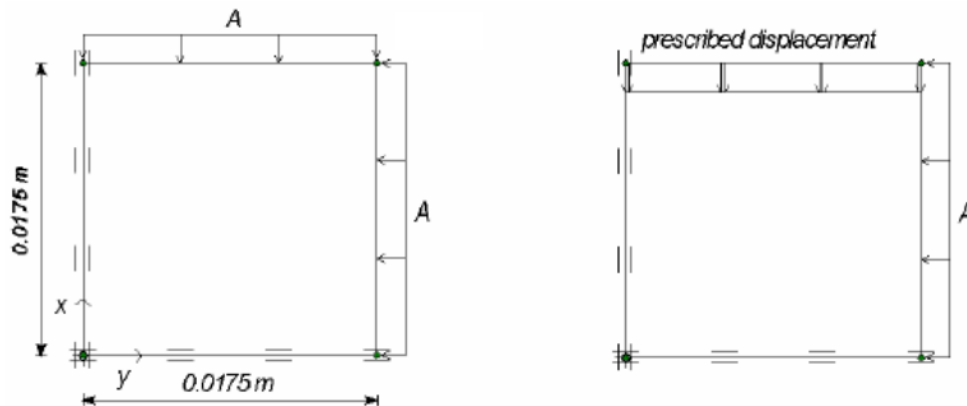


Figure 94: Modelling of triaxial test on Haney clay. Left, Initial configuration. Right, configuration for phases 9 to 11

The *Very coarse* option is selected for the *Element distribution*. To generate the graphs presented further below, mesh points need to be selected. More specifically, a node located at the top model boundary (e.g. with coordinates (0.0175, 0.0175)) is needed to generate [Figure 95](#) (on page 213), while a stress point with coordinates (0.0110, 0.0050) is needed for [Figure 96](#) (on page 213).

## Application of advanced soil models

Soft Soil Creep model : Undrained triaxial tests at different loading rates

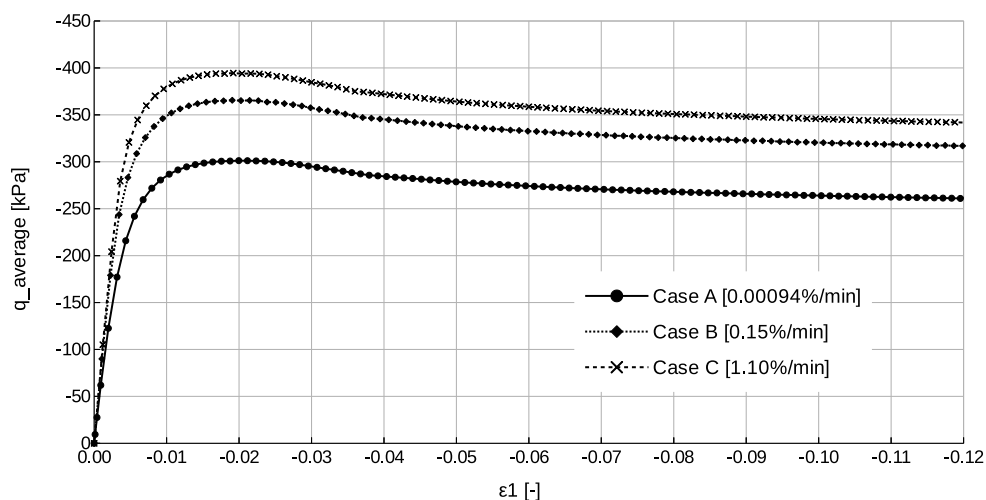


Figure 95: Average deviatoric stress versus axial strain for different strain rates

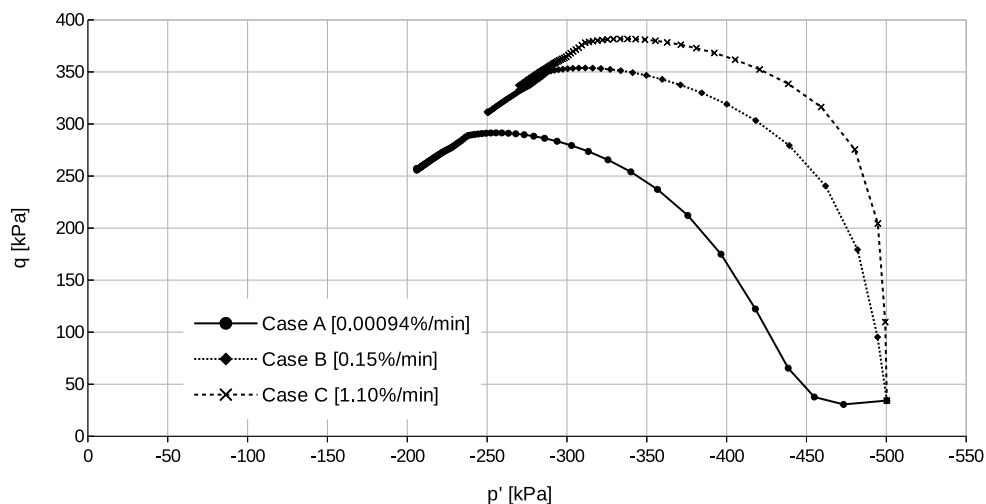


Figure 96:  $p'$ - $q$  stress paths for different strain rates for a point at position (0.0110, 0.0050)

In addition to isotropic loading, prescribed displacements are also applied. Both types of loading are simulated using the *Staged construction* option. During isotropic loading, horizontal and vertical loads are applied. The calculation phases for isotropic loading consist of undrained plastic and consolidation analyses.

After the isotropic loading phases, the displacements are reset to zero. The vertical load is deactivated and the prescribed displacement is activated. Rate of loading is simulated by applying prescribed displacements at different velocities. As such, a total of 12% axial strain (2.1 mm, vertical displacement) is applied in 8.865 days (0.00094%/min), 0.0556 days (0.15%/min) and 0.00758 days (1.10%/min) respectively. Each of the prescribed displacement loading phases 9 to 11 starts from the end of the last consolidation phase 8. The calculation scheme is listed in [Table 15](#) (on page 214).

## Application of advanced soil models

Soft Soil Creep model : Undrained triaxial tests at different loading rates

**Table 15: Loading scheme for triaxial tests at different loading rates**

Phase	Starts from	Calculation type	Top load [kPa]	Side load [kPa]	Displacement [m]	Time interval [day]
1	0	Plastic	-65	-65	Inactive	0.00
2	1	Consolidation	-65	-65	Inactive	0.01
3	2	Plastic	-130	-130	Inactive	0.00
4	3	Consolidation	-130	-130	Inactive	0.01
5	4	Plastic	-260	-260	Inactive	0.00
6	5	Consolidation	-260	-260	Inactive	0.01
7	6	Plastic	-520	-520	Inactive	0.00
8	7	Consolidation	-520	-520	Inactive	0.01
9	8	Plastic	Inactive	-520	0.0021	8.865
10	8	Plastic	Inactive	-520	0.0021	0.0556
11	8	Plastic	Inactive	-520	0.0021	0.00758

The computational results are presented in [Figure 95](#) (on page 213) and [Figure 96](#) (on page 213). [Figure 95](#) (on page 213) illustrates the average deviatoric strain  $q_{average}$  versus the principal strain  $\varepsilon_1$  for phases 9 to 11. The average deviatoric strain is obtained as:

$$q_{average} = \frac{2F_Y}{R^2} \cdot \sigma_3 \quad Eq. [355]$$

where:

$$R=0.0175 \text{ and } \sigma_3=-520 \text{ kN/m}^3$$

In Eq. [355],  $F_Y$  is the reaction force against the applied prescribed displacement ( $Force_Y$ ). The principal strain  $\varepsilon_1$  is obtained by dividing the vertical displacement  $u_y$  of a node located at the top boundary by the height of the model (0.0175 m). The starting point in [Figure 95](#) (on page 213) is deliberately selected to be zero.

Based on [Figure 95](#) (on page 213), it can be seen that the shear strength highly depends on the strain rate; the higher strain rate the higher the shear strength.

[Figure 96](#) (on page 213) shows the  $p'$  -  $q$  stress paths from the prescribed displacement loading phases. For higher strain rates there is a smaller reduction of the mean effective stress, which allows for larger ultimate deviatoric stress. It should be noted that the stress state is not homogeneous at all, because of the inhomogeneous (excess) pore pressure distribution. This is due to the fact that points close to draining boundaries consolidate faster than points at a larger distance.

In addition to the full tests as described before, the last part of the test can also be done in a simplified way using the **Soil Test** facility. Since the **Soil Test** facility operates on a single stress point, it is not possible to start the

## Application of advanced soil models

### Soft Soil Creep model: Response in one-dimensional compression test

undrained triaxial tests from an inhomogeneous stress state, as considered in the full finite element based model. Instead, we start from an isotropic effective stress of  $500 \text{ kN/m}^2$ .

**Table 16: Input parameters for the Soil Test facility**

Input parameter	A(0.00094%/min)	B(0.15%/min)	C(1.10%/min)
Type of test	Triaxial, Undrained	Undrained & Triaxial	Undrained
Direction	Compression	Compression	Compression
Consolidation	Isotropic	Isotropic	Isotropic
Initial effect. stress $ \sigma_3' $	$500 \text{ kN/m}^2$	$500 \text{ kN/m}^2$	$500 \text{ kN/m}^2$
Maximum strain $ \varepsilon_1 $	12.0%	12.0%	12.0%
Time $\Delta t$	8.865 days	0.0556 days	0.00758 days
Number of steps	200	200	200
Vert. precons. stress	$433 \text{ kN/m}^2$	$433 \text{ kN/m}^2$	$433 \text{ kN/m}^2$

## 17.5 Soft Soil Creep model: Response in one-dimensional compression test

In this section the behaviour of the Soft Soil Creep model is illustrated on the basis of a one-dimensional compression test on clay. Two types of analysis are performed. First, the test is simulated assuming drained conditions in order to demonstrate the logarithmic stress-strain relationship and the logarithmic time-settlement behaviour on the long term (secondary compression). Second, the test is simulated more realistically by including undrained conditions and consolidation. Since the consolidation process depends on the drainage length, it is important to use actual dimensions of the test set-up. In this case an axisymmetric configuration with specimen height of 0.01 m, [Figure 97](#) (on page 216), is used. The material parameters are shown in [Table 17](#) (on page 216). The parameter values are selected arbitrarily, but they are realistic for normally consolidated clay. The vertical preconsolidation stress is fixed at 50 kPa (POP = 50 kPa).

## Application of advanced soil models

Soft Soil Creep model: Response in one-dimensional compression test

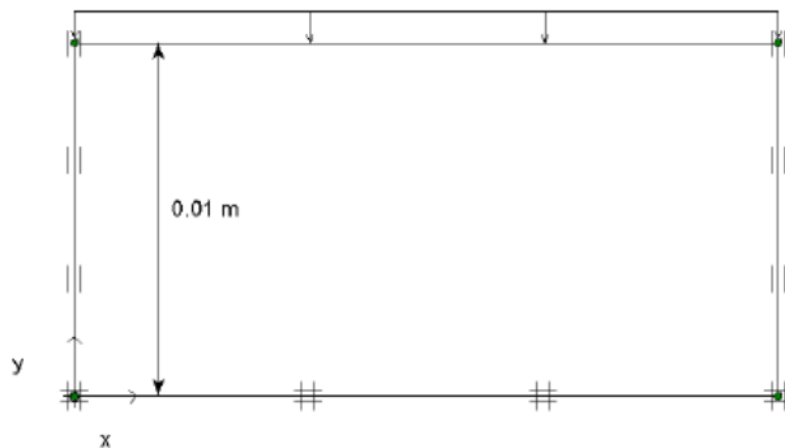


Figure 97: One-dimensional compression test

Table 17: Soft Soil Creep model parameters for one-dimensional compression test

Parameter	Symbol	Value	Unit
Unit Weight	$\gamma$	19	kN/m <sup>3</sup>
Permeability	$k_x, k_y$	0.0001	m/day
Modified compression index	$\lambda^*$	0.10	-
Modified swelling index	$\kappa^*$	0.02	-
Secondary compression index	$\mu^*$	0.005	-
Poisson's ratio	$\nu_{ur}$	0.15	-
Cohesion	$c$	1.0	kN/m <sup>2</sup>
Friction angle	$\varphi$	30	°
Dilatancy angle	$\psi$	0.0	°
Coefficient of lateral stress	$K_0^{nc}$	0.5	-

### 17.5.1 Drained analysis

In the first analysis successive plastic loading steps are applied using drained conditions. The load is doubled in every step using *Staged construction* with time increments of 1 day. After the last loading step an additional creep period of 100 days is applied. The calculation scheme is listed in [Table 18](#) (on page 217). All calculations are performed with a tolerance of 1%.

## Application of advanced soil models

Soft Soil Creep model: Response in one-dimensional compression test

**Table 18: Calculation scheme for the drained case**

Phase	Calculation type	Loading input	Load [kPa]	Time interval [day]	End time [day]
1	Plastic	Staged construction	10	1	1
2	Plastic	Staged construction	20	1	2
3	Plastic	Staged construction	40	1	3
4	Plastic	Staged construction	80	1	4
5	Plastic	Staged construction	160	1	5
6	Plastic	Staged construction	320	1	6
7	Plastic	Staged construction	640	1	7
8	Plastic	Staged construction	640	100	107

### 17.5.2 Undrained analysis

In the second analysis the loading steps are instantaneously applied using undrained conditions. After each loading step a consolidation of 1 day is applied to let the excess pore pressures fully dissipate. After the last loading step, an additional creep period of 100 days is again introduced. The calculation scheme for this analysis is listed in [Table 19](#) (on page 217). All calculations are performed with a reduced tolerance of 1%.

**Table 19: Calculation scheme for second analysis**

Phase	Calculation type	Loading input	Load [kPa]	Time interval [day]	End time [day]
1	Plastic	Staged construction	10	0	0
2	Consolidation	Staged construction	10	1	1
3	Plastic	Staged construction	20	0	1

## Application of advanced soil models

Soft Soil Creep model: Response in one-dimensional compression test

Phase	Calculation type	Loading input	Load [kPa]	Time interval [day]	End time [day]
4	Consolidation	Staged construction	20	1	2
5	Plastic	Staged construction	40	0	2
6	Consolidation	Staged construction	40	1	3
7	Plastic	Staged construction	80	0	3
8	Consolidation	Staged construction	80	1	4
9	Plastic	Staged construction	160	0	4
10	Consolidation	Staged construction	160	1	5
11	Plastic	Staged construction	320	0	5
12	Consolidation	Staged construction	320	1	6
13	Plastic	Staged construction	640	0	6
14	Consolidation	Staged construction	640	1	7
15	Consolidation	Staged construction	640	100	107

[Figure 98](#) (on page 219) shows the load-settlement curves of both analyses. It can be seen that, after consolidation, the results of the undrained test match those of the drained test. The influence of the preconsolidation stress can clearly be seen, although the transition between reloading and primary loading is not as sharp as when using the Soft Soil model. In fact, the results presented here are more realistic. The transition is indeed around 50 kPa.

## Application of advanced soil models

Soft Soil Creep model: Response in one-dimensional compression test

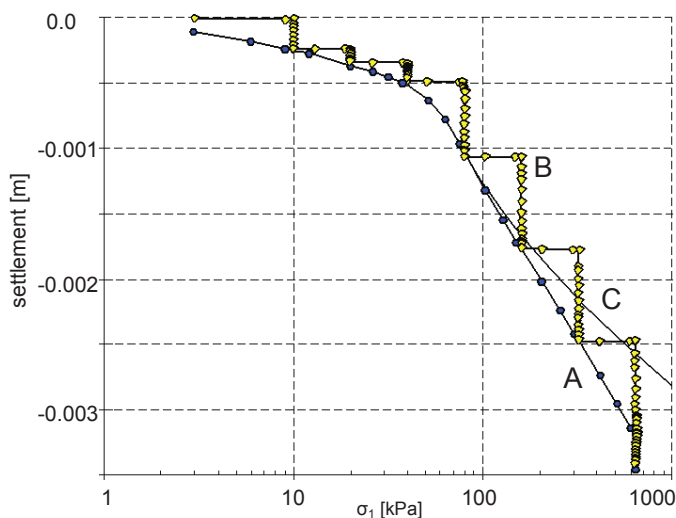


Figure 98: Load-settlement curve of oedometer test with Soft Soil Creep model. A) Transient loading with doubling of loading within one day. B) Instantaneous loading with doubling of load at the beginning of a new day. C) As 'A' using Updated Mesh calculation

From the slope of the primary loading line one can back-calculate the modified compression index  $\lambda^* = \Delta \varepsilon_1 / \ln(\sigma_1 + \Delta \sigma_1) / \sigma_1 \approx 0.10$ . Note that 1 mm settlement corresponds to  $\varepsilon_1 = 10\%$ . For an axial strain of 30% one would normally use an *Updated mesh* analysis, which has not been done in this simple analysis. If, however, the Soft Soil Creep model would have been used in an *Updated mesh* analysis with axial strains over 15% one would observe a stiffening effect as indicated by line C in [Figure 98](#) (on page 219).

[Figure 99](#) (on page 220) shows the time-settlement curves of the drained and the undrained analyses. From the last part of the curve one can back-calculate the secondary compression index  $\mu^* = \Delta \varepsilon_1 / \ln(\Delta t / t_0) \approx 0.005$  (with  $t_0 = 1$  day).

## Application of advanced soil models

Soft Soil Creep model: Response in one-dimensional compression test

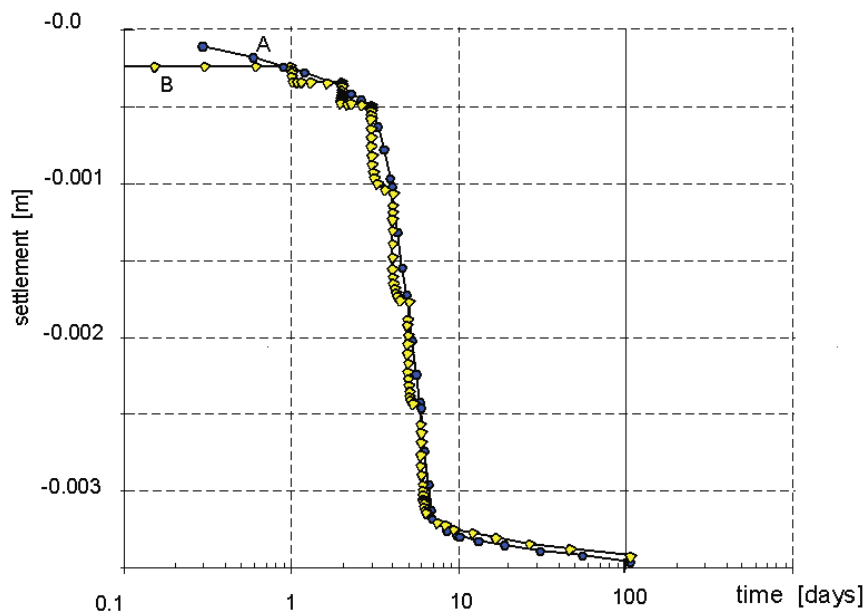


Figure 99: Time-settlement curve of oedometer test with Soft Soil Creep model. A) Transient loading with doubling of loading within one day. B) Instantaneous loading with doubling of load at the beginning of a new day

Another interesting phenomenon is the development of lateral stresses. During primary loading, the lateral stress is determined by  $K_0^{nc}$ , appropriate for normally consolidated soil. During unloading, the lateral stress decreases much less than the vertical stress, so that the ratio  $\sigma'_{xx} / \sigma'_{yy}$  increases.

To show these effects the calculation is continued after with a new drained unloading phase that starts from phase 7 (see Table 18 (on page 217)) in which the vertical stress is reduced to -80 kPa.

Figure 100 (on page 220) shows the stress state for two different calculation phases, both at a vertical stress level of 80 kPa. The plot in the left hand side shows the stress state after primary loading. As expected the horizontal stress is found to be approximately -40 kPa (corresponding to  $K_0^{nc} = 0.5$ ). The plot in the right hand side shows the final situation after unloading down to -80 kPa. In this case the horizontal stress is decreased from -320 kPa to approximately -220 kPa, ( $\Delta \sigma'_{xx} = 100$  kPa), i.e., much less than the decrease of the vertical stress ( $\Delta \sigma'_{yy} = 560$  kPa). Thus, a situation where  $\sigma'_{xx}$  is larger than  $\sigma'_{yy}$  is obtained.

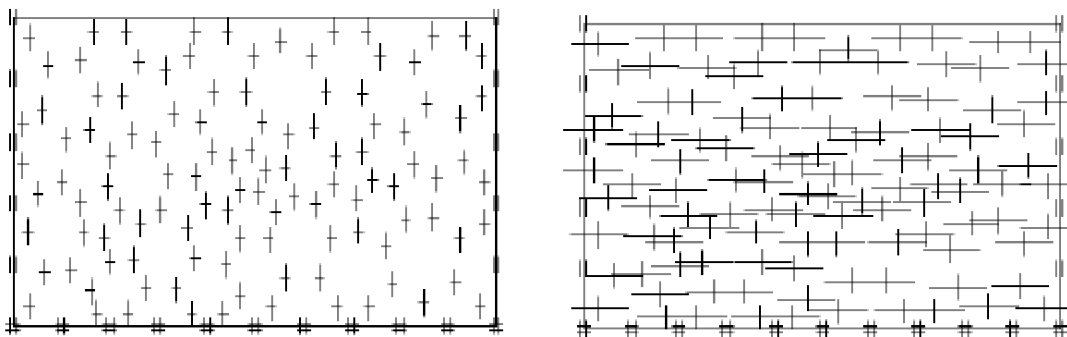


Figure 100: Stress states at vertical stress level of -80 kPa. Left, after primary loading  $\sigma'_{xx} \approx 40$  kPa. Right, after unloading from -640 kPa  $\sigma'_{xx} \approx -220$  kPa  $\sigma'_{yy} \approx 40$  kPa. Right, after unloading from -640 kPa  $\sigma'_{xx} \approx -220$  kPa

## Application of advanced soil models

### Soft Soil model: Response in isotropic compression test

During sudden unloading in a one-dimensional compression test, the behaviour is purely elastic. Hence, the ratio of the horizontal and vertical stress increments can be determined as:

$$\frac{\Delta\sigma'_{xx}}{\Delta\sigma'_{yy}} = \frac{\nu_{ur}}{1 - \nu_{ur}} \quad Eq. [356]$$

It is easy to verify that the results correspond to Poisson's ratio  $\nu_{ur} = 0.15$  as listed in [Table 13](#) (on page 208).

## 17.6 Soft Soil model: Response in isotropic compression test

In this section it will be demonstrated that the Soft Soil model obeys a logarithmic relationship between the volumetric strain and the mean stress in isotropic compression. For this purpose the test set up is simulated as that presented in [Figure 75](#) (on page 196). The vertical load (A) and the horizontal load (B) are simultaneously applied to the same level so that a fully isotropic stress state occurs. The parameters of the Soft Soil model are chosen arbitrarily, but the values are realistic for normally consolidated clay. The parameters are presented in [Table 20](#) (on page 221).

**Table 20: Soft Soil model parameters for isotropic compression test**

Modified compression index	$\lambda^*$	0.1
Modified swelling index	$\kappa^*$	0.02
Poisson's ratio	$\nu_{ur}$	0.15
Friction angle	$\varphi$	30°
Cohesion	$c$	1.0 kPa
Normally consolidated $K_0$	$K_0$ & $K_0^{nc}$	0.5

From a stress-free state, the model is isotropically loaded to a mean stress of  $p' = 100$  kPa, after which the displacements are reset to zero. As a result, the material becomes 'normally consolidated', i.e., the preconsolidation stress is equivalent to the current state-of-stress. After that, the isotropic pressure is increased to  $p' = 1000$  kPa. This loading path is denoted as 'primary loading'. Then, the sample is isotropically 'unloaded' to  $p' = 100$  kPa. Finally, the sample is loaded up to  $p' = 10000$  kPa. In the last loading path, the maximum preload of 1000 kPa is exceeded, and hence, it consists of two parts: the part of the loading path for which  $p' < 1000$  kPa is referred to as 'reloading', and the part of the loading path for  $p' > 1000$  kPa consists of further primary loading. The calculation phases are indicated in [Table 21](#) (on page 221).

**Table 21: Calculation phases for isotropic compression test on clay**

Stage		Initial stress	Final stress
0	Initial situation	-	$p^0 = 100$ kPa
1	Primary loading	$p^0 = 100$ kPa	$p^1 = 1000$ kPa

## Application of advanced soil models

Soft Soil model: Response in isotropic compression test

Stage		Initial stress	Final stress
2	Unloading	$p^1 = 1000 \text{ kPa}$	$p^2 = 100 \text{ kPa}$
3	Reloading	$p^2 = 100 \text{ kPa}$	$p^3 = 1000 \text{ kPa}$
4	Primary loading	$p^3 = 1000 \text{ kPa}$	$p^4 = 10000 \text{ kPa}$

The computational results are presented in [Figure 101](#) (on page 222), which shows the relation between the vertical strain  $\varepsilon_{yy}$  and the vertical stress  $\sigma'_{yy}$ .

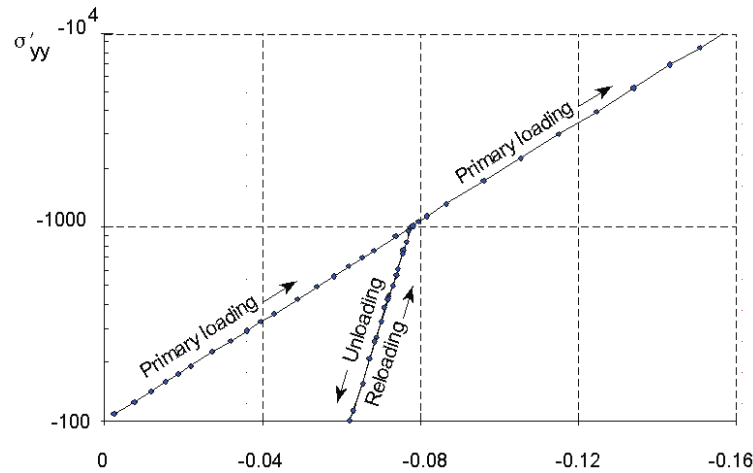


Figure 101: Results of isotropic compression test

The latter quantity is plotted on a logarithmic scale. The plot shows two straight lines, which indicates that there is indeed a logarithmic relation for loading and unloading. The vertical strain is 1/3 of the volumetric strain,  $\varepsilon_v$ , and the vertical stress is equal to the mean stress,  $p'$ . The volumetric strains obtained from the calculation are given in [Table 22](#) (on page 222).

Table 22: Volumetric strains from various calculation phases

Phase	Initial strain	Final strain
0	-	$\varepsilon_v^0 = 0.000$
1	$\varepsilon_v^0 = 0.000$	$\varepsilon_v^1 = -0.235$
2	$\varepsilon_v^1 = -0.235$	$\varepsilon_v^2 = -0.188$
3	$\varepsilon_v^2 = -0.188$	$\varepsilon_v^3 = -0.235$
4	$\varepsilon_v^3 = -0.235$	$\varepsilon_v^4 = -0.471$

From these strains and corresponding stresses, the parameters  $\lambda^*$  and  $\kappa^*$  can be back-calculated using Eq. [236] and Eq. [237].

## Application of advanced soil models

Hardening Soil model and Hardening Soil model with small-strain stiffness: Excavation in Berlin sand

---

$$\text{Phase 1: } \lambda^* = - \frac{\varepsilon_v^1 - \varepsilon_v^0}{\ln(p^1/p^0)} = \frac{0.235}{\ln(1000/100)} = 0.102$$

$$\text{Phase 2: } \kappa^* = - \frac{\varepsilon_v^2 - \varepsilon_v^1}{\ln(p^2/p^1)} = \frac{0.188 - 0.235}{\ln(100/1000)} = 0.020$$

$$\text{Phase 3: } \kappa^* = - \frac{\varepsilon_v^3 - \varepsilon_v^2}{\ln(p^3/p^2)} = \frac{0.235 - 0.188}{\ln(1000/100)} = 0.020$$

$$\text{Phase 4: } \lambda^* = - \frac{\varepsilon_v^4 - \varepsilon_v^3}{\ln(p^4/p^3)} = \frac{0.471 - 0.235}{\ln(10000/1000)} = 0.102$$

The back-calculated values correspond to the input values as given in [Table 20](#) (on page 221).

Note that the Soft Soil model does not include time effects such as in the secondary compression. Such behaviour is included in the Soft Soil Creep model.

## 17.7 Hardening Soil model and Hardening Soil model with small-strain stiffness: Excavation in Berlin sand

In the previous example, the advantage of the Hardening Soil model's distinct loading and unloading stiffness was highlighted. With those, the calculated excavation heave could be reduced to a more realistic, but in most cases still too high value. In the Berlin excavation example, now the further advantage of considering small-strain stiffness in the analysis is demonstrated.

The working group 1.6 Numerical methods in Geotechnics of the German Geotechnical Society (DGGT) has organised several comparative finite element studies (benchmarks). One of these benchmark examples is the installation of a triple anchored deep excavation wall in Berlin sand. The reference solution by [Schweiger \(2002\)](#) (on page 249) is used here as the starting point for the next validation example: Both, the mesh shown in [Figure 102](#) (on page 224), and the soil parameters given in [Table 23](#) (on page 224) are taken from this reference solution. However, the bottom soil layer 3 defined by [Schweiger \(2002\)](#) (on page 249) is assigned the parameters of layer 2 in the HSsmall analysis. In the reference solution this layer's only purpose is the simulation of small-strain stiffness due to a lack of small-strain stiffness constitutive models back then.

## Application of advanced soil models

Hardening Soil model and Hardening Soil model with small-strain stiffness: Excavation in Berlin sand

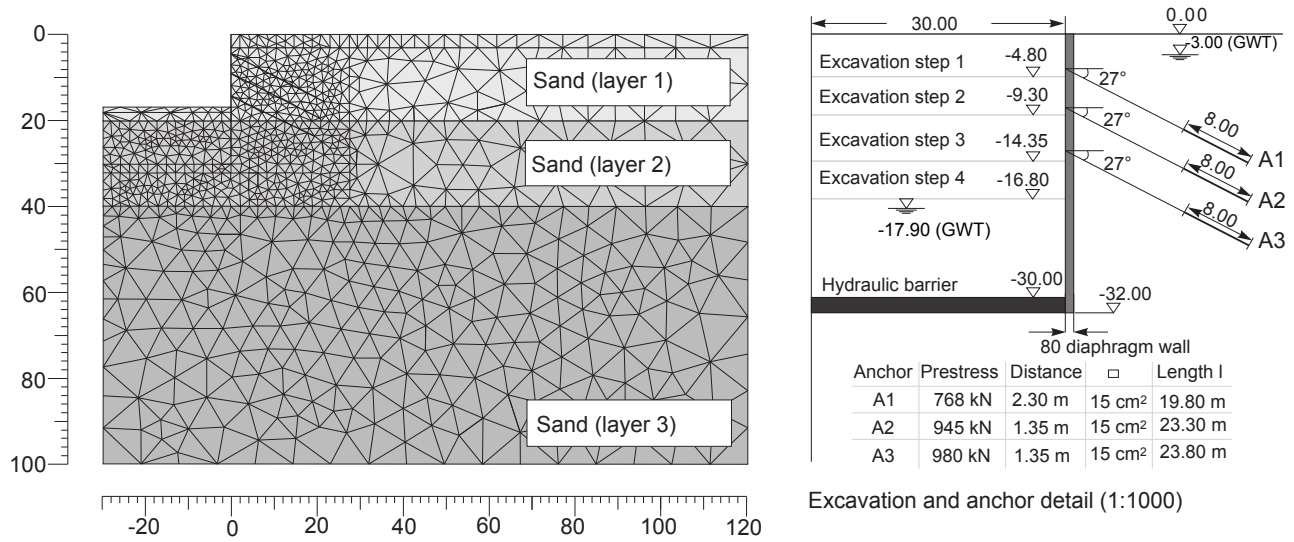


Figure 102: Excavation in Berlin sand: plane strain mesh (left) and geometry detail (right)

Table 23: Hardening Soil model and HS small model parameters for the three sand layers in the excavation project

Parameter	Layer 1	Layer 2	Layer 3	Unit
Unit weight above/ below phreatic level	19 / 20	19 / 20	19 / 20	kN/m <sup>3</sup>
$E_{50}^{ref} (p_{ref} = 100 \text{ kPa})$	45000	75000	105000	kN/m <sup>2</sup>
$E_{ur}^{ref} (p_{ref} = 100 \text{ kPa})$	45000	75000	105000	kN/m <sup>2</sup>
$E_{oed}^{ref} (p_{ref} = 100 \text{ kPa})$	180000	300000	315000	kN/m <sup>2</sup>
$G_0^{ref} (p_{ref} = 100 \text{ kPa})$	168750	281250	NA	kN/m <sup>2</sup>
Shear strain $\gamma_0^{ref} (p_{ref} = 100 \text{ kPa})$	0.0002	0.0002	NA	-
Cohesion c	1	1	1	kN/m <sup>2</sup>
Friction angle $\varphi$	35	38	38	°
Dilatancy angle $\psi$	5	6	6	°
Poisson's ratio $\nu_{ur}$	0.2	0.2	0.2	-
Power m	0.55	0.55	0.55	-
$K_0^{nc}$	0.43	0.38	0.38	-

## Application of advanced soil models

Hardening Soil model and Hardening Soil model with small-strain stiffness: Excavation in Berlin sand

Parameter	Layer 1	Layer 2	Layer 3	Unit
Tensile strength	0	0	0	kN/m <sup>2</sup>
Failure ratio	0.9	0.9	0.9	-

[Figure 103](#) (on page 225) shows results from the finite element calculation using the original Hardening Soil model and the Hardening Soil model with small-strain stiffness. The small-strain stiffness formulation in the Hardening Soil model with small-strain stiffness accumulates more settlements right next to the wall, whereas the settlement trough is smaller. The triple anchored retaining wall is deflected less when using the HSsmall model, almost fitting the measured deflection. Calculated excavation heave at the end of excavation is shown in [Figure 104](#) (on page 226). Compared to the HS results, the heave which is due to elastic unloading, is roughly halved when using the Hardening Soil model with small-strain stiffness.

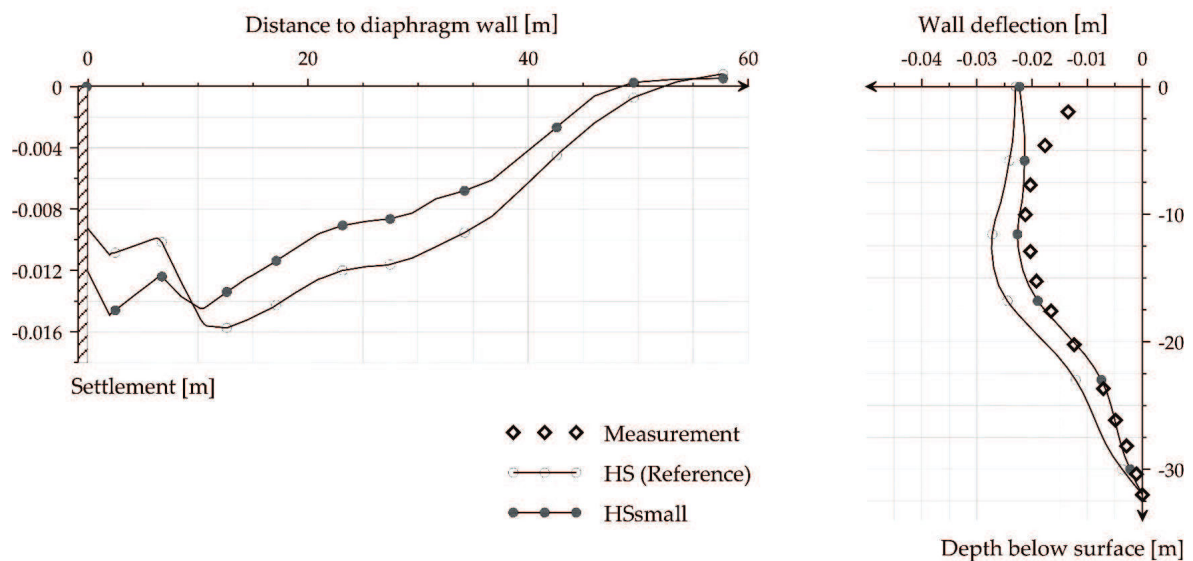


Figure 103: Hardening Soil model and Hardening Soil model with small-strain stiffness predictions versus measured displacements after the final excavation step. Left: Surface settlement trough. Right: Lateral wall deflection.

## Application of advanced soil models

Hardening Soil model and Hardening Soil model with small-strain stiffness: Excavation in Berlin sand

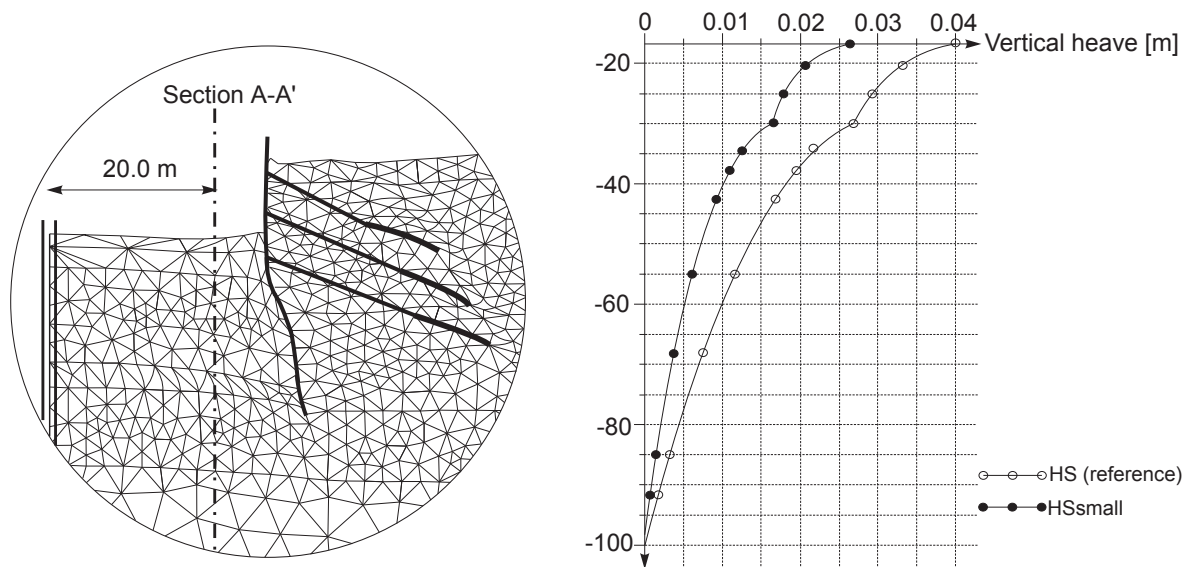


Figure 104: Vertical displacements in the excavation pit at a distance of 10 m from the retaining wall (Section A-A)

## 18.1 Anchors

The elastic behaviour of an anchor involves only a relationship between axial force  $N$  and displacement (elongation)  $u$  of the form:

$$N = \frac{EA}{L} U \quad \text{Eq. [357]}$$

The anchor stiffness  $EA$  is defined by the user based on the material stiffness  $E$  and cross section  $A$ .

In case of elastoplastic behaviour of the anchor the maximum tension force is bound by  $F_{max,tens}$  and the maximum compression force is bound by  $F_{max,comp}$ .

## 18.2 3D Beams

The local system of axes of a beam element is such that the first axis corresponds with the axial beam direction. The second and third axis are always perpendicular to the beam axis.

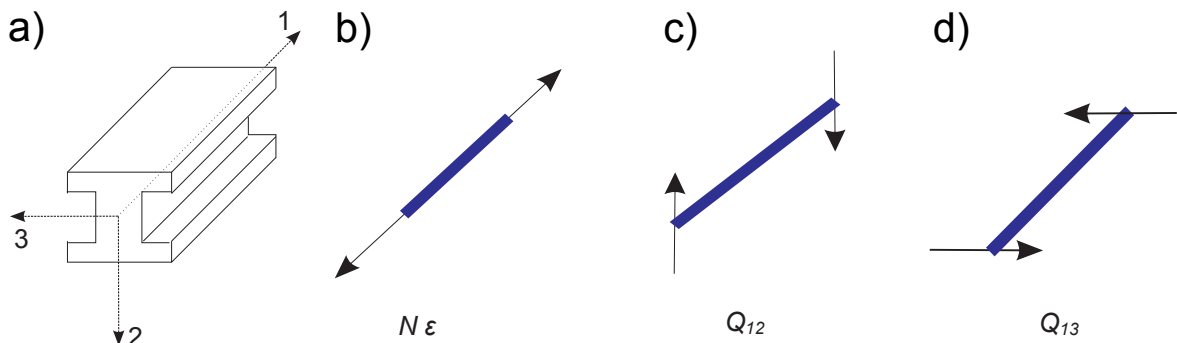


Figure 105: Axial force and shear forces. a- Local axes. b- Axial force  $N$ . c- Shear force  $Q_{12}$ . d- Shear force  $Q_{13}$ .

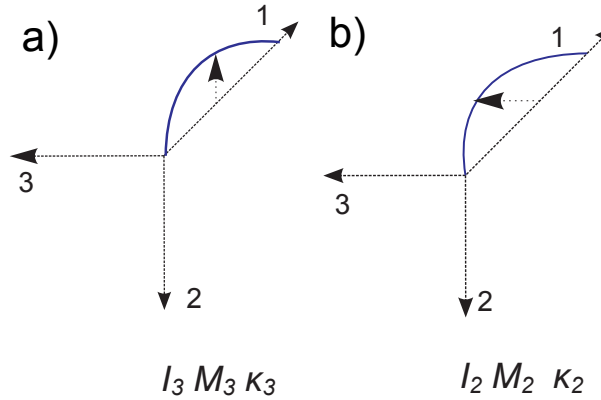


Figure 106: Bending moments. a- Bending moment  $M_3$ . b- Bending moment  $M_2$

Elastic behaviour of beam elements is defined by the following parameters:

$A$	Beam cross section area	$[\text{m}^2]$
$E$	Young's modulus in axial direction	$[\text{kN}/\text{m}^2]$
$I_2$	Moment of inertia against bending around the second axis	$[\text{m}^4]$
$I_3$	Moment of inertia against bending around the third axis	$[\text{m}^4]$

The relationships between the different force components and the strain / gradient / curvature components are defined as:

$$\begin{aligned}
 N &= EA\varepsilon \\
 Q_{12} &= kGA\gamma_{12} \\
 Q_{13} &= kGA\gamma_{13} \\
 M_2 &= EI_2\kappa_2 \\
 M_3 &= EI_3\kappa_3
 \end{aligned}
 \quad \text{Eq. [358]}$$

In which  $k$  is the shear correction factor, which is taken as  $5/6$ . The shear modulus is taken as  $G = \frac{1}{2}E$ .

When plasticity is considered, the maximum bending moment  $M_p$  in the local direction  $i$  and the maximum normal force  $N_p$  are calculated as:

$$\begin{aligned}
 N_{p,eq} &= A_{eq}\sigma_{y,eq} \\
 M_{p,i,eq} &= W_{i,eq}\sigma_{y,eq}
 \end{aligned}
 \quad \begin{aligned} &\text{Eq. [359]} \\ &\text{Eq. [360]} \end{aligned}$$

where  $i$  is the index number for the selected local direction where plasticity can occur (i.e. *Local direction 2* or *Local direction 3*),  $\sigma_{y,eq}$  is the equivalent yield stress,  $W_{i,eq}$  is the equivalent plastic section modulus in the  $i$  local direction,  $A_{eq}$  is the equivalent area.

Based on the input parameters  $A$ ,  $I_2$ ,  $I_3$  and  $\sigma_y$ , the equivalent properties are calculated:

$$h_{i,eq} = \sqrt[3]{12 \frac{I_i}{A}} \quad \text{Eq. [361]}$$

$$A_{eq} = h_{2,eq} h_{3,eq} \quad Eq. [362]$$

$$W_{i,eq} = \frac{\sqrt{3}}{6} A_{eq} h_{i,eq} \quad Eq. [363]$$

The maximum bending moments are given in units of force times length. The maximum axial force is computed in units of force. By default the maximum moment is set to  $1 \cdot 10^{15}$  units if the material type is set to elastic (the default setting).

Bending moments and axial forces are calculated at the stress points of the beam elements. When the yield function is violated, stresses are redistributed according to the theory of plasticity, so that the maxima are complied with. This will result in irreversible deformations. Output of bending moments and axial forces is given in the nodes, which requires extrapolation of the values at the stress points. Nodal forces are not checked against the maximum forces.

## 18.3 3D Geogrids

The PLAXIS 3D program allows for orthotropic as well as anisotropic material behaviour in geogrid elements, which is defined by the following parameters:

$$\begin{aligned} N_1 &= EA_1 \varepsilon_1 \\ N_2 &= EA_2 \varepsilon_2 \\ Q_{12} &= GA_{12} \end{aligned} \quad Eq. [364]$$

In the case of orthotropic behaviour  $EA_1 = EA_2$  and  $GA = \frac{1}{2} EA_1$  in the general three dimensional case.

When plasticity is considered, the maximum tensile forces can be defined:

$N_{p,1}$	Maximum tensile force in 1-direction.	[kN/m]
$N_{p,2}$	Maximum tensile force in 2-direction.	[kN/m]

A non-linear  $N$ - $\varepsilon$  diagram may be specified in case of elastoplasticity:

$N_1$ - $\varepsilon_{ps1}$	The $N$ - $\varepsilon$ diagram in 1-direction.
$N_2$ - $\varepsilon_{ps2}$	The $N$ - $\varepsilon$ diagram in 2-direction.

Axial forces are calculated at the stress points of the geogrid elements. If  $N_p$  is exceeded, stresses are redistributed according to the theory of plasticity, so that the maximum forces are complied with. This will result in irreversible deformations. Output of axial forces is given in the nodes, which requires extrapolation of the values at the stress points. Nodal forces are not checked against the maximum forces. Hence, it is possible that the nodal values of the axial force may slightly exceed  $N_p$ .

A *Visco-elastic (time-dependent)* behaviour may be specified based on a visco-elastic perfectly-plastic Kelvin-Voigt model in each direction. Parameters which are required for time-dependent visco-elasticity are:

$EA_{I,short}$	Elastic stiffness during initial(instantaneous) strain increment in 1-direction.	[kN/m]
----------------	--	--------

$EA_{2,short}$	Elastic stiffness during initial(instantaneous) strain increment in 2-direction.	[kN/m]
$EA_{1,long}$	Elastic stiffness during (infinitely) long strain increment in 1-direction.	[kN/m]
$EA_{2,long}$	Elastic stiffness during (infinitely) long strain increment in 1-direction.	[kN/m]
<i>Retardation time</i>	The time where a linear extrapolation of the initial creep rate intersects the long-term displacement line.	[day]
$N_{p,1}$	Maximum force in 1-direction (in-plane).	[kN/m]
$N_{p,2}$	The maximum force in 2-direction.	[kN/m]

For more information about the determination of the parameters see the Reference Manual - Chapter 6 - *Material data sets for geogrids*.

## 18.4 3D Plates

The PLAXIS 3D program allows for orthotropic material behaviour in plate elements, which is defined by the following parameters:

$E_1$	Young's modulus in first axial direction.	[kN/m <sup>2</sup> ]
$E_2$	Young's modulus in second axial direction.	[kN/m <sup>2</sup> ]
$G_{12}$	In-plane shear modulus.	[kN/m <sup>2</sup> ]
$G_{13}$	Out-of-plane shear modulus related to shear deformation over first direction.	[kN/m <sup>2</sup> ]
$G_{23}$	Out-of-plane shear modulus related to shear deformation over second direction.	[kN/m <sup>2</sup> ]
$\nu_{12}$	Poisson's ratio ( $\nu < \sqrt{E_1 / E_2}$ ).	[-]

The material behaviour in plate elements is defined by the following relationship between strains and stresses, which is based on the general three-dimensional continuum mechanics theory and the assumption that  $\sigma_{33}=0$ .

$$\begin{bmatrix} \varepsilon_{11} \\ \varepsilon_{22} \\ \gamma_{12} \\ \gamma_{13} \\ \gamma_{23} \end{bmatrix} = \begin{bmatrix} 1/E_1 & -\nu_{12}/E_1 & 0 & 0 & 0 \\ -\nu_{12}/E_1 & 1/E_2 & 0 & 0 & 0 \\ 0 & 0 & 1/G_{12} & 0 & 0 \\ 0 & 0 & 0 & 1/kG_{13} & 0 \\ 0 & 0 & 0 & 0 & 1/kG_{23} \end{bmatrix} \begin{bmatrix} \sigma_{11} \\ \sigma_{22} \\ \sigma_{12} \\ \sigma_{13} \\ \sigma_{23} \end{bmatrix} \quad Eq. [365]$$

In which  $k$  is the shear correction factor, which is taken as  $5/6$ . Inverting this relationship and ignoring the higher order terms in  $\nu$  gives the following stress-strain relationship:

$$\begin{bmatrix} \sigma_{11} \\ \sigma_{22} \\ \sigma_{12} \\ \sigma_{13} \\ \sigma_{23} \end{bmatrix} = \begin{bmatrix} E_1 & \nu_{12}E_2 & 0 & 0 & 0 \\ \nu_{12}E_2 & E_2 & 0 & 0 & 0 \\ 0 & 0 & G_{12} & 0 & 0 \\ 0 & 0 & 0 & kG_{13} & 0 \\ 0 & 0 & 0 & 0 & kG_{23} \end{bmatrix} \begin{bmatrix} \varepsilon_{11} \\ \varepsilon_{22} \\ \gamma_{12} \\ \gamma_{13} \\ \gamma_{23} \end{bmatrix} \quad \text{Eq. [366]}$$

This approximation holds as long as the Poisson's ratio is small. These stress-strain relationships can be transformed into relationships for structural forces:

$$\begin{bmatrix} N_1 \\ N_2 \end{bmatrix} = \begin{bmatrix} E_1 d & \nu_{12} E_2 d \\ \nu_{12} E_2 d & E_2 d \end{bmatrix} \begin{bmatrix} \varepsilon_1 \\ \varepsilon_2 \end{bmatrix} \quad \text{Eq. [367]}$$

$$\begin{bmatrix} Q_{12} \\ Q_{13} \\ Q_{23} \end{bmatrix} = \begin{bmatrix} G_{12} d & 0 & 0 \\ 0 & k G_{13} d & 0 \\ 0 & 0 & k G_{23} d \end{bmatrix} \begin{bmatrix} \gamma_{12} \\ \gamma_{13}^* \\ \gamma_{23}^* \end{bmatrix} \quad \text{Eq. [368]}$$

$$\begin{bmatrix} M_{11} \\ M_{22} \\ M_{12} \end{bmatrix} = \begin{bmatrix} \frac{E_1 d^3}{12} & \frac{\nu_{12} E_2 d^3}{12} & 0 \\ \frac{\nu_{12} E_2 d^3}{12} & \frac{E_2 d^3}{12} & 0 \\ 0 & 0 & \frac{G_{12} d^3}{12} \end{bmatrix} \begin{bmatrix} \kappa_{11} \\ \kappa_{22} \\ \kappa_{12} \end{bmatrix} \quad \text{Eq. [369]}$$

In which  $d$  is the thickness of the plate, which also determines the distributed weight of the plate together with the unit weight of the plate material:  $\gamma \cdot d$ . The modified shear strain  $\gamma^*$  takes into account the shear strain  $\gamma$  and some additional terms in order to give a more accurate approximation of the problem.

The local system of axes in a plate element is such that the first and the second local axis lie in the plane of the plate whereas the third axis is perpendicular to the plane of the plate ([Figure 107](#) (on page 232)).

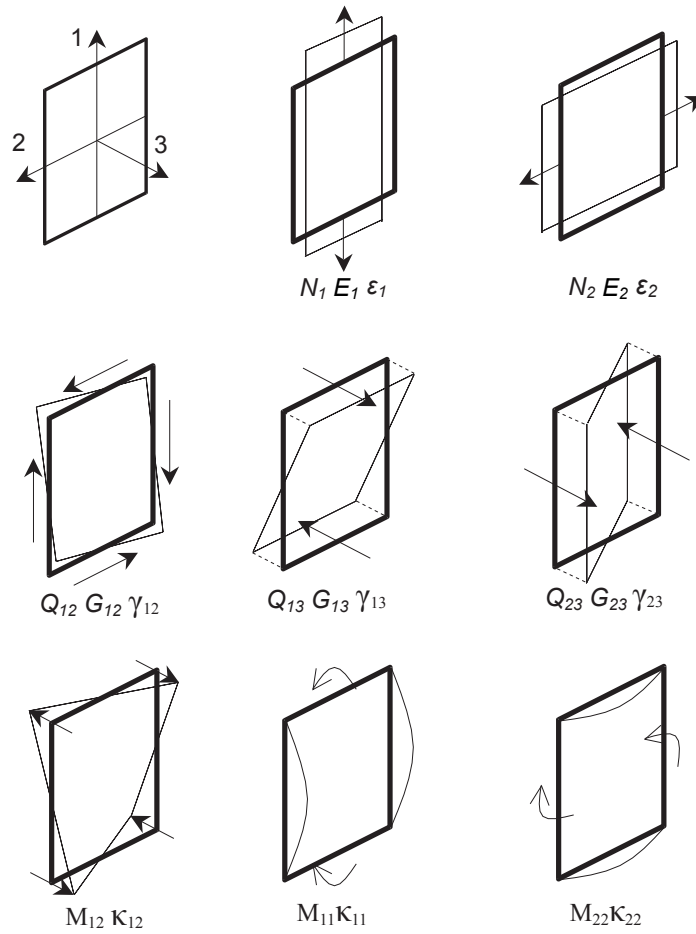


Figure 107: Definition of positive axial forces ( $N$ ), shear forces ( $Q$ ) and bending moments ( $M$ ) for a plate based on local system of axes

When geometric orthotropy is considered rather than material orthotropy, the following relationships for structural forces apply:

$$\begin{bmatrix} N_1 \\ N_2 \end{bmatrix} = \begin{bmatrix} EA_1/(1-\nu^2) & \nu EA_1/(1-\nu^2) \\ \nu EA_1/(1-\nu^2) & EA_2/(1-\nu^2) \end{bmatrix} \begin{bmatrix} \varepsilon_1 \\ \varepsilon_2 \end{bmatrix} \approx \begin{bmatrix} EA_1 & \nu EA_1 \\ \nu EA_1 & EA_2 \end{bmatrix} \begin{bmatrix} \varepsilon_1 \\ \varepsilon_2 \end{bmatrix} \quad Eq. [370]$$

$$\begin{bmatrix} Q_{12} \\ Q_{13} \\ Q_{23} \end{bmatrix} = \begin{bmatrix} \frac{EA_{12}}{2(1+\nu)} & 0 & 0 \\ 0 & \frac{EA_{13}}{2(1+\nu)} & 0 \\ 0 & 0 & \frac{EA_{23}}{2(1+\nu)} \end{bmatrix} \begin{bmatrix} \gamma_{12} \\ \gamma_{13}^* \\ \gamma_{23}^* \end{bmatrix} \quad Eq. [371]$$

where the approximations hold for a small Poisson's ratio. In these relations the following alternative parameters are used:

$A_1$	Effective material cross section area for axial forces in the first direction.	$[m^2]$
-------	--	---------

$A_2$	Effective material cross section area for axial forces in the second direction.	[m <sup>2</sup> ]
$A_{12}$	Effective material cross section area for shear forces $Q_{12}$ .	[m <sup>2</sup> ]
$A_{13}$	Effective material cross section area for shear forces $Q_{13}$ .	[m <sup>2</sup> ]
$A_{23}$	Effective material cross section area for shear forces $Q_{23}$ .	[m <sup>2</sup> ]
$I_1$	Moment of inertia against bending over the first axis.	[m <sup>4</sup> ]
$I_2$	Moment of inertia against bending over the second axis.	[m <sup>4</sup> ]
$I_{12}$	Moment of inertia against torsion.	[m <sup>4</sup> ]

In order to use the available plate elements for geometric orthotropy, the basic material parameters should be chosen in such a way that the resulting axial stiffness  $E_1 A$  is equal to the axial stiffness  $E A_1$  of the plate. Here  $E_1$  is the input value for the Young's modulus in the first direction,  $A$  is the internally calculated area of the plate,  $E$  is the actual Young's modulus of the material and  $A_1$  is the cross sectional area of the element to be modelled. Similar parameter choices should be made for the other axial stiffness, bending stiffness and shear stiffnesses. However, for a given choice of the equivalent plate thickness  $d$  it will not be possible to match all stiffness components exactly. The thickness  $d$  is the equivalent plate thickness such that the average distributed weight of the plate corresponds to  $\gamma d$ .

When bending is considered as the most important type of deformation, the following choices are recommended:

$$E_1 = 12EI_1/d^3 \quad E_2 = 12EI_2/d^3$$

$$G_{12} = \frac{6EI_{12}}{(1+\nu)d^3} \quad G_{13} = \frac{EA_{13}}{2(1+\nu)d} \quad G_{23} = \frac{EA_{23}}{2(1+\nu)d} \quad \text{Eq. [372]}$$

$$\nu_{12} = \nu$$

In this case the resulting bending stiffness  $E_1 d^3/12$  and  $E_2 d^3/12$  and shear stiffnesses  $G_{13}d$  and  $G_{23}d$  prove to be independent of the chosen value for equivalent plate thickness. Only the axial stiffnesses  $E_1 A$  and  $E_2 A$  and shear stiffness  $G_{12}d$  are not independent of the chosen value of the equivalent plate thickness, and a suitable selection for  $d$  has to be made. What is the most suitable selection for  $d$  depends on the construction that is to be modelled. Two examples are given below.

When plasticity is considered, the maximum bending moment  $M_p$  and the maximum axial force  $N_p$  are calculated in the two axial directions (1 and 2) as:

$$N_{p,1,eq} = d \quad \sigma_{y,11,eq} \quad \text{Eq. [373]}$$

$$N_{p,2,eq} = d \quad \sigma_{y,22,eq} \quad \text{Eq. [374]}$$

$$M_{p,11} = W_{11} \quad \sigma_{y,11} \quad \text{Eq. [375]}$$

$$M_{p,22} = W_{22} \quad \sigma_{y,22} \quad \text{Eq. [376]}$$

where

$$\begin{aligned} \sigma_{y,11,eq}, \sigma_{y,22,eq} &= \text{Yield stresses.} \\ W_{11}, W_{22} &= \text{Plastic section moduli.} \\ d &= \text{(Equivalent) Thickness.} \end{aligned}$$

In order to obtain the plastic axial forces  $N_p$  the equivalent stresses are calculated:

$$\sigma_{y,11,eq} = \sigma_{y,11} / \sqrt{3}$$

$$\sigma_{y,22,eq} = \sigma_{y,22} / \sqrt{3}$$

The maximum bending moments are given in units of force times length per unit width. The maximum axial forces are computed in units of force per unit width. The yield surfaces are a diamond shape in the  $N_1 - M_{11}$  plane and in the  $N_2 - M_{22}$  plane. The two directions are treated separately. Force combinations inside the diamonds will result in elastic deformations only.

By default the maximum moment is set to  $1 \cdot 10^{15}$  units if the material type is set to elastic (the default setting).

Bending moments and axial forces are calculated at the stress points of the beam elements. When yield function is violated, stresses are redistributed according to the theory of plasticity, so that the maxima are complied with. This will result in irreversible deformations. Output of bending moments and axial forces is given in the nodes, which requires extrapolation of the values at the stress points. Nodal forces are not checked against the maximum forces.

### 18.4.1 Engineering example:

In the following, two types of applications are given that frequently occur in the engineering practice. The first example is a sheet-pile wall, as depicted in [Figure 108](#) (on page 234). From the sheet-pile manufacturer, the following properties are known:  $t$  (wall thickness),  $h$  (total height),  $A$  (per m wall width),  $I_1$ ,  $E_{steel}$  and  $\gamma_{steel}$ .

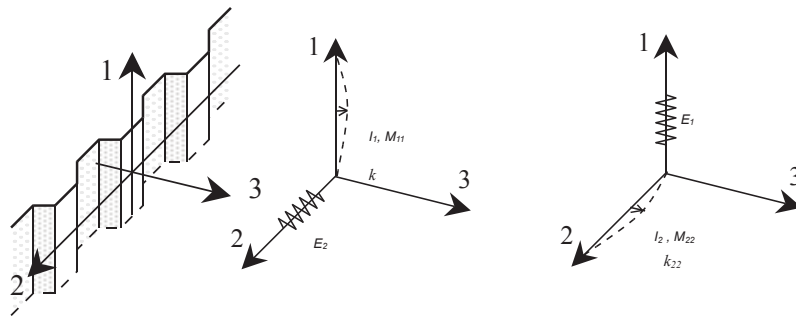


Figure 108: Example of sheet-pile wall with its major quantities

The structure is geometrically orthotropic with significant different stiffnesses in horizontal and vertical direction. It is known that the axial stiffness in vertical direction is larger than the effective stiffness in horizontal direction ( $E_1 > E_2$ ). Moreover, the stiffness against bending over the vertical direction,  $I_1$ , is much larger than the stiffness against bending over the horizontal direction,  $I_2$ , ( $I_1 \gg I_2$  say  $I_1 \approx 20 I_2$  and  $I_1 \gg I_{12}$  say  $I_1 \approx 10 I_{12}$ ).<sup>3</sup>

Furthermore, it is assumed that the cross section area that is effective against shear deformation over the vertical direction is about 1/3 of the total cross section area, whereas the area that is effective against shear deformation over the horizontal direction is about 1/10 of the total cross section area. Finally, the Poisson's ratio's for sheet pile walls can be assumed zero. With these assumptions, the situation could be modelled by selecting the model parameters in the following way:

$$d = h$$

<sup>3</sup> A factor of 20 is used here to move the bending stiffness over the first direction sufficiently small compared to the bending stiffness over the second direction, whilst the matrix condition is still OK. Note that in reality bending stiffness differences in order of 1000 may exist.

$$E_1 = 12E_{steel}I_1/d^3$$

$$E_2 = 12E_{steel}I_2/d^3 \approx I_2/I_1 E_1 \approx E_1/20$$

$$G_{12} = \frac{6E_{steel}I_{12}}{(1+\nu_{steel})d^3} \approx 6E_{steel}I_1/10d^3$$

$$G_{13} = \frac{E_{steel}A_{13}}{2(1+\nu_{steel})d} \approx E_{steel}(A/3)/2d \approx E_{steel}A/6d$$

$$G_{23} = \frac{E_{steel}A_{23}}{2(1+\nu_{steel})d} \approx E_{steel}(A/10)/2d \approx E_{steel}A/20d$$

$$\nu_{12} \approx 0$$

$$\gamma = Ay_{steel}/d$$

The second example is a concrete T-shaped floor profile, as depicted in [Figure 108](#) (on page 234). In addition to the precise geometry dimensions, the following properties are known:

$E_{concrete}, \nu_{concrete}$

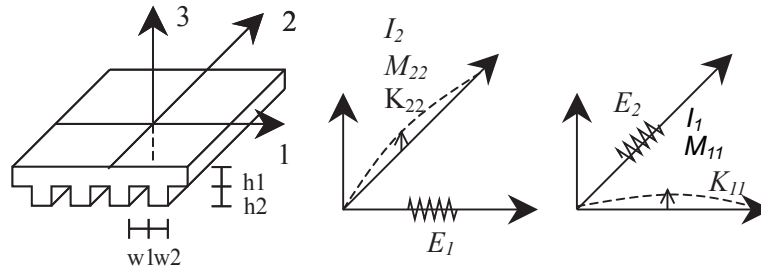


Figure 109: Example of concrete floor profile with its major quantities

The structure is again geometrically orthotropic with significant different stiffnesses in the two major floor directions. The stiffness against bending over the second direction,  $I_2$ , is larger than the stiffness against bending over the first direction,  $I_1$ , ( $I_2 > I_1$ ), since  $I_2$  is dominated by  $h_1 + h_2$  whereas  $I_1$  only depends on  $h_1$ . Furthermore, the cross section area (per unit of width) that is effective against shear deformation over the second direction ( $G_{23}$ ) is equal to the total cross section area  $A$ , whereas the area that is effective against shear deformation over the first direction ( $G_{13}$ ) is equal to  $h_1$ . With these assumptions, the situation could be modelled by selecting the model parameters in the following way:

$$d = \frac{h_1 w_1 + (h_1 + h_2) w_2}{w_1 + w_2}$$

$$E_1 = 12E_{concrete}I_1/d^3 = 12E_{concrete}\frac{1}{12}h_1^3/d^3 = E_{concrete}h_1^3/d^3$$

$$E_2 = 12E_{concrete}I_2/d^3; \text{ where } I_2 = \frac{\frac{1}{12}h_1^3w_1 + \frac{1}{12}(h_1 + h_2)^3w_2}{w_1 + w_2}$$

$$G_{12} = \frac{6E_{concrete}I_{12}}{(1 + \nu_{concrete})d^3} \text{ where } I_{12} \approx I_1 = \frac{1}{12}h_1^3$$

$$G_{13} = \frac{E_{concrete}A_{13}}{2(1 + \nu_{concrete})d} = \frac{E_{concrete}h_1}{2(1 + \nu_{concrete})d}$$

$$G_{23} = \frac{E_{concrete}A_{23}}{2(1 + \nu_{concrete})d} = \frac{E_{concrete}d}{2(1 + \nu_{concrete})d} = \frac{E_{concrete}}{2(1 + \nu_{concrete})}$$

$$\nu_{12} = \nu_{concrete}$$

## 18.5 3D Embedded beams

An embedded beam in PLAXIS 3D consists of beam elements with embedded interface elements to describe the interaction with the soil at the pile skin and at the pile foot (bearing capacity). The material parameters of the embedded beam distinguish between the parameters of the beam and the parameters of the skin resistance and foot resistance. The beam elements can be linear elastic or elastoplastic. Their behaviour and material parameters are defined as a regular 3D beam element ([3D Beams](#) (on page 227)).

The interaction of the pile with the soil at the skin of the pile is described by linear elastic behaviour with a finite strength and is defined by the following parameter:

**$T_{max}$**  Maximum traction allowed at the skin of the embedded beam (can vary along the pile)

The constitutive equation at the skin of the pile is defined by (see [Figure 110](#) (on page 237)):

$$\begin{bmatrix} t_s \\ t_n \\ t_t \end{bmatrix} = \begin{bmatrix} K_s & 0 & 0 \\ 0 & K_n & 0 \\ 0 & 0 & K_t \end{bmatrix} \begin{bmatrix} u_s^p - u_s^s \\ u_s^p - u_n^s \\ u_s^p - u_t^s \end{bmatrix} \quad Eq. [377]$$

where

$u^p$	=	Displacement of the pile
$u^s$	=	Displacement of the soil
$K_s$	=	The elastic shear stiffness (against parallel displacement differences) of the embedded interface elements
$K_t$	=	Elastic normal stiffness (against perpendicular displacement differences) of the embedded interface elements.

By default these values are defined such that the stiffness of the embedded interface elements does not influence the total elastic stiffness of the pile-soil structure:

$$K_s > G_{soil}$$

$$K_n = K_t = \frac{2(1 - \nu)}{1 - 2\nu} K_s \quad Eq. [378]$$

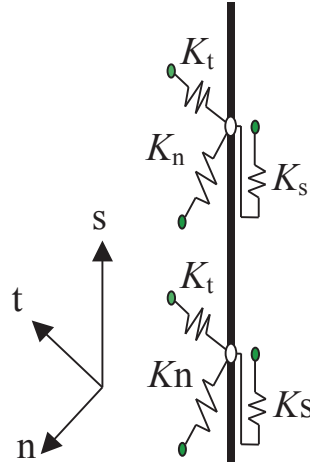


Figure 110: Stiffness of the embedded interface elements at the skin of the pile

The normal stresses  $t_n$  and  $t_t$  always remain elastic. The transverse forces are not limited in the special interface element that connects the pile with the soil but, in general, they are limited due to failure conditions in the surrounding soil itself outside the elastic zone.

For the shear stress in axial direction  $t_s$ , to remain elastic, it is given by:

$$|t_s| < T_{max} \quad \text{Eq. [379]}$$

For plastic behaviour the shear force  $t_s$  is given by:

$$|t_s| = T_{max} \quad \text{Eq. [380]}$$

In case of defining a layer dependent skin resistance the shear force  $t_s$  will remain elastic as long as:

$$|t_s| < (\sigma_n^{avg} \tan \varphi_i + c_i) \pi D_{eq} \quad \text{and} \quad |t_s| < T_{max} \quad \text{Eq. [381]}$$

where

$$\begin{aligned} D_{eq} &= \text{Diameter or the equivalent diameter (in the case alternative beam properties have been specified) of the embedded beam} \\ & \quad (D_{eq} = 2 \max \{ \sqrt{A / \pi}, \sqrt{(2I_{avg} / A)} \} \text{ with } I_{avg} = (I_2 + I_3) / 2) \\ \sigma_n^{avg} &= \text{Average lateral (perpendicular) stress of the soil around the pile:} \end{aligned}$$

$$\sigma_n^{avg} = \frac{1}{2} (\sigma_{xx} + \sigma_{yy}) \quad \text{Eq. [382]}$$

The parameters  $\varphi_i$  and  $c_i$  are the friction angle and cohesion of the embedded interface. The strength properties of embedded interfaces with layer dependent skin resistance are linked to the strength properties of a soil layer. Each data set has an associated strength reduction factor for interfaces  $R_{inter}$ . The embedded interface properties are calculated from the soil properties in the associated data set and the strength reduction factor by applying the following rules:

$$\begin{aligned} \tan \varphi_i &= R_{inter} \tan \varphi_{soil} \\ c_i &= R_{inter} c_{soil} \end{aligned} \quad \text{Eq. [383]}$$

In the case of a layer dependent skin resistance where the actual bearing capacity is not known,  $T_{max}$  can be used as an ultimate cut-off value. The interaction of the pile with the soil at the foot of the pile is described by a linear elastic perfectly plastic interface element. The strength of the base is described by the following parameter:

For plastic behaviour  $t_s$  is given by:

$$|t_s| = (\sigma_n^{avg} \tan \varphi_i + c_i) \pi D ; \text{ provided that } (\sigma_n^{avg} \tan \varphi_i + c_i) \pi D \leq T_{max} \quad Eq. [384]$$

In the case of a layer dependent skin resistance where the actual bearing capacity is not known,  $T_{max}$  can be used as an ultimate cut-off value. The interaction of the pile with the soil at the foot of the pile is described by a linear elastic perfectly plastic interface element. The strength of the base is described by the following parameter:

$F_{max}$	Maximum force allowed at the foot of the embedded beam.
-----------	---

In addition, no tension forces are allowed. The constitutive relationship at the foot of the pile and its failure criterion are defined by (see [Figure 110](#) (on page 237)):

$$F_{foot} = K_{foot} (u_{foot}^p - u_{foot}^s) < F_{max} \quad Eq. [385]$$

where

$$K_{foot} = \text{Stiffness of the spring which is defined in the same way as the stiffness of the embedded interface elements:}$$

$$K_{foot} > G_{soil}$$

In case of plastic behaviour, the foot force  $F_{foot}$  is given by:

$$F_{foot} = F_{max} \quad Eq. [386]$$

In order to ensure that a realistic pile bearing capacity as specified can actually be reached, a zone in the soil volume elements surrounding the beam is identified where any kind of soil plasticity is excluded (elastic zone [Figure 108](#)). The size of this zone is determined by the embedded beam's equivalent radius  $R_{eq} = \max \{ \sqrt{(A / \pi)}, \sqrt{(2I_{avg} / A)} \}$  with  $I_{avg} = (I_2 + I_3) / 2$ . The elastic zone makes the embedded beam almost behave like a volume pile. However, installation effects of piles are not taken into account and the pile-soil interaction is modelled at the centre rather than at the circumference.

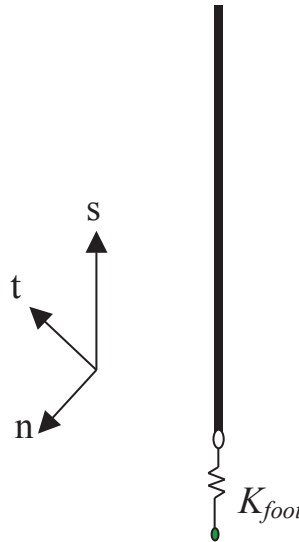


Figure 111: Stiffness of the embedded interface element at the foot of the pile

# 19

## Hydraulic Models

### 19.1 Van Genuchten model

A Soil Water Characteristic Curve (SWCC) is introduced to describe hydraulic parameters of the groundwater flow in unsaturated zones (usually above the phreatic surface). The SWCC describes the capacity of the soil to keep water at different stresses. There are many models which describe the hydraulic behaviour of unsaturated soils. The most common in the groundwater literature is the model proposed by [van Genuchten \(1980\)](#) (on page 249), which is used in PLAXIS. The Van Genuchten function is a three-parameter equation and relates the saturation to the pressure head  $\psi$ :

$$S(\psi) = S_{res} + (S_{sat} - S_{res}) \left[ 1 + (g_a |\psi|)^{g_n} \right]^{g_c} \quad Eq. [387]$$

where

$\psi$	=	$-\frac{p_w}{\gamma_w}$	
$p_w$	=	Suction pore stress.	
$\gamma_w$	=	Unit weight of the pore fluid.	
$S_{res}$	=	A residual saturation which describes a part of the fluid that remains in the pores even at high suction heads.	
$S_{sat}$	=	In general at saturated conditions the pores will not be completely filled with water as air can get trapped and the saturation in this situation, $S_{sat}$ will be less than one. However, the default is $S_{sat} = 1.0$	
$g_a$	=	A fitting parameter which is related to the air entry value of the soil and has to be measured for a specific material. It is in the unit of $1/L$ and is a positive value.	
$g_n$	=	A fitting parameter which is a function of the rate of water extraction from the soil once the air entry value has been exceeded. This parameter has to be measured for a specific material.	
$g_c$	=	A fitting parameter which is used in the general Van Genuchten equation. In PLAXIS the following assumption is made to convert the Van Genuchten to a two-parameter equation (Eq. [382]).	
$g_c$	=	$\left( \frac{1 - g_n}{g_n} \right)$	Eq. [388]

The Van Genuchten relationship provides reasonable results for low and intermediate suctions. For very high suction values, saturation remains at the residual saturation.

## Hydraulic Models

Van Genuchten model

[Figure 112](#) (on page 240) and [Figure 113](#) (on page 240) show the effect of the parameters  $g_a$  and  $g_n$  on the shape of the SWCC.

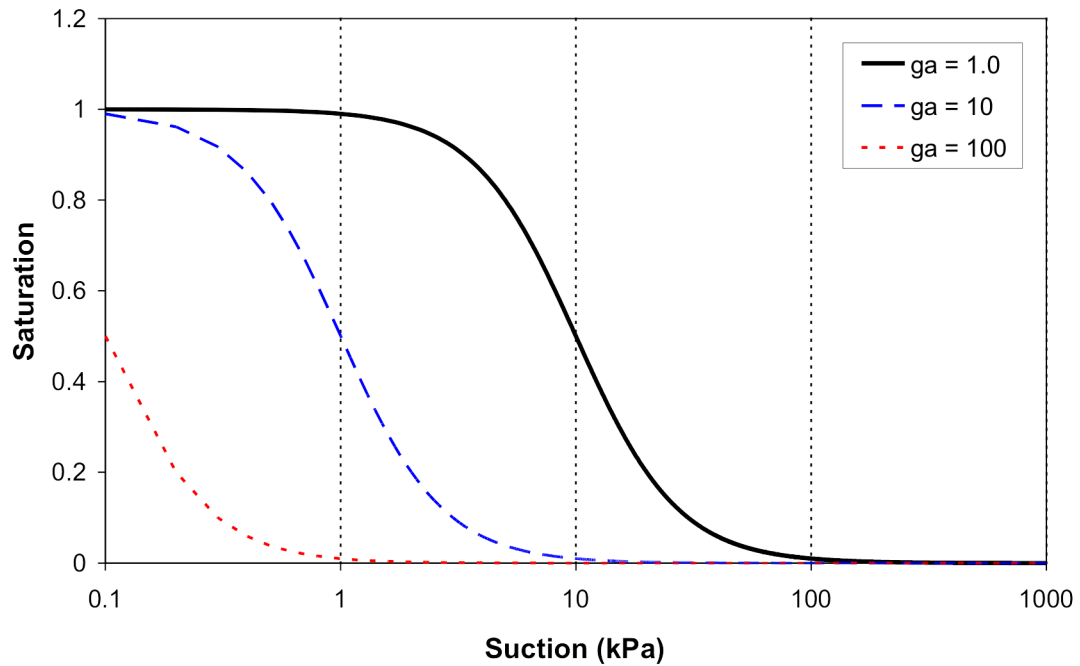


Figure 112: Effect of the parameter  $g_a$  on the SWCC  $g_a$  on the SWCC

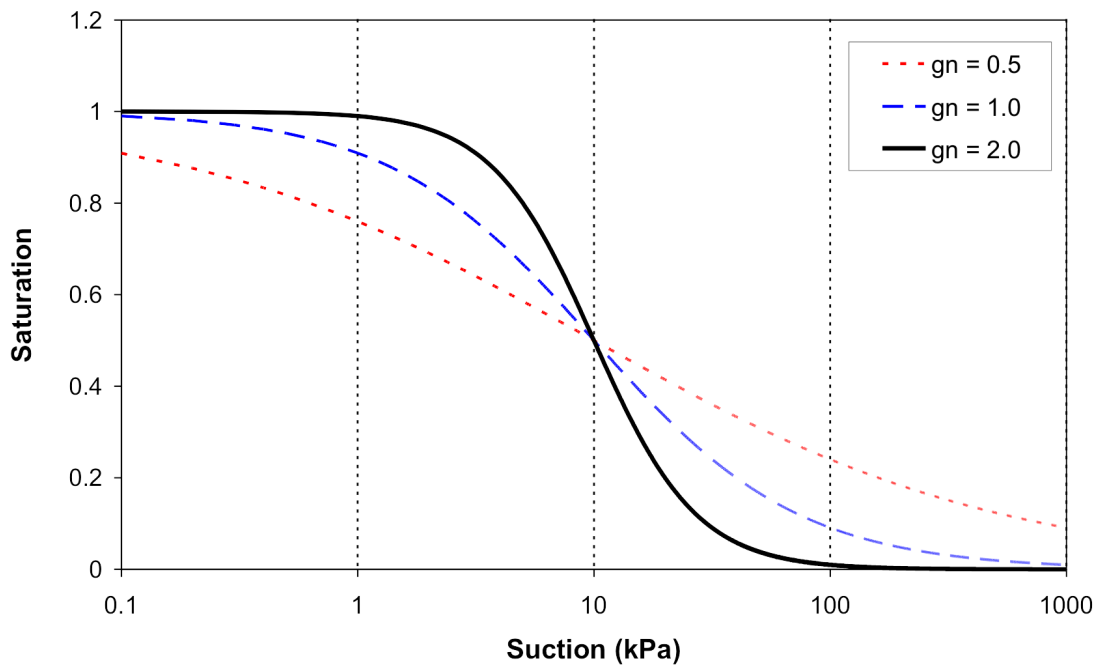


Figure 113: Effect of the parameter  $g_n$  on the SWCC  $g_n$  on the SWCC

## Hydraulic Models

### Van Genuchten model

Relative permeability is related to the saturation via the effective saturation. The effective saturation  $S_{eff}$  is expressed as:

$$S_{eff} = \frac{S - S_{res}}{S_{sat} - S_{res}} \quad Eq. [389]$$

The relative permeability according to Van Genuchten now reads:

$$k_{rel}(S) = \max \left[ (S_{eff})^{g_l} \left( 1 - \left[ 1 - S_{eff}^{\left( \frac{g_n}{g_n - 1} \right)} \right]^{\left( \frac{g_n - 1}{g_n} \right)^2} \right), 10^{-4} \right] \quad Eq. [390]$$

$g_l$  is a fitting parameter and has to be measured for a specific material. Note that using the above expressions, the relative permeability can be related to the suction pore pressure directly.

The derivative of the degree of saturation with respect to the suction pore pressure reads:

$$\frac{\partial S(p_w)}{\partial p_w} = (S_{sat} - S_{res}) \left[ \frac{1 - g_n}{g_n} \right] \left[ g_n \left( \frac{g_a}{y_w} \right)^{g_n} \cdot p_w^{(g_n - 1)} \right] \left[ 1 + \left( g_a \cdot \frac{p_w}{y_w} \right)^{g_n} \right]^{\left( \frac{1 - 2g_n}{g_n} \right)} \quad Eq. [391]$$

[Figure 114](#) (on page 241) and [Figure 115](#) (on page 242) present the Van Genuchten relations for a sandy material with parameters  $S_{sat} = 1.0$ ,  $S_{res} = 0.027$ ,  $g_a = 2.24 \sim m^{-1}$ ,  $g_l = 0.0$  and  $g_n = 2.286$  graphically.

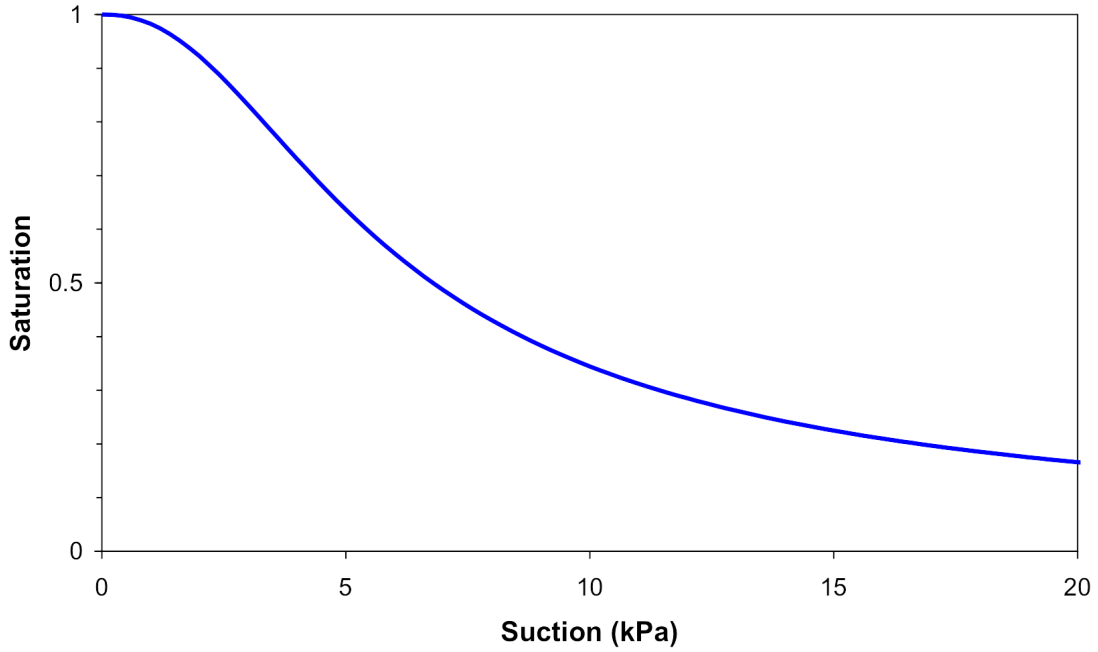


Figure 114: Van Genuchten pressure-relative permeability

## Hydraulic Models

Approximate Van Genuchten model

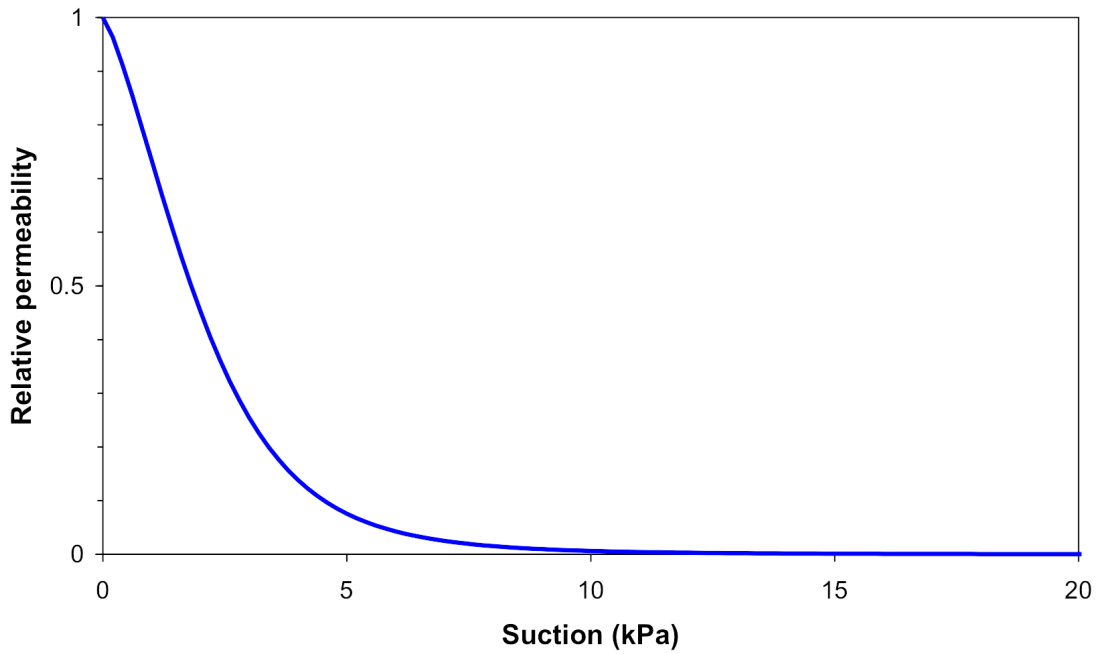


Figure 115: Approximate Van Genuchten pressure-relative permeability

## 19.2 Approximate Van Genuchten model

As an alternative, PLAXIS for flow analysis supports a linearised Van Genuchten model for which the approximate Van Genuchten parameters can be derived. According to this concept saturation relates to the pore pressure head as:

$$S(\psi) = \begin{cases} 1 & \text{if } \psi \geq 0 \\ 1 + \frac{\psi}{|\psi_s|} & \text{if } \psi_s < \psi < 0 \\ 0 & \text{if } \psi \leq \psi_s \end{cases} \quad \text{Eq. [392]}$$

The variable  $\psi_s$  is a material dependent pressure head which specifies the extent of the unsaturated zone under hydrostatic conditions. Below this threshold value the saturation is assumed to be zero. For saturated conditions the degree of saturation equals one.

The linearised Approximate Van Genuchten relation between relative permeability and pressure head is written as:

$$k_{rel}(\psi) = \begin{cases} 1 & \text{if } \psi \geq 0 \\ 10 \frac{4\psi}{|\psi_k|} & \text{if } \psi_k < \psi < 0 \\ 10^{-4} & \text{if } \psi \leq \psi_k \end{cases} \quad \text{Eq. [393]}$$

## Hydraulic Models

### Approximate Van Genuchten model

According to this formulation the permeability in the transition zone is described as a log-linear relation of pressure head where  $\psi_k$  is the pressure head at which the relative permeability is reduced to  $10^{-4}$ . In the Approximate Van Genuchten model the permeability remains constant for values of the pressure head higher than  $\psi_k$ . Under saturated conditions the relative permeability equals one and the effective permeability is equal to the saturated permeability which is assumed to be constant.

The input parameters of the "approximate Van Genuchten model" are derived from the classical Van Genuchten model. These parameters are translated into approximately equivalent process parameters for the numerically more robust linearised model. For  $\psi_S$  the translation is as follows:

$$\psi_S = \frac{1}{S_{\psi=-1.0 \text{ m}} \cdot S_{sat}} \quad \text{Eq. [394]}$$

The parameter  $\psi_k$  is set equal to the pressure head at which the relative permeability according to Van Genuchten is  $10^{-2}$ , with a lower limit of -0.5~m. [Figure 116](#) (on page 243) presents the functional relation between pressure and saturation according to the approximate Van Genuchten model using  $\psi_k = 1.48 \text{ m}$ . The corresponding pressure-relative saturation relation  $\psi_s = 1.15 \text{ m}$  is given in [Figure 117](#) (on page 244).

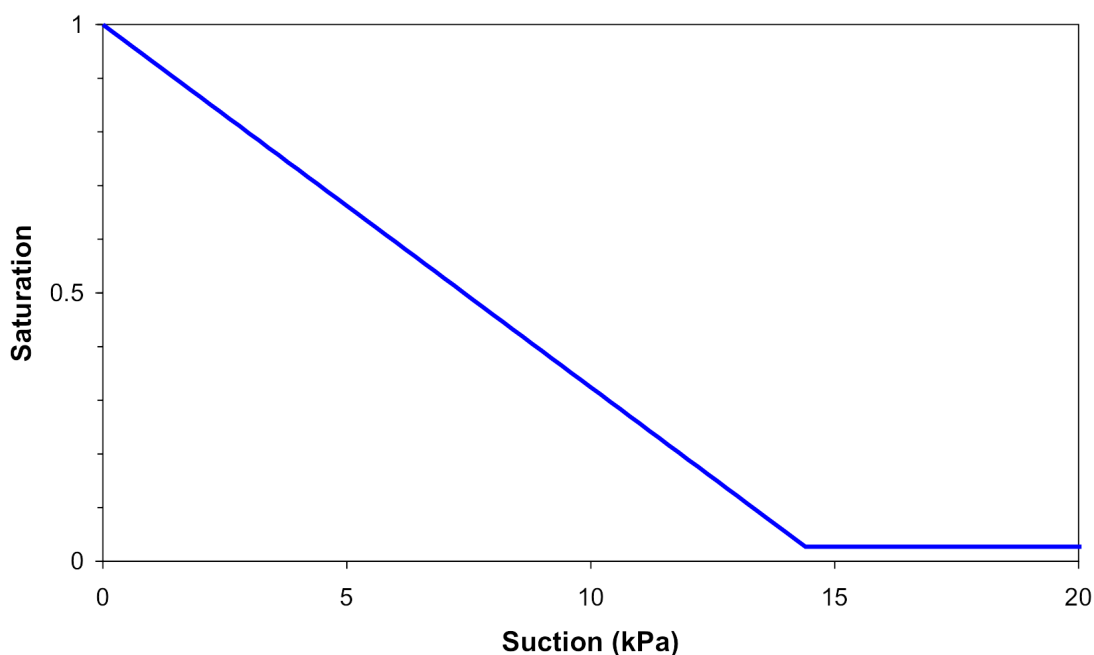
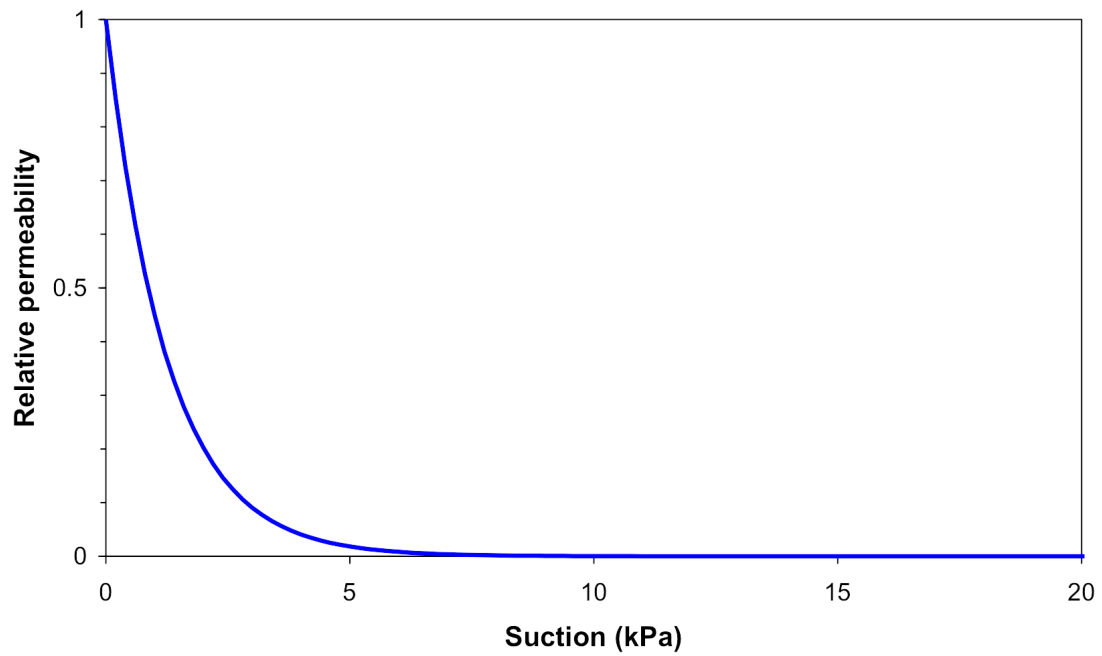


Figure 116: Approximate Van Genuchten pressure-saturation

## Hydraulic Models

Approximate Van Genuchten model

---



*Figure 117: Approximate Van Genuchten pressure-relative permeability*

# 20

## References

---

1. (1990). CEB-FIP model code Fédération internationale du béton.
2. (1992). ACI 209R-92 American Concrete Institute.
3. (2004). Eurocode 2: Design of concrete structures . European Committee for Standardization.
4. Adachi, T., Oka, F. (1982). Constitutive equation for normally consolidated clays based on elasto-viscoplasticity. *Soils and Foundations*, 22, 57–70.
5. Alpan, I. (1970). The geotechnical properties of soils. *Earth-Science Reviews*, 6, 5–49.
6. Andersen, K., Kleven, A., Heien, D. (1988). Cyclic soil data for design of gravity structures. *Journal of Geotechnical engineering*, 114, 517–539.
7. Andersen, K.H. (2009). Bearing capacity under cyclic loading offshore, along the coast, and on land. *Canadian Geotechnical Journal*, 46, 513–535.
8. Andersen, K.H. (2015). Cyclic soil parameters for offshore foundation design. *Frontiers in Offshore Geotechnics III*, 5–82.
9. Andresen, L. (2002). Capacity analysis of anisotropic and strain-softening clay. Ph.d. thesis, University of Oslo, Institute of Geology.
10. Andresen, L., Jostad, H.P. (1999). Application of an anisotropic hardening model for undrained response of saturated clay. *Proc. NUMOG VII*, 581–585.
11. Andresen, L., Jostad, H.P. (2009). A fe procedure for calculation of displacements and capacity of foundations subjected to cyclic loading. *Proc. COMGEO I*.
12. Atkinson, J.H., Bransby, P.L. (1978). *The Mechanics of Soils*. McGraw-Hill, London.
13. Atkinson, J.H., Sallfors, G. (1991). Experimental determination of soil properties. In *Proc. 10th ECSMFE*, 3, 915–956.
14. Austin, S.A., Robins, P.J. (1995). *Sprayed Concrete: Properties, Design and Installation*. Whittles Publishing, Dunbeath.
15. Barros, J.A.O., Figueiras, J.A. (1999). Flexural behaviour of sfrc: testing and modelling. *Journal of Materials in Civil Engineering*, ASCE 11, 331–339.
16. Beaty, M.H., Byrne, P.M. (1998). An effective stress model for predicting liquefaction behaviour of sand. *Geotechnical Earthquake Engineering and Soil Dynamics*, ASCE Geotechnical Special Publication 75, 766–777.
17. Beaty, M.H., Byrne, P.M. (2011). Ubcsand constitutive model. Itasca UDM website 904aR.
18. Beaty, M.H., Perlea, V.G. (2011). Several observations on advanced analyses with liquefiable materials. *Thirty first annual USSD conference on 21st century dam design-advances and adaptations*, 1369–1397.
19. Belytschko, T., Lasry, D. (1989). Localization limiters and numerical strategies for strain-softening materials. In *Proc. France-US Workshop on Strain localization and size effect due to cracking and Damage* editor= (Mazars & Bazant). 349–362.
20. Benz, T. (2006). Small-Strain Stiffness of Soils and its Numerical Consequences. Ph.d. thesis, Universität Stuttgart.

## References

---

21. Benz, T., Schwab, R., Vermeer, P.A., Kauther, R.A. (2007). A hoek-brown criterion with intrinsic material strength factorization. *Int.J. of Rock Mechanics and Mining Sci.*, 45(2), 210–222.
22. Biarez, J., Hicher, P.Y. (1994). *Elementary Mechanics of Soil Behaviour*. A A Balkema, Rotterdam, The Netherlands.
23. Billington, E.W. (1988). Generalized isotropic yield criterion for incompressible materials. *Acta Mechanica*, 72, 1–20.
24. Bjerrum, L. (1967). Engineering geology of norwegian normally-consolidated marine clays as related to settlements of buildings. *Seventh Rankine Lecture, Geotechnique* 17, 81–118.
25. Bolton, M.D. (1986). The strength and dilatancy of sands. *Géotechnique*, 36(1), 65–78.
26. Borja, R.I., Kavazanjian, E. (1985). A constitutive model for the  $\sigma$ - $\epsilon$  behaviour of wet clays. *Geotechnique*, 35, 283–298.
27. Borja, R.I., Lee, S.R. (1990). Cam-clay plasticity, part 1: implicit integration of elasto-plastic constitutive relations. *Computer Methods in Applied Mechanics and Engineering*, 78, 48–72.
28. Branque, D. (1997). Utilisation d'un modèle Élasto-plastique avec dilatance dans l'interprétation de l'essai pressiométrique sur sable. Ph.d. thesis, Ecole Centrale Paris.
29. Brinkgreve, R.B.J. (1994). *Geomaterial Models and Numerical Analysis of Softening*. Dissertation. Delft University of Technology.
30. Brinkgreve, R.B.J. (2004). Time-dependent behaviour of soft soils during embankment construction - a numerical study. *Proc. NUMOG IX*, 631–637.
31. Brinkgreve, R.B.J., Engin, E., Engin, H. (2010). Validation of empirical formulas to derive model parameters for sands. In T. Benz, S. Nordal (eds.), *7th European Conference Numerical Methods in Geotechnical Engineering*. Numge 2010, Trondheim, volume 1, 137–174.
32. Brinkgreve, R.B.J., Kappert, M.H., Bonnier, P.G. (2007). Hysteretic damping in a small-strain stiffness model. *Proc. NUMOG X*, 737–742.
33. Brinkgreve, R.B.J., Vermeer, P.A. (1992). On the use of cam-clay models. In *Proc. IV Int. Symposium on Numerical Models in Geomechanics* (eds. G.N. Pande, S. Pietruszczak). Balkema, Rotterdam, volume 2, 557–565.
34. Buisman, K. (1936). Results of long duration settlement tests. *Proceedings 1st International Conference on Soil Mechanics and Foundation Engineering, Mass. Vol. 1*, 103–107.
35. Burland, J.B. (1965). The yielding and dilation of clay. *Géotechnique*, 15, 211–214. (Correspondence).
36. Burland, J.B. (1967). *Deformation of Soft Clay*. Dissertation. Cambridge University.
37. Burns, N.H., Siess, C.P. (1962). Load-deformation characteristics of beam-column connections in reinforced concrete. *Civil Engineering Studies, SRS no. 234*. University of Illinois, Urbana.
38. Butterfield, R. (1979). A natural compression law for soils (an advance on  $e$ - $\log p'$ ). *Geotechnique*, 29, 469–480.
39. Carranza-Torres, C. (2004). Elastoplastic solution of tunnel problems using the generalized form of the hoek-brown failure criterion. *Int.J. of Rock Mechanics and Mining Sci.*, 41(3), 480–481.
40. Chen, W.F. (1975). *Limit analysis and soil plasticity*. Elsevier, Amsterdam.
41. Davis, E.H., Christian, J.T. (1971). Bearing capacity of anisotropic cohesive soil. *Journal of Soil Mechanics and Foundation Division*, 97, 753–769.
42. Deere, D.U. (1968). *Rock mechanics in engineering practice*. London: Wiley.
43. den Haan, E.J. (1994). *Vertical Compression of Soils*. Thesis, Delft University.
44. Drucker, D.C., Prager, W. (1952). Soil mechanics and plastic analysis or limit design. *Quart. Appl. Math.*, 10(2), 157–165.
45. Duncan, J.M., Chang, C.Y. (1970). Nonlinear analysis of stress and strain in soil. *ASCE J. of the Soil Mech. and Found. Div.*, 96, 1629–1653.
46. Fung, Y.C. (1965). *Foundations of Solid Mechanics*. Prentice-Hall, New Jersey, USA.

## References

---

47. Garlanger, J.E. (1972). The consolidation of soils exhibiting creep under constant effective stress. *Géotechnique*, 22, 71–78.
48. Grimstad, G., Andresen, L., Jostad, H.P. (2010). Anisotropic shear strength model for clay. *International Journal for Numerical and Analytical Methods in Geomechanics*, (Accepted for publication).
49. Hardin, B.O., Black, W.L. (1969). Closure to vibration modulus of normally consolidated clays. *Proc. ASCE: Journal of the Soil Mechanics and Foundations Division*, 95(SM6), 1531–1537.
50. Hardin, B.O., Drnevich, V.P. (1972). Shear modulus and damping in soils: Design equations and curves. *Proc. ASCE: Journal of the Soil Mechanics and Foundations Division*, 98(SM7), 667–692.
51. Hill, R. (1950). *The Mathematical Theory of Plasticity*. Oxford University Press, London, U.K.
52. Hoek, E. (1999). Putting numbers to geology-an engineers's viewpoint. *Quarterly Journal of Engineering Geology*, 32, 1–9.
53. Hoek, E. (2006). *Practical Rock Engineering*. E-book.
54. Hoek, E., Carranza-Torres, C., Corkum, B. (2002). Hoek-brown failure criterion - 2002 edition. volume 1, 267–273.
55. Hoek, E., Diederichs, M.S. (2006). Empirical estimation of rock mass modulus. volume 43, 203–215.
56. Iizuka, A., Ohta, H. (1987). A determination procedure of input parameters in elasto-viscoplastic finite element analysis. *Soils and Foundations*, 27, 71–87.
57. Jaky, J. (1944). The coefficient of earth pressure at rest. *J. Soc. Hung. Eng. Arch.*,
58. Janbu, N. (1963). Soil compressibility as determined by oedometer and triaxial tests. *Proc. ECSMFE Wiesbaden*, 1, 19–25.
59. Janbu, N. (1969). The resistance concept applied to soils. *Proceedings of the 7th ICSMFE, Mexico City*, 1, 191–196.
60. Janbu, N. (1985). Soil models in offshore engineering (25th Rankine lecture). *Géotechnique*, 35, 241–280.
61. Jostad, H.P., Torgerstrud, Engin, H. (2015). A FE procedure for calculation of fixity of jack-up foundations with skirts using cyclic strain contour diagrams. In *The 15th International Conference: The Jack-up Platform*. London.
62. Koiter, W.T. (1953). Stress-strain relations, uniqueness and variational theorems for elasto-plastic materials with a singular yield surface. *Quart. Appl. Math.*, 11, 350–354.
63. Koiter, W.T. (1960). General theorems for elastic-plastic solids. In I.N. Sneddon, R. Hill (eds.), *Progress in Solid Mechanics*. North-Holland, Amsterdam, volume 1, 165–221.
64. Kondner, R.L. (1963). A hyperbolic stress strain formulation for sands. 2. *Pan. Am. ICOSFE Brazil*, 1, 289–324.
65. Kormeling, H.A., Reinhardt, H.W. (1969). Determination of the fracture energy of normal concrete and epoxy modified concrete. *Delft University of Technology*.
66. Kulhawy, F.H., Mayne, P.W. (1990). *Manual on Estimating Soil Properties for Foundation Design*. Cornell University, Ithaca, New York.
67. Kwak, H.G., Filippou, F.C. (1996). Nonlinear FE analysis of R/C structures under monotonic loads. *Computer and Structures*, 65(1), 1–16.
68. Laera, A., Brinkgreve, R.B.J. (2015). Liquefaction analysis with the use of the finite element code PLAXIS. In *5th Int. Conf. IAGIG. Roma*.
69. Leroueil, S. (1977). *Quelques considérations sur le comportement des argiles sensibles*. Ph.D. thesis, Laval University, Québec.
70. Li, X.S., Dafalias, Y.F. (2000). Dilatancy for cohesionless soils. *Geotechnique*, 50(4), 449–460.
71. Marinos, P., Hoek, E. (2001). Estimating the mechanical properties of heterogeneous rock masses such as flysh. *Bulletin of Engineering Geology*, 92, 60–85.
72. Masing, G. (1926). *Eigenspannungen und verfestigung beim messing*. In *In Proc. 2nd Int. Congr. Appl. Mech. Zurich*.
73. Mayne, P.W. (2001). Keynote: Stress-strain-strength-flow parameters from enhanced in-situ tests. In *In-Situ Measurement of Soil Properties and Case Histories. Indonesia*, 27–47.

## References

---

74. Meschke, G., Kropik, C., Mang, H.A. (1996). Numerical analysis of tunnel linings by means of a viscoplastic material model for shotcrete. *International Journal for Numerical Methods in Engineering*, 39, 3145–62.
75. Mesri, G., Godlewski, P.M. (1977). Time and stress-compressibility inter-relationship. *Journal of the Geotechnical Engineering Division, ASCE*, 103(GT5), 417–430.
76. Muir Wood, D. (1990). *Soil Behaviour and Critical State Soil Mechanics*. Cambridge University Press. 1, 355–358.
77. Murayama, S., Shibata, T. (1966). Flow and stress relaxation of clays. In *I.U.T.A.M. Symp. on Rheology and Soil Mechanics*. Grenoble, 99–129.
78. Naesgaard, E. (2011). A hybrid effective stress-total stress procedure for analysing soil embankments subjected to potential liquefaction and flow. Ph.d. thesis, University of British Columbia.
79. Niemunis, A., Herle, I. (1997). I.: Hypoplastic model for cohesionless soils with elastic strain range. *Mechanics of Cohesive Frictional Materials*, 2(3), 279–299.
80. Ohta, H., Hata, S. (1973). Immediate and consolidation deformations of clay. In *8th. Int. Conf. S.M.F.E. volume 1*, 193–196.
81. Oluokun, F.A., Burdette, E.G., Deatherage, J.H. (1991). Splitting tensile strength and compressive strength relationship at early ages. *ACI Materials Journal*, 88(2), 115–121.
82. Petalas, A., Galavi, V. (2012). Plaxis liquefaction model ubc3d-plm. PLAXIS knowledge base.
83. Pipatpongsa, T., Iizuka, A., Kobayashi, I., Ohta, H. (2002). Fem formulation for analysis of soil constitutive model with a corner on the yield surface. *Journal of Structural Engineering*, 48, 185–194.
84. Polling, R. (2000). Eine praxisnahe, schÄd’digungsorientierte Materialbeschreibung von Stahlbeton fÄijr Strukturanalysen. Ph.d. thesis, Ruhr-Universität, Bochum.
85. Prevost, J.H. (1976). Undrained stress-strain-time behaviour of clays. *Journal of the Geotechnical Engineering Division, GT12*, 1245–1259.
86. Puebla, H., Byrne, M., Phillips, P. (1997). Analysis of canlex liquefaction embankments prototype and centrifuge models. *Canadian Geotechnical Journal*, 34, 641–657.
87. Randolph, M., Gourvenec, S. (2011). *Offshore Geotechnical Engineering*. Spoon Press, New York.
88. Roscoe, K.H., Burland, J.B. (1968). On the generalized stress-strain behaviour of “wet” clay. In *Heyman & Leckie, Engineering Plasticity*, Cambridge University Press. 535–609.
89. Roscoe, K.H., Schofield, A.N., Thurairajah, A. (1963). Yielding of clays in states wetter than critical. *Geotechnique*, 13(3), 211–240.
90. Rots, J.G. (1988). Computational modelling of concrete fracture. PhD Thesis. Delft University of Technology.
91. Rowe, P.W. (1962). The stress-dilatancy relation for static equilibrium of an assembly of particles in contact. In *Proc. Roy. Soc. A.*, No. 269. 500–527.
92. Santos, J.A., Correia, A.G. (2001). Reference threshold shear strain of soil. its application to obtain a unique strain-dependent shear modulus curve for soil. In *Proceedings 15th International Conference on Soil Mechanics and Geotechnical Engineering*. Istanbul, Turkey, volume 1, 267–270.
93. Schädlich, B., Schweiger, H.F. (2014). A new constitutive model for shotcrete. In *T.F. Group (ed.), Numerical Methods in Geotechnical Engineering*. 103–108.
94. Schanz, T. (1998). *Zur Modellierung des Mechanischen Verhaltens von Reibungsmaterialien*. Habilitation, Stuttgart Universität.
95. Schanz, T., Vermeer, P.A. (1996). Angles of friction and dilatancy of sand. *Géotechnique*, 46, 145–151.
96. Schanz, T., Vermeer, P.A. (1998). Special issue on pre-failure deformation behaviour of geomaterials. *Géotechnique*, 48, 383–387.
97. Schanz, T., Vermeer, P.A., Bonnier, P.G. (1999). The hardening-soil model: Formulation and verification. In *R.B.J. Brinkgreve, Beyond 2000 in Computational Geotechnics*, Balkema, Rotterdam. 281–290.
98. Schütz, R., Potts, D.M., Zdravković, L. (2011). Advanced constitutive modelling of shotcrete: Model formulation and calibration. *Computers and Geotechnics*, 38(6), 834–845.

## References

---

99. Schweiger, H.F. (2002). Results from numerical benchmark exercises in geotechnics. In P. Mestat (ed.), 5th European Conference Numerical Methods in Geotechnical Engineering. Numge 2002, Paris, volume 1, 305–314.
100. Sekiguchi, H. (1977). Rheological characteristics of clays. In Proceedings of the 9th ICSMFE. Tokyo, volume 1, 289–292.
101. Sekiguchi, H., Ohta, H. (1977). Induced anisotropy and time dependency in clays. In Proceedings of the 9th ICSMFE. Tokyo, volume 3, 542–544.
102. Simpson, B. (1992). "retaining structures: displacement and design", the 32nd rankine lecture. Geotechnique, 42(4), 541–576.
103. Sluis, J. (2012). Validation of embedded pile row in PLAXIS 2D. Master's thesis. Delft University of Technology.
104. Smith, I.M., Griffiths, D.V. (1982). Programming the Finite Element Method. John Wiley & Sons, Chisester, U.K, second edition.
105. Souliotis, C., Gerolymos, N. (2016). Seismic analysis of quay wall in liquefiable soil with the ubc3d-plm constitutive model: Calibration methodology and validation. In 1th International Conference on Natural Hazards & Infrastructure. Chania.
106. Stolle, D.F.E. (1991). An interpretation of initial stress and strain methods, and numerical stability. International Journal for Numerical and Analytical Methods in Geomechanics, 15, 399–416.
107. Stolle, D.F.E., Bonnier, P.G., Vermeer, P.A. (1997). A soft soil model and experiences with two integration schemes. In Numerical Models in Geomechanics. Numog 1997, 123–128.
108. Taiebat, H.A., Carter, J.P. (2008). Flow rule effects in the tresca model. Computers and Geotechnics, 35, 500–503.
109. Takeyama, T., Ohno, S., Pipatpongsa, T., Iizuka, A., Ohta, H. (2010). The stress update using implicit integration for the viscid version of sekiguchi-ohta model. Technical report, Technical report.
110. Tsegaye, A. (2010). Plaxis liquefaction model. external report. PLAXIS knowledge base.
111. Ukritchon, B., Whittle, A.J., Sloan, S.W. (2003). Undrained stability of braced excavations in clay. Journal of Geotechnical and Geoenvironmental Engineering, 129(8), 738–755.
112. Vaid, Y., Campanella, R.G. (1977). Time-dependent behaviour of undisturbed clay. ASCE Journal of the Geotechnical Engineering Division, 103(GT7), 693–709.
113. van Genuchten, M. (1980). A closed-form equation for predicting the hydraulic conductivity of unsaturated soils. Soil science society of America journal, 44(5), 892–898.
114. van Langen, H., Vermeer, P.A. (1990). Automatic step size correction for non-associated plasticity problems. Int. J. Num. Meth. Engng., 29, 579–598.
115. Vermeer, P.A., Borst, R. (1984). Non-associated plasticity for soils, concrete and rock. Heron, 29(3).
116. Vermeer, P.A., Neher, H. (1999). A soft soil model that accounts for creep. In R.B.J. Brinkgreve, Beyond 2000 in Computational Geotechnics, Balkema, Rotterdam. 249–261.
117. Vermeer, P.A., Stolle, D.F.E., Bonnier, P.G. (1998). From the classical theory of secondary compression to modern creep analysis. Proc. 9th Int. Conf. Comp. Meth. and Adv. Geomech., Wuhan, China, 4, 2469–2478.
118. Vermeer, P.A., van Langen, H. (1989). Soil collapse computations with finite elements. In Ingenieur-Archiv 59. 221–236.
119. von Mises, R. (1913). Mechanik der festen körper in plastisch deformablem zustand. Göttinger Nachrichten Math.-Phys. Klasse, 1, 582–592.
120. von Soos, P. (1990). Properties of soil and rock (in german). In In: Grundbautaschenbuch Part 4. Ernst & Sohn, Berlin.
121. Vucetic, M., Dobry, R. (1991). Effect of soil plasticity on cyclic response. Journal of Geotechnical Engineering, ASCE, 117(1), 89–107.
122. Wyllie, D.C., Mah, C. (2004). Rock slope engineering. CRC Press, Boca Raton.

# Appendices

---

# A

## Symbols

General Symbols	Name
$A$	Cross section area
$c$	Cohesion
$csp$	Current stiffness parameter
$C$	Correction factor for SPT value
$C_{\alpha}$	Creep index for secondary compression
$C_c$	Compression index
$C_r$	Ricompaction index
$C_s$	Swelling index
$C_u, S_u$	Undrained shear-strength
$d$	Thickness
$D$	Disturbance factor
$\mathbf{D}^e$	Elastic material matrix representing Hooke's law
$e$	Void ratio
$E$	Young's modulus
$E_{oed}$	Oedometer modulus
$f$	Yield function
$f_{dens}$	Densification factor
$f_{Epost}$	Post-liquefaction factor
$g$	Plastic potential function

## Symbols

General Symbols	Name
$G$	Shear modulus
$GSI$	Geological Strength Index
$G_{ur}$	Unloading/reloading shear modulus
$I$	Moment of inertia
$k^*e_B$	Elastic bulk modulus factor
$k^*e_G$	Elastic shear modulus factor
$k^*p_G$	Plastic shear modulus factor
$k^*p_{G,secondary}$	Secondary plastic shear modulus factor
$K$	Bulk modulus
$K_0$	Coefficient of lateral earth pressure (initial stress state)
$K_0^{nc}$	Coefficient of lateral earth pressure for a normally consolidated stress state
$me$	Power in stress-dependent relation for elastic bulk modulus
$m_i$	Intact rock parameter
$ne$	Power in stress-dependent relation for elastic shear modulus
$np$	Power in stress-dependent relation for plastic shear modulus
$M$	Slope of critical state line in $p'$ - $q$ space
$M$	Bending moment
$n_{rev}$	Number of shear stress reversals
$N$	Normal force
$N_{1,60}$	Corrected SPT value
OCR	overconsolidation ratio
$p$	Isotropic stress or mean stress, negative for pressure; positive for tension
$p_w$	Pore pressure
$p_p$	Isotropic pre-consolidation stress, negative for pressure
POP	Pre overburden pressure, positive for (over)pressure

## Symbols

General Symbols	Name
$q$	Equivalent shear stress or deviatoric stress
$Q$	Shear force
$R_f$	Failure ratio
$r_{u,\sigma'v}$	Excess pore pressure ratio in terms of vertical effective stresses
$r_{u,p'}$	Excess pore pressure ratio in terms of mean effective stresses
$RD$	Relative density
$s_u^a$	Undrained active shear strength
$s_u^{c,TX}$	Undrained triaxial compressive shear strength
$s_u^{DSS}$	Undrained direct simple shear strength
$s_u^p$	Undrained passive shear strength
$t$	Time
$\underline{u}$	Vector with displacement components
$\gamma$	Unit weight
$\gamma$	Various types of shear strain
$\alpha_1$	dip angle
$\alpha_2$	dip direction
$\Delta$	Increment
$\underline{\varepsilon}$	Vector with Cartesian strain components, normal components positive for extension; negative for compression
$\varepsilon_q$	Deviatoric strain (invariant)
$\varepsilon_v$	Volumetric strain, negative for compression; positive for extension
$\kappa$	Cam-Clay swelling index
$\kappa^*$	Modified swelling index
$\lambda$	Plastic multiplier
$\lambda$	Cam-Clay compression index
$\lambda^*$	Modified compression index

## Symbols

General Symbols	Name
$\mu^*$	Modified creep index
$\nu$	Poisson's ratio
$\underline{\sigma}$	Vector with Cartesian stress components, normal components positive for tension; negative for pressure
$\sigma_\psi$	Confining pressure at which $\psi = 0$
$\sigma_{ci}$	Uni-axial compressive strength
$\sigma_p$	Vertical pre-consolidation stress, negative for pressure
$\varphi$	Friction angle
$\varphi_{cv}$	Constant volume friction angle
$\varphi_{mob}$	Mobilised friction angle
$\varphi_p$	Peak friction angle
$\psi$	Dilatancy angle
$\psi_m$	Mobilised dilatancy angle
$\psi_{max}$	Maximum dilatancy angle
$x^c$	Denotes creep component
$x^e$	Denotes elastic component
$x^p$	Denotes plastic component
$x^{ref}$	Denotes reference value (related to a reference stress)
$x_u$	Denotes undrained
$x_{ur}$	Denotes unloading and reloading
$x_m$	Denotes mobilised

Concrete model symbols	Name
$a$	Increase of $\varepsilon_{cp}$ with increase of $p$
$f$	Yield stress
$f_{xxn}$	Normalised strength
$F$	Yield function

## Symbols

Concrete model symbols	Name
$G$	Fracture energy
$H$	Normalised hardening/softening
$J$	Shotcrete strength class
$k_{\sigma}$	Degree of concrete utilisation in compression
$L_{eq}$	Characteristic length of the finite element
$s$	Power in time-dependent strength/stiffness relations
$t_{hydr}$	Time of full curing
$\gamma_{fx}$	Safety factor for strength
$\varphi_{cr}$	Creep factor
$\varphi_{max}$	Maximum friction angle
$\psi$	Dilatancy angle
$x^{cr}$	denotes creep
$x^{shr}$	denotes shrinkage
$x_{\infty}$	Denotes a time $t = \infty$
$x_{28}$	Denotes a value of cured concrete
$x_{50}$	Denotes a time $t$ when 50% of the phenomenon has occurred
$x_{cp}$	Denotes peak in uniaxial compression
$x_{xf}$	Denotes a uniaxial failure value

# B

## Applicability of the material model

In this appendix, an overview of the applicability of the material models is given.

Considering different materials:

Model	Concrete	Rock	Gravel	Sand	Silt	OC clay	NC clay	Peat(org)
Linear Elastic Model	C	C						
Mohr-Coulomb model	B	B	C	C	C	C	C	C
Hardening soil model			B	B	B	B	B	
HS small model			A	A	A	A	B	
UBC3D-PLM model			B*	B*	B*			
Soft Soil creep model							A*	A*
Soft soil model							A*	A*
Jointed rock model		A**						
Modified Cam-Clay model							C	C
NGI-ADP model						A*	A*	A*

## Applicability of the material model

Model	Concrete	Rock	Gravel	Sand	Silt	OC clay	NC clay	Peat(org)
UDCAM-S model						A*	A*	A*
Hoek-Brown model		A**						
Concrete model	A							
A : The best standard model in PLAXIS for this application								
B : Reasonable modelling								
C : First order (crude) approximation								
* : Soft Soil Creep model in case time-dependent behaviour is important; UBC3D-PLM model for dynamics analysis of sandy soils involving liquefaction								
* : NGI-ADP model for short-term analysis and UDCAM-S model for cyclic analysis, in case only undrained strength is known								
** : Jointed Rock model in case of anisotropy and stratification; Hoek-Brown model for rock in general								

Considering different types of applications(consider also type of soil!)

Model	Foundation	Excavation	Tunnel	Embankment	Slope	Dam	Offshore	Other
Linear Elastic model	C		C					
Mohr-Coulomb model	C	C	C	C	C	C	C	C
Hardening Soil model	B	B	B	B	B	B	B	B
HS small model	A	A	A	A	A	A	A	A
UBC3D-PLM model*	B	B	B	B	B	B	B	B

## Applicability of the material model

Model	Foundation	Excavation	Tunnel	Embankment	Slope	Dam	Offshore	Other
Soft Soil Creep model	B	B	B	A	A	B	B	B
Soft Soil model	B	B	B	A	A	B	B	B
Jointed Rock model	B	B	B	B	B	B	B	B
Modified Cam-Clay model	C	C	C	C	C	C	C	C
NGI-ADP model	B	B	B	A	A	B	A	B
UDCAM-S model*							A	
Hoek-Brown model	B	B	B	B	B	B	B	B
Concrete model	A	A	A	A	A	A	A	A
A : The best standard model in PLAXIS for this application								
B : Reasonable modelling								
C : First order (crude) approximation								
* : UDCAM-S model for cyclic analysis, in case only undrained strength is known; UBC3D-PLM model for dynamics analysis of sandy soils involving undrained cyclic loading								
* : As an alternative PM4Sand is available as a user-defined soil model under [GSE]								

Considering different types of loading and soils (consider also type of soil!):

## Applicability of the material model

Model	Primary compression	Unloading / Reloading	Shear / Deviatoric loading	Undrained loading	Cyclic	Compression + Shear	Extension + Shear
Linear Elastic model	C	C					
Mohr-Coulomb model	C	B	C	C		C	C
Hardening Soil model	A	B	B	B	C	A	A
HS small model	A	A	A	B	B	A	A
UBC3D-PLM model*	B	B	B	B	B	B	B
Soft Soil Creep model	A	B	B	B	C	A	B
Soft Soil model	A	B	B	B	C	A	B
Jointed Rock model	B	B	B			B	B
Modified Cam-Clay model	C	C	C	C	C	C	C
NGI ADP model	B	B	B	A	C	B	B
UDCAM-S model*	B	B	B	A	A*	A	B
Hoek-Brown model	B	B	B			B	B
Concrete model**	A	A	A		C	A	A
A : The best standard model in PLAXIS for this application							
B : Reasonable modelling							

## Applicability of the material model

Model	Primary compression	Unloading / Reloading	Shear / Deviatoric loading	Undrained loading	Cyclic	Compression + Shear	Extension + Shear
C : First order (crude) approximation							
* : UDCAM-S model for cyclic analysis, in case only undrained strength is known; UBC3D-PLM model for dynamics analysis of sandy soils involving undrained cyclic loading							
* : As an alternative PM4Sand is available as a user-defined soil model upon request							



## Modelling of embedded structures

In this appendix, an overview of the applicability of the different modelling techniques for embedded structures is given. In addition to displacement differences and shear forces in axial direction, the embedded structures can undergo transverse forces due to lateral displacements. The lateral displacements can be induced by a transverse force applied at the top of the pile (*Pile head loading*) or as a consequence of the transverse distributed load induced by the lateral displacement field of the surrounding soil (*Horizontal soil displacement*).

PLAXIS 2D	Axial behaviour			Lateral behaviour Pile head loading		Lateral behaviour Lateral soil movement	
	Wall behaviour	Pile row	Single pile	Pile row	Single pile	Pile row	Single Pile
Volume elements	B	C	-	-	-	-	-
Plate	A	C	-	B	-	C	-
Node to node anchor	-	C	-	-	-	-	-
Embedded beam row	-	B	C	B	-	B	-

PLAXIS 3D	Axial behaviour			Lateral behaviour Pile head loading		Lateral behaviour Lateral soil movement	
	Wall behaviour	Pile row	Single pile	Pile row	Single pile	Pile row	Single Pile
Volume elements	A	A	A	A	A	A	A
Plate	A	C	-	-	-	-	-
Node to node anchor	-	C	-	-	-	-	-
Embedded beam	-	B	C	C	C	B	B

## Modelling of embedded structures

---

A : The best modelling choice for the correspondent application

B : Reasonable modelling

C : First order (crude) approximation

- : Not recommended



# Fortran subroutines for User-defined soil models

## D.1 Subroutines

In this appendix, a listing is given of the subroutines and functions which are provided by PLAXIS in libraries and source code in the User-defined soil model directory. These can be called by the User\_Mod subroutine:

Subroutine	Description
MZeroR( R , K )	To initialize K terms of double array R to zero.
MZeroI( I, K )	To initialize K terms of integer array I to zero.
SetRVal( R, K, V )	To initialize K terms of double array R to V.
SetIVal( I, K, IV )	To initialize K terms of integer array I to IV.
CopyIVec( I1, I2, K )	To copy K values from integer array I1 to I2.
CopyRVec( R1, R2, K )	To copy K values from double array R1 to R2.
MulVec( V, F, n )	To multiply a vector V by a factor F, n values.
MatVec( xMat, im, Vec, n, VecR )	<ul style="list-style-type: none"><li>Matrix (xMat)-vector(Vec) operation.</li><li>First dimension of matrix is im; resulting vector is VecR.</li></ul>
AddVec( Vec1, Vec2, R1, R2, n, VecR )	To add n terms of two vectors; result in VecR <ul style="list-style-type: none"><li><math>VecR_i = R1 \cdot Vec1_i + R2 \cdot Vec2_i</math></li></ul>
MatMat( xMat1, id1, xMat2, id2, nR1, nC2, nC1, xMatR, idR)	<ul style="list-style-type: none"><li>Matrix multiplication <math>xMatR_{ij} = xMat1_{ik} \cdot xMat2_{kj}</math></li><li>id1, id2, idR: first dimension of matrices</li><li>nR1 number of rows in xMat1 and resulting xMatR</li><li>nC2 number of column in xMat2 and resulting xMatR</li><li>nC1 number of columns in xMat2 = rows in xMat2</li></ul>

## Fortran subroutines for User-defined soil models

Subroutine	Description
MatMatSq( n, xMat1, xMat2, xMatR )	<ul style="list-style-type: none"> <li>Matrix multiplication <math>xMatR_{ij} = xMat1_{ik} \cdot xMat2_{kj}</math></li> <li>Fully filled square matrices with dimensions n</li> </ul>
MatInvPiv( AOrig, B, n )	<p>Matrix inversion of square matrices AOrig and B with dimensions n.</p> <ul style="list-style-type: none"> <li>AOrig is NOT destroyed, B contains inverse matrix of AOrig.</li> <li>Row-pivoting is used.</li> </ul>
WriVal( io, C, V )	<p>To write a double value V to file unit io (when io &gt; 0).</p> <ul style="list-style-type: none"> <li>The value is preceded by the character string C.</li> </ul>
WriIVl( io, C, I )	<ul style="list-style-type: none"> <li>As WriVal but for integer value I.</li> </ul>
WriVec( io, C, V, n )	<ul style="list-style-type: none"> <li>As WriVal but for n values of double array V.</li> </ul>
WriIVc( io, C, iV, n )	<ul style="list-style-type: none"> <li>As WriVal but for n values of integer array iV</li> </ul>
WriMat( io, C, V, nd, nr, nc )	<ul style="list-style-type: none"> <li>As WriVal but for double matrix V. nd is first dimension of V, nr and nc are the number of rows and columns to print respectively.</li> </ul>
PrnSig( iOpt, S, xN1, xN2, xN3, S1, S2, S3, P, Q )	<p>To determine principal stresses and (for iOpt=1) principal directions.</p> <ul style="list-style-type: none"> <li>iOpt = 0 to obtain principal stresses without directions.</li> <li>iOpt = 1 to obtain principal stresses and directions.</li> <li>S array containing 6 stress components (XX, YY, ZZ, XY, YZ, ZX).</li> <li>xN1, xN2, xN3 array containing 3 values of principal normalised directions only when iOpt=1.</li> <li>S1, S2, S3 sorted principal stresses (<math>S1 \leq S2 \leq S3</math>)</li> <li>P isotropic stress (negative for compression).</li> <li>Q deviatoric stress.</li> </ul>
CarSig( S1, S2, S3, xN1, xN2, xN3, SNew )	<p>To calculate Cartesian stresses from principal stresses and principal directions.</p> <ul style="list-style-type: none"> <li>S1, S2, S3 principal stresses.</li> <li>xN1, xN2, xN3 arrays containing principal directions (from PrnSig).</li> <li>SNew contains 6 stress components (XX, YY, ZZ, XY, YZ, ZX).</li> </ul>
CrossProd( xN1, xN2, xN3 )	<p>Cross product of vectors xN1 and xN2</p>

## Fortran subroutines for User-defined soil models

Subroutine	Description
SetVecLen( xN, n, xL )	To multiply the n components of vector xN such that the length of xN becomes xL (for example to normalize vector xN to unit length).

## D.2 Functions

Functions	Description
Logical Function LEqual( A, B, Eps )	Returns TRUE when two values A and B are almost equal, FALSE otherwise. <ul style="list-style-type: none"><li>LEqual = <math> A - B  &lt; Eps * ( A  +  B  + Eps) / 2</math></li></ul>
Logical Function Is0Arr( A, n )	Returns TRUE when all n values of real (double) array A are zero, FALSE otherwise.
Logical Function Is0IArr( IArr, n )	Returns TRUE when all n values of integer array IArr are zero, FALSE otherwise.
Double Precision Function DInProd( A, B, n )	Returns the dot product of two vectors with length n

## Overview of Soil Models and Licence levels

In the table below, it is a summary of the different Soil Models Available in PLAXIS with their required licence level. To know more about PLAXIS licencing please visit the [General Information Manual](#).

**Table 24: Available soil models in PLAXIS 3D**

Soil Model	Licence Level		
	PLAXIS 3D	PLAXIS 3D Advanced [ADV]	PLAXIS 3D Ultimate [ULT]
Mohr-Coulomb/Linear Elastic	✓	✓	✓
Hoek & Brown (rock behaviour)	✓	✓	✓
Jointed Rock (anisotropy)	✓	✓	✓
Hardening Soil (isotropic hardening)	✓	✓	✓
Hardening Soil (Isotropic hardening)	✓	✓	✓
The Hardening Soil with small-strain stiffness	✓	✓	✓
Modified Cam-Clay	✓	✓	✓
NGI-ADP (anisotropic undrained shear strength)	✓	✓	✓
Soft soil	-	✓	✓
Soft Soil Creep	-	✓	✓
Sekiguchi-Ohta	-	✓	✓
UDCAM-S	-	✓	✓

## Overview of Soil Models and Licence levels

Soil Model	Licence Level		
	PLAXIS 3D	PLAXIS 3D Advanced [ADV]	PLAXIS 3D Ultimate [ULT]
Concrete	-	✓	✓
UBC3D-PLM	-	-	✓
<b>User defined Soil Models (UDSM)</b>			
Barcelona Basic	-	✓ + [GSE]	✓ + [GSE]
Creep-SCLAY1S	-	✓ + [GSE]	✓ + [GSE]
Fluid model	-	✓ + [GSE]	✓ + [GSE]
Generalized Hardening Soil	-	✓ + [GSE]	✓ + [GSE]
Hoek & Brown with softening	-	✓ + [GSE]	✓ + [GSE]
Hypoplastic model with inter-granular strain	-	✓ + [GSE]	✓ + [GSE]
Isotropic Jointed Rock with Mohr-Coulomb Failure Criterion	-	✓ + [GSE]	✓ + [GSE]
Masonry	-	✓ + [GSE]	✓ + [GSE]
NorSand	-	✓ + [GSE]	✓ + [GSE]
N2PC-Salt	-	✓ + [GSE]	✓ + [GSE]
OC-Clay	-	✓ + [GSE]	✓ + [GSE]
SHANSEP Mohr Coulomb	-	✓ + [GSE]	✓ + [GSE]
SHANSEP NGI-ADP	-	✓ + [GSE]	✓ + [GSE]
Swelling Rock Model	-	✓ + [GSE]	✓ + [GSE]
Visco-elastic perfectly plastic	-	✓ + [GSE]	✓ + [GSE]

**Note:** For detailed information about the User Defined Soil Models please check the [Bentley Communities website](#). Some user-defined soil models have been developed and are supported by the PLAXIS team itself.